To the Graduate Council:

I am submitting herewith a thesis written by Robert Lewis Partin entitled "Depolarization and Backscatter of 0.904 Micrometer Radiation by Various Surfaces." I recommend that it be accepted in partial fulfillment of the requirements for the degree of Master of Science, with a major in Physics.

Ronald H. Kohl, Major Professor

We have read this thesis
and recommend its acceptance:

Accepted for the Council:

Hilton A. Smith
Vice Chancellor
Graduate Studies and Research

DEPOLARIZATION AND BACKSCATTER OF 0.904 MICROMETER RADIATION BY VARIOUS SURFACES

A Thesis

Presented for the

Master of Science

Degree

The University of Tennessee

Robert Lewis Partin

June 1976

128932

ACKNOWLEDGMENTS

The author wishes to express his appreciation to Dr. Ronald H. Kohl, Committee Chairman and Advisor, for his advice and encouragement throughout this study.

Thanks go also to the other members of the Faculty Advisory Committee, Dr. William A. Dunnill and Dr. Arthur A. Mason.

The author would also like to express his thanks to Michael Flaherty for his help in the collection of data.

He especially would like to thank his wife for her patience and support during this study.

The work presented in this thesis was supported by the Air Force Armament Laboratory, Air Force Systems Command, United States Air Force, Eglin Air Force Base, Florida.

ABSTRACT

The objectives of this study were to determine experimentally the polarization ratios, the related percent depolarizations, and the reflective characteristics occurring in the backscatter from several commonly occurring surfaces for 0.904 micrometer radiation. In general, the variations of these quantities with change in angle of incidence are shown. The reflective characteristics are compared to a standard reflective surface. The surfaces investigated include leaves, barks, woods, petroleum products, rock-like materials, sand, ice, paper products, cloth products, a movie screen, and paint.

The equipment and equipment calibration procedures are discussed.

The theoretical expressions for the measured quantities are derived. The data reduction procedures are outlined.

The results obtained are discussed by groups of similar surfaces.

TABLE OF CONTENTS

CHAPTER		PAGE
I.	INTRODUCTION	1
II.	EXPERIMENTAL APPARATUS	4
	General Description	4
	Sources	8
	Detectors	14
	Signal Processing	18
	Polarizers	19
	Component Mounting and Alignment	21
	Sample Holders	27
	Power Supplies	30
	Standard Reflective Surface	31
III.	THEORETICAL EXPRESSIONS	35
IV.	DATA COLLECTION AND REDUCTION	44
	Data Collection Procedures	44
	Oscilloscope Calibration	49
	Polarizer Leakage	55
	Laser and Detector Calibration	58
	Polarization Ratio	62
	Percent Depolarization	65
	Backscattered Fractions	67
	Error Analysis	69
V.	DISCUSSION OF EXPERIMENTAL RESULTS	83
	Leaves	167

CHAPTER PAGE

Barks..... 172

Dirts..... 172

Woods..... 173

Metals..... 176

Petroleum Products..... 178

Rock-Like Materials..... 180

Sands..... 183

Ice..... 186

Miscellaneous..... 187

Effects Produced by Paints..... 188

VI. CONCLUSIONS..... 191

BIBLIOGRAPHY..... 194

APPENDIX..... 196

I. RADIATION SCATTERED FROM A PERFECTLY REFLECTING LAMBERTIAN SURFACE..... 197

VITA..... 203

LIST OF FIGURES

FIGURE		PAGE
1.	Laboratory Equipment	5
2.	Sketch of Experimental Setup	6
3.	Beam Geometries for Perpendicular and Parallel Lasers	13
4.	Spectral Distributions of Lasers	15
5.	Field of View Geometry for Detectors	17
6.	Position of Optical Components as seen from Data Surface	23
7.	Alignment of Laser Beams and Receiver Fields of View	26
8.	Standard Surface	32
9.	Polarization Ratios	84
10.	Percentages of Depolarization	102
11.	Basic Backscattered Fractions	120
12.	Backscattered Fractions involving Unpolarized Radiation	143
13.	Leaves	169
14.	Woods	174
15.	Metals	177
16.	Petroleum Products	179
17.	Stone and Ice	181
18.	Sands	184
19.	Sketches for Deriving Scattering Equations	198

NOMENCLATURE

A_l	The surface area on a sphere between two given values of the polar angle.
A_c	Area intercepted by a cone.
A_t	Total scattering area of a surface.
A_n^s	The slope of the oscilloscope calibration curve for detector n and sensitivity setting s.
ΔA_n^s	The standard error in A_n^s.
${}_iA_n^s$	The slope of the i^{th} oscilloscope calibration curve set for detector n and sensitivity setting s.
${}_i^jA_n^s$	${}_iA_n^s$ calculated from the corresponding slope in calibration curve set j.
${}_i^cA_n^s$	${}_iA_n^s$ during the collection of the oscillosope calibration data.
B_d^ℓ	The fraction of incident radiation of polarization ℓ which is backscattered such that it would pass through an analyzer having transmission direction d.
$B_U^\perp$	$B_\perp^\perp + B_{/\!/}^\perp$.
$B_U^{/\!/}$	$B_{/\!/}^{/\!/} + B_\perp^{/\!/}$.
$B_\perp^U$	$\frac{1}{2}(B_\perp^\perp + B_\perp^{/\!/})$.
$B_{/\!/}^U$	$\frac{1}{2}(B_{/\!/}^{/\!/} + B_{/\!/}^\perp)$.
B_U^U	$(B_\perp^U + B_{/\!/}^U)$ or $(B_U^\perp + B_U^{/\!/})$.
c	Calibration data.
C	Correlation coefficient of regression line.

D_n^s	Drift in trace baseline for detector n and sensitivity setting s.
ΔD_n^s	Standard error in D_n^s.
d	Orientation of receiver polarizer.
d´	Orthogonal to d.
E_n	Amplification factor for detector n.
E_n^s	Amplification factor for detector n when used with oscilloscope sensitivity setting s.
${}_n\dot{F}_d^\ell$	${}_1S_d^\ell / {}_nS_d^\ell$.
G_n^ℓ	$\int_{x,y\ \text{plane}} \rho^\ell(x,y,R)K_n(x,y)\,dx\,dy$.
${}_n\eta_d^\ell$	$(M_n^\ell)^{-1}\,{}_nS_d^\ell$.
$\Delta_n\eta_d^\ell$	Experimental error in ${}_n\eta_d^\ell$.
I_1	Intensity scattered per unit area of surface into a cone.
I_2	$I_1/(R+1)^2$.
I_3	$I_2\cos\theta_i$.
I_4	$2\pi I_3 R^2 \sin\theta_i\, d\theta_i$.
I_5	The total intensity scattered from a surface into the annular cone defined by the polar angles θ_1 and θ_2.
I_j	The value of the j^{th} I_n in a particular set of I_n.
I_n	Fraction of P^ℓ allowed into the laser beam during collection of calibration curve data.

I_s	The intensity per unit solid angle scattered from a surface.
I_t	The total intensity scattered from a surface.
${}_nI_d^{\ell}$	The effective power originating from the laser with polarization ℓ which is backscattered into receiver n through an analyzer having transmission direction d.
K_n^o	Response of detector n.
${}^cK_n^o$	K_n^o during the collection of the oscilloscope calibration data.
${}_i^cK_n^o$	${}^cK_n^o$ for the i^{th} calibration curve set.
$K_n(x,y,R)$	Distribution function for field of view of receiver n.
k	Detector number.
L_n	Fraction of orthogonally polarized radiation leaked by polarizer on detector n.
ℓ	Direction of linear polarization of laser output.
ℓ'	Orthogonal to ℓ.
M_n^{ℓ}	$({}^cM_n^{\ell}\ {}^cK_n^o\ {}^cP^{\ell})/(K_n^oP^{\ell})$.
${}^cM_n^{\ell}$	$\left[T_n\ {}^c\sigma_d^{\ell}(\theta_i) + L_n\ {}^c\sigma_d^{\ell'}(\theta_i)\right]\Omega_nG_n^{\ell}$.
${}_i^cM_n^{\ell}$	${}^cM_n^{\ell}$ for calibration curve set i.
m	Detector number.
N_n^{ℓ}	$(M_n^{\ell})^{-1}({}_n^cS_{\ell}^{\ell} + {}_n^cS_{\ell}^{\ell'})$.
n	Detector number.
n_j	Order number of the j^{th} data set.

n_t	Total number of data sets for one collection period.
Ω_n	Solid angle subtended by receiver number n.
Ω_1	Solid angle subtended by area A_1.
P^ℓ	Total power output in polarization ℓ.
$_cP^\ell$	P^ℓ during the collection of the oscilloscope calibration data.
$_cP^\ell_i$	$_cP^\ell$ for the i^{th} calibration curve set.
PD^ℓ	Percent depolarization, laser polarization ℓ .
PD^ℓ_{kmn}	PD^ℓ measured using detectors k, m and n.
$Q(X_1, X_2, \ldots, X_n)$	General function.
ΔQ	Standard error in Q.
R	Distance to surface.
R^ℓ	Polarization ratio, laser polarization ℓ.
ΔR^ℓ	Experimental error in R^ℓ.
R^ℓ_{mn}	R^ℓ measured using detectors m and n.
ΔR^ℓ_{mn}	Experimental error in R^ℓ_{mn}.
$\rho^\ell(x,y,R)$	Laser beam distribution function.
$_nS^\ell_d$	$\Omega_n \sigma^\ell_d(\theta_i) G^\ell_n$.
$_nS^\ell_d$	$_nS^\ell_d$ measured from the standard surface.
s	An oscilloscope sensitivity setting.
$\Sigma^\ell(x,y,\theta_i,\theta_s,\psi_s)$	The fraction of power incident at x,y,θ_i with polarization ℓ scattered in the direction of θ_s, ψ_s.

$\sigma_d^{\ell}(\theta_i)$	Fraction of power incident with polarization ℓ and angle θ_i which is scattered in polarization d.
${}^{c}\sigma_d^{\ell}(\theta_i)$	$\sigma_d^{\ell}(\theta_i)$ measured from the standard surface.
T_n	Transmission of the polarizer on detector n.
t	An oscilloscope sensitivity setting.
θ_1	A polar angle in spherical co-ordinates.
θ_2	A polar angle in spherical co-ordinates.
θ_i	Angle of incidence.
θ_c	Angle of receiver field of view axis with respect to surface normal.
θ_s	Angle of scattering with respect to surface normal.
u	No directional preference (unpolarized).
V	The oscilloscope signal given by the calibration curve when $I_n = I_j$.
V_j	The oscilloscope signal obtained when $I_n = I_j$ where I_j is from the same set as V_j.
${}_nV_d^{\ell}$	Oscilloscope signal, detector n, laser polarization ℓ, backscattered component polarization d.
${}_n^{s}V_d^{\ell}$	${}_nV_d^{\ell}$ using oscilloscope sensitivity setting s.
${}_n^{c}V_d^{\ell}$	${}_nV_d^{\ell}$ from the standard.
${}_nW_d^{\ell}$	Total response of receiver n, laser polarization ℓ, backscattered component polarization d.
X_n	General measurement.
ΔX_n	Experimental error in X_n.
x	Abscissa of point on surface.

y	Ordinate of point on surface.
ψ_c	Angle of receiver field of view axis with respect to plane of incidence.
ψ_s	Angle of scattering with respect to the plane of incidence.
z	Axis of laser beam.

CHAPTER I

INTRODUCTION

Electromagnetic radiation whose electric field oscillation pattern exhibits a directional preference is called polarized radiation (1).[1] Linearly polarized radiation is radiation whose electric field oscillation is confined to a given axis, and the polarization is given by defining the axis. Unpolarized radiation is radiation whose electric field oscillation pattern exhibits no directional preference, and has the property (2) that the intensity of the radiation measured in any direction perpendicular to the direction of propagation is the same. Unpolarized radiation can be considered to be made up of two linearly polarized components having electric field oscillations orthogonal to each other and having entirely random phases with respect to one another. The intensity of the radiation is the time averaged energy per unit cross section of the radiation and is given by the average value of the Poynting vector (3) which in free space is approximately 2.05 watts per meter squared times the square of the amplitude of the electric field oscillation. For radiation which is a mixture of polarized and unpolarized radiation (partially polarized radiation), if the electric field oscillation is split

---

[1]Numbers in parentheses refer to similarly numbered references in the bibliography.

vectorally into two orthogonal components such that one has the same direction as the polarized radiation, the intensity of the component in the direction of the polarized vibration will be greater than that of the orthogonal component and will be equal to the intensity of the polarized electric field oscillation plus the intensity of the orthogonal component. The ratio of the lesser intensity to the greater intensity is the polarization ratio. The fraction of the intensity of the total radiation which is due to the polarized radiation is given by the difference of the maximum intensity and the minimum intensity divided by the sum. The fraction of the total intensity due to the unpolarized radiation is then one minus the fraction due to the polarized radiation or twice the minimum intensity divided by the sum. The reflectivity of a surface is the fraction of the total incident intensity which is scattered by the surface. Backscattered radiation is radiation whose direction of propagation after being scattered from a surface is opposite to its direction of propagation before being scattered.

The backscattered radiation due to incident linearly polarized radiation consists of a linearly polarized component and an unpolarized component (4). The linearly polarized component of the backscattered radiation will have the same orientation for the electric field oscillation as the incident linearly polarized component.

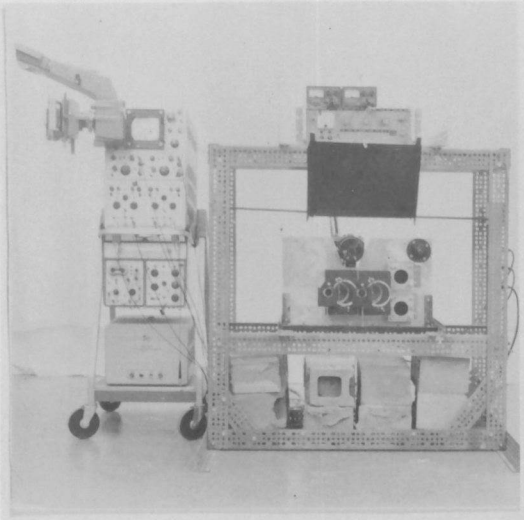
The primary objective of this study was to determine experimentally the polarization ratios and reflective characteristics occurring in the backscatter from several commonly occurring surfaces for radiation of 0.904 micrometers wavelength. These are presented, as are the respective fractions or percentages of depolarization of incident polarized radiation. For most cases, whenever possible, the variations of these quantities with change in angle of incidence are shown. The reflective characteristics are compared to a standard reflective surface having a known reflectivity. The surfaces used include leaves, barks, woods, petroleum products, rock-like materials, sand, ice, paper products, cloth products, and a movie screen. Several of these surfaces were subsequently painted, and the polarization ratios, percentages of depolarization, and reflective characteristics were reevaluated. Previous work in this area using a He-Ne laser at 0.6328 micrometers wavelength has been done by Egan, Grusaukas, and Hallock (5), and by Renau, Cheo, and Cooper (4).

CHAPTER II

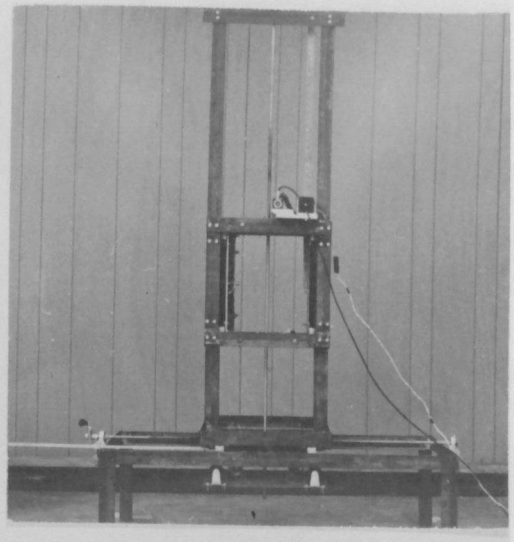
EXPERIMENTAL APPARATUS

I. GENERAL DESCRIPTION

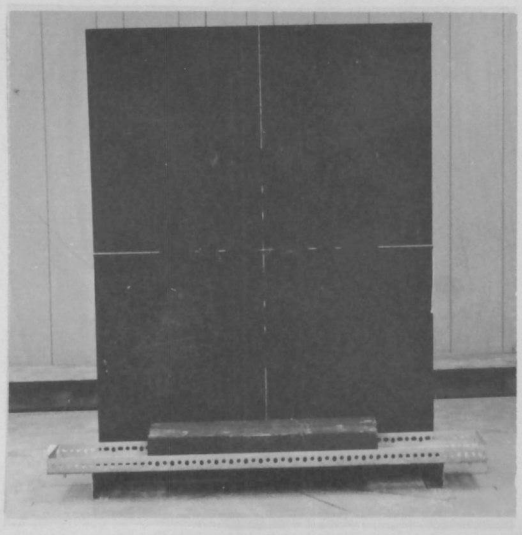
The equipment used for obtaining the data consisted of two radiation sources which provided radiation at about 0.904 micrometers (9040 angstroms); two detectors (mounted in receivers); an oscilloscope for recording data; a sample holder for holding surfaces which could be mounted vertically; a mirror and sample holder for holding surfaces horizontally; a camera for visually recording the surfaces; an alignment sight; and Polaroid Type HD polarizing sheets mounted in front of each of the sources and receivers. These, along with other equipment which will be discussed later, are shown in Figure 1. The sources, receivers, camera, and alignment sight were mounted on a metal plate within sixteen inches of each other and facing the surface from which data were to be collected. The optical components were aligned such that the locus of the centers of the beams or fields of view made lines which were approximately parallel to the floor and which converged to a common point twenty-five feet from the plate. A sketch of this setup is shown in Figure 2. The source beams had a beam spread of about 6 milliradians, and the fields of view of the receivers



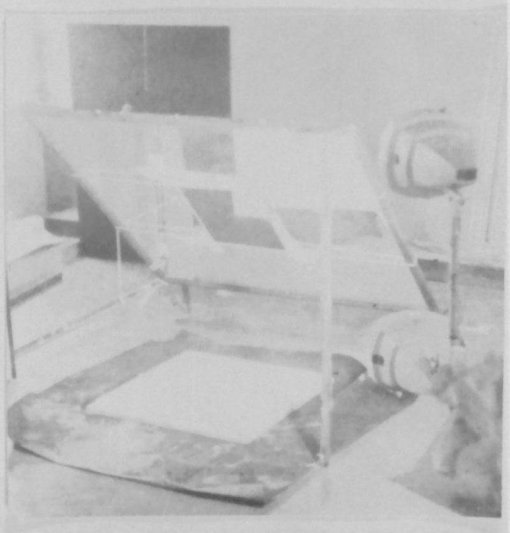
(a)



(b)



(c)



(d)

Figure 1. Laboratory equipment. (a) Optical and signal processing components; (b) Alignment equipment; (c) Data mounting board; (d) Mirror arrangement.

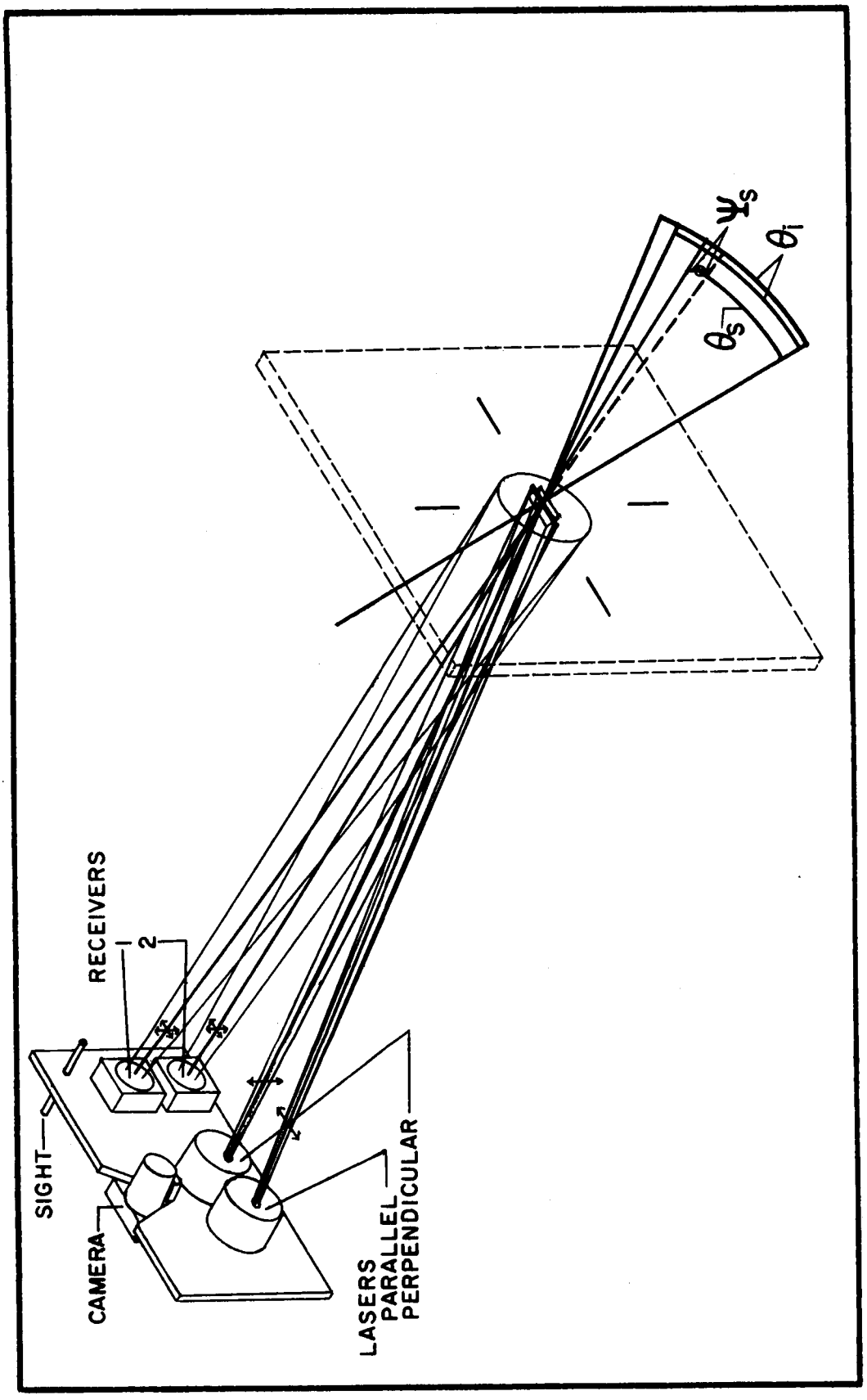


Figure 2. Sketch of experimental setup.

had a beam spread of about 32 milliradians. The sources were pulsed at approximately one thousand pulses per second. Each pulse had a rise time of about one nanosecond and a pulse width of about twelve nanoseconds. The receivers had a collecting area of one square inch, a responsivity of 2×10^5 volts per watt, and a demodulation band width of 50 megahertz. The oscilloscope main amplifier also had a band width of 50 megahertz. The polarizing sheets passed approximately 80% of the radiation with oscillation parallel to the transmission direction of the material and between 1% to 4% of the radiation with oscillation perpendicular to the transmission direction of the material. Each sheet was mounted such that it could be rotated about the normal to its surface. For convenience, the polarizers in front of the sources were oriented so that one source always emitted radiation with the electric vibration perpendicular to the plane of incidence, and the other emitted radiation with the electric vibration parallel to the plane of incidence. These polarizers were not usually rotated during a data taking period. An extra source, an extra detector, and an x,y traverse were available for aligning and testing the other equipment.

Rigid surfaces from which data were taken were mounted at the focal point of the beams with the plane of the surface perpendicular to the floor. The surfaces

could be rotated about a vertical line lying on the surface such that the plane of incidence was parallel to the floor. For most of the rigid surfaces, data were taken at zero, thirty, and sixty degrees angle of incidence. For nonrigid surfaces, the surface was held in a container on the floor, and a mirror was used to direct the beams of the sources and the fields of view of the other optical components onto the surface such that the angle of incidence was either zero or two to five degrees when specular reflections needed to be eliminated.

The surfaces from which data were taken included plant leaves, tree barks, woods, metals, petroleum products, cotton materials, paper products, rock-like materials, painted surfaces, soils, and ice. The reflective properties of these surfaces were compared with a standard reflective surface having known reflective characteristics.

The sections which follow provide a detailed description of the apparatus.

II. SOURCES

Three solid state Gallium Arsenide single diode pulsed injection lasers (two with associated optics) were available. The two lasers which were already equipped with optics were used to illuminate the surfaces, and the remaining bare-diode laser was used for equipment checkout

and alignment. Several important characteristics of Gallium Arsenide diode lasers are the wavelength at which intensity peaks; the shift in the wavelength of the peak intensity as a function of diode case temperature; spectral distribution of the power output; the change in power output as a function of case temperature; diode efficiencies; physical dimensions of the lasing area; beam width of the beam from a bare diode; and the possible polarization of the emitted radiation.

The following are typical output characteristics (6) for a diode laser operating with the case at room temperature (27^{o} Centigrade). (Specific characteristics for the sources used will be given later.) The peak intensity has a wavelength of 0.904 micrometers and increases with increasing temperature at the rate of 2.2 angstroms per degree Kelvin. The spectral distribution between half power points is between forty and four hundred angstroms, depending on the design of the lasing junction. The power output for pulsed operation is generally five to ten watts, but can, with good heat sinks, be as high as 80 watts for some single diode devices. The output intensity is about 28% higher with a case temperature of zero degrees Centigrade and about 32% lower with a case temperature of seventy degrees Centigrade, as compared to the intensity output with a case temperature of twenty-seven degrees Centigrade.

The quantum efficiency, defined as the ratio of the photon current out to the electrical current in, varies with peak pulse input current and has a maximum of about 7%. The incremental quantum efficiency, defined as the slope of the linear portion of the photon current out to electrical current in curve, is typically 10%. The power efficiency, defined as the ratio of the optical output power to electrical input power, is typically 1.6%. All efficiencies decrease with increasing temperature. The emitting region is from three to fifty-five mills long, depending on the output power designed for, and eight hundredths of a mill wide. The beam spread to half power points in a plane parallel to the plane of the junction is about fifteen degrees, and the beam spread in a plane perpendicular to the plane of the junction is about eighteen degrees. The distribution of intensity is not usually symmetrical about the center of beam. Since the intensity decreases rapidly outside the half power beam spread, almost all of the power is contained within a twenty degree beam spread. The electric field oscillations in the output radiation can generally be divided into two orthogonal components, within the cross section of the beam of radiation, such that one component is significantly larger than the other component. The rise time and duration of the laser pulse generally depend upon the pulsing circuit as long as the duty factor (typically

one-tenth of one percent) is not exceeded. The duty factor is the percentage of the time of each power output cycle during which the diode is operating and depends on material, manufacturing processes, and designs. The diode acts as an 0.11 ohm resistor (7) in the pulsing circuit and typically draws over thirty amperes peak current.

The two sources used to illuminate the surface used an RCA SG2007 GaAs diode laser followed by a meniscus lens that collected all of the radiation within $\pm 15^{o}$ of the optical axis followed by a nonsymmetrical bioconvex lens. The combination collimated the collected radiation into a beam with an approximately 10 milliradian beam spread. The electronics were such that, at room temperature, the typical output was ten watts and was contained in a pulse approximately 12 nanoseconds wide with a rise time of approximately one nanosecond and with a repetition rate of one thousand pulses per second. The lasers were equipped with polarizers following the lens system. Each polarizer was mounted such that it could be rotated about an axis parallel to the transmitted beam. The two lasers and their polarizers were arranged so that one laser always transmitted radiation with the electric field oscillation perpendicular to the plane of incidence and will be referred to as the perpendicular laser. (See Figure 2, page 6.) The other laser polarizer was arranged

so as to transmit radiation with the electric field oscillation parallel to the plane of incidence and will be known as the parallel laser. By measuring the laser outputs while rotating the polarizers, both lasers were found to have polarized outputs with the maximum electric field oscillation being about twice the minimum electric field oscillation. The orientation of each laser and its polarizer was such as to take advantage of the particular polarization of the radiation from the diode in order to obtain the maximum possible intensity for each polarized beam. In the final arrangement, the perpendicular laser always produced a slightly higher output power than the parallel laser produced. The relative intensity versus angular displacement in both the horizontal and vertical directions is shown for the beam of the perpendicular laser and for the beam of the parallel laser in Figure 3. The third laser produced a ten watt peak power pulse using a typical ten watt RCA diode. (Information as to the exact type was not obtainable.) The laser had a rise time of about sixty nanoseconds with a pulse duration of one hundred fifty nanoseconds, and with a repetition rate of thirty-three pulses per second. No lenses were used with this laser so that the output beam was relatively wide and its alignment was not a critical factor. The output spectrums were measured for both the perpendicular and parallel

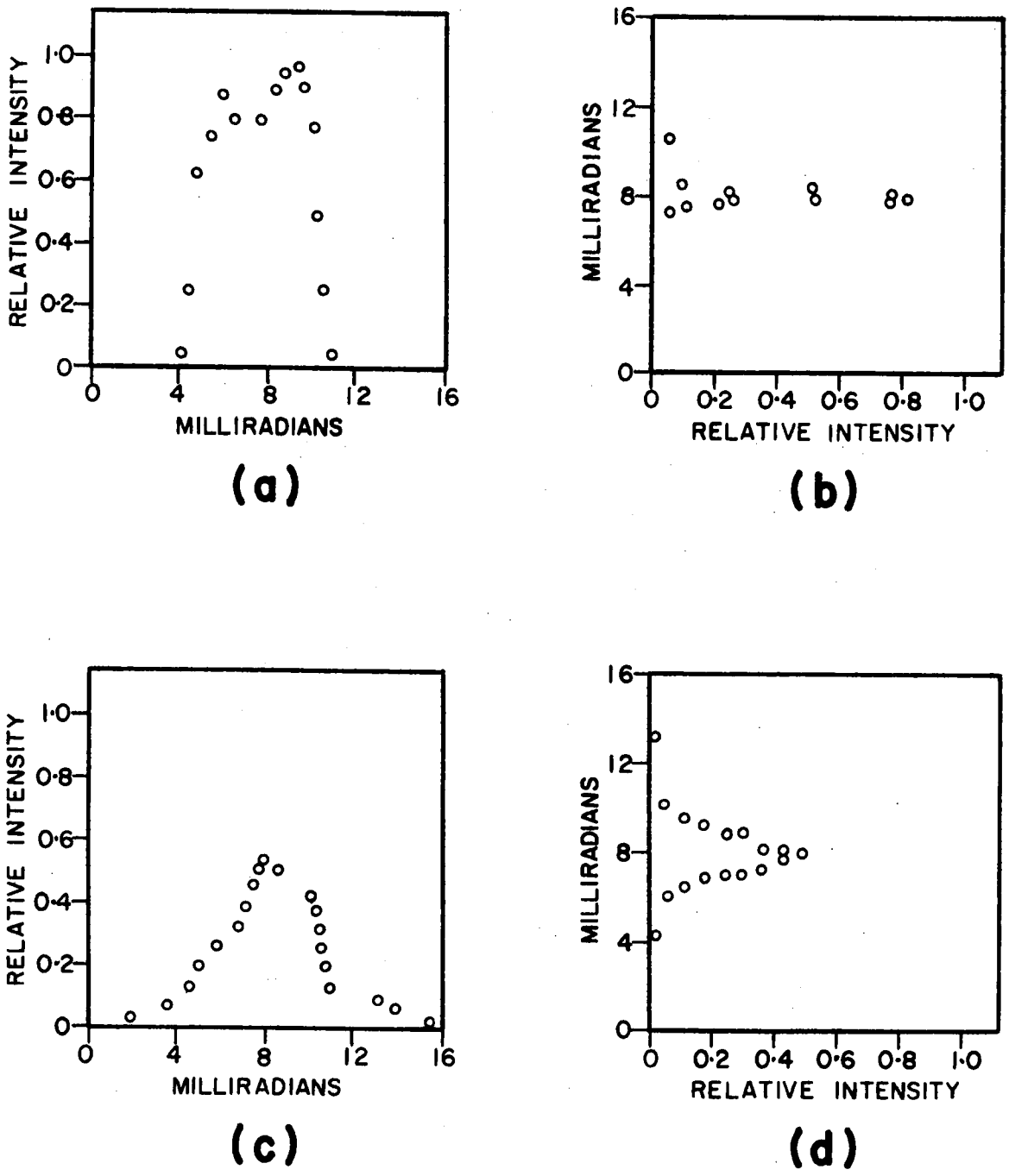


Figure 3. Beam geometries for perpendicular and parallel lasers. (a) Perpendicular laser, horizontal axis; (b) Perpendicular laser, vertical axis; (c) Parallel laser, horizontal axis; (d) Parallel laser, vertical axis.

lasers as well as for the bare-diode laser and are shown in Figure 4.

III. DETECTORS

Three detectors, each with associated electronics, and with peak response near 0.9 micrometers were available. The two detectors which were used in the experiment to detect the backscattered radiation were Texas Instruments TIXL-79 low-profile silicon avalanche photodetector modules with pre-amplifiers and with a photo avalanche gain of one hundred twenty-five. The devices have typical responsivities (6) of 2×10^{5} volts per watt; a noise equivalent power of 2×10^{-13} watts per $(\text{hertz})^{\frac{1}{2}}$ at 0.9 micrometers; and a demodulation band width of 50 megahertz. Each unit contains a silicon avalanche photodiode with a circular active area 0.030 inches in diameter and a temperature sensing voltage reference diode. Since the detectors reach saturation when approximately 10^{-5} watts is incident on the photodiode, the collecting system was designed to collect and focus 10^{-6} watts on the detector from a 20% reflecting surface twenty-five feet away. The 10^{-6} watts is three orders of magnitude above the noise equivalent power of 10^{-9} watts which would result from using the full fifty megahertz band width. Using the approximate calculations from Equation 95 in Appendix I, and a conservative estimate of five watts for the power

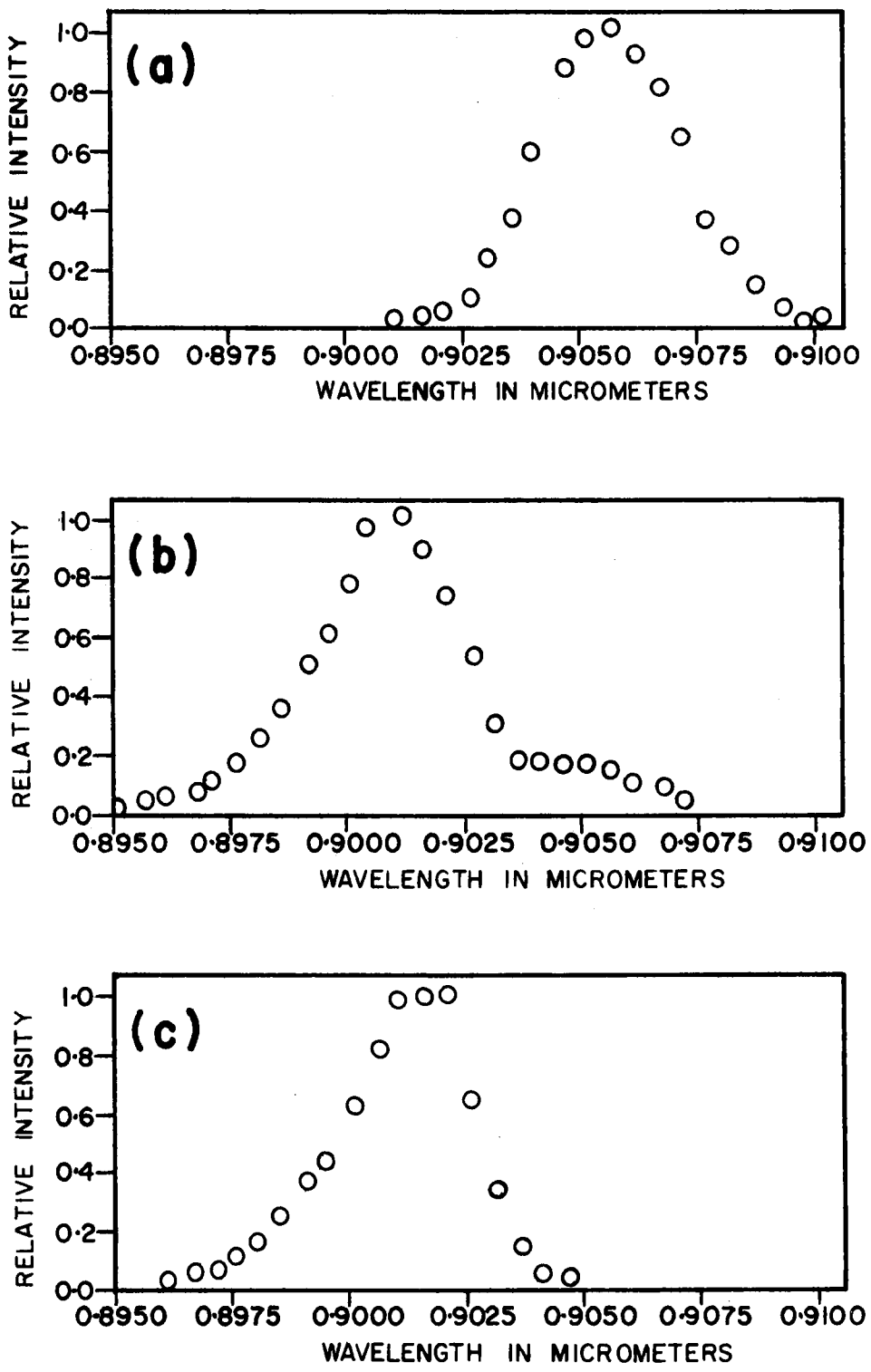


Figure 4. Spectral distributions of lasers. (a) Perpendicular laser; (b) Parallel laser; (c) Alignment laser.

from the laser, the receiver should have a collecting area greater than 0.6 square inches to collect 10^{-6} watts of the radiation scattered from a 20% reflective surface. The field of view of each receiver was designed to have a spread of thirty milliradians wide in order to insure a good overlap with each laser beam. A single aspheric lens with a diameter of 34 millimeters and a focal length of 21.5 millimeters was used as the collector for each receiver. The relative sensitivity versus angular displacement in the field of view is shown in Figure 5 for both the horizontal and vertical directions. A polarizer was mounted in front of the lens of each receiver such that it could be rotated about an axis parallel to the field of view of the receiver. Using this lens, with the polarizer rotated to pass the perpendicular electric field oscillations, the return from the stronger perpendicular laser at normal incidence to a Lambertian surface, which was almost 100% reflective, was just below the saturation level of each detector. The third detector was an EG&G Lite Mike and was used for alignment and checkout. The unit contained a silicon photodiode with an active area 0.1 inch in diameter. The diode rise time was five nanoseconds, and with the output fed into a one megaohm input impedance scope, the detector output was 78.7 millivolts per watt per square centimeter. While the detector was being used to map the laser beams,

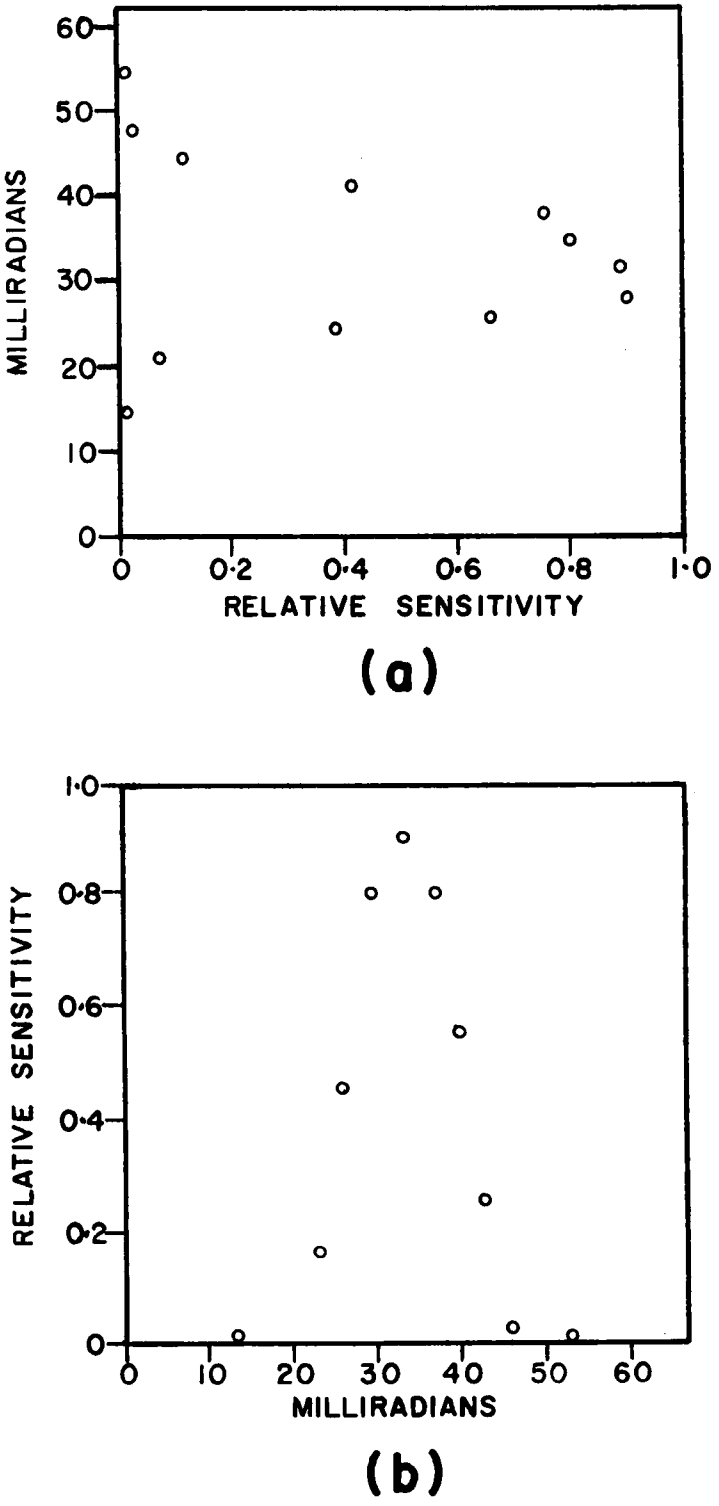


Figure 5. Field of view geometry for detectors. (a) Vertical axis; (b) Horizontal axis.

sufficient intensity was incident upon the detector to allow operation without the collecting lens. The removal of the lens eliminated the need for careful alignment of the detector beam, since the detector then had a 70^{o} field of view.

IV. SIGNAL PROCESSING

The oscilloscope which was used was a Tektronix Type 555 dual beam oscilloscope with a dual time base and two dual trace Type 1A1 plug-in units. The rise time of the 50 megahertz band width main amplifier coupled with the plug-in units varies from 11 nanoseconds for the 5 millivolts per division setting to 14.5 nanoseconds for the 20 volts per division setting. The synchronization pulses (pulses immediately preceeding the laser output) from the lasers were connected to separate time bases allowing separate adjustments of trigger level and sweep rate, and allowing both synchronization pulses to be readily available. The outputs from the two detectors were connected to separate oscilloscope beams giving brighter traces with less wash than would be possible with both on the same oscilloscope beam and allowing for separate adjustment of both trace intensity and trace position. The oscilloscope traces from both detectors were generally recorded simultaneously by photographing the oscilloscope screen with a one-fiftieth second

exposure, thus, averaging over approximately twenty detector signals for each data point. The data collecting and recording process was accelerated by shifting the traces and recording four or more sets of data on the same photograph.

The camera used was a Tektronix Type C-31 with a Polaroid camera back. Polaroid Polascope Type 410 Land roll film was used since it has a high recording speed, and the sweep rate of the trace was twenty nanoseconds per division. A slower film was tried, but with poor results. The slower film displayed the trace very faintly for exposure times up to one-fiftieth of a second and was completely washed for longer exposure times.

V. POLARIZERS

The polarizers were made of Polaroid Type HD sheets, an experimental product which has improved features at 0.9 micrometers wavelength, as opposed to the Type AP sheets which they replaced. When new, the sheets passed on the order of 80% of the radiation with electric field oscillation parallel to the transmission direction of the material and approximately 1% of the perpendicular oscillation. The quality of the sheets deteriorates with exposure to ultraviolet radiation. The polarizers used were taken from two different shipments, which were received several months apart, and even though covered

when not used, deteriorated to 84% parallel transmission and 4.8% perpendicular transmission for the older sheets placed on the lasers and receiver one, and to 78% parallel transmission and 3.1% perpendicular transmission for the newer material placed on the other receiver. The sheets were mounted in metal rings which were held in metal sleeves by retaining screws. The polarizers could be rotated about an axis perpendicular to their surfaces. The transmission directions of several polarizing sheets were determined by measuring the transmitted radiation while rotating them in a beam of 0.9 micrometers radiation which was linearly polarized by reflecting it from glass at Brewster's angle (8). The transmission directions of additional sheets which were later used were determined in a similar manner using linearly polarized radiation obtained by passing radiation through sheets having a known transmission direction. Marks were placed on the rings around each laser polarizer to show the direction parallel to the transmission direction and the direction orthogonal to the transmission direction. The edges of the sleeves on the lasers were marked to indicate the direction perpendicular to the plane of incidence and the direction parallel to the plane of incidence using the floor as a reference. The marks were within 5^{o} of the actual directions they indicated. (The leakage due to the misalignment would be on the order of one-half the

square of the sine of the angle involved, or 0.4%.) The polarizers on the detectors were then aligned by rotating the polarizers in their sleeves while detecting back-scattered radiation from a diffuse surface and observing the maximum and minumum returns. Marks were placed on the sleeves to indicate the directions of the maxima and minima. The detector polarizers could then be rotated to the desired position to within 3^{o}. (Less than 0.15% leakage could be due to misalignment.) The directions could have been determined with less chance of error by detecting radiation scattered from a diffuse surface and choosing two orthogonal directions such that as the polarizer was rotated, the ratio of the minimum radiation detected in one direction to the maximum radiation detected in the orthogonal direction was minimized.

VI. COMPONENT MOUNTING AND ALIGNMENT

The lasers and receivers were rigidly mounted on a 3/8 inch aluminum plate along with a telephoto camera and an alignment sight. The mounted components along with the oscilloscope, the power supplies, and the mechanical shutter are shown in Figure 1a, page 5. Also, a sketch of the component mounting and alignment is shown in Figure 2, page 6. The two smaller dark circles on a horizontal line are the lasers. The parallel laser

is on the left, and the perpendicular laser is on the right. A holder for neutral density filters stands in front of each laser. The two larger apertures beside each laser are receivers which were not used. The receivers which were used are the two dark circular apertures in a vertical line on the right side of the plate. The alignment sight is in the upper right hand corner, and the telephoto camera is centered at the top of the plate. The mechanical shutter which could be lowered in front of the lasers and detectors, completely blocking their beams or fields of view, is above the mounting plate. All components were placed as symmetrically and as close as mechanical considerations would allow. The positions of the components as seen from the point twenty-five feet away at which data were taken are shown in Figure 6. The lasers are 18.1 milliradians apart. The receivers are 16.7 milliradians apart. The perpendicular laser and each receiver are 22.7 milliradians apart. The parallel laser and each receiver are 40 milliradians apart. For a Lambertian reflector, the return varies as the cosine of the angle from the normal. Therefore, for surfaces which approximate Lambertian reflectors, the correction to the return due to the angular displacements of the optical components is less than 0.08%. For some very specularly reflecting surfaces, such as very shiny metal or water, the fact that the lasers and

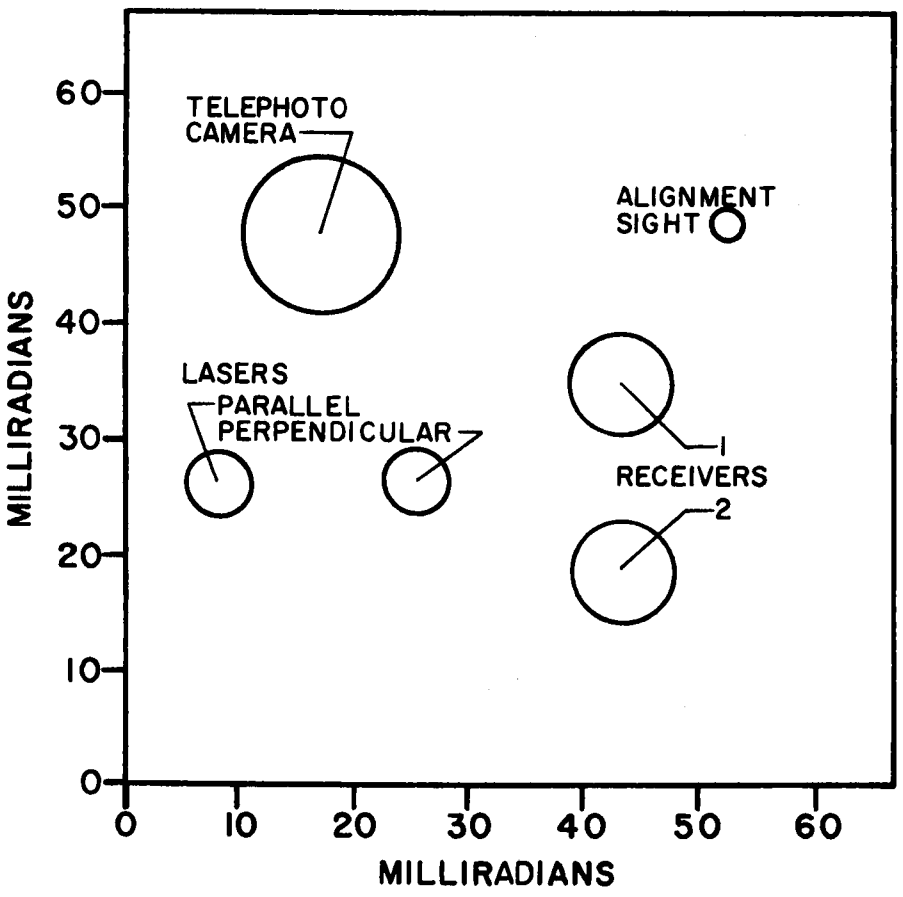


Figure 6. Position of optical components as seen from data surface.

receivers were at different angles from the data surface normal was very noticeable.

The beams and fields of view of the components were aligned at 25 feet by means of the spare laser and spare detector mounted on an x,y traverse shown in Figure 1b, page 5. The run of the traverse was 90 centimeters (118 milliradians, or about 7^{o} as seen by the optical components) in both the vertical and horizontal directions. This proved to be about right for initially finding the positions of the beams after they had been aligned only by assuming each beam to be perpendicular to the face of its own system housing. The alignment laser and detector were mounted on the traverse at the same vertical level (within 1 millimeter or 0.13 milliradians as seen by the optical components) and separated on the horizontal axis by a distance of 10 centimeters. This allowed rapid comparison between the x-y coordinates of the two alignment devices. The measurements made to determine the alignment of the laser beams and the receiver fields of view were repeated several times. The values obtained for the lasers varied by 0.5 millimeters (0.7 milliradians). The values obtained for the receivers varied by 3 millimeters (4 milliradians). The larger error in the receiver alignment measurements as compared to the laser alignment measurements was due to the differences in the beam and field of view variations with angular displacement. The

beams, as well as the camera and the alignment sight, were oriented by placing varying thicknesses of shim stock between the proper edges of the components and the aluminum plate to which they were bolted. The alignment of the laser beams and receiver fields of view is shown in Figure 7 by the contours through the half power points of the beam or field of view of each optical component.

The telephoto camera was aligned at 25 feet by placing the alignment detector in the center of the laser beams and shimming the lens bracket until the detector appeared to be near the center of the camera sight. Photographs of the alignment detector were then taken. The alignment sight, which consisted of a tube 3/8 inch in diameter and eight inches long with a 0.01 inch pin hole in one end and a set of crosshairs at the other, was aligned in similar fashion, such that the alignment detector window appeared at the intersection of the crosshairs. The alignment of the sight was to within 2 millimeters (0.3 milliradians). At the beginning of each roll of film used in the telephoto camera, a picture was taken of two white strings situated in the same plane as surfaces from which data were taken and coincident with the crosshairs of the alignment sight. This was intended to give the alignment of optical beams with respect to each set of telephoto pictures. It was later found that due to variations in framing the

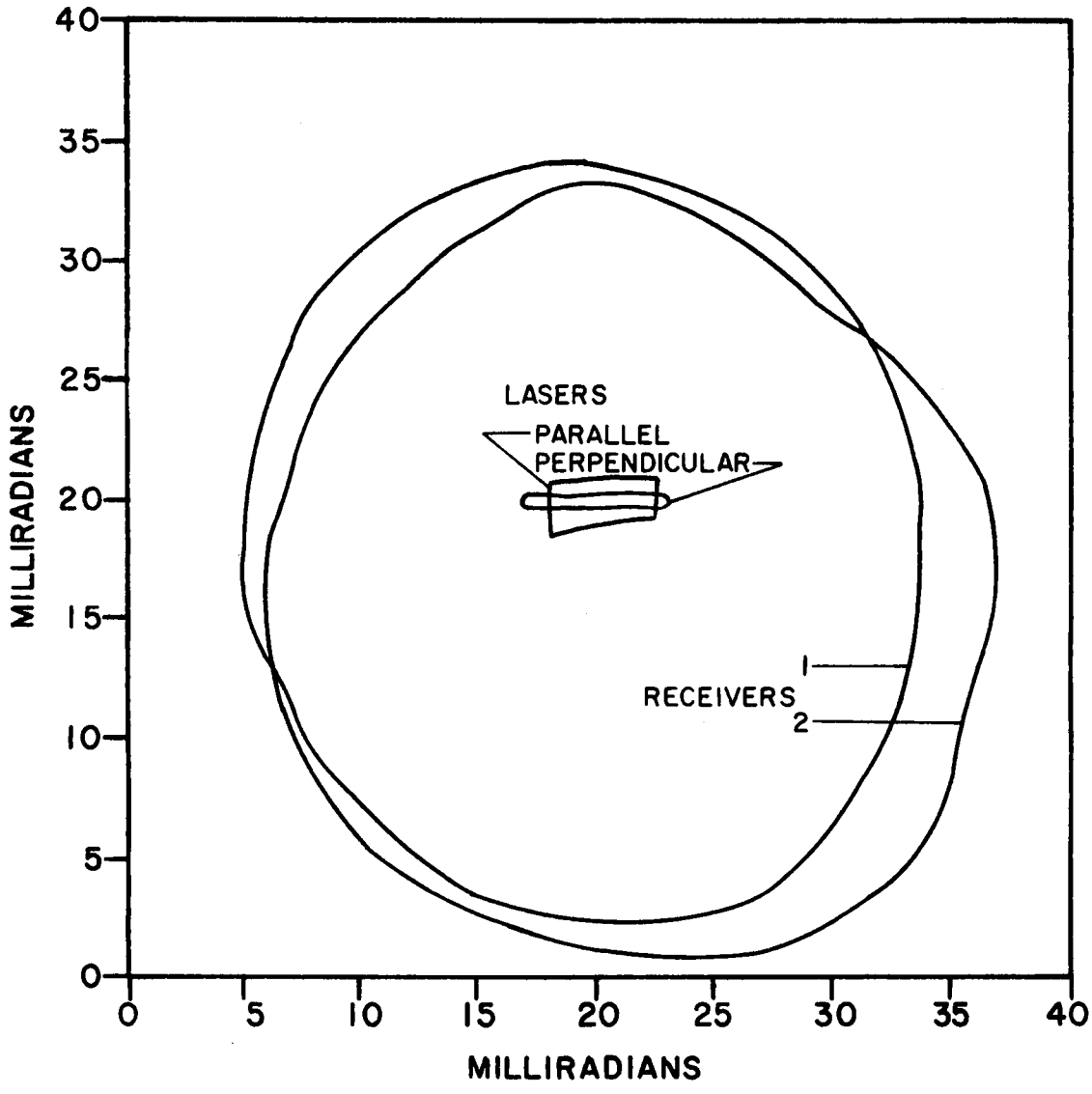


Figure 7. Alignment of laser beams and receiver fields of view.

35 millimeter color slides, the alignment varied by about 15 milliradians. An attempt was then made to include the white strings in the edges of each picture.

The alignment of the laser beams, the detector fields of view, and the alignment sight were checked at various times during the period over which data were being collected.

VII. SAMPLE HOLDERS

A sample holder, shown in Figure 1c, page 5, was made by fastening a three foot by four foot by three-quarter inch piece of plyboard painted ultraflat black to a metal frame. A set of axes were drawn at the base of the frame, and marks were placed on the base of the frame so that the sample holder could be rotated about its base such that the point of intersection of the axes of the beams and fields of view with the mounted surface remained unchanged while selecting 0^{o}, 30^{o}, or 60^{o} as the angle of incidence. The errors in the angles were checked by observing the backscattered intensity from a specularly reflecting surface and noting the magnitude of the adjustments required to maximize the intensity incident on the receivers. The error in the angle of incidence was less than 1^{o} (17 milliradians) for diffuse surfaces and was minimized for specularly reflecting surfaces by maximizing the intensity incident on the

receivers. Dry, rigid surfaces were fastened to the plyboard by nails, bolts or strings, or were placed on a stand attached to the frame.

For wet surfaces and those such as sand, water, and gravel which could not be placed in an upright position, a metal container with the inside painted ultraflat black was placed on the floor, and the surfaces were placed in the container. The beams were directed perpendicular to the bottom of the container by a front surface gold mirror mounted on a stand. A rear surface glass mirror was initially used, but was discarded due to the decrease occurring in the backscattered intensities and to the fact that the fraction of radiation reflected by the glass mirror was different for each of the two orthogonal components in the backscattered radiation. Due to absorption in the glass after two reflections by the glass mirror, the backscattered intensity from a surface was less than 20% of the backscattered intensity from the same surface placed on the vertical sample holder. A front surface aluminum mirror with a reflectivity of approximately 80% was tried and discarded since, possibly due to a special coating or surface imperfections, it depolarized about 6% of the polarized radiation on each reflection. The aluminum mirror also rotated the electric fields although this effect was small in the mirror orientation used, and the effect was essentially cancelled with the second

reflection. The glass mirror with the aluminum mirror attached is shown in Figure 1d, page 5. The gold mirror was situated similarly to the aluminum mirror. The proper orientation of the mirror was achieved by placing a specularly reflecting surface parallel to the bottom surface of the surface holder and adjusting the mirror to maximize the backscattered intensity incident on the receivers. The combination was positioned so that correct alignment of the beams at the surface from which data were being taken was maintained, and the distance of the surfaces from the optical components remained the same as for surfaces mounted vertically.

The surface holders which were painted ultraflat black did not act as perfect beam dumps, but rather had reflectivities of up to 9%, which decreased with aging to about 4%. This problem was of little concern, however, since the laser beams were very concentrated. All of the detectable energy was found to be within an area of 8 by 13 centimeters, since a mirror of this size deflected all but an amount of the return which was less than the system noise. By measuring the backscattered intensity from a large uniform surface with a high reflectivity and comparing with the backscattered intensity from the same surface, but with a portion removed at the position of the center of the beams, it was found that 87% of the beam was contained in a 2.5 by 7 centimeter area. With

samples larger than this area, the backscattered intensity due to the sample holders would be less than 1.2%. Since most surfaces were several times larger than the 2.5 by 7 centimeter area and were centered in the beams as verified by the alignment sight, the backscattered intensity from the sample holders was insignificant. For other surfaces, mirrors were used to deflect overflow radiation outside of the receiver fields of view.

VIII. POWER SUPPLIES

The two lasers used for collecting data each required 100 milliamps at 24 to 32 volts for proper operation. No change in laser output power could be detected as the voltage was varied from 24 to 32 volts. The detectors used for taking data required two power supplies, one providing 20 milliamps at 8.5 ± 0.5 volts and one providing 1.5 milliamps at 240 ± 15 volts. No difference in detector outputs resulting from a constant amount of power being incident on the photodiode could be observed when these voltages were varied between their respective limits. Two Hewlett Packard Model 6215A power supplies were used to supply the low voltages. A Power Designs Model HV-1547 power supply was used to supply the high voltage. The power supplies were set to the midrange voltages and were capable of supplying the proper currents while maintaining the low voltages to within 0.1 volt and high

voltage to within 1 volt. The power supply for the third laser was a portable battery pack which was capable of maintaining the laser at a constant output for the periods of time over which it was used. The alignment and checkout detector contained its own power supply and operated on line voltage.

IX. STANDARD REFLECTIVE SURFACE

The standard surface shown in Figure 8, and also in Figure 1b, page 5, was made by painting a two foot square of plyboard with Eastman White Reflectance Paint. The absolute reflectance of the paint (8), a mixture of barium sulfate and purified polyvinyl alcohol in the ratio 100:1, at 0.9 micrometers is 0.992. It was recommended by Eastman Kodak that the surface be primed with an inert plastic primer such as Krylon 1502 flat white spray enamel and then the reflectance paint be sprayed on with an aerosol powered sprayer such as the "Jet Pack" supplied by Sprayon Products Company. Eastman Kodak also recommended that the thickness of the paint be such that one pint uniformly covered four square feet of surface. This took six to eight coats using the "Jet Pack" sprayer. Spurting resulted unless the paint was thinned by approximately 10% (15% is the maximum allowed thinning) using a mixture of distilled water and an anhydrous ethyl alcohol (1:1v/v), and unless the aerosol

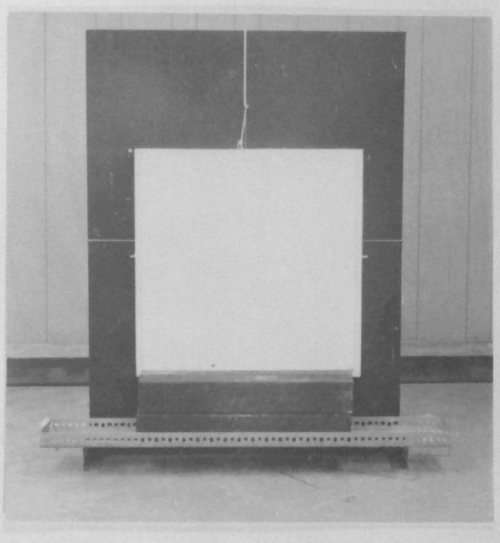


Figure 8. Standard surface.

can was heated when it began to chill. The paint should be sprayed onto the surface in such a manner that the surface appears wet and gleams. Each successive coat should be applied just after the paint has lost its gleam. The paint obtained the required state of dryness in approximately forty-five minutes when the painting was done in an unventilated room at room temperature. If the paint was allowed to dry very much beyond this point, the next coat would run unless it was an extremely light coat not capable of wetting the surface. When too much drying occurred, the best procedure seemed to be to moisten the surface with a light spray of the thinning mixture before applying the next coat. Grum and Luckey (9) prepared surfaces by pouring the paint onto a flat surface. When this was attempted, the paint sat in a glob similar to a malted milk shake until its base separated out even though the paint had been properly prepared before being poured. Spraying seems to be the better method of applying the paint if a sprayer of sufficient force and which is free of contaminates is available.

The standard was checked for nonhomogeneities by setting it on the sample holder and translating it perpendicular to an axis parallel to the optical beams while recording the signals from the backscattered intensity. Anisotropy was checked for by rotating the standard about

an axis parallel to the optical beams while recording the signals. The standard was uniform and isotropic to within 2%.

CHAPTER III

THEORETICAL EXPRESSIONS

The expressions for the backscattered intensities detected by the detectors are derived in this chapter in terms of the basic parameters involved in the experiment which is sketched in Figure 2, page 6. The expressions for the polarization ratios, percentages of depolarization, and backscattered fractions are written in terms of these basic parameters.

Linearly polarized radiation collimated into a beam with a beam spread of approximately 10 milliradians between half power points is incident onto a surface at an angle θ_i with respect to the normal. With the beam of radiation which is along the z-axis and whose electric field oscillation has the orientation ℓ with respect to the plane of incidence, the radiation power per unit area at a point x,y,z on a surface at a distance z=R from the radiation source is $P^{\ell}\rho^{\ell}(x,y,R)\cos\theta_i$. P^{ℓ} is the total power in the beam, and ρ^{ℓ} is the distribution of the intensity in the beam such that

$$1 = \int_{x,y \text{ plane}} \rho^{\ell}(x,y,R)\,dx\,dy. \qquad (1)$$

The magnitude of ρ^{ℓ} is significant only for values of x and y which are small compared to R.

With linear polarization incident on a surface element dA located at x,y,z=R, the fraction of the power that is scattered per steradian into a direction which makes an angle θ_s with respect to the normal to the surface and an angle ψ_s with respect to the plane of incidence and which has polarization d is $\Sigma_d^{\ell}(x,y,\theta_i,\theta_s,\psi_s)$. The solid angle subtended by the aperture of receiver n which contains detector n is Ω_n. The receiver aperture is covered by a polarization analyzer oriented to pass polarization d. When power having polarization d is incident on this polarization analyzer, the fraction of the power which passes the analyzer is T_n. The responsivity of the detector to radiation which has passed the analyzer after originating from or being scattered from the point x,y,z=R is independent of the polarization of the radiation and is $(K_n^o)K_n(x,y,R)$ where $K_n(x,y,R)$ is a distribution function such that

$$1 = \int_{x,y \text{ plane}} K_n(x,y,R)\,dx\,dy. \tag{2}$$

The total response of receiver n to the scattered radiation with polarization d from the surface is found by integrating the scattered intensity over the area of the receiver aperture, and is given by

$$ {}_{n}W_{d}^{\ell} = \int_{\Omega_n} \int_{\text{surface}} (K_n^{o}) K_n(x,y,R) T_n \, \Sigma_d^{\ell}(x,y,\theta_i,\theta_i,\psi_s) \, \rho^{\ell}(x,y,R) P^{\ell} \cos\theta_i \, dA \, d\Omega_n . \qquad (3) $$

The solid angle subtended by the receiver is sufficiently small that Σ_d^{ℓ} is essentially constant over the limits of integration in θ_s, ψ_s for scattering from diffuse surfaces or when observing the diffuse component of scattering from specular surfaces. Since $\rho^{\ell} K_n$ is significant over an area on the surface on the order of four square centimeters, and since this area subtends an angle of less than ten milliradians as seen from the receiver, Σ_d^{ℓ} is essentially constant in the integration over a homogeneous surface. Then $\Sigma_d^{\ell}(x,y,\theta_i,\theta_s,\psi_s)$ can be replaced by $\Sigma_d^{\ell}(\theta_i,\theta_c,\psi_c)$ where θ_c and ψ_c are the angles between the direction from the center of the incident beam on the surface to the center of the detector and the surface normal and from this same direction to the plane of incidence, respectively. For an inhomogeneous surface, $\Sigma_d^{\ell}(\theta_i,\theta_c,\psi_c)$ is taken to be the average value over the surface where $\rho^{\ell} K_n$ is significant.

For a specularly reflecting surface, $\Sigma_d^{\ell}(\theta_i,\theta_c,\psi_c)$ is, in addition, an average of the scattering over the solid angle subtended by the receiver. Then the expression for the response of detector n becomes

$$ {}_nW_d^{\ell} = K_n^o T_n \Omega_n \Sigma_d^{\ell}(\theta_i, \theta_c, \psi_c) $$

$$ P^{\ell} \int_{\text{surface}} \rho^{\ell}(x,y,R) K_n(x,y,R) \cos\theta_i \, dA. \qquad (4) $$

The receivers, lasers and surfaces from which the data were collected were positioned such that ψ_c was approximately zero. For the diffusely reflecting component of the reflection from a surface, the angle between the incident beam and the receiver field of view was much smaller than any directional characteristics of the scattered radiation, and Σ_d^{ℓ} had essentially the same value as it would have had if the detector had been mounted in the same space as the laser. When the specular component was being observed (the specular component is observed only for θ_i in the neighborhood of zero), the peak of the specularly scattered radiation was made to be incident on the receiver such that $\theta_i \simeq \theta_c$, and both θ_i and θ_c were essentially zero. The angle ψ_c was approximately divided between the receivers and was, in any case, less than one-half of a degree. Then under these conditions $\Sigma_d^{\ell}(\theta_i, \theta_i, \psi_c)$ is essentially $\sigma_d^{\ell}(\theta_i)$ where $\sigma_d^{\ell}(\theta_i)$ is the fraction of the incident radiation which is backscattered when the radiation incident is incident at angle θ_i. Since R is essentially a constant over the x,y plane as far as ρ^{ℓ} and K_n are concerned, and $\cos\theta_i \, dA = dx\,dy$ where dA is a surface element and dxdy is the projected area element in the cross section

of the beam, the total response of the detector is given by

$$ {}_nW_d^{\ell} = K_n^{o} T_n \Omega_n \sigma_d^{\ell}(\theta_i) G_n^{\ell} P^{\ell} = K_n^{o} T_n \, {}_nS_d^{\ell} \, P^{\ell} \tag{5} $$

where G_n^{ℓ} is the beam geometry factor given by

$$ G_n^{\ell} = \int_{x,y \text{ plane}} \rho^{\ell}(x,y,R) K_n(x,y,R) \, dx \, dy, \tag{6} $$

and ${}_nS_d^{\ell}$ is the effective fraction of the total power in the laser beam which is incident on the receiver aperture after being scattered by the surface and is given by

$$ {}_nS_d^{\ell} = \Omega_n \sigma_d^{\ell}(\theta_i) G_n^{\ell}. \tag{7} $$

The oscilloscope signal ${}_nV_d^{\ell}$ originating from detector n will be the total response of the detector multiplied by an amplification factor E_n . The signal ${}_nV_d^{\ell}$ is given by

$$ {}_nV_d^{\ell} = E_n K_n^{o} T_n \Omega_n \sigma_d^{\ell}(\theta_i) G_n^{\ell} P^{\ell}. \tag{8} $$

The backscatter surface parameters of interest in this investigation are the backscattered fractions, the polarization ratios, and the percent depolarizations. The polarization ratio is the ratio of the fraction of the backscattered radiation which is polarized orthogonal to the incident polarization direction ℓ to the fraction backscattered which is polarized parallel to the incident

polarization direction ℓ. The percent depolarization is one hundred times the ratio of the unpolarized backscatter to the total backscatter.

The polarization ratio is given by

$$\frac{\sigma^{\ell}_{\ell'}(\theta_i)}{\sigma^{\ell}_{\ell}(\theta_i)} = \frac{{}_nV^{\ell}_{\ell'}}{{}_nV^{\ell}_{\ell}} \tag{9}$$

where ℓ' is orthogonal to ℓ. If some of the surface parameters vary with time, it might be advantageous to measure both components simultaneously using two detectors n and m. The polarization ratio would then be given by

$$\frac{\sigma^{\ell}_{\ell'}(\theta_i)}{\sigma^{\ell}_{\ell}(\theta_i)} = \frac{{}_mV^{\ell}_{\ell'}}{{}_nV^{\ell}_{\ell}} \left(\frac{E_n K^o_n T_n \Omega_n G^{\ell}_n}{E_m K^o_m T_m \Omega_m G^{\ell}_m} \right). \tag{10}$$

The numerator and the denominator in the last factor of Equation 10 may be calculated from Equation 5 by observing the signals from a standard surface of known σ's. Less error is involved in eliminating the factor by observing identical σ's from a surface with the two detectors m and n giving the relation

$$1 = \frac{{}_mV^{\ell}_d}{{}_nV^{\ell}_d} \left(\frac{E_n K^o_n T_n \Omega_n G^{\ell}_n}{E_m K^o_m T_m \Omega_m G^{\ell}_m} \right) \tag{11}$$

which can be solved to give the factor in terms of the observed signals ${}_{m}V_{d}^{\ell}$ and ${}_{n}V_{d}^{\ell}$.

The percent depolarization is given by

$$\frac{2\sigma_{\ell'}^{\ell}(\theta_i)\ (100)}{\sigma_{\ell}^{\ell}(\theta_i) + \sigma_{\ell'}^{\ell}(\theta_i)} = \frac{2\ {}_{n}V_{\ell'}^{\ell}(100)}{{}_{n}V_{\ell}^{\ell} + {}_{n}V_{\ell'}^{\ell}} . \qquad (12)$$

If it is advantageous to use signals from two (or three) detectors, the expression becomes

$$\frac{2\sigma_{\ell'}^{\ell}(\theta_i)\ (100)}{\sigma_{\ell}^{\ell}(\theta_i) + \sigma_{\ell'}^{\ell}(\theta_i)} = \frac{\dfrac{2\ {}_{m}V_{\ell'}^{\ell}\ (100)}{E_m K_m^{o} T_m \Omega_m G_m^{\ell} P^{\ell}}}{\dfrac{{}_{n}V_{\ell}^{\ell}}{E_n K_n^{o} T_n \Omega_n G_n^{\ell} P^{\ell}} + \dfrac{{}_{k}V_{\ell'}^{\ell}}{E_k K_k^{o} T_k \Omega_k G_k^{\ell} P^{\ell}}} \qquad (13)$$

where the ratios involving E, K^{o}, Ω, T, G^{ℓ}, and P^{ℓ} can be eliminated through expressions of the type in Equation 11.

The value of the backscattered fraction $\sigma_{d}^{\ell}(\theta_i)$ can be obtained by comparing the signal ${}_{n}V_{d}^{\ell}$ for the surface in question with the signal ${}_{n}^{c}V_{d}^{\ell}$ obtained using a surface for which σ is known, such as the surface described in Chapter II, Section IX. The value of the total backscattered fraction for normally incident radiation polarized along ℓ for a perfect Lambertian surface is given by Equation 91 in Appendix I,

$$ {}^{c}\sigma_{\ell}^{\ell}(0) + {}^{c}\sigma_{\ell'}^{\ell}(0) = \pi^{-1}(\text{steradian})^{-1}. \tag{14} $$

To obtain $\sigma_d^{\ell}(\theta_i)$ from any surface at any angle of incidence the ratio

$$ \frac{\sigma_d^{\ell}(\theta_j)}{{}^{c}\sigma_{\ell}^{\ell}(0) + {}^{c}\sigma_{\ell'}^{\ell}(0)} = \frac{{}_{n}V_d^{\ell}}{{}_{n}^{c}V_{\ell}^{\ell} + {}_{n}^{c}V_{\ell'}^{\ell}} \tag{15} $$

is used, or

$$ \sigma_d^{\ell}(\theta_j) = \frac{{}_{n}V_d^{\ell}}{{}_{n}^{c}V_{\ell}^{\ell} + {}_{n}^{c}V_{\ell'}^{\ell}} \pi^{-1}(\text{steradian})^{-1} . \tag{16} $$

The expressions derived above can correctly be applied to the data in this experiment except for the neglect of the analyzer leakage of the orthogonal polarization component and the fact that in our equipment, E_n was different on different oscilloscope settings. The latter problem is dealt with in Chapter IV, Section II. The correction to Equation 8 due to leakage L_n of the orthogonal polarization component by the analyzer on the aperture of the receiver n is given by

$$ {}_{n}V_d^{\ell} = \left[T_n \sigma_d^{\ell}(\theta_i) + L_n \sigma_d^{\ell}(\theta_i) \right] E_n K_n^{o} \Omega_n G_n^{\ell} P^{\ell} \tag{17} $$

where the analyzer on the receiver n is oriented to pass

polarization d and d' is the orthogonal polarization. With a second observation with the same or another receiver whose analyzer is oriented to pass polarization d', the system of Equations 17 can be solved for the σ's. The problem is dealt with in greater detail in Chapter IV, Section III.

CHAPTER IV

DATA COLLECTION AND REDUCTION

I. DATA COLLECTION PROCEDURES

The equipment was always operated for at least one hour before data were recorded. This was sufficient in most cases to stabilize the temperature dependent components: two lasers, two detectors, and the oscilloscope.

Some small drift in the system parameters was usually observed in collecting data over a typical six hour period. This was assumed to be due to slight temperature changes in certain components of the equipment. The major effects of these temperature changes might have been a variation in the laser diode output power and pulse width. Any changes in the system parameters which occurred after an hour of operation were small and approximately linear in time. These changes were generally compensated for by comparing the signals obtained from the standard surface (described in Chapter II, Section IX), before and after each data collection period.

The calibration data (data collected from the standard surface) were used to determine the signals produced from a known surface. These signals were proportional to the laser output power, beam geometry factor, detector response, and the amplification factor. The calibration

data were also used to compare the product of the detector response and amplification factor for each of the two detector-amplifier chains. In order to compare the latter, data were recorded simultaneously from both detectors while detecting identical optical returns. Using ${}_nV_d^{\ell}$ for the signal recorded for detector n using the laser with polarization ℓ with respect to the plane of incidence (sketched in Figure 2, page 6) and with the receiver polarizer oriented to transmit radiation with electric field oscillation in direction d, the sets of calibration data which were taken are as follows: $({}_1V_{\perp}^{\perp}, {}_2V_{\perp}^{\perp})$, $({}_1V_{\perp}^{/\!/}, {}_2V_{\perp}^{/\!/})$, $({}_1V_{/\!/}^{\perp}, {}_2V_{/\!/}^{\perp})$, and $({}_1V_{/\!/}^{/\!/}, {}_2V_{/\!/}^{/\!/})$.

Flickering changes of about 20% occurred randomly in the linearly polarized power output of the lasers in less than about 5% of the data recordings made. These changes never lasted long, as the calibration data from the beginning and the end of a data collection period always agreed except for the small drift mentioned above. These changes were believed to be due to a change in the relative intensity of the components of the polarized laser output and, thus, a change in the power transmitted by the laser polarizer. (It is believed that the total power output of the lasers remained constant while the relative intensity of the polarization components changed since this flickering was never observed with the polarizers off of the lasers.) Due to the possibility of such a

change occurring during the collection of the data from a given surface, both orthogonal polarization components of the backscattered intensity originating from each laser were measured simultaneously in order that the dependence on laser power output would cancel in any ratio formed between the measurements in each pair. Therefore, the data were collected from each surface in the following four sets: $({}_1V_{\perp}^{\perp}, {}_2V_{/\!/}^{\perp})$, $({}_1V_{\perp}^{/\!/}, {}_2V_{/\!/}^{/\!/})$, $({}_1V_{/\!/}^{\perp}, {}_2V_{\perp}^{\perp})$, $({}_1V_{/\!/}^{/\!/}, {}_2V_{\perp}^{/\!/})$.

Surfaces from which data were to be collected were mounted either on the vertical mounting board or in the holder under the mirror. In most cases where there was some doubt as to surface uniformity, the surface was translated with fixed angle of incidence so that the radiation was scattered from different areas on the surface while both components of the scattered radiation were observed. The data were then collected from the most uniform portion of the surface, and the magnitude of the variations over the surface was noted. The alignment sight was used to monitor the position on the surface from which the scattering was taking place. Generally, the nonrigid surfaces could be placed only at 0° angle of incidence. Data were usually recorded from the rigid surfaces at 0°, 30°, and 60° angle of incidence.

For surfaces which were suspected of having specular reflections, the dependence of the backscattered radiation on small changes in the angle of incidence about the normal

was observed. When specular reflections were being observed, the surface was positioned such that the peak intensity of the backscattered radiation was incident at a point which was within two inches (less than one-half of a degree as seen from the surface) of the midpoint between the two detectors.

The baselines of the oscilloscope traces drifted slowly throughout the data collection period. To overcome this, the following procedure was adopted. Each time, before data were recorded, all radiation was blocked away from the detectors, and the two trace baselines were set to a given value. The systems were then unblocked and the signals recorded immediately. Any drift which occurred between the time the trace baselines were set and the data were recorded was subtracted from the data before they were used.

The same procedures were followed for collecting each pair or set of data points. In order to correct the data for the linear drift time dependence in the systems, an effort was made to collect the data such that the time between recording each pair of data was the same and the time between collecting data from each surface orientation was the same. The data were usually recorded by photographing the oscilloscope screen. In order to reduce the time span between sets of data, multiple exposures (up to five) were made when possible. Generally, all of the data

which were collected from a surface at one angle of incidence were recorded on one photograph.

Detector number one was inoperative during the latter part of the data collection portion of the experiment. The data collection procedures were modified so that the collection of the data was repeated using detector number two. The order in which all the data were collected was then as follows: ${}_2V_{\perp}^{\perp}$, ${}_2V_{\perp}^{/\!/}$, ${}_2V_{/\!/}^{\perp}$, ${}_2V_{/\!/}^{/\!/}$, ${}_2V_{\perp}^{\perp}$, ${}_2V_{\perp}^{/\!/}$, ${}_2V_{/\!/}^{\perp}$, and ${}_2V_{/\!/}^{/\!/}$. The data were then reduced assuming that the first four measurements had been taken using detector number one. All of the expressions and other procedures remained unchanged.

The surfaces were visually recorded on thirty-five millimeter color slides by the telephoto camera. This was used to record the alignment of the laser beams and detector fields of view on each surface as well as to record the visual surface characteristics. The alignment was found to vary among the slides due to variations in mounting the slides. This was somewhat overcome by two strings fastened to the surface of the sample board, shown in Figure 1c, page 5, which intersected at the beam midpoint and generally could be seen extending beyond the object or surface in question. Unfortunately, several of the initial photographs of the surfaces were out of focus due to a defect in the camera. The surfaces shown in the text were printed by exposing Kodak R. C. Rapid

Polycontrast paper with light which had been passed through the slides. The resulting negatives were used to make positives by contact printing on other sheets of Kodak photographic paper. These positives were then photographed and the negatives used to expose Kodak Ektamatic S.C. paper.

II. OSCILLOSCOPE CALIBRATION

The signal height of a trace on the oscilloscope display is proportional to the product of the response of the detector and the amplification by the electronics. The responsivity and amplification were expected to be constant, independent of the signal height, but plots of oscilloscope output in millivolts versus the fractional peak radiation power incident on the detector contained distinct deviations from linearity. The detected radiation was backscattered radiation from the standard surface using either the perpendicular or the parallel laser as the source. The plotted points were obtained by placing calibrated neutral density filters in the laser beams, thus, reducing the radiation intensity incident on the detector by a known amount, I_n, and recording the resulting signal. A plot was made for each plug-in unit covering the scale settings from five millivolts per division to two hundred millivolts per division.

Upon examination of each plot of oscilloscope output versus the fractional power incident, the plot appeared to be made up of disjointed straight line segments, each segment corresponding to a scale setting on the vertical amplifier of the oscilloscope.. The plots which were subsequently made of oscilloscope output versus fractional detected radiation for each individual scale setting and plug-in unit combination were found to be linear. The variation of oscilloscope amplification between different scale settings was probably due to the pulse width of the transmitters being on the order of the rise times of the amplifiers and to the slight variation of oscilloscope amplifier rise time with scale setting due to the differing attenuation components.

Calibration curves were then obtained using a straight line least squares fit for each plug-in unit and each sensitivity scale setting which might be used. The sensitivities which were used were the 5, 10, 20, 50, 100, and 200 millivolt per division settings. At least ten points were obtained on each of the twelve curves. It was found that the curves were linear with a typical variation of the data points from the curve of less than 5% except where the signal on each scale became less than one-half of a division. Since data were seldom collected using trace heights lower than one division, this deviation from the curve was ignored.

The calibration curves were in the form

$$ {}^{c}V_n^s - D_n^s = {}^{c}A_n^s I_n = E_n^s \, {}^{c}M_n^{\ell} \, {}^{c}K_n^o I_n \, {}^{c}P^{\ell} \qquad (18) $$

where

n is the detector number,

s is the oscilloscope sensitivity (scale) setting,

c indicates the signals are calibration signals taken from the standard surface,

${}^{c}V_n^s$ is the oscilloscope calibration signal including drift which is obtained for detector n and scale setting s,

${}^{c}A_n^s = E_n^s \, {}^{c}M_n^{\ell} \, {}^{c}K_n^o \, {}^{c}P^{\ell}$, is the slope of the calibration curve for detector n and oscilloscope sensitivity setting s,

I_n is the fraction of ${}^{c}P^{\ell}$ which is allowed into the laser beam,

E_n^s is the amplification factor for the combination of detector n and oscilloscope sensitivity setting s,

${}^{c}M_n^{\ell}$ is the fraction of the incident radiation on a particular surface which is scattered into receiver n. If a polarizer is on the receiver, then ${}^{c}M_n^{\ell}$ is given by ${}^{c}M_n^{\ell} = \left[T_n \, {}^{c}\sigma_d^{\ell}(\theta_i) + L_n \, {}^{c}\sigma_{d'}^{\ell}(\theta_i) \right] \Omega_n G_n^{\ell}$, where Ω_n is the solid angle subtended by receiver n and G_n^{ℓ} is the beam geometry factor given in Equation 6,

D_n^s is the magnitude of the oscilloscope trace drift which occurs in the data point collecting time on scale s.

Equation 18 is equivalent to Equation 17 with a correction added for trace drift and with the dependence of E_n^s on the oscilloscope scale setting taken into consideration.

The small drifts D_n^s in the baseline of the traces persisted even after the systems had been operated for an hour or more and were different for each detector and scale setting combination. The magnitude of the drift was a linear function of time and was independent of the incident intensity. Since the time spent between zeroing the trace and recording the data was the same each time, the drifts D_n^s are functions only of the scale setting s and amplifier plug-in with detector n.

Five sets of calibration curves were obtained at various times throughout the period of data collection. A typical set of values of scale (in millivolts), ${}^cA_n^s$ (in millivolts per fraction of ${}^cP^{\ell}$), and D_n^s (in millivolts) is (5, 428, 0.336), (10, 434, 0.416), (20, 432, -0.693), (50, 455, -2.76), (100, 466, -6.67), and (200, 430, 19.5) for detector one; and (5, 462, 0.046), (10, 469, 0.332), (20, 447, 0.290), (50, 488, 0.593), (100, 474, 6.90), and (200, 444, 20.5) for detector two.

Since the power output of the laser varied significantly from one data collection period to the next, the

slopes ${}^{c}A_{n}^{s}$ of the calibration curves of ${}^{c}V_{n}^{s}$ versus I_n also varied from one data collection period to the next. Assuming that there were no changes in the amplifiers between two sets of calibration curves, the ratios of any two slopes in one set to the corresponding ratios of the slopes in the other set would be equal. The relation between the ratio of the slopes of scales s and t of calibration set i to the same for calibration set j is

$$\frac{{}^{c}_{i}A^{s}_{n}}{{}^{c}_{i}A^{t}_{n}} = \frac{E^{s}_{n}\ {}^{c}_{i}M^{\ell}_{n}\ {}^{c}_{i}K^{o}_{n}\ {}^{c}P^{\ell}_{i}}{E^{t}_{n}\ {}^{c}_{i}M^{\ell}_{n}\ {}^{c}_{i}K^{o}_{n}\ {}^{c}P^{\ell}_{i}} = \frac{E^{s}_{n}\ {}^{c}_{j}M^{\ell}_{n}\ {}^{c}_{j}K^{o}_{n}\ {}^{c}P^{\ell}_{j}}{E^{t}_{n}\ {}^{c}_{j}M^{\ell}_{n}\ {}^{c}_{j}K^{o}_{n}\ {}^{c}P^{\ell}_{j}} = \frac{{}^{c}_{j}A^{s}_{n}}{{}^{c}_{j}A^{t}_{n}}. \quad (19)$$

This relation was found to hold within experimental error for all but a few of the slopes where the disagreement was greater than 10%. The probable causes for the disagreements were either found to be uncorrectable errors in recording the values of the calibration data or believed to be due to observed temporarily poor connections in the oscilloscope switch contacts. Average slope values were substituted for those slopes which were found to be in error. The values to be substituted were calculated by the following procedure:

1. The slope ${}_{i}A^{s}_{n}$ was found to be in error.
2. The ratio R_{ij} between the m slopes of calibration sets i and j was calculated by the expression

$$R_{ij} = \frac{1}{m} \sum_{k=1}^{m} \frac{{}_{i}A_{n}^{k}}{{}_{j}A_{n}^{k}} \tag{20}$$

where none of the terms in the sum contains a slope which was in error. R_{ij} is an experimental determination of

$${}^{c}P_{i}^{\ell}\ {}^{c}K_{i\,n}^{o} \Big/ {}^{c}P_{j}^{\ell}\ {}^{c}K_{j\,n}^{o} .$$

3. A substitute slope from the j^{th} calibration set, ${}_{i}^{j}A_{n}^{s}$, was calculated from the expression

$${}_{i}^{j}A_{n}^{s} = R_{ij}\ {}_{j}A_{n}^{s} \tag{21}$$

where ${}_{j}A_{n}^{s}$ was not in error.

4. The substitute slope used, ${}_{i}A_{n}^{s}$, was an average of these expressions, one for each of the other calibration sets j where ${}_{j}A_{n}^{s}$ was not in error and is given by the expression

$${}_{i}A_{n}^{s} = \frac{1}{m_{j}} \sum_{j=1}^{m_{j}} {}_{i}^{j}A_{n}^{s} . \tag{22}$$

Since no significant differences were observed among any of the sets of calibration curves, the results were calculated using all the sets of curves. The results were calculated from each set of curves independently, and the results of the independent calculations were averaged.

III. POLARIZER LEAKAGE

Polarizers made from sheets of Polaroid Type HD polarizing material transmitted, when new, about 80% of the intensity having an electric field oscillation parallel to the transmission direction and leaked about 1% of the intensity of incident radiation having an electric field oscillation perpendicular to the transmission direction. Measurements of the leakage taken several months into the data collection period showed 4.8% leakage and 84% transmission for the polarizing material on the lasers and on detector one; and 3.1% leakage and 78% transmission for the material on detector number two. The material on detector two was several months newer than the other material.

The amount of intensity which might have been transmitted due to possible misalignment of the polarizers would have been most pronounced when the incident radiation was completely polarized and zero for completely unpolarized radiation. For completely polarized radiation and the maximum misalignment of five degrees, the error in the detected intensity would have been on the order of $\frac{1}{2}\sin^2(5^o)$ or 0.38% and can be ignored.

The leakage through one of these polarizers has the same polarization direction (to one part in 99) as the transmitted radiation (i.e., the leakage has its

polarization rotated 90° from its original state). For this reason, the transmitter beam issuing from the laser polarizer is essentially 100% polarized despite the leakage which occurs.

Any misalignment of the laser polarizers with respect to the plane of incidence to the surface from which data were being collected would have been undetectable at 0° angle of incidence. For other angles of incidence, the misalignment should have been detectable only for the specularly reflecting surfaces, and then the effect on any measured quantity should have always been less than 0.4%.

The effective power I_d^ℓ of the radiation of polarization d which is backscattered from a surface and is incident on the detector is given in terms of the effective power of the backscattered radiation of both polarizations incident on the receiver polarizer by the expression

$$ {}_nI_d^\ell = (T_n \, {}_nS_d^\ell + L_n \, {}_nS_{d'}^\ell) P^\ell \qquad (23) $$

where

n is the detector number,

ℓ is the polarization of the laser beam,

d is the orientation of the receiver polarizer,

d' is orthogonal to d,

T_n is the fractional transmission of the polarizer on detector n,

L_n is the fractional leakage of the polarizer on detector n, and

${}_nS_d^{\ell} = \Omega_n \sigma_d^{\ell}(\theta_i) G_n^{\ell}$ as is given by Equation 7.

The resulting peak oscilloscope signal is then

$$ {}_n^sV_d^{\ell} = E_n^s K_n^o (T_n \, {}_nS_d^{\ell} + L_n \, {}_nS_{d'}^{\ell}) P^{\ell} + D_n^s \qquad (24) $$

where

s is the oscilloscope sensitivity setting.

Let the product of the responsivity of detector n and the output power of the laser of polarization ℓ when the calibration curves are obtained be designated ${}^cK_n^o \, {}^cP^{\ell}$. Then as ${}^cA_n^s = E_n^s \, {}^cM_n^{\ell} \, {}^cK_n^o \, {}^cP^{\ell}$, we have the relation

$$ E_n^s K_n^o P^{\ell} = \frac{{}^cA_n^s \; K_n^o \; P^{\ell}}{{}^cM_n^{\ell} \; {}^cK_n^o \; {}^cP^{\ell}} = \frac{A_n^s}{M_n^{\ell}} \qquad (25) $$

where M_n^{ℓ} is defined to be

$$ M_n^{\ell} = \frac{{}^cM_n^{\ell} \; {}^cK_n^o \; {}^cP^{\ell}}{K_n^o \; P^{\ell}} \; . \qquad (26) $$

So Equation 24 becomes

$$ {}_n^sV_d^{\ell} = \frac{{}^cA_n^s}{M_n^{\ell}} (T_n \, {}_nS_d^{\ell} + L_n \, {}_nS_{d'}^{\ell}) + D_n^s . \qquad (27) $$

Consider the equation for the peak oscilloscope signal when the analyzer on the receiver is rotated to transmit

polarization d'. The oscilloscope scale setting used is called t. Within the constant M_n^{ℓ}, the effective fraction of the laser power incident on the receiver polarizer can be found by solving the system of these two equations giving the relation

$$ {}_nS_d^{\ell}(M_n^{\ell})^{-1} = \frac{1}{T_n^2 - L_n^2}\left(\frac{T_n}{cA_n^s}\left({}_nV_d^{\ell} - D_n^s\right) - \frac{L_n}{cA_n^t}\left({}_nV_d^{\ell} - D_n^t\right)\right) \qquad (28) $$

where

t is the oscilloscope sensitivity setting.

Equation 28 gives the backscattered fractions of the incident laser beam in terms of measured quantities and an unknown factor M_n^{ℓ} which, as will be seen, cancels out of all the final results.

IV. LASER AND DETECTOR CALIBRATION

The lasers and detectors were calibrated by taking data from the standard surface at 0° angle of incidence. From Appendix I, Equation 91, the fraction of the power incident on the standard from each of the perpendicular and parallel laser beams at 0° angle of incidence which is backscattered is $\pi^{-1}(\text{steradian})^{-1}$.

The signals were recorded simultaneously from both receivers while detecting the same polarization in the backscattered return from a given laser. In each case, the optical returns incident on the receivers were

essentially identical, and the differences in output signals were due to differences between the two detectors in solid angle subtended, sensitivity over the field of view, amplification, and polarizer transmission. In order to compensate for the differences between the two detectors in calculations where both appeared, equality factors were associated with detector number two. The equality factors for the four different laser-receiver polarization cases are given by

$$
\begin{aligned}
{}_2F_d^{\ell} &= (M_1^{\ell})^{-1}\, {}_1^{c}S_d^{\ell} \Big/ (M_2^{\ell})^{-1}\, {}_2^{c}S_d^{\ell}\ , \\
{}_1F_d^{\ell} &= 1, \text{ by definition,}
\end{aligned}
\tag{29}
$$

where

ℓ is the polarization of the laser,

d is the polarization being detected,

c indicates the signals are calibration signals taken from the standard surface,

${}_2F_d^{\ell}$ and ${}_1F_d^{\ell}$ are the equality factors, and

$(M_1^{\ell})^{-1}\, {}_1^{c}S_d^{\ell}$ and $(M_2^{\ell})^{-1}\, {}_2^{c}S_d^{\ell}$ are given by Equation 28.

Laser output power normalization factors were also obtained within the constant $(M_n^{\ell})^{-1}$ while viewing the standard surface at 0^{o} angle of incidence. These power normalization factors are, within the factor $(M_n^{\ell})^{-1}$, the effective fraction of the power from the laser of polarization ℓ which was backscattered from the standard

onto the aperture of receiver n in both polarizations ℓ and ℓ':

$$\begin{aligned} N_n &= (M_n^{\ell})^{-1}\ {}^{c}_{n}S^{\ell}_{\ell} + (M_n^{\ell})^{-1}\ {}^{c}_{n}S^{\ell}_{\ell'} \\ &= (M_n^{\ell})^{-1}\Omega_n G_n^{\ell}\left[{}^{c}\sigma^{\ell}_{\ell}(0) + {}^{c}\sigma^{\ell}_{\ell'}(0)\right] \\ &= (M_n^{\ell})^{-1}\Omega_n G_n^{\ell}\ \pi^{-1} \end{aligned} \tag{30}$$

where the result of Equation 91 in Appendix I was used.

The calibration data were collected after the equipment had been operational for at least one hour and before any other data were taken and usually were taken again after the data collecting period before the equipment was turned off. Small changes in the receiver equality factors and the laser power normalization factors due to slight changes in K_n^o and P^{ℓ} (or changes which can be considered to be in K_n^o and P^{ℓ}) persisted throughout most of the data collection periods. These changes were believed to be due either to the relatively large dependence of laser output power on temperature or to variations in pulse width producing changes because of the relatively long amplifier rise time or some combination of both. The magnitudes and even the direction of the changes varied between data collection periods. However, these changes were observed to be relatively slow and approximately linear. When calibration data were collected at

the end of a data collection period, since the data sets were generally equally spaced in time, the equality factors and normalization factors for the j^{th} data set were taken to be

$$({}_nF_d^{\ell})_j = ({}_nF_d^{\ell})_i + \frac{n_j}{n_t}\left[({}_nF_d^{\ell})_f - ({}_nF_d^{\ell})_i\right] \tag{31}$$

and

$$(N_n^{\ell})_j = (N_n^{\ell})_i + \frac{n_j}{n_t}\left[(N_n^{\ell})_f - (N_n^{\ell})_i\right] \tag{32}$$

where

j is the data point being considered,

n_j is the number of the j^{th} data point,

n_t is the total number of data sets collected during the period,

i indicates initial values of the parameters, and

f indicates the final values of the parameters.

The variation of the receiver equality factors and laser normalization factors from the beginning to the end of a data collection period was typically 5% and never more than 10%.

V. POLARIZATION RATIO

The polarization ratio is given by

$$R^{\ell}_{mn} = \left(\frac{{}_{n}F^{\ell}_{\ell'}}{{}_{m}F^{\ell}_{\ell}} \right) \frac{(M^{\ell}_{n})^{-1}\,{}_{n}S^{\ell}_{\ell'}}{(M^{\ell}_{m})^{-1}\,{}_{m}S^{\ell}_{\ell}} = \frac{\sigma^{\ell}_{\ell'}(\theta_i)}{\sigma^{\ell}_{\ell}(\theta_i)} \qquad (33)$$

where

the ratio of the F's is to be used only for $m \neq n$,

m,n are the receiver numbers, either 1 or 2,

ℓ is the polarization of the laser beam,

ℓ' is orthogonal to ℓ.

R^{ℓ}_{mn} is the polarization ratio obtained using the laser with polarization ℓ calculated using the measurements from receiver numbers m and n,

F is the equality factor given by Equation 29,

M is given by Equation 26,

S is given by Equation 7, and

σ is the backscattered fraction.

There are, thus, four ways to calculate the polarization ratio from Equation 33 for each laser. Of these values and the averaged combinations (including linear or non-linear combinations) which could be formed from these values, the one which should be used (10) is the value having the least variance or standard error. The

value with the least standard error is generally the arithmetic average of the independent values from the set of values (i.e., R^{ℓ}_{11}, R^{ℓ}_{22}, R^{ℓ}_{12}, R^{ℓ}_{21}) which individually have the least and approximately equal relative errors. Of the different combinations which can be formed from the R^{ℓ}_{mn}, the one containing the values from Equation 33 with the smallest relative errors is

$$R^{\ell} = \tfrac{1}{2}(R^{\ell}_{11} + R^{\ell}_{22}) \quad . \tag{34}$$

The relative errors for R^{ℓ}_{11} and R^{ℓ}_{22} are smaller than the relative errors for R^{ℓ}_{12} and R^{ℓ}_{21} since the latter involve the equality factors. The effects due to the difference between the two receivers in their positions with respect to the surface, apparent in the case of specular reflections, should tend to cancel in the ratios R^{ℓ}_{11} and R^{ℓ}_{22}. The only error which is introduced into R^{ℓ} in Equation 34 which would not occur in any of the other possible expressions would occur when the laser output power changes during the collection of the data, i.e., while the receiver polarizer is being rotated. This error is less than 1% for laser changes less than 10%. When this occurs, R^{ℓ} could be calculated from

$$R^{\ell} = \tfrac{1}{2}(R^{\ell}_{12} + R^{\ell}_{21}) \tag{35}$$

in which the laser power cancels in the ratios. However,

this expression typically has much more error as it contains many more experimentally determined quantities. Additional error can be introduced if the detector or amplifier characteristics change during the collection of the data from a particular surface. The expression

$$R^{\ell} = \tfrac{1}{4} \sum_{mn} R^{\ell}_{mn} \tag{36}$$

is shown in Section VII to have typically 12% more error in R^{ℓ} than for R^{ℓ} from Equation 34 except when some of the oscilloscope signal peaks approach the noise. Since the expression for R^{ℓ} in Equation 34 generally contains less error, it was used exclusively for the calculation of the polarization ratios.

In connection with the larger error in Equation 36, it is interesting to note that the quantities involved are not independent. A relation exists of the form

$$R^{\ell}_{12} = \frac{R^{\ell}_{11} \, R^{\ell}_{22}}{R^{\ell}_{21}} \quad . \tag{37}$$

A value with less standard error might have been obtained using a weighted or nonlinear form of Equation 36. This was never attempted, however, since the value of R^{ℓ} from Equation 34 proved sufficient and reliable and was less susceptible to such indeterminate errors as those which could occur when observing specular reflections.

VI. PERCENT DEPOLARIZATION

One-half of the unpolarized backscattered radiation is contained in each of the orthogonal polarizations. Since the backscattered radiation which is still polarized is of the same orientation as the incident radiation, none of the scattered polarized radiation will be detected in the polarization direction perpendicular to the polarization of the incident radiation. The total unpolarized backscattered fraction will then be twice the fraction measured with the receiver polarization perpendicular to the laser beam polarization; and the total backscattered fraction will be the sum of the fractions detected in both polarizations. The percentage of backscattered radiation which is depolarized is then, in terms of experimentally determined quantities,

$$PD^{\ell}_{kmn} = \frac{2\,{}_kF^{\ell}_{\ell'}\,(M^{\ell}_k)^{-1}\,{}_kS^{\ell}_{\ell'}\quad(100)}{{}_mF^{\ell}_{\ell}\,(M^{\ell}_m)^{-1}\,{}_mS^{\ell}_{\ell}\;+\;{}_nF^{\ell}_{\ell'}\,(M^{\ell}_n)^{-1}\,{}_nS^{\ell}_{\ell'}} \tag{38}$$

$$= \frac{2\sigma^{\ell}_{\ell'}(\theta_i)\quad(100)}{\sigma^{\ell}_{\ell}(\theta_i)\;+\;\sigma^{\ell}_{\ell'}(\theta_i)}$$

where,

if k=m=n=1 or 2, the F's are not used,

k, m and n are the receiver numbers,

ℓ is the polarization of the laser beam,

ℓ' is the polarization orthogonal to ℓ ,

PD^{ℓ}_{kmn} is the percent depolarization of the backscattered radiation incident from the laser with polarization ℓ and calculated using the measurements from receivers k, m and n,

F is the equality factor given by Equation 29,

M is given by Equation 26,

S is given by Equation 7, and

σ is the backscattered fraction.

There are eight different ways to calculate the percent depolarization from Equation 38 for each laser. The percent depolarization can be related to the polarization ratio by using Equation 7 in Equation 38.

$$PD^{\ell}_{kmn} = \frac{2R^{\ell}_{kn}}{R^{\ell}_{mn} + 1} (100). \tag{39}$$

For the same reasons discussed in Section V, the percent depolarizations were calculated from the equation

$$PD^{\ell} = \tfrac{1}{2}(PD^{\ell}_{111} + PD^{\ell}_{222}). \tag{40}$$

VII. BACKSCATTERED FRACTIONS

The relative backscattered fraction is the fraction per steradian of the incident radiation which is backscattered normalized to the total fraction backscattered from a perfect Lambertian surface at 0^{o} angle of incidence. (See Appendix I.) The relative fraction of incident radiation of a particular polarization ℓ which is backscattered with polarization d is, in terms of experimental quantities,

$$B_d^{\ell} = \frac{(M_n^{\ell})^{-1}\, {}_nS_d^{\ell}}{N_d^{\ell}} = \sigma_d^{\ell}(\theta_i)\ (\pi) \qquad (41)$$

where

n is the detector number,

ℓ is the polarization of the incident radiation,

d is the orientation of the detector polarizer,

B_d^{ℓ} is the intensity per steradian of radiation incident with polarization ℓ which is backscattered and detected in orientation d,

${}_nS_d^{\ell}$ is the scattered intensity given by Equation 7,

N_d^{ℓ} is the normalization factor given by Equation 30,

σ_d^{ℓ} is the backscattered fraction.

Due to error considerations, the backscattered fractions were calculated from

$$B_d^{\ell} = \tfrac{1}{2}\left(\frac{(M_1^{\ell})^{-1}\,{}_1S_d^{\ell}}{N_d^{\ell}} + \frac{(M_2^{\ell})^{-1}\,{}_2S_d^{\ell}}{N_d^{\ell}}\right) . \tag{42}$$

From these four basic relative backscattered fractions $B_{\perp}^{\perp}$, $B_{/\!/}^{\perp}$, $B_{/\!/}^{/\!/}$, and $B_{\perp}^{/\!/}$, the total relative backscattered fraction of the radiation initially polarized in the perpendicular direction $B_U^{\perp}$; the total relative backscattered fraction of the radiation initially polarized in the parallel direction $B_U^{/\!/}$; the relative fraction of incident unpolarized radiation to be found in the perpendicularly polarized backscattered component $B_{\perp}^{U}$; the relative fraction of incident unpolarized radiation to be found in the parallel polarized backscattered component $B_{/\!/}^{U}$; and the total relative backscattered fraction for incident unpolarized radiation B_U^U, (i.e., the relative reflectivity in the backscatter direction at angle of incidence θ_i); can be calculated from the following relations

$$B_U^{\perp} = B_{\perp}^{\perp} + B_{/\!/}^{\perp}, \tag{43}$$

$$B_U^{/\!/} = B_{/\!/}^{/\!/} + B_{\perp}^{/\!/}, \tag{44}$$

$$B_{\perp}^{U} = \tfrac{1}{2}(B_{\perp}^{\perp} + B_{\perp}^{/\!/}), \tag{45}$$

$$B_{/\!/}^{U} = \tfrac{1}{2}(B_{/\!/}^{/\!/} + B_{/\!/}^{\perp}), \tag{46}$$

$$B_U^U = B_{\perp}^{U} + B_{/\!/}^{U} = B_U^{\perp} + B_U^{/\!/} , \tag{47}$$

where

u superscript denotes unpolarized incident radiation,

u subscript denotes an unbiased detector, and all the backscatter fractions are functions of the angle of incidence.

The factors of ½ in Equations 45 and 46 come from the fact that for unpolarized radiation incident, the radiation power in the parallel component is equal to the radiation power in the perpendicular polarized component and both are one-half of the total radiation power incident.

VIII. ERROR ANALYSIS

The calculated error in the experimental results arises from the error in reading each independently measured quantity. Since most of the data were recorded on photographs of the oscilloscope trace, and a transparent grid with about 1% error was used to read the data, the reading error was of the order of one-half the trace width of the oscilloscope. The trace width was typically 0.2 to 0.4 divisions and the maximum trace height was 4.5 divisions.

The errors in the quantities A_n^s and D_n^s in the oscilloscope calibration curves of Equation 18 were taken to be the standard errors arising from the curve fitting. The quantities A_n^s and D_n^s were calculated by linear regression (a least squares straight line fit) to a set of points of oscilloscope peak signal versus fraction of laser power passed. Let V_j and I_j be one of n pairs of

signal and laser power fractions and V be given by Equation 18 for $I_n = I_j$, then the definition (11) of standard error in A_n^s is

$$\Delta A_n^s = \left[\frac{n}{n-2} \sum_{j=1}^{n} (V_j - V)^2 \Big/ \left(n \sum_{j=1}^{n} I_j^2 - \left(\sum_{j=1}^{n} I_j \right)^2 \right) \right]^{\frac{1}{2}} . \qquad (48)$$

The numerator is the standard error of estimate of V on I, and the denominator is the variance of I. The definition of standard error in D_n^s is

$$\Delta D_n^s = \left[\frac{\sum_{j=1}^{n} I_j^2}{n-2} \sum_{j=1}^{n} (V_j - V)^2 \Big/ \left(n \sum_{j=1}^{n} I_j^2 - \left(\sum_{j=1}^{n} I_j \right)^2 \right) \right]^{\frac{1}{2}} . \qquad (49)$$

A quantity which gives the closeness of the curve fit to the data is the correlation coefficient or coefficient of determination C defined by

$$C^2 = \frac{\left[n \sum_{j=1}^{n} V_j I_j - \sum_{j=1}^{n} V_j \sum_{j=1}^{n} I_j \right]^2}{\left[\sum_{j=1}^{n} I_j^2 - \left(\sum_{j=1}^{n} I_j \right)^2 \right] \left[\sum_{j=1}^{n} V_j^2 - \left(\sum_{j=1}^{n} V_j \right)^2 \right]} . \qquad (50)$$

The numerator is the covariance between V and I. The standard error in A_n^s, ΔA_n^s is typically 7.3% of A_n^s. The standard error in D_n^s, ΔD_n^s, is typically 80% of D_n^s but is of little significance since the drift was very small on

each scale. The coefficient C was typically 0.991 versus 1.0 for a perfect fit.

The error in an experimentally derived quantity was taken to be the RMS error found by taking the differential of the expression for the quantity in terms of independently measured quantities and taking the square root of the sum of the squares of the terms so found, with the measurement's errors substituted for the differentials of the independent quantities. This is sometimes referred to as the expected error in a calculation. To obtain the expression for this error, consider a function of n independently measured variables $Q(X_1, X_2, \ldots, X_n)$ and evaluate the function for small changes (errors) in the X by expanding it in a Taylor's series.

$$Q(X_1+\Delta X_1, X_2+\Delta X_2, \ldots, X_n+\Delta X_n) = Q(X_1, X_2, \ldots, X_n) + \sum_{j=1}^{n} \pm \frac{\partial Q}{\partial X} \Delta X_j + \text{higher order terms.}$$

$$= Q + \Delta Q + \text{higher order terms.} \qquad (51)$$

The magnitude of the suspected error in Q, ΔQ is then

$$\Delta Q = \left[\sum_{j=1}^{n} \left(\frac{\partial Q}{\partial X_j} \right)^2 (\Delta X_j)^2 \right]^{\frac{1}{2}} . \qquad (52)$$

Each of the calculations which was made was one of the following two cases.

1. $Q = X_1 \pm X_2$.

$$\Delta Q = \left[(\Delta X_1)^2 + (\Delta X_2)^2\right]^{\frac{1}{2}} . \tag{53}$$

2. $Q = X_1 (X_2)^{\pm 1}$

$$\Delta Q = Q\left[\frac{\Delta X_1^{\,2}}{X_1} + \frac{\Delta X_2^{\,2}}{X_2}\right]^{\frac{1}{2}} . \tag{54}$$

For a calculation involving any number of independent variables in ratios and products, applying Equation 54 shows that the error in the result is the result times the square root of the sum of the squares of the relative errors of each variable. For sums and differences, applying Equation 53 shows that the error is the square root of the sum of the squares of the errors of each variable.

The expected error in the expressions for the polarization ratio can now be calculated. Considering first the polarization ratio involving only the terms R_{11}^{ℓ} and R_{22}^{ℓ} as given by Equation 34, the error is found by substituting Equation 34 into Equation 52 giving the result

$$\frac{\Delta R^{\ell}}{R^{\ell}} = \tfrac{1}{2}\left[\frac{\Delta R_{11}^{\ell}}{R_{11}^{\ell}} + \frac{\Delta R_{22}^{\ell}}{R_{22}^{\ell}}\right]. \tag{55}$$

For error estimation purposes, all of the polarization ratios can be considered to be approximately equal or $R^{\ell} \simeq R^{\ell}_{11} \simeq R^{\ell}_{22}$. Applying Equation 52 to the definition of R^{ℓ}_{mn} into Equation 33 gives

$$\frac{\Delta R^{\ell}_{mn}}{R^{\ell}_{mn}} = \frac{\Delta\, {}_n\eta^{\ell}_{\ell'}}{{}_n\eta^{\ell}_{\ell'}} - \frac{\Delta\, {}_n\eta^{\ell}_{\ell}}{{}_n\eta^{\ell}_{\ell}} \tag{56}$$

where ${}_n\eta^{\ell}_{d}$ is defined to be

$$\begin{aligned} {}_n\eta^{\ell}_{d} &= (M^{\ell}_{n})^{-1}\, {}_nS^{\ell}_{d} \\ &= \frac{1}{T_n^2 - L_n^2}\left(\frac{T_n}{A^s_n}({}^s_nV^{\ell}_{d} - D^s_n) - \frac{L_n}{A^t_n}({}^t_nV^{\ell}_{d} - D^t_n)\right) . \end{aligned} \tag{57}$$

Since the error in ${}^s_nV^{\ell}_{d}$ is essentially the independent reading error and the term involving ${}^t_nV^{\ell}_{d}$ is small compared to the term involving ${}^s_nV^{\ell}_{d}$, the errors in ${}_n\eta^{\ell}_{d}$, $\Delta\, {}_n\eta^{\ell}_{d}$, are essentially independent. Also, the relative errors $\frac{\Delta\, {}_n\eta^{\ell}_{d}}{{}_n\eta^{\ell}_{d}}$ of each of the ${}_n\eta^{\ell}_{d}$ are approximately equal. The magnitude of the error in the polarization ratio as given by Equation 34 is

$$\frac{\Delta R^{\ell}}{R^{\ell}} \simeq \tfrac{1}{2}\left[4\left(\frac{\Delta\eta^{\ell}}{\eta^{\ell}}\right)^2\right]^{\frac{1}{2}} = \frac{\Delta\eta^{\ell}}{\eta^{\ell}} . \tag{58}$$

For the polarization ratio calculated by the expression $R^{\ell} = \frac{1}{4}\sum_{mn} R^{\ell}_{mn}$, as given by Equation 36, the relative error is given by

$$\frac{\Delta R^{\ell}}{R^{\ell}} = \frac{1}{4}\left(\frac{\Delta R^{\ell}_{11}}{R^{\ell}_{11}} + \frac{\Delta R^{\ell}_{22}}{R^{\ell}_{22}} + \frac{\Delta R^{\ell}_{12}}{R^{\ell}_{12}} + \frac{\Delta R^{\ell}_{21}}{R^{\ell}_{21}}\right) . \tag{59}$$

Again, for error consideration purposes, the polarization ratios can be considered to be approximately equal or $R^{\ell}_{11} \simeq R^{\ell}_{22} \simeq R^{\ell}_{12} \simeq R^{\ell}_{21} \simeq R^{\ell}$. Substituting R^{ℓ}_{mn} from Equation 33 and ${}_2F^{\ell}_d$ from Equation 29 into Equation 52 and combining terms gives the expression

$$\frac{\Delta R^{\ell}}{R^{\ell}} \simeq \frac{1}{4}\left[2\left(\frac{\Delta_1 \eta^{\ell}_{\ell'}}{{}_1\eta^{\ell}_{\ell'}} + \frac{\Delta_2 \eta^{\ell}_{\ell'}}{{}_2\eta^{\ell}_{\ell'}} - \frac{\Delta_1 \eta^{\ell}_{\ell}}{{}_1\eta^{\ell}_{\ell}} - \frac{\Delta_2 \eta^{\ell}_{\ell}}{{}_2\eta^{\ell}_{\ell}}\right)\right.$$

$$\left. + \left(\frac{\Delta^c_1 \eta^{\ell}_{\ell'}}{{}^c_1\eta^{\ell}_{\ell'}} + \frac{\Delta^c_2 \eta^{\ell}_{\ell'}}{{}^c_2\eta^{\ell}_{\ell'}} - \frac{\Delta^c_1 \eta^{\ell}_{\ell}}{{}^c_1\eta^{\ell}_{\ell}} - \frac{\Delta^c_2 \eta^{\ell}_{\ell}}{{}^c_2\eta^{\ell}_{\ell}}\right)\right] \tag{60}$$

where the ${}^c\eta$ are the numerators and denominators used in the equality factors of Equation 29 or

$${}_2F^{\ell}_d = \frac{{}^c_1\eta^{\ell}_d}{{}^c_2\eta^{\ell}_d} . \tag{61}$$

As the relative errors in the η are usually approximately the same size, the magnitude of the error in the polarization ratio as given in Equation 36 is

$$\frac{\Delta R^{\ell}}{R^{\ell}} = \tfrac{1}{4}\left[4\left(4\left(\frac{\Delta\eta^{\ell}}{\eta^{\ell}}\right)^2\right) + \left(4\left(\frac{\Delta\eta^{\ell}}{\eta^{\ell}}\right)^2\right)\right]^{\frac{1}{2}} = \left(\frac{5}{4}\right)^{\frac{1}{2}} \frac{\Delta\eta^{\ell}}{\eta^{\ell}} . \qquad (62)$$

Then typically, the expression for the polarization ratios involving R_{11}^{ℓ}, R_{22}^{ℓ}, R_{12}^{ℓ}, and R_{21}^{ℓ} as given by Equation 36 has 12% more error than the one given by Equation 34 involving only R_{11}^{ℓ} and R_{22}^{ℓ}.

When the surface from which data were being collected was such that only small signal peak heights could be obtained on the oscilloscope (this seldom was the case), the relative errors in the first term of Equation 60 approach one since they are proportional to the reading errors which approach one for small signal peak heights. This is large compared to the second term of Equation 60 which arises from measurements on the standard which backscatters well enough to produce signals which can always be displayed with peak heights of at least two divisions. Neglecting the second term of Equation 60 with respect to the first, in this case causes the results of Equations 55 and 59 to be equal.

Errors created due to the misalignment of the optics or of the receiver polarizers were taken to be random in occurrence and magnitude and, since they have been shown to be much smaller than 1%, were neglected. As discussed in Section III above, any errors associated with the laser polarizers would be much less than 1%

and were, therefore, neglected. The error in the values for the receiver polarizer leakages could produce very large relative errors in the orthogonal polarization components of the specular reflectors. The values assumed for leakages were the accurately measured values of 4.8% and 3.1% which were measured near the end of the experiment. The polarizers had been protected from ultraviolet light as much as possible since it was known to deteriorate them. However, they did deteriorate much more than expected, perhaps due to aging alone. Near the beginning of the experiment, these values could have been as low as 1%, as measured on new material by others in the laboratory. The transmission factors T_n did not appear to change appreciably with age. If L_n is the actual polarizer leakage and R^{ℓ} the actual polarization ratio, the measured peak oscilloscope signals are given by Equation 27 as

$$ {}_{n}V_{d}^{\ell s} = \frac{A_n^s}{M_n^{\ell}} \left(T_n \, {}_{n}S_{d}^{\ell} + L_n \, {}_{n}S_{d}^{\ell}{}_{\cdot}\right) + D_n^s \qquad (63) $$

where

$$ {}_{n}S_{d} = \Omega_n \sigma_d^{\ell}(\theta_i) G_n^{\ell} \text{ , by Equation 7.} $$

The polarization ratio is given by

$$R^{\ell} = \frac{\sigma^{\ell}_{\ell'}(\theta_i)}{\sigma^{\ell}_{\ell}(\theta_i)} = \frac{{}_nS^{\ell}_{\ell'}}{{}_nS^{\ell}_{\ell}} \quad . \tag{64}$$

The values A^s_n, M^{ℓ}_n, ${}_nS^{\ell}_{\ell}$, and ${}_nS^{\ell}_{\ell'}$ can be eliminated by substituting Equation 64 into Equation 63 to obtain the following two expressions:

$$\frac{M^{\ell}_n}{A^s_n} = {}^sV^{\ell}_n - D^s_n = {}_nS^{\ell}_{\ell}\, T_n + L_n R^{\ell} \quad , \text{ and} \tag{65}$$

$$\frac{M^{\ell}_n}{A^s_n} = {}^tV^{\ell}_{n\,\ell'} - D^t_n = {}_nS^{\ell}_{\ell}\, R^{\ell} T_n + L_n \quad . \tag{66}$$

The expression for R^{ℓ} which depends only on the polarizer transmission and leakage and the measured oscilloscope signal height can then be found by solving Equations 65 and 66 for R^{ℓ}

$$R^{\ell} = \frac{({}^sV^{\ell}_n - D^s_n)L_n - ({}^tV^{\ell}_{n\,\ell'} - D^t_n)T_n}{({}^tV^{\ell}_{n\,\ell'} - D^t_n)L_n - ({}^sV^{\ell}_n - D^s_n)T_n} \quad . \tag{67}$$

If the polarizer leakage is believed to be L'_n, then in place of $(M^{\ell}_n)^{-1}S^{\ell}_d$ and $(M^{\ell}_n)^{-1}S^{\ell}_{d'}$ in Equation 63, the numbers ${}_n\eta^{\ell}_d$ and ${}_n\eta^{\ell}_{d'}$ are calculated such that

$$(A^s_n)^{-1}({}^sV^{\ell}_n - D^s_n) = {}_n\eta^{\ell}_{\ell}(T_n + L'_n R'^{\ell}) \tag{68}$$

and

$$(A_n^t)^{-1}({}_nV_\ell^t - D_n^t) = {}_n\eta_\ell^{\ell}(R'^{\ell}T_n + L_n') \quad . \tag{69}$$

Substituting Equations 68 and 69 into Equation 67 gives an expression for the actual polarization ratio R^{ℓ} in terms of the actual polarizer transmission T_n, the actual polarizer leakage L_n, the assumed values T_n' and L_n' and the polarization ratio R'^{ℓ} calculated from the assumed values. The expression for R^{ℓ} is

$$R^{\ell} = \frac{T_n^2R'^{\ell} + L_n'T_n - L_nT_n - L_nL_n' R'^{\ell}}{T_n^2 + L_n'T_nR'^{\ell} - L_nT_nR'^{\ell} - L_nL_n'} \quad . \tag{70}$$

The largest relative changes occur for small values of the polarization ratio R^{ℓ}. For the pair (L_n', L_n) equal to (4%,1%), where L_n' has been taken as the average of the measured leakages for the two detectors for the purposes of comparison, examples of pairs of (R'^{ℓ}, R^{ℓ}) are (0.0, 0.0375), (0.01, 0.0475), (0.02, 0.0575), (0.05, 0.0874), (0.1, 0.137), (0.25, 0.0285), (0.5, 0.0528), and (0.8, 0.817). Polarization ratios for data taken during the first part of the experiment and which have have been calculated to be on the order of 0.01 using the higher leakage values could be actually on the order of 0.05 with the possible error becoming negligible for ratios over 0.8.

The effect of error in polarizer leakage on the percent depolarization can best be analyzed by expressing the percent depolarization in terms of the polarization ratio as in Equation 39,

$$PD^{\ell} = \frac{2R^{\ell}(100)}{R^{\ell} + 1} . \tag{71}$$

The relative magnitude of the error which could exist in the percent depolarization is on the same order as the relative error which could exist in the polarization ratio for small values of either. The error in the percent depolarization due to polarizer leakage becomes negligible as the polarization ratio and thus the percent depolarization increases, becoming negligible at values larger than 80%. Only two relative backscattered fractions $B_{//}^{\perp}$ and $B_{\perp}^{//}$, are significantly affected. For data where the lower leakage values should be used, the values of $B_{//}^{\perp}$ and $B_{\perp}^{//}$ which were calculated using the higher values should be $B_{//}^{\perp}$ and $B_{\perp}^{//}$ given by

$$B_{//}^{\perp} \simeq B_{//}^{\perp} + (0.04)B_{\perp}^{\perp} , \tag{72}$$

and

$$B_{\perp}^{//} \simeq B_{\perp}^{//} + (0.04)B_{//}^{//} . \tag{73}$$

In order to determine the error introduced into the polarization ratios due to changes in the laser power outputs, first consider R^{ℓ} when no change occurs in the output power of the laser between the recording of the oscilloscope signal for one of the backscattered radiation components and the recording of the signal for the orthogonal component. The polarization ratio is given by

$$R^{\ell} = \tfrac{1}{2}(R^{\ell}_{11} + R^{\ell}_{22}) \simeq R^{\ell}_{11} , \tag{74}$$

assuming no other system changes occur in the same time period. If the power output (of the perpendicular laser, for example) after recording the first set of data becomes I_n as great for the second set of data, then considering the order in which the data were collected, as discussed in Section I above, the polarization ratio becomes

$$R'^{\ell} = \tfrac{1}{2}\left(I_n R_{11} + (I_n)^{-1} R_{22}\right) \simeq R_{11}(\tfrac{1}{2})\left(I_n + (I_n)^{-1}\right). \tag{75}$$

If the laser output power were to change by 10%, then $I_n=0.9$ or $I_n=1.1$, and

$$R'^{\ell} \simeq 1.005R^{\ell}. \tag{76}$$

For the polarization ratios obtained from data taken when only one detector was available, the relative changes in the results for the polarization ratios would be

one-half of the relative change of the laser output power. For the laser with polarization ℓ, the relative errors introduced into the backscattered fractions due to changes in the laser power outputs would be one-half the laser output power change for B_{ℓ}^{ℓ}, B_{ℓ}^{ℓ}, and B_{u}^{ℓ}, and one-fourth of the laser change for B_{u}^{u}.

For data which were taken from surfaces at normal incidence, the results for both lasers should have been the same. Considering all such data which were collected, the polarization ratios for the perpendicular laser were 0.8% ± 8% greater than for the parallel laser for approximately non-specularly reflecting surfaces and 16% ± 68% greater when very specularly reflecting surfaces were also considered. At normal incidence, the backscattered fraction $B_{U}^{\perp}$ was 1% ± 11% greater than $B_{U}^{/\!/}$ when only approximately non-specularly reflecting surfaces were considered and was 2% ± 24% greater when the very specularly reflecting surfaces were also considered. Thus, the differences between the two lasers were much less than the experimental errors.

Throughout the data collection period, the detectors were operated within the region of their linear response. Any intensities which produced saturation were reduced by placing calibrated neutral density filters in the beam of the laser whose backscattered intensity was causing

the saturation thus reducing the incident intensity and bringing the detector back into its linear response region. The errors in the densities given for the filters were believed to be small but were not accurately known. The differences in the results from the two lasers when specular reflections were being detected could be due, in part, to the difference in laser output power and in the errors in the values for the densities of the filters since they were generally used when very specular reflections were being detected.

CHAPTER V

DISCUSSION OF EXPERIMENTAL RESULTS

The polarization ratios $R^{\perp}$ and $R^{/\!/}$ given by Equation 34 are shown in Figure 9. (Superscripts denote the polarization of the incident beam, with superscript u denoting unpolarized. Subscripts denote the transmission direction of the receiver polarizers with subscript u implying the receiver is unbiased with respect to polarization.) The percent depolarizations $PD^{\perp}$ and $PD^{/\!/}$ given by Equation 40 are shown in Figure 10. The basic backscattered fractions $B_{\perp}^{\perp}$, $B_{/\!/}^{\perp}$, $B_{\perp}^{/\!/}$, and $B_{/\!/}^{/\!/}$ given by Equation 42 are shown in Figure 11. The backscattered fractions measured by a detector unbiased with respect to polarization and the backscattered fractions for unpolarized incident radiation $B_{U}^{\perp}$, $B_{U}^{/\!/}$, $B_{\perp}^{U}$, $B_{/\!/}^{U}$, and B_{U}^{U} given by Equations 43, 44, 45, 46, and 47, are shown in Figure 12. For the polarization ratios and percent depolarizations, the inner error bars give the expected error of the plotted data point, which is an average, and the outer error bars are the limits of the expected error bars of the values which were averaged to obtain the plotted data point. The latter gives an indication of the dispersion of the individual measurements. The error bars on the backscattered fractions indicate the expected errors.

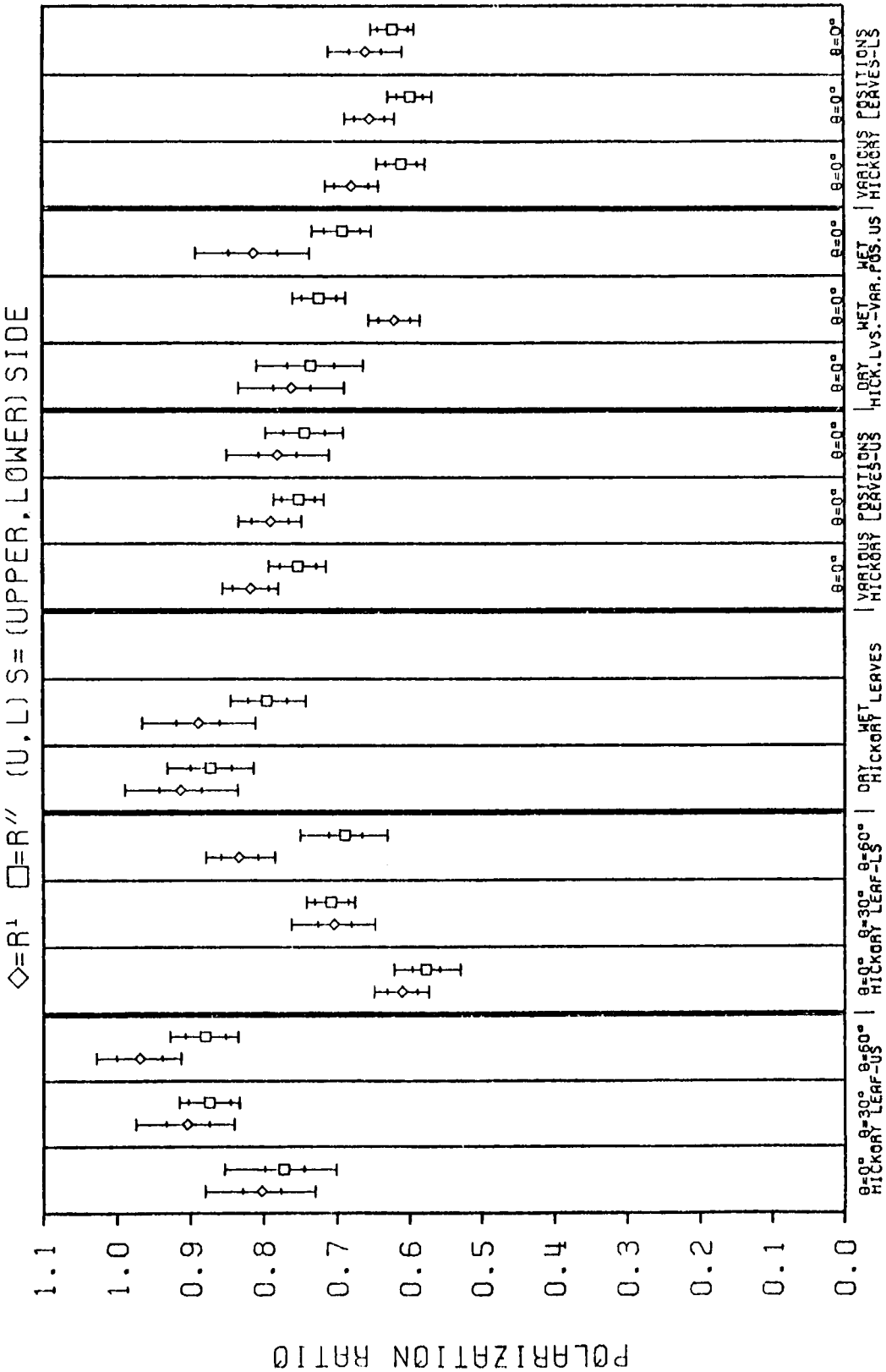


Figure 9. Polarization ratios.

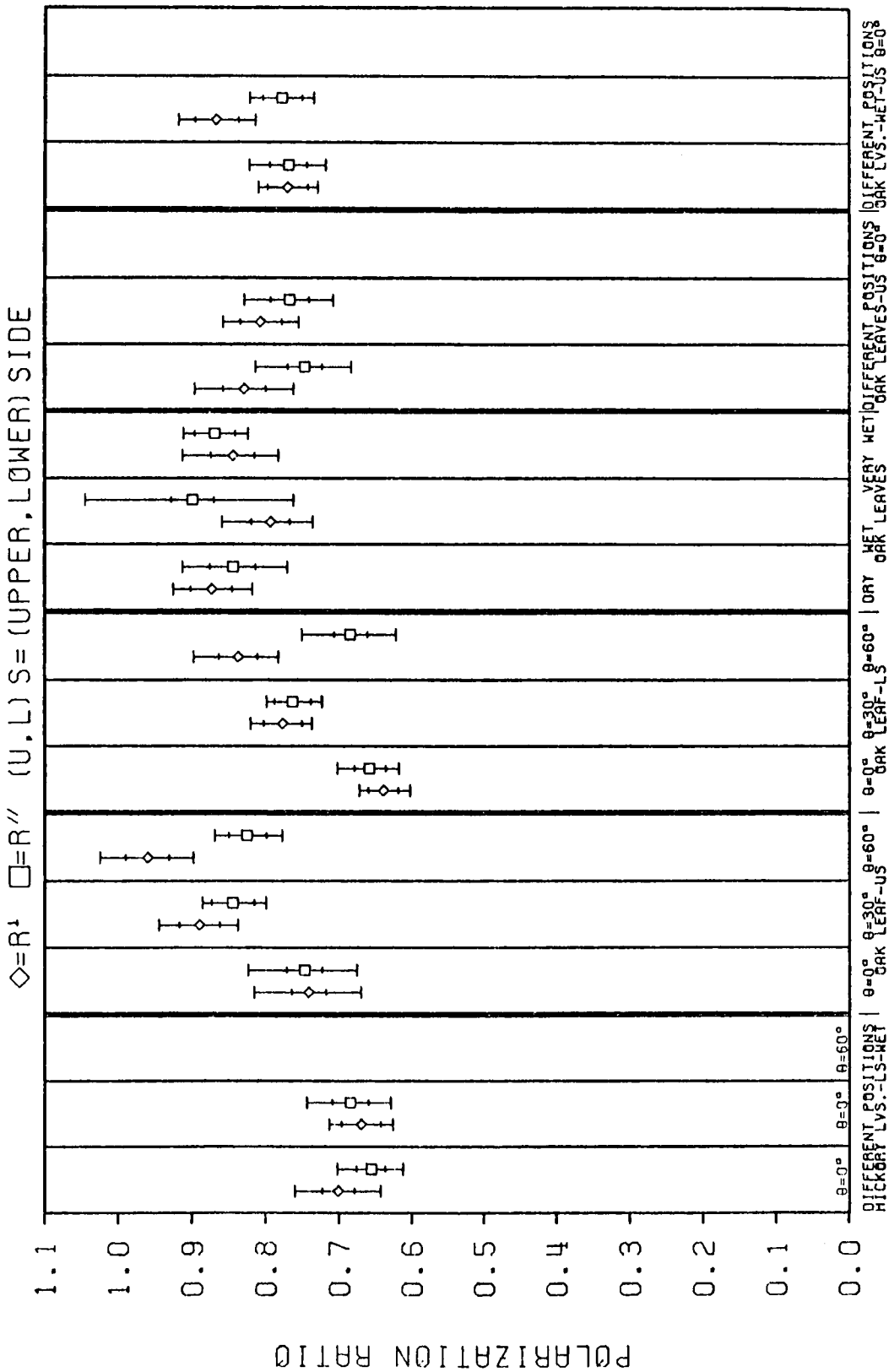


Figure 9. (continued)

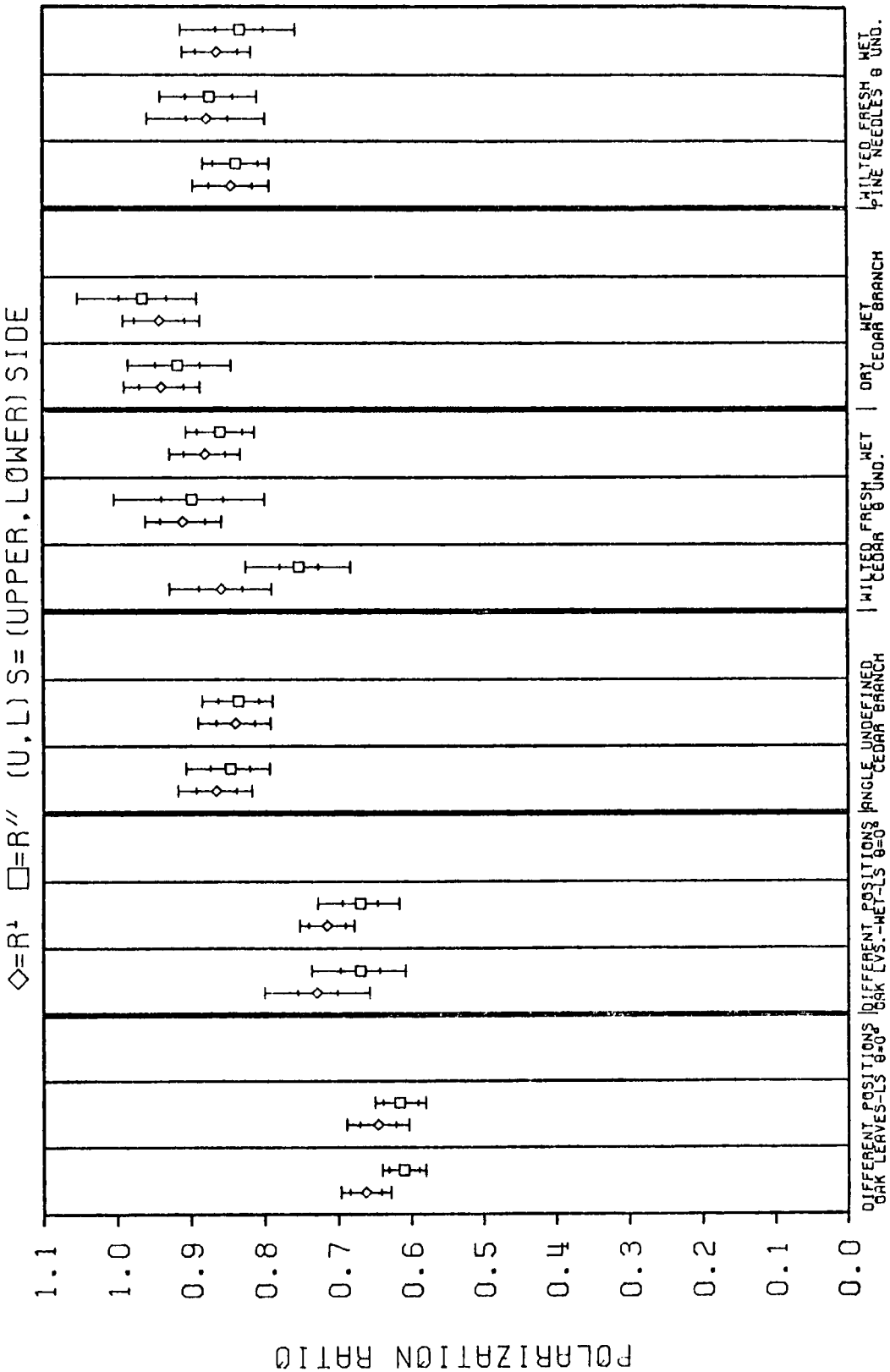


Figure 9. (continued)

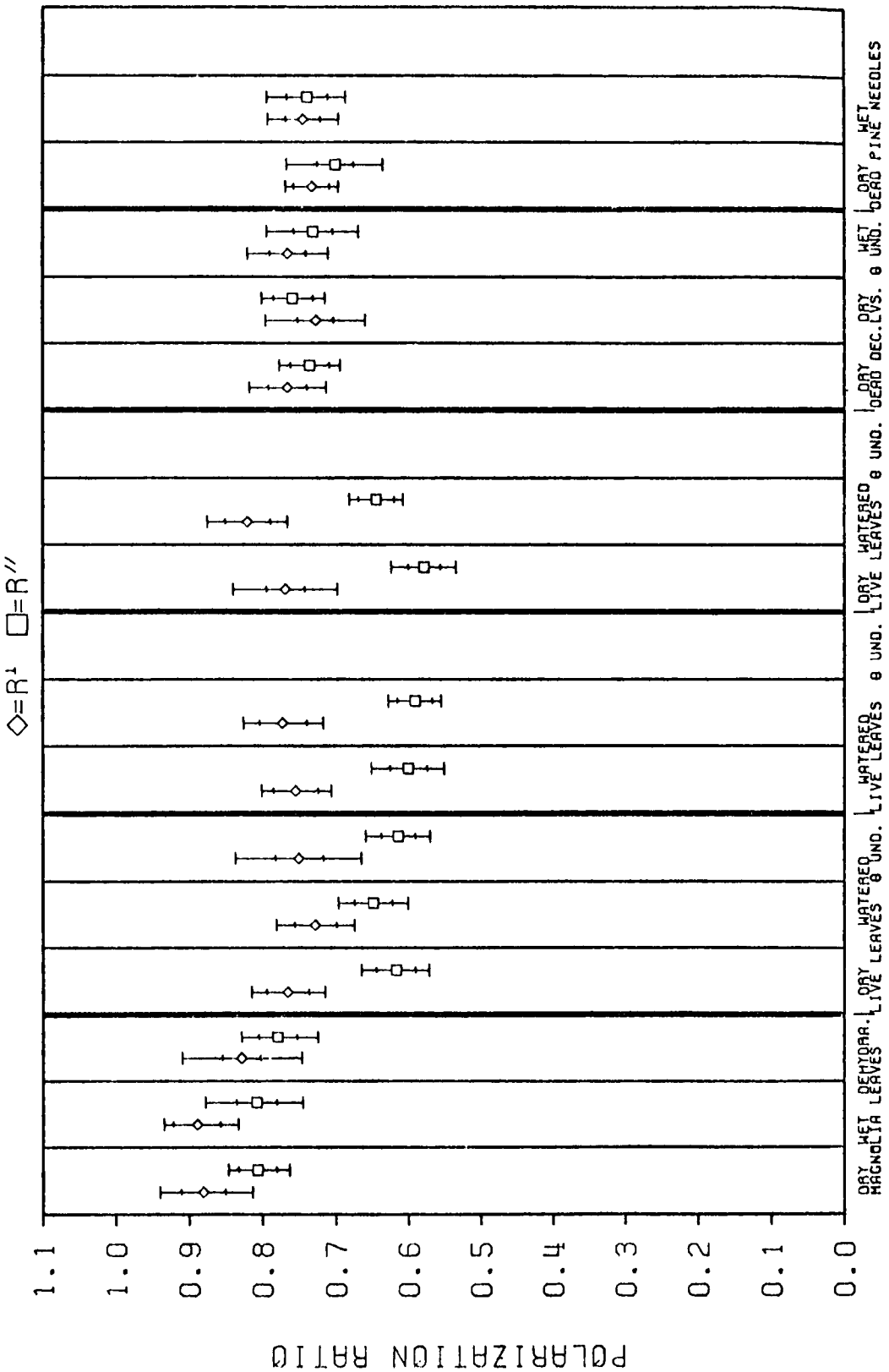


Figure 9. (continued)

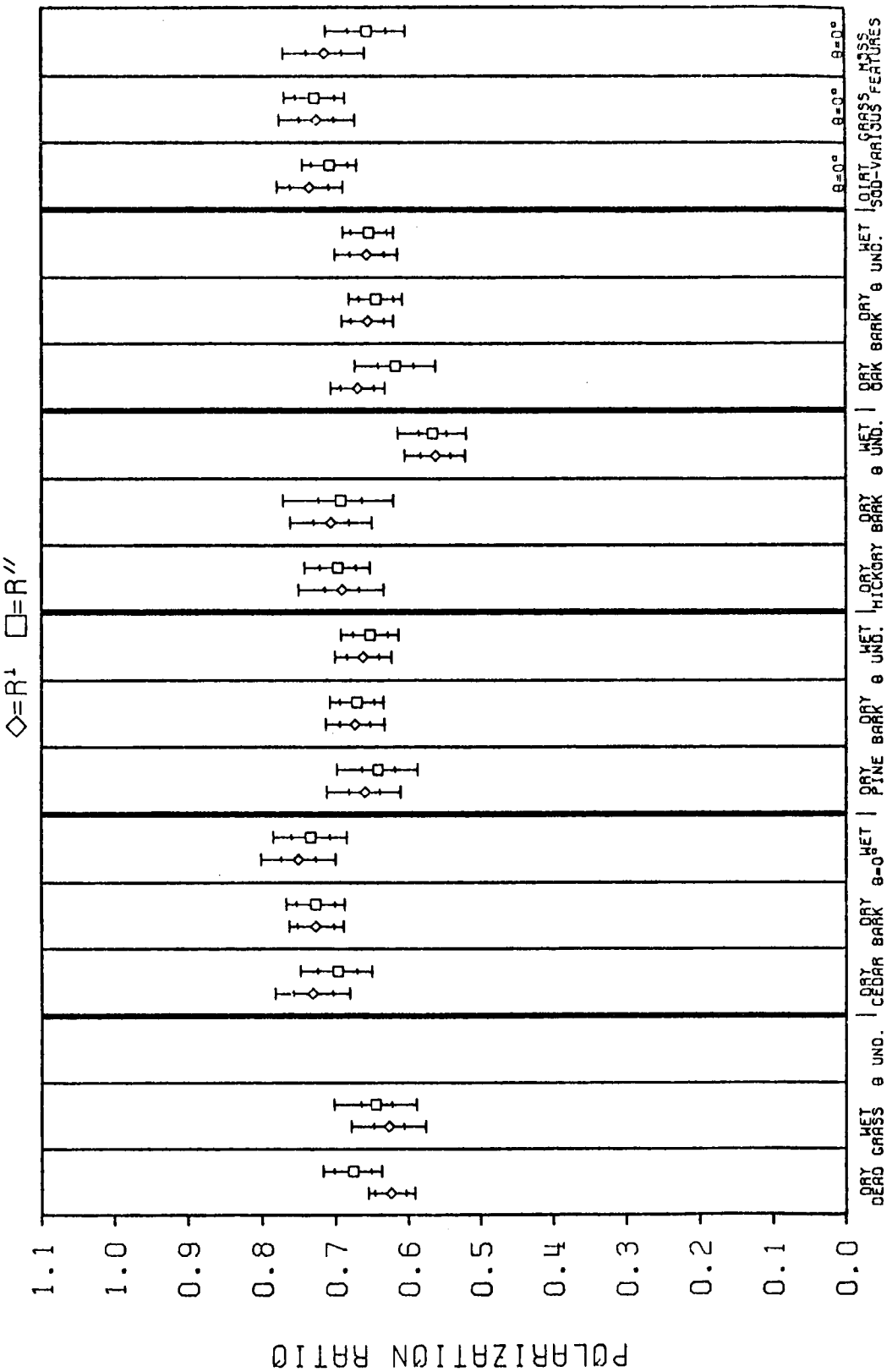


Figure 9. (continued)

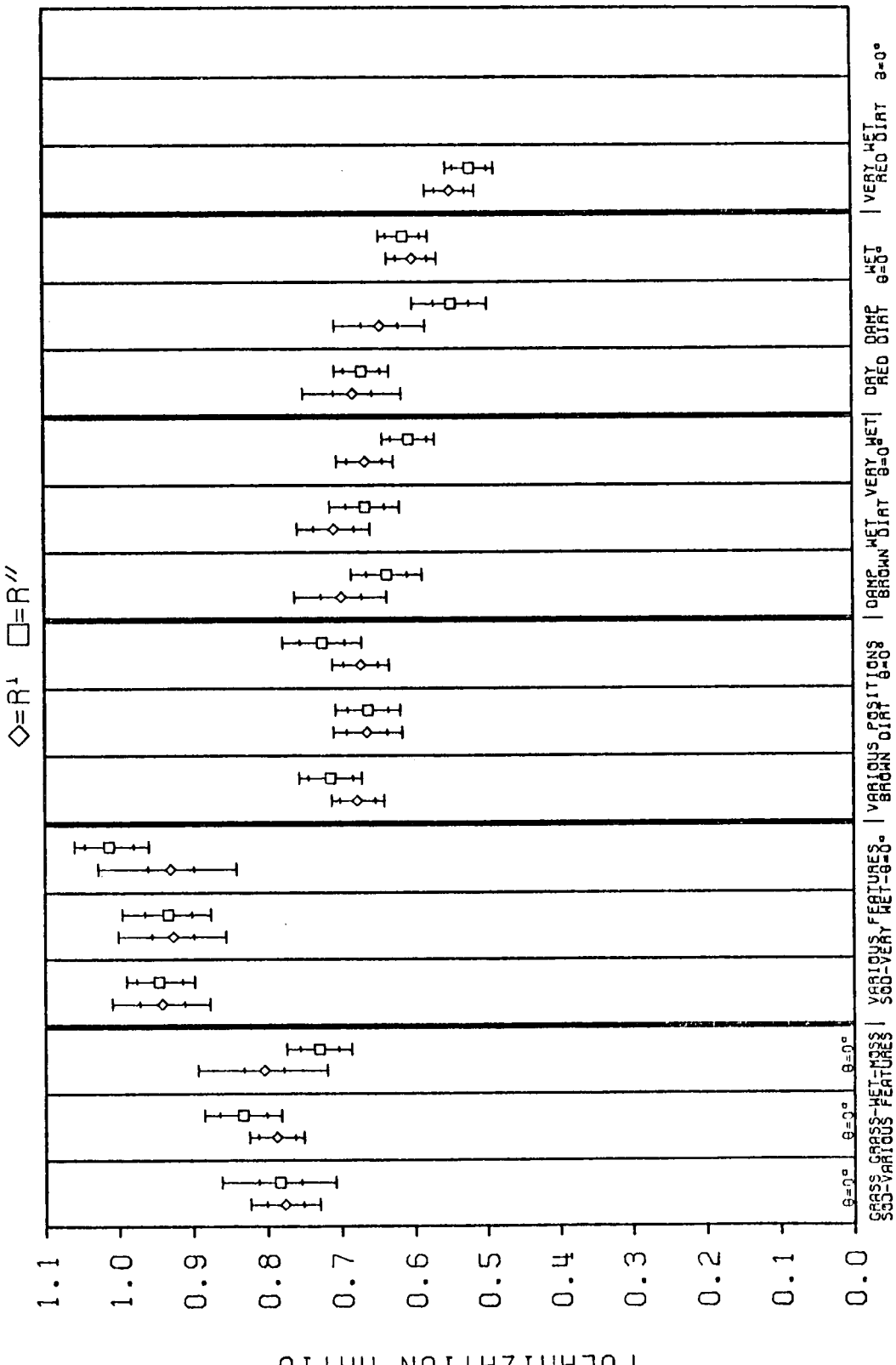


Figure 9. (continued)

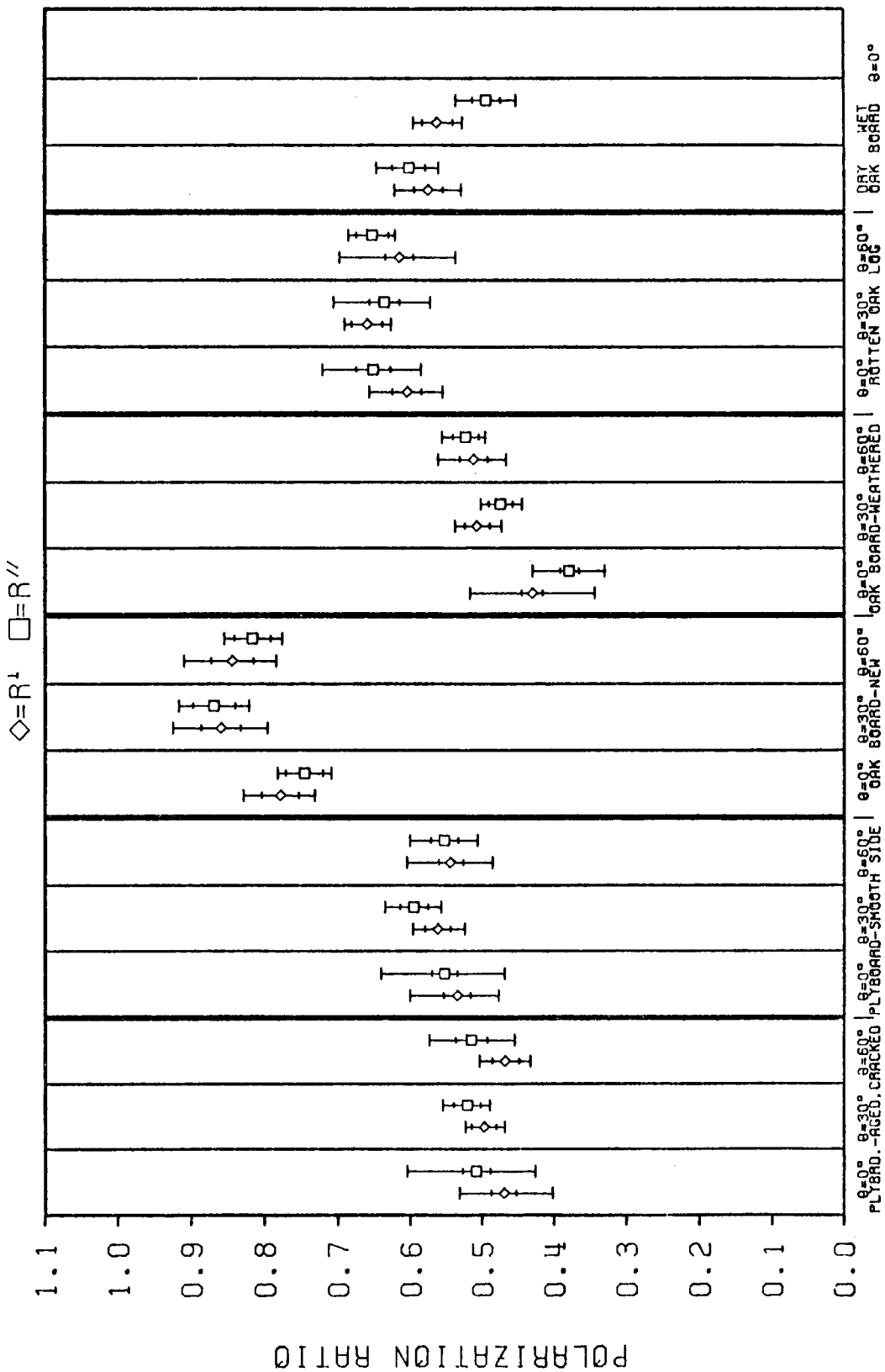


Figure 9. (continued)

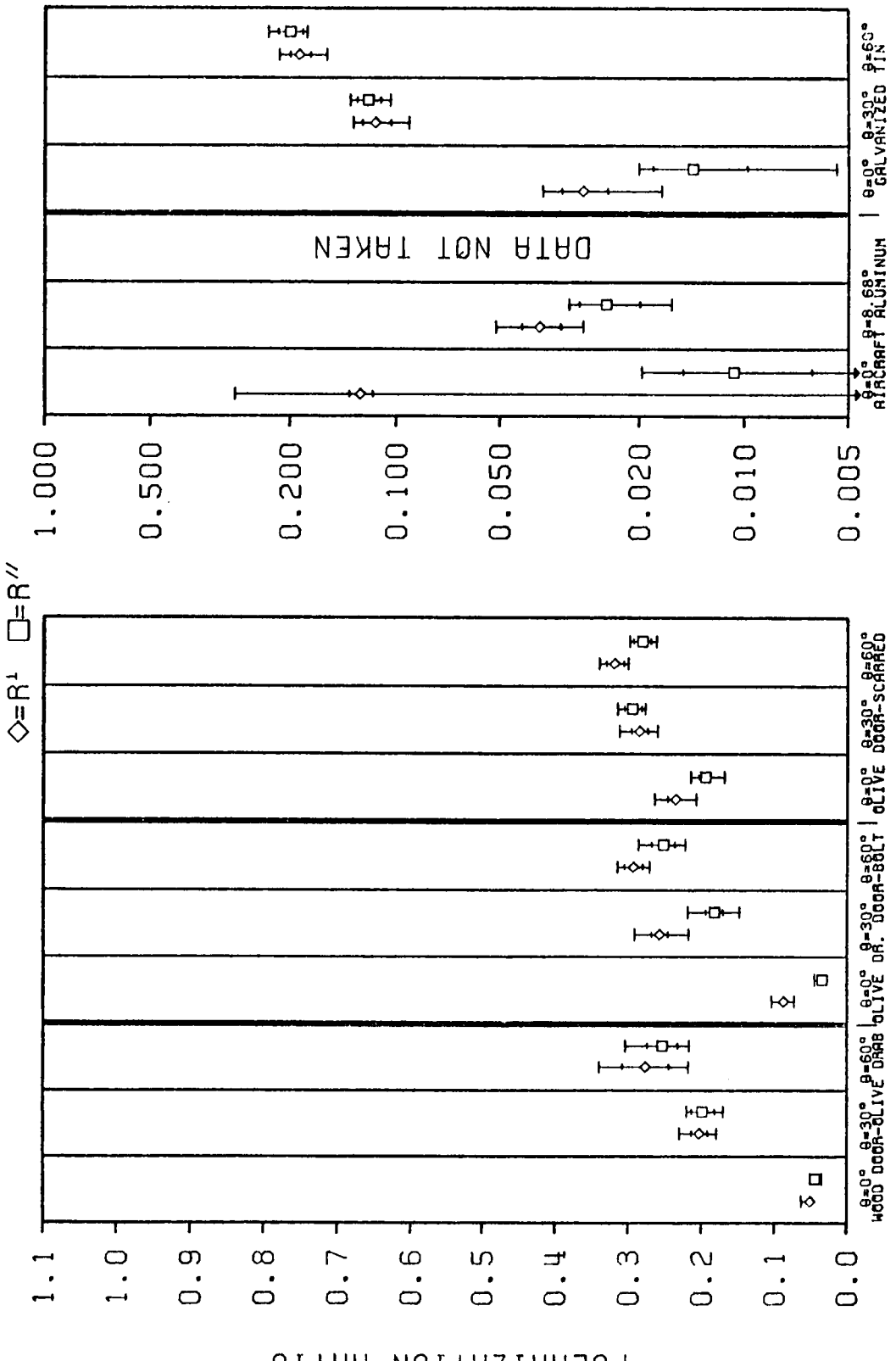


Figure 9. (continued)

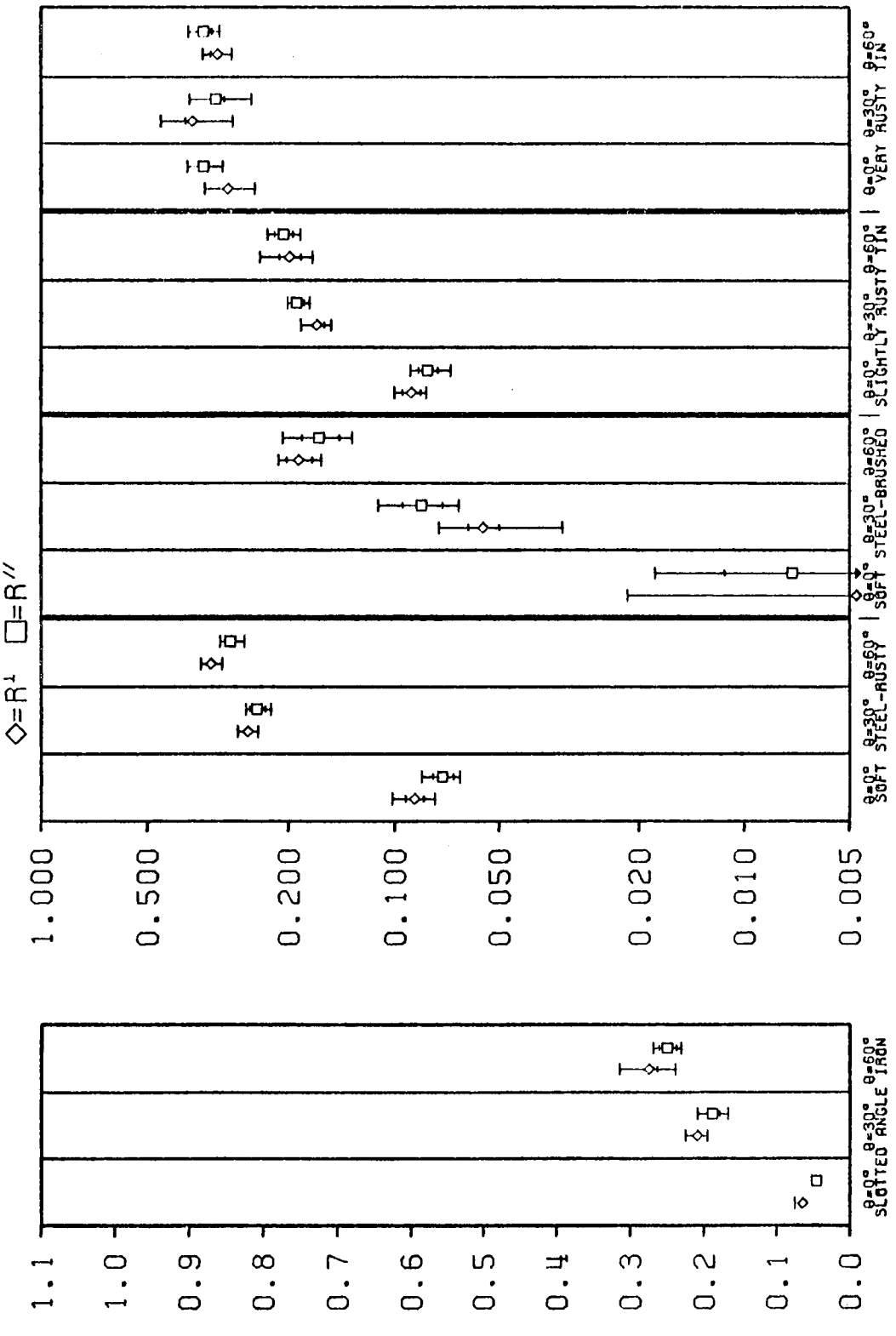


Figure 9. (continued)

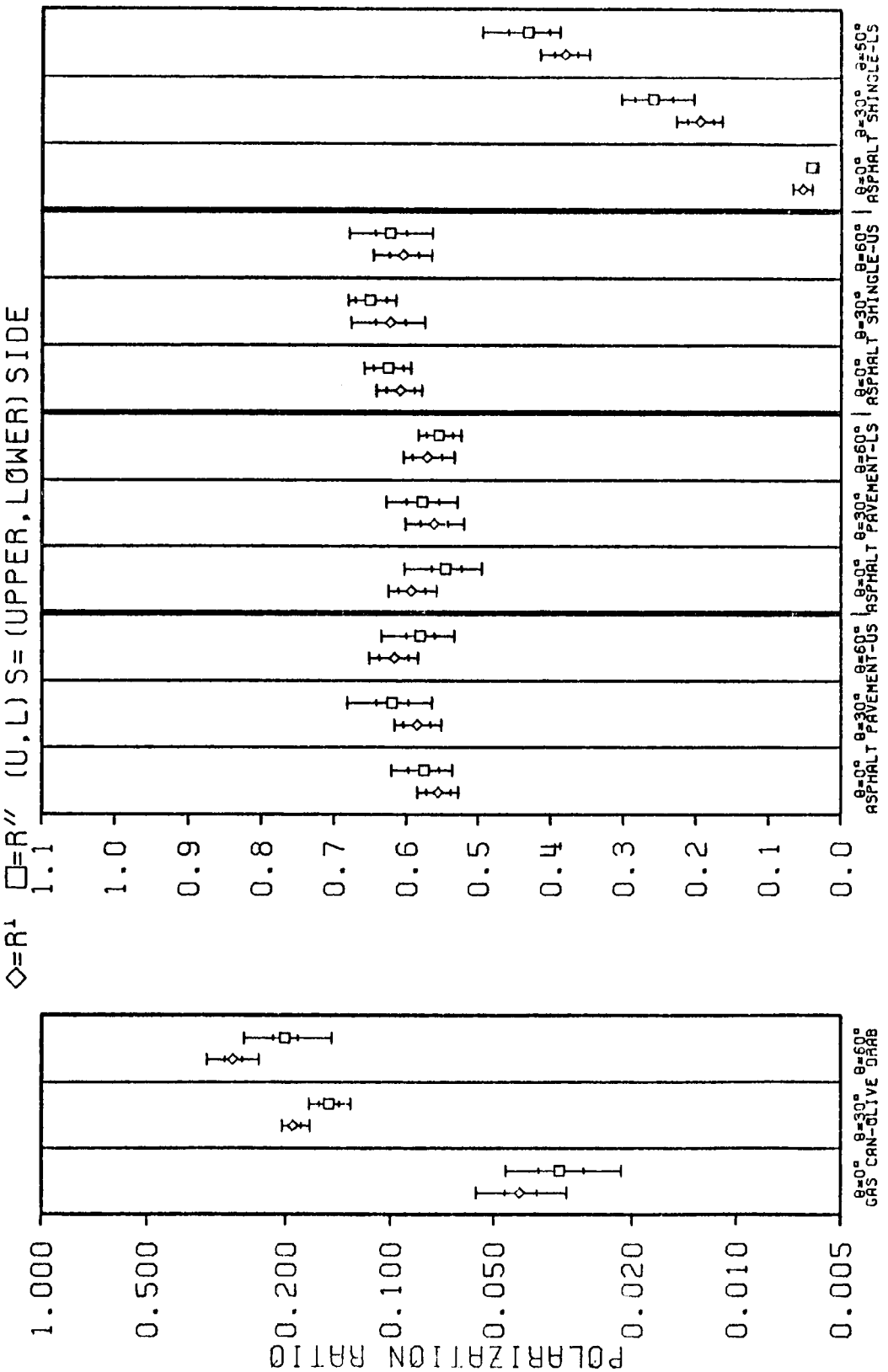


Figure 9. (continued)

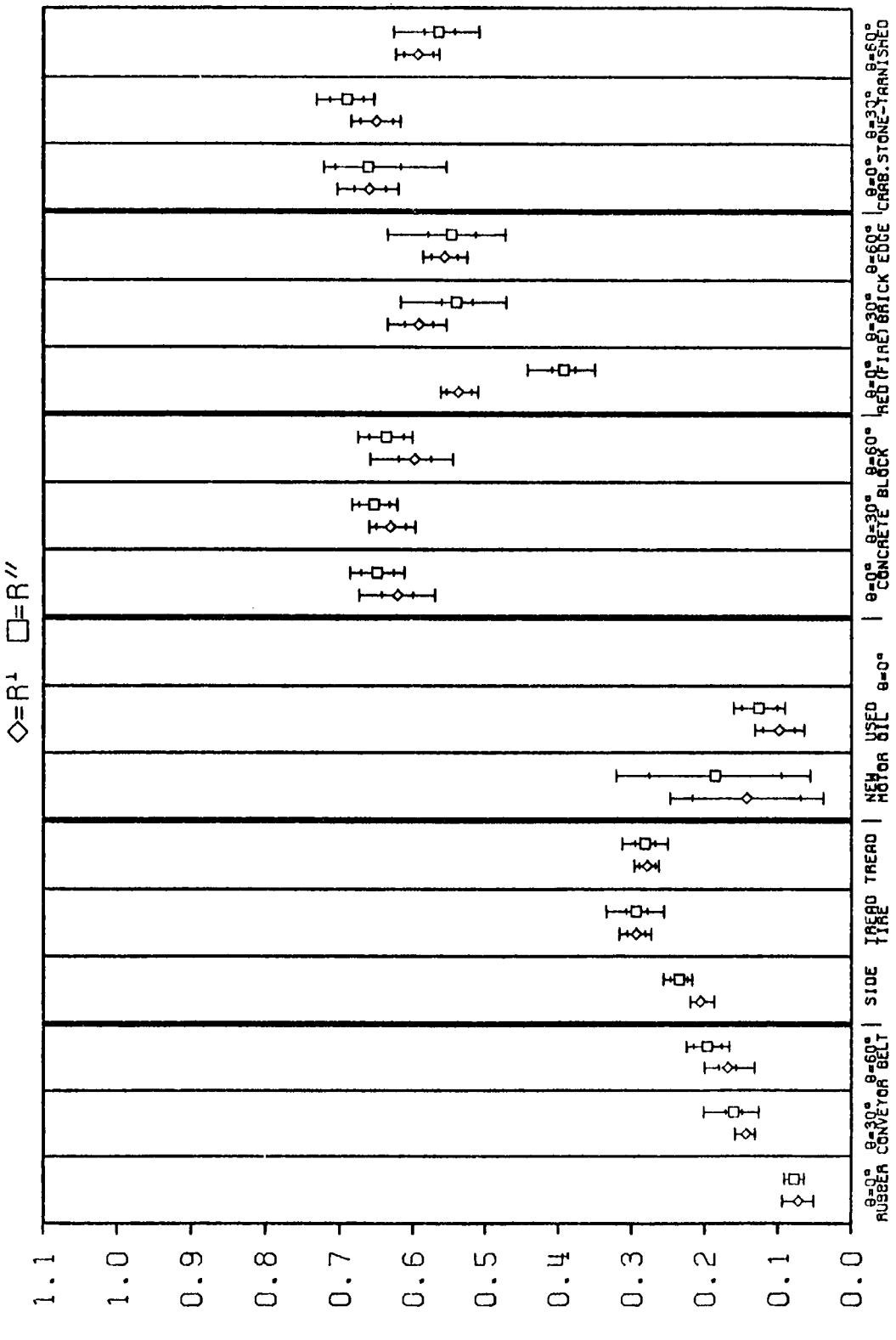


Figure 9. (continued)

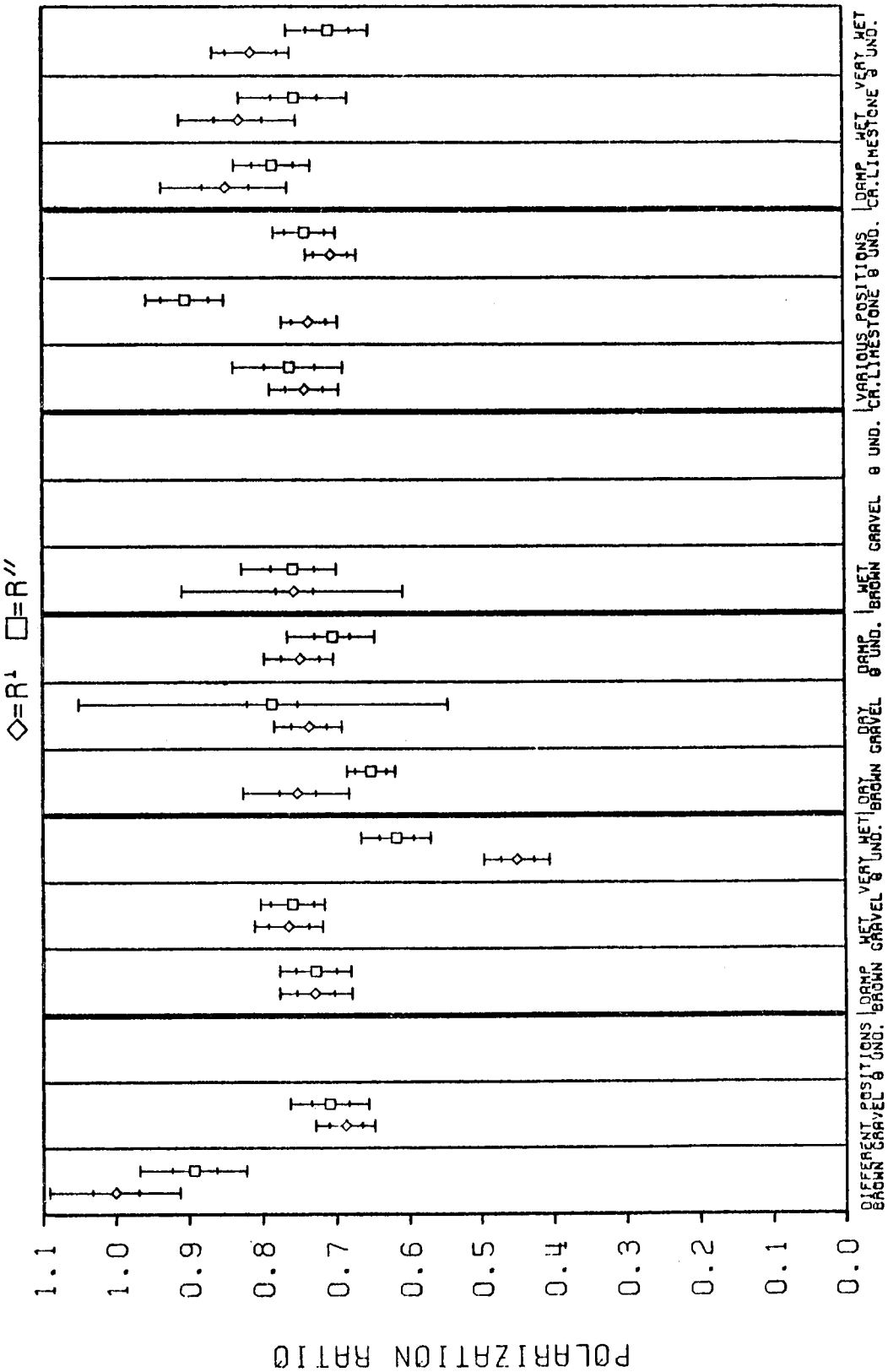


Figure 9. (continued)

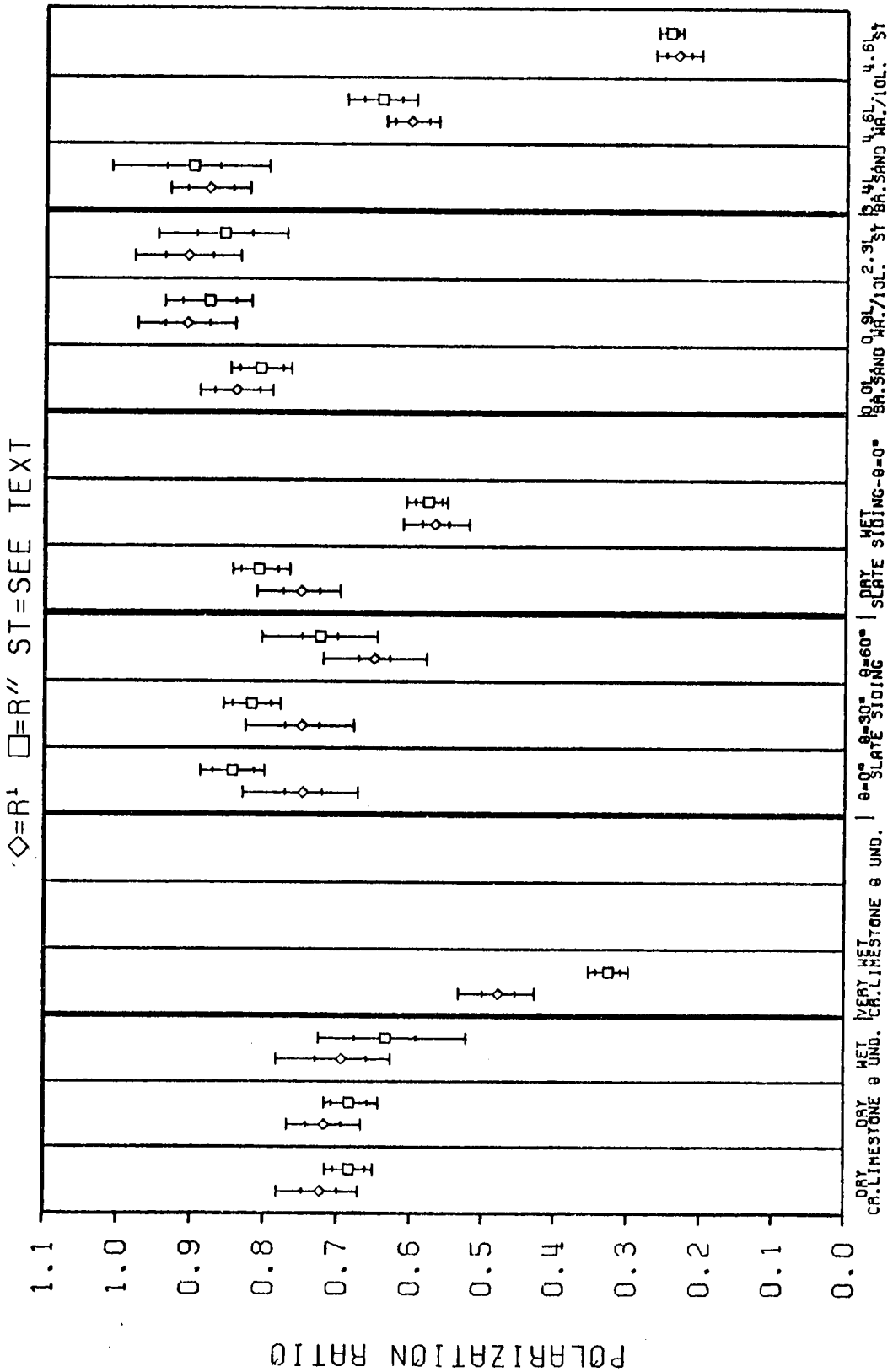


Figure 9. (continued)

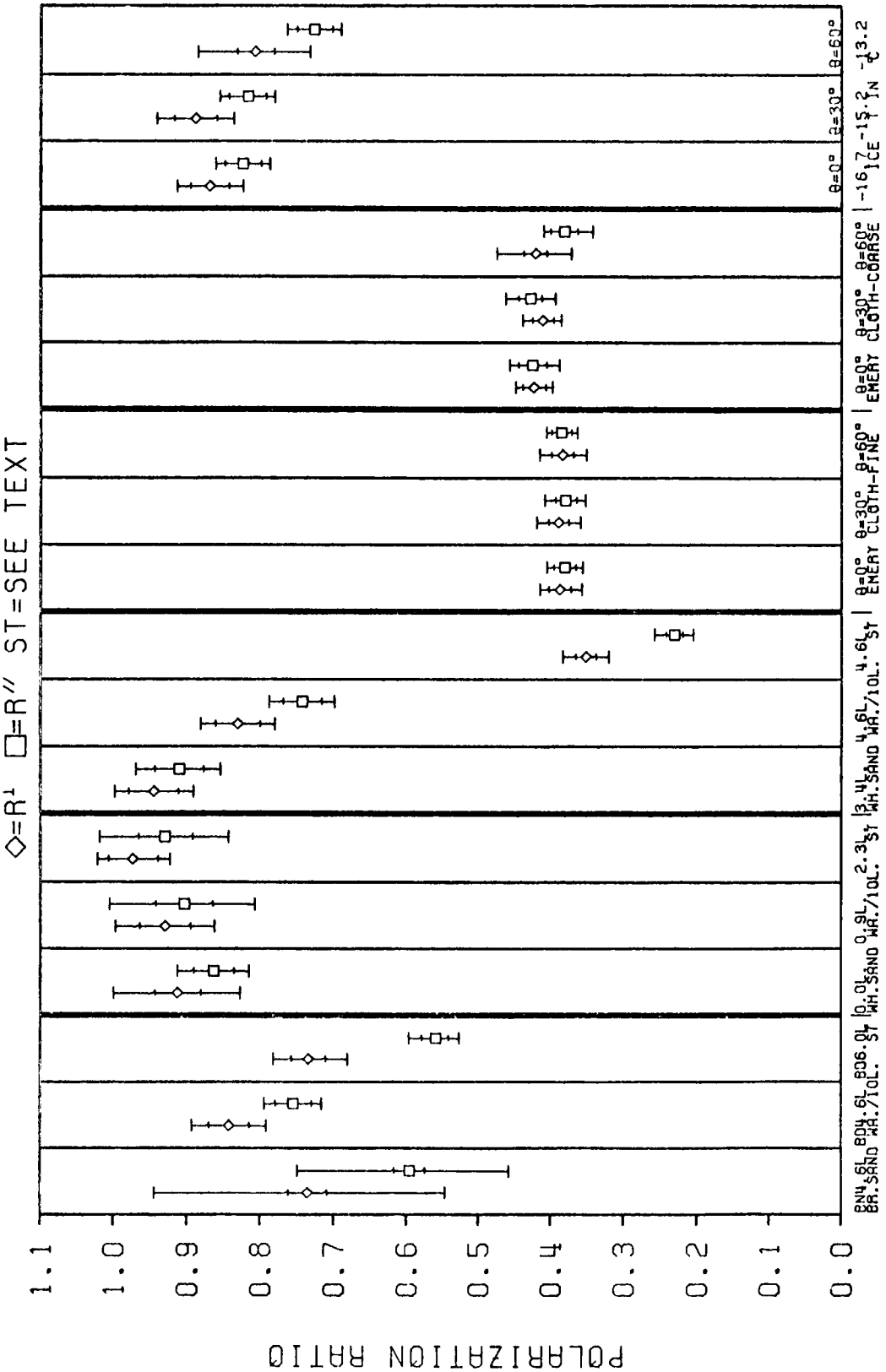


Figure 9. (continued)

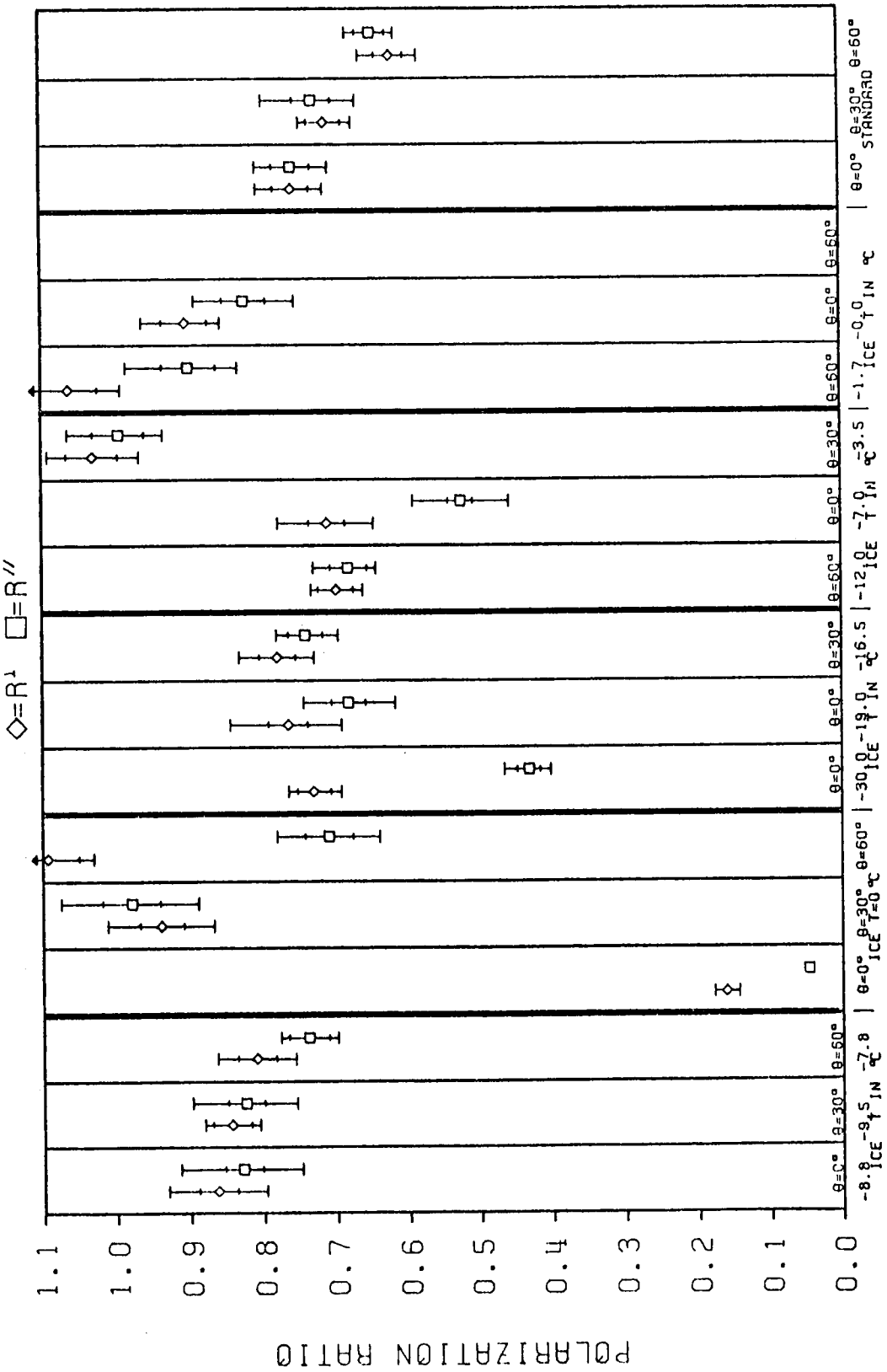


Figure 9. (continued)

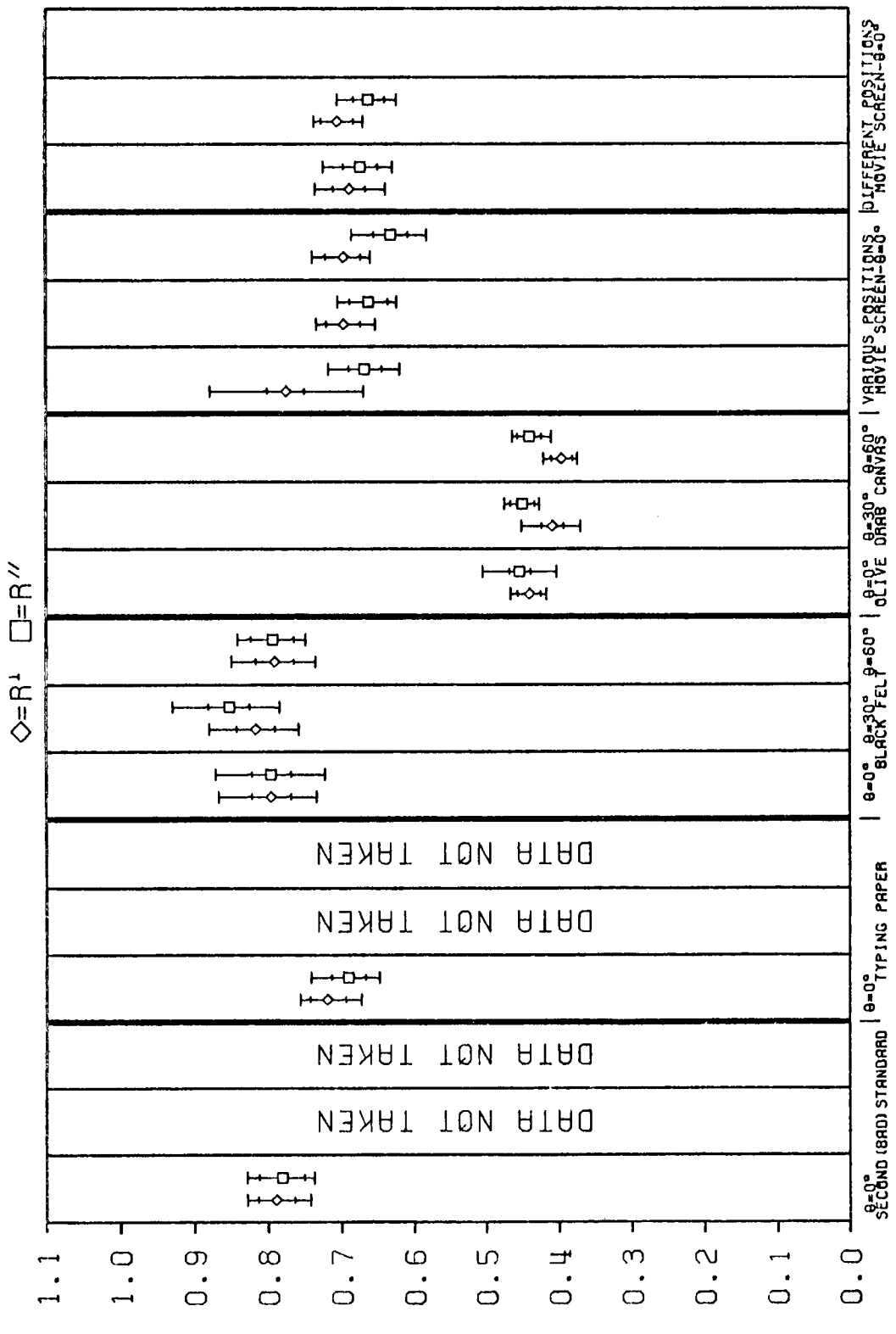


Figure 9. (continued)

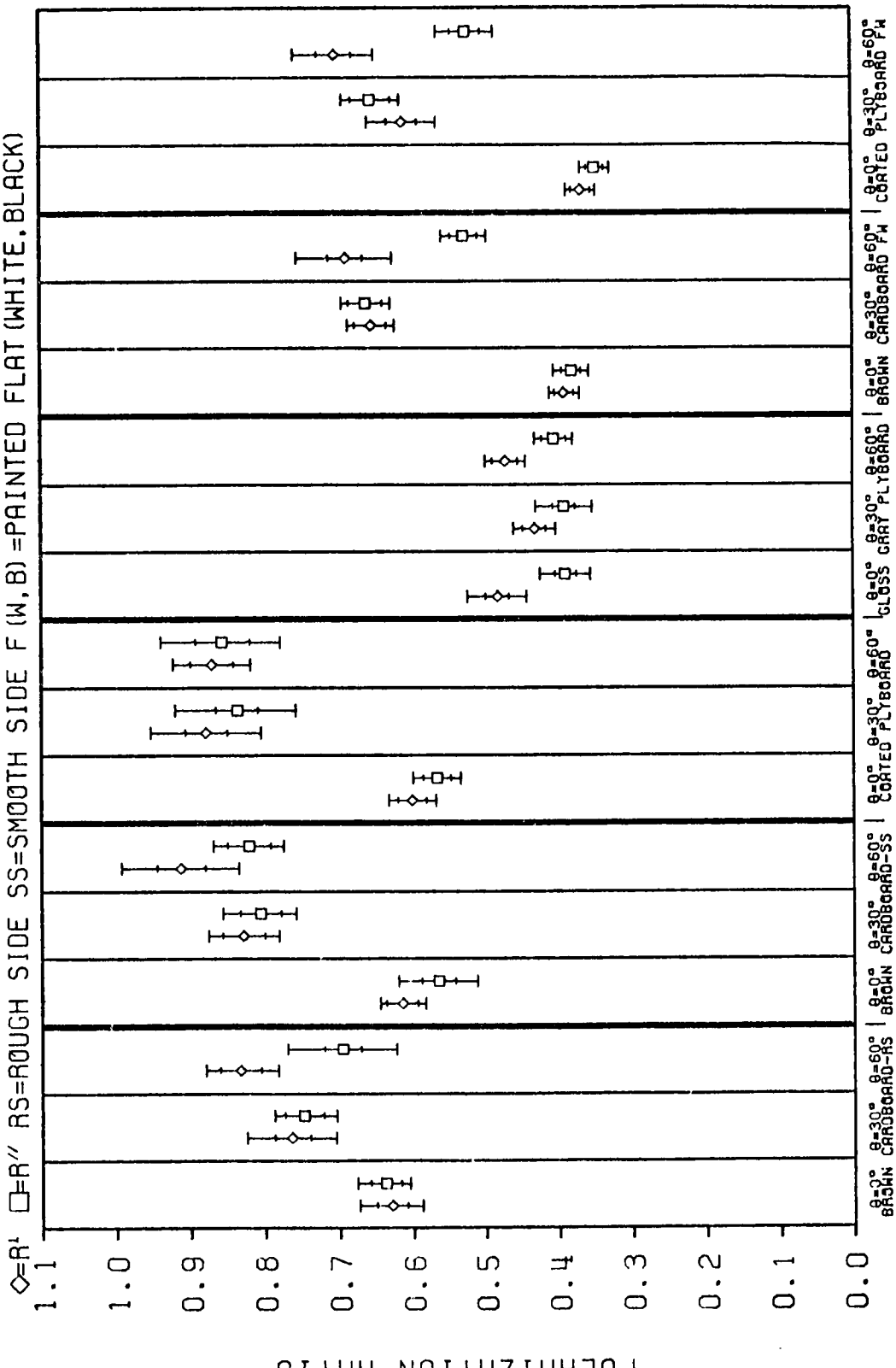


Figure 9. (continued)

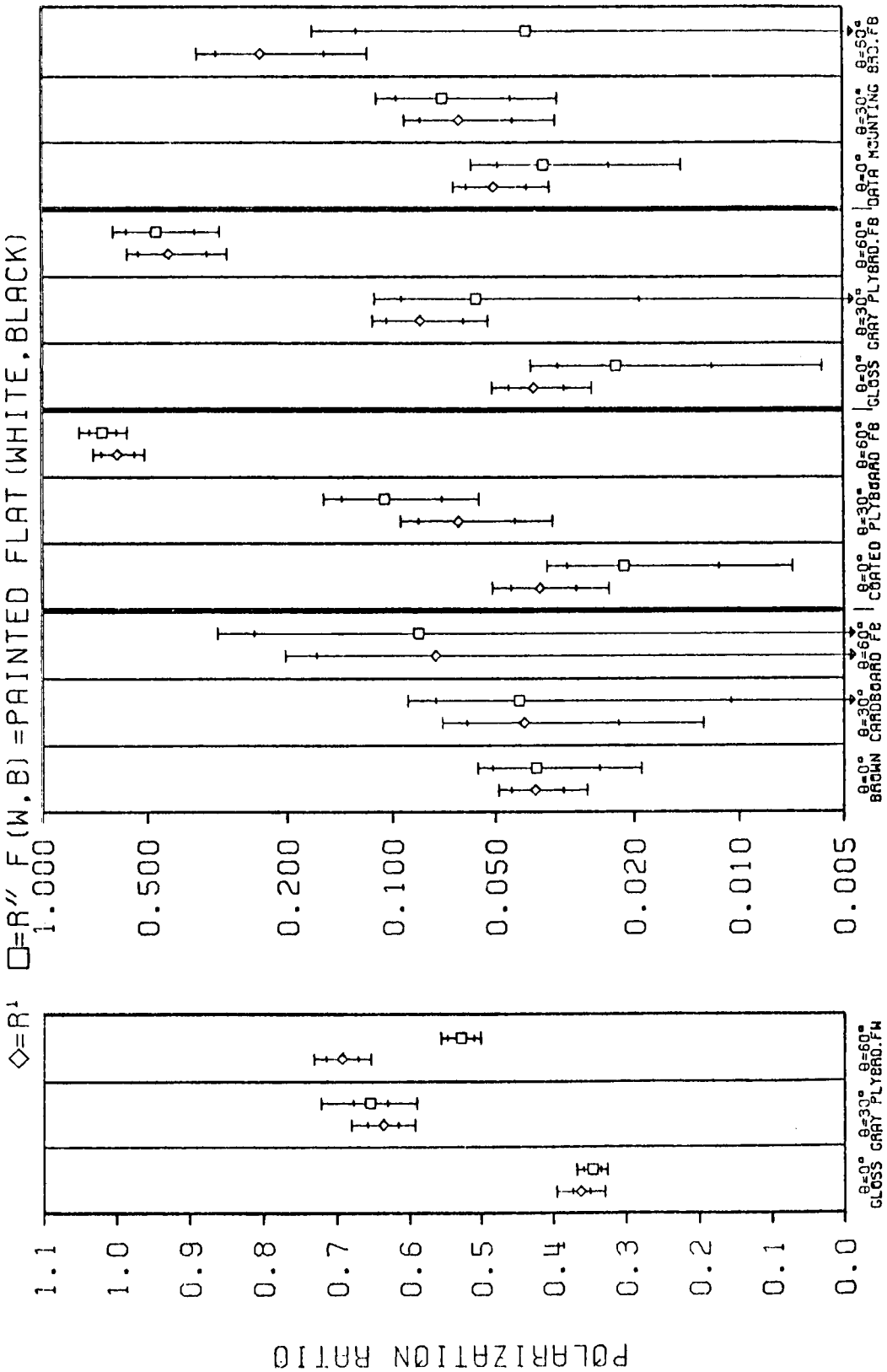


Figure 9. (continued)

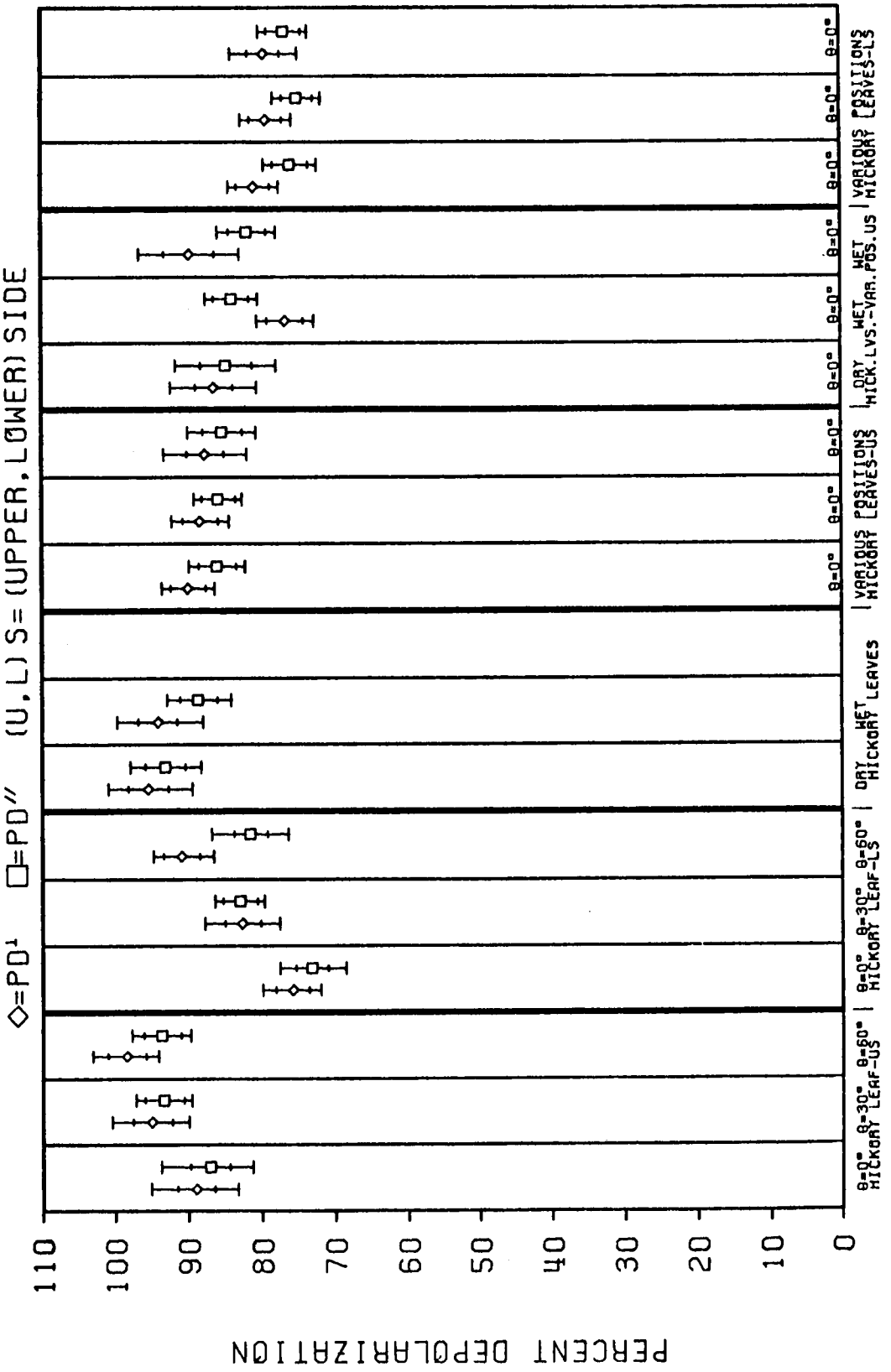


Figure 10. Percentages of depolarization.

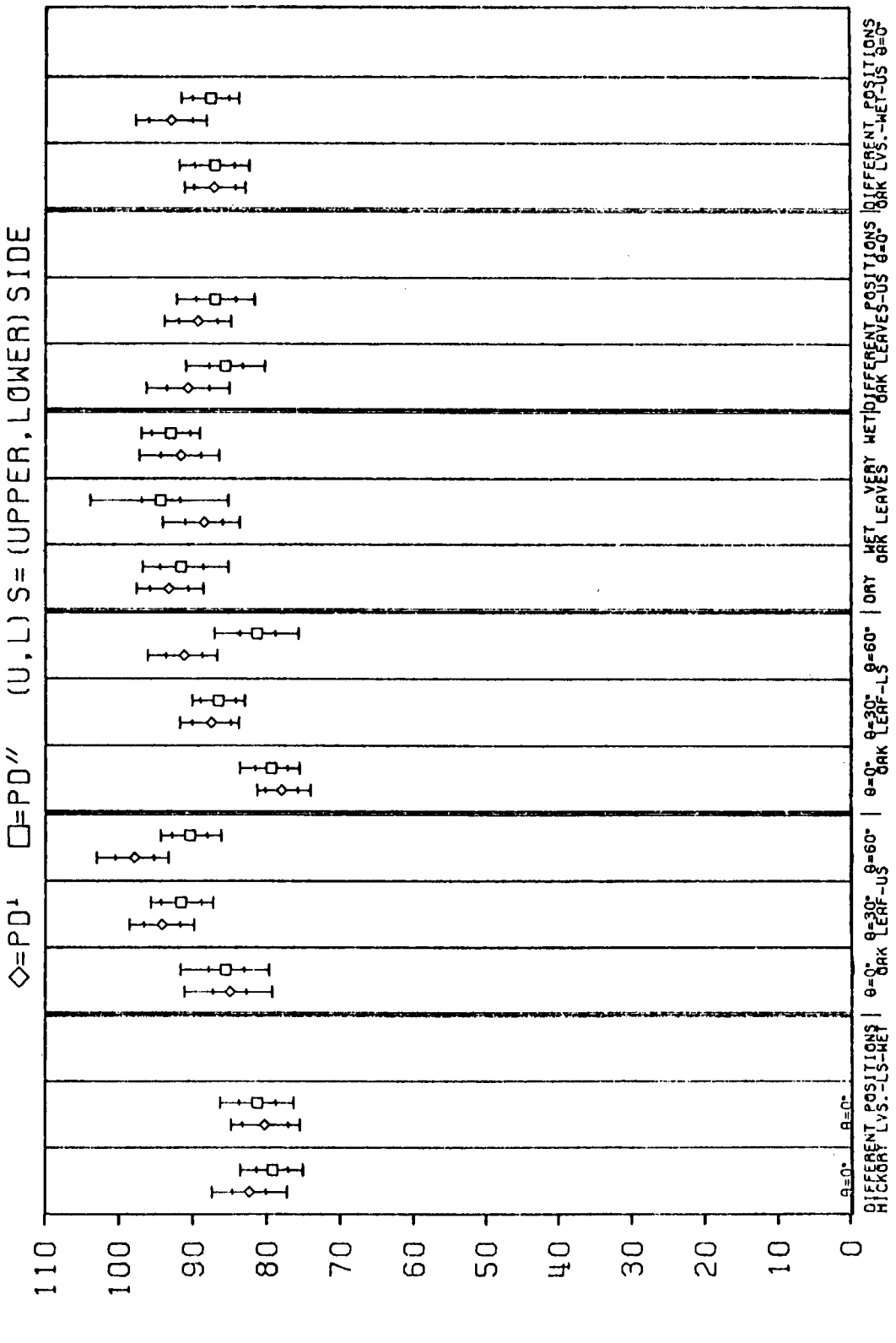


Figure 10. (continued)

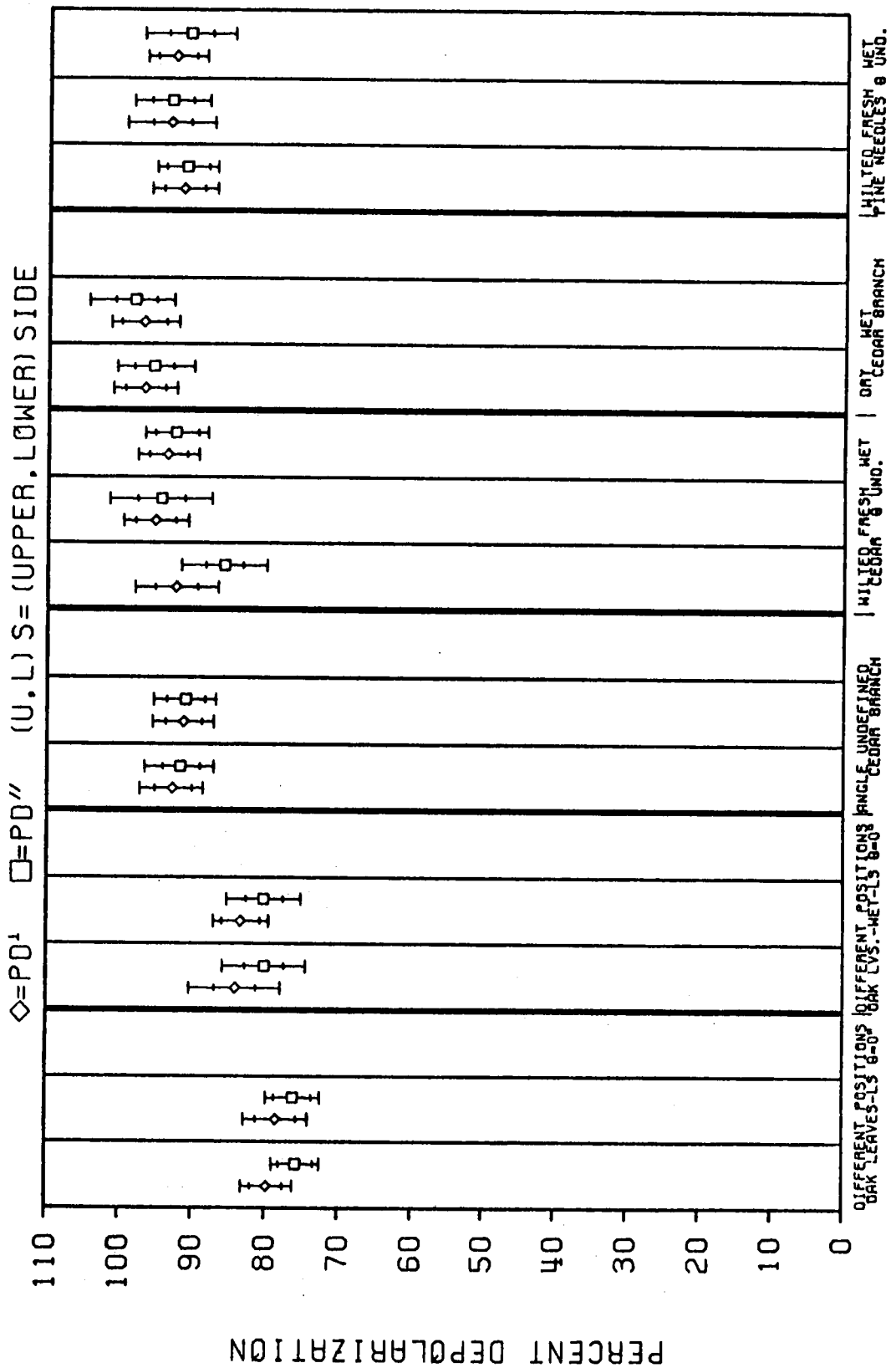


Figure 10. (continued)

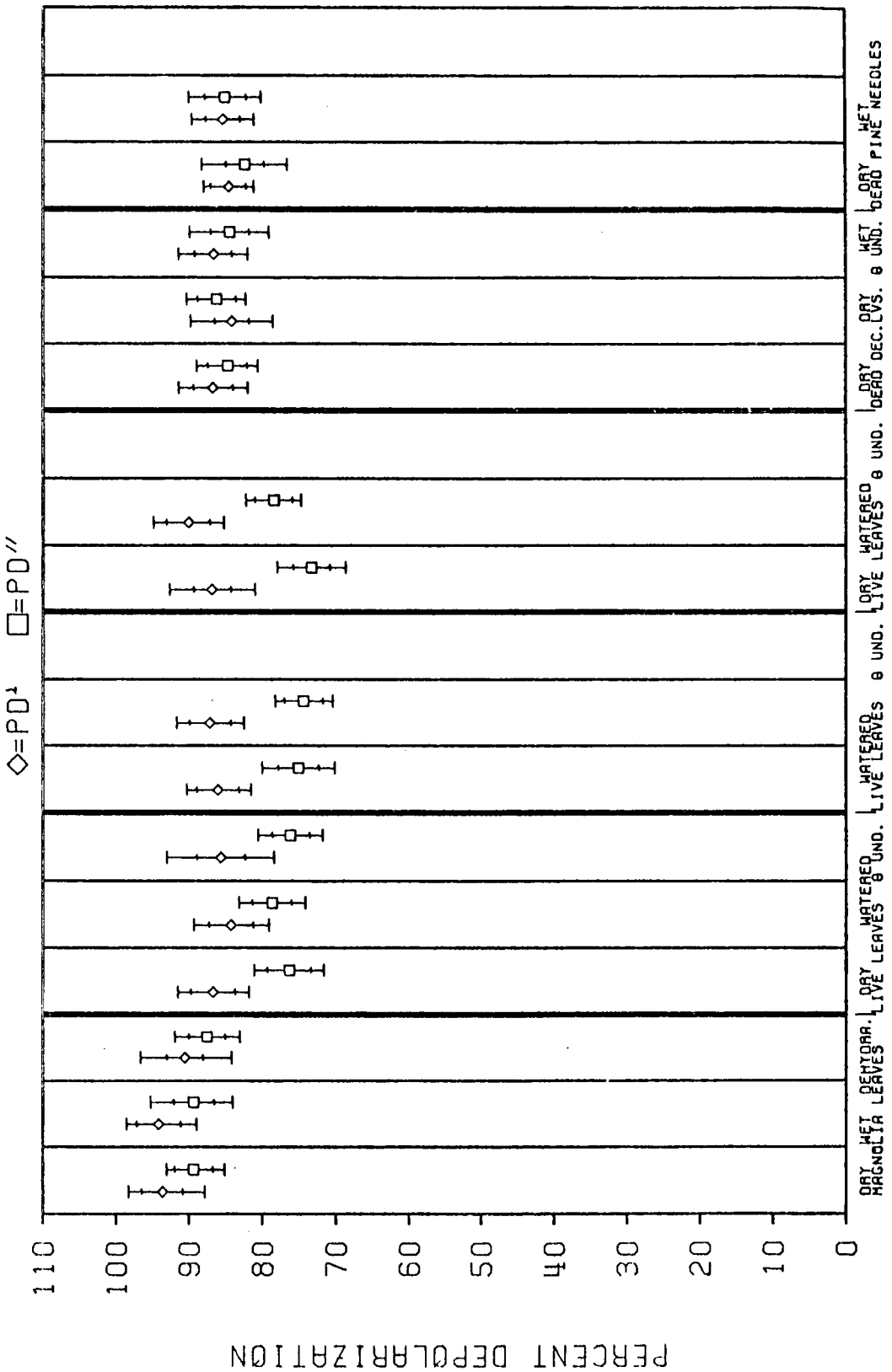


Figure 10. (continued)

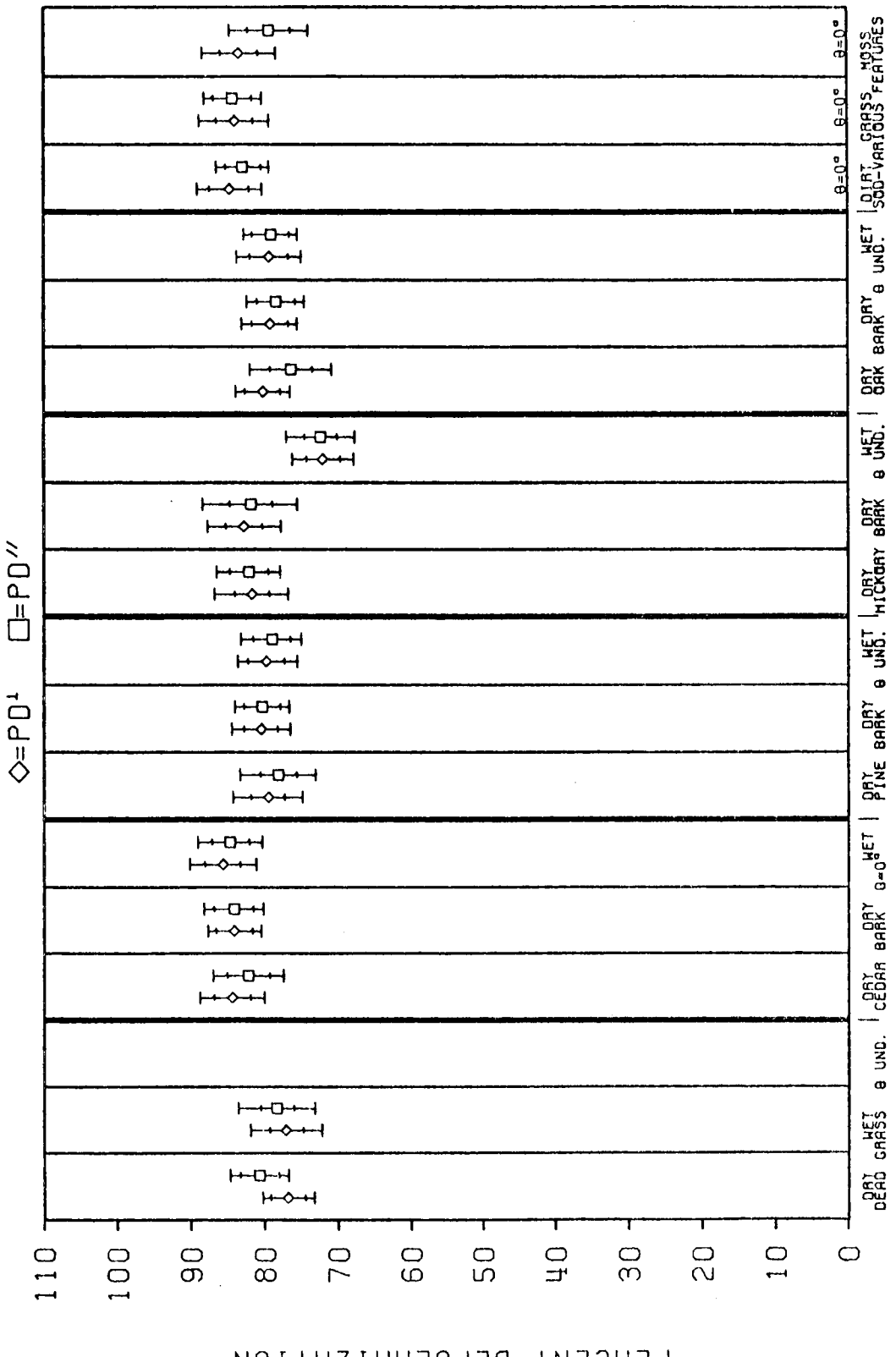


Figure 10. (continued)

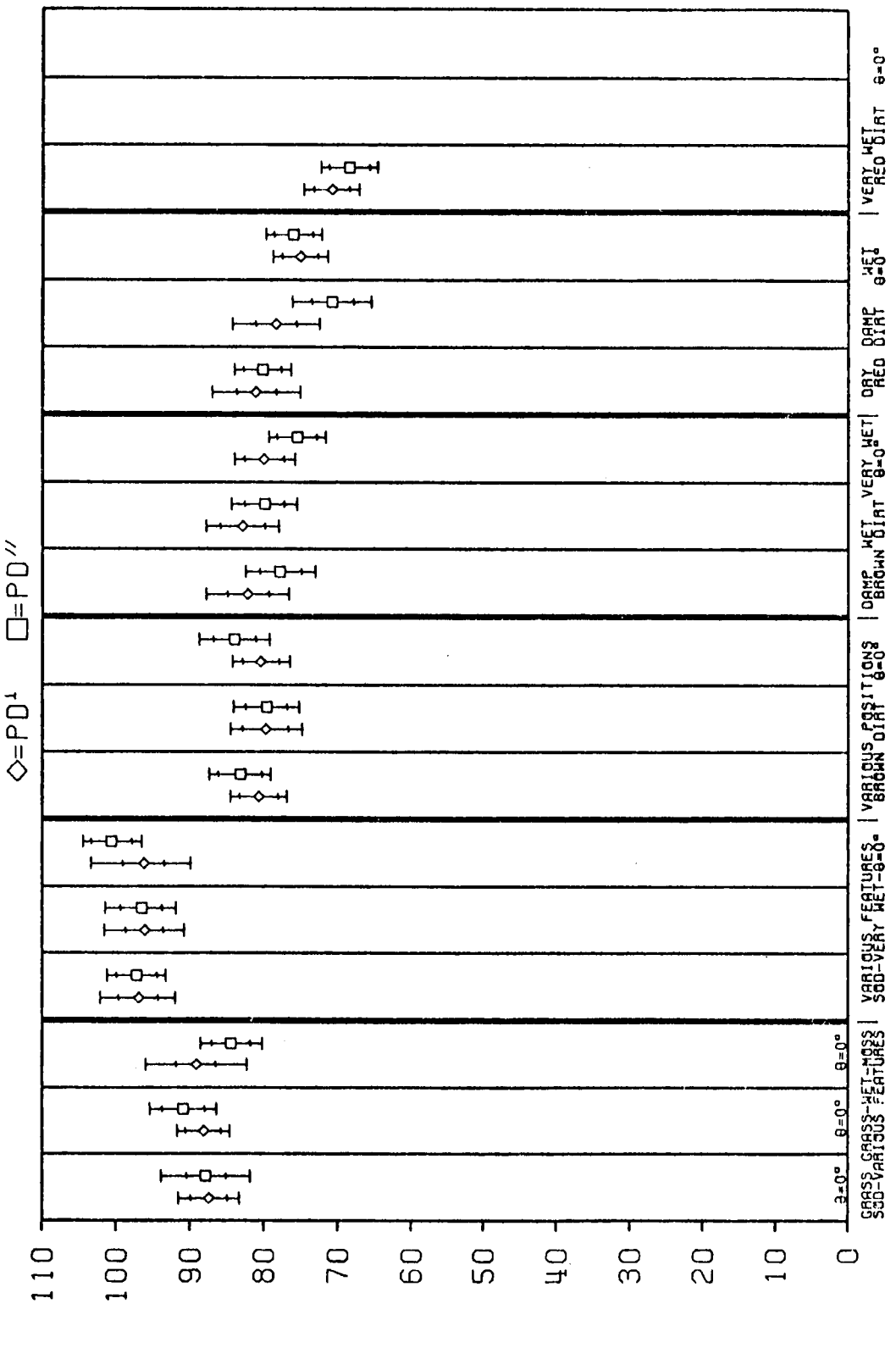


Figure 10. (continued)

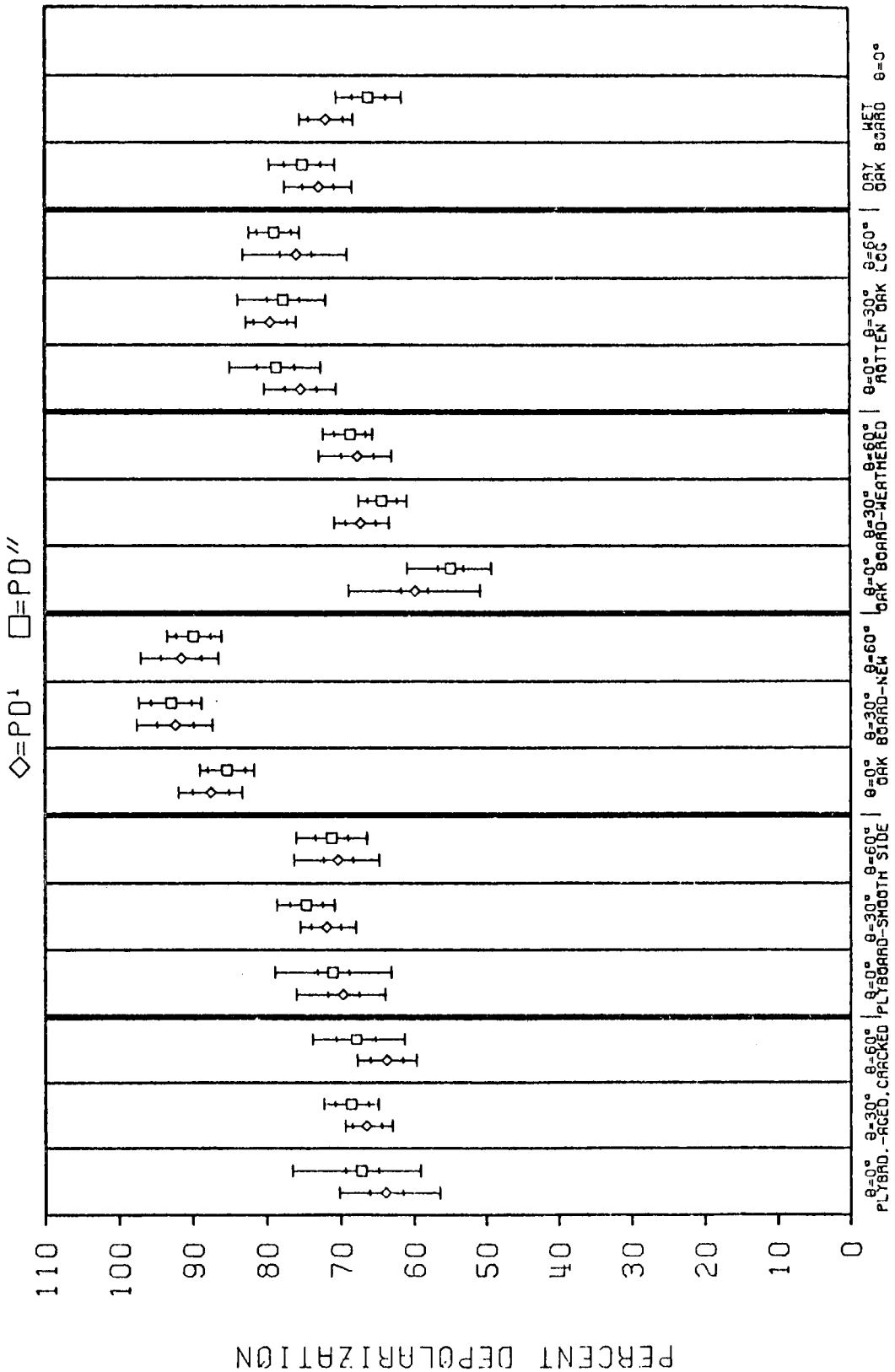


Figure 10. (continued)

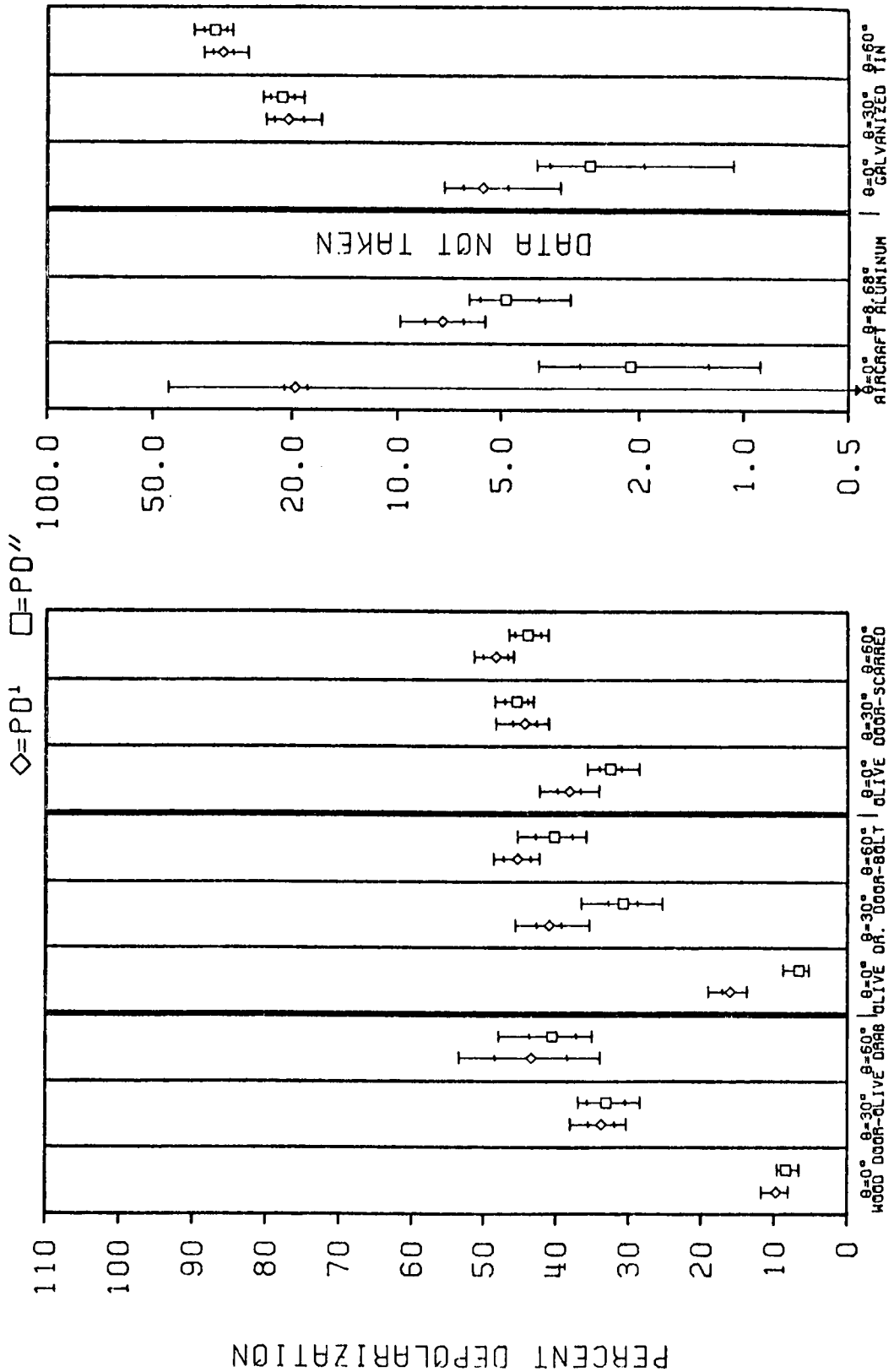


Figure 10. (continued)

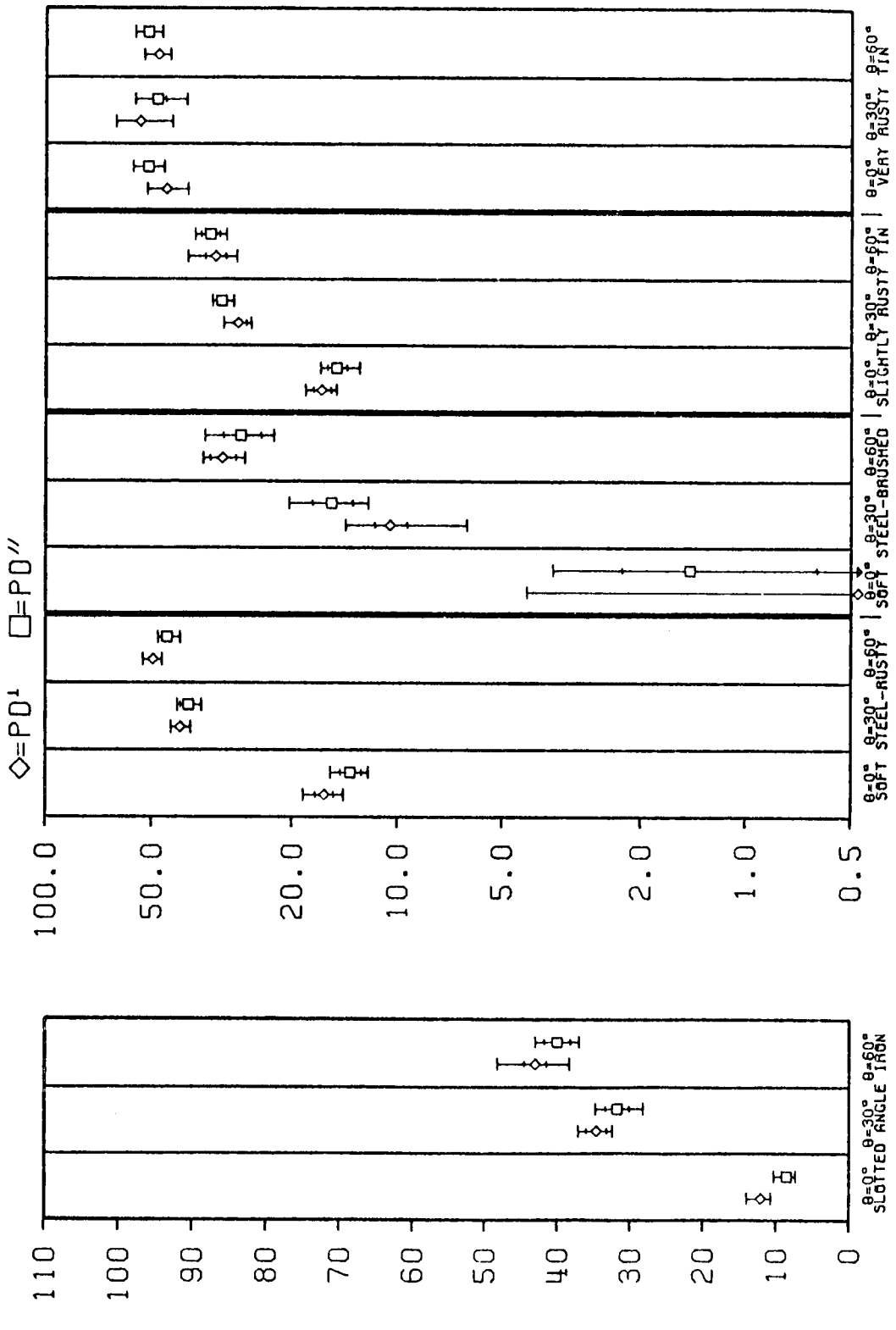


Figure 10. (continued)

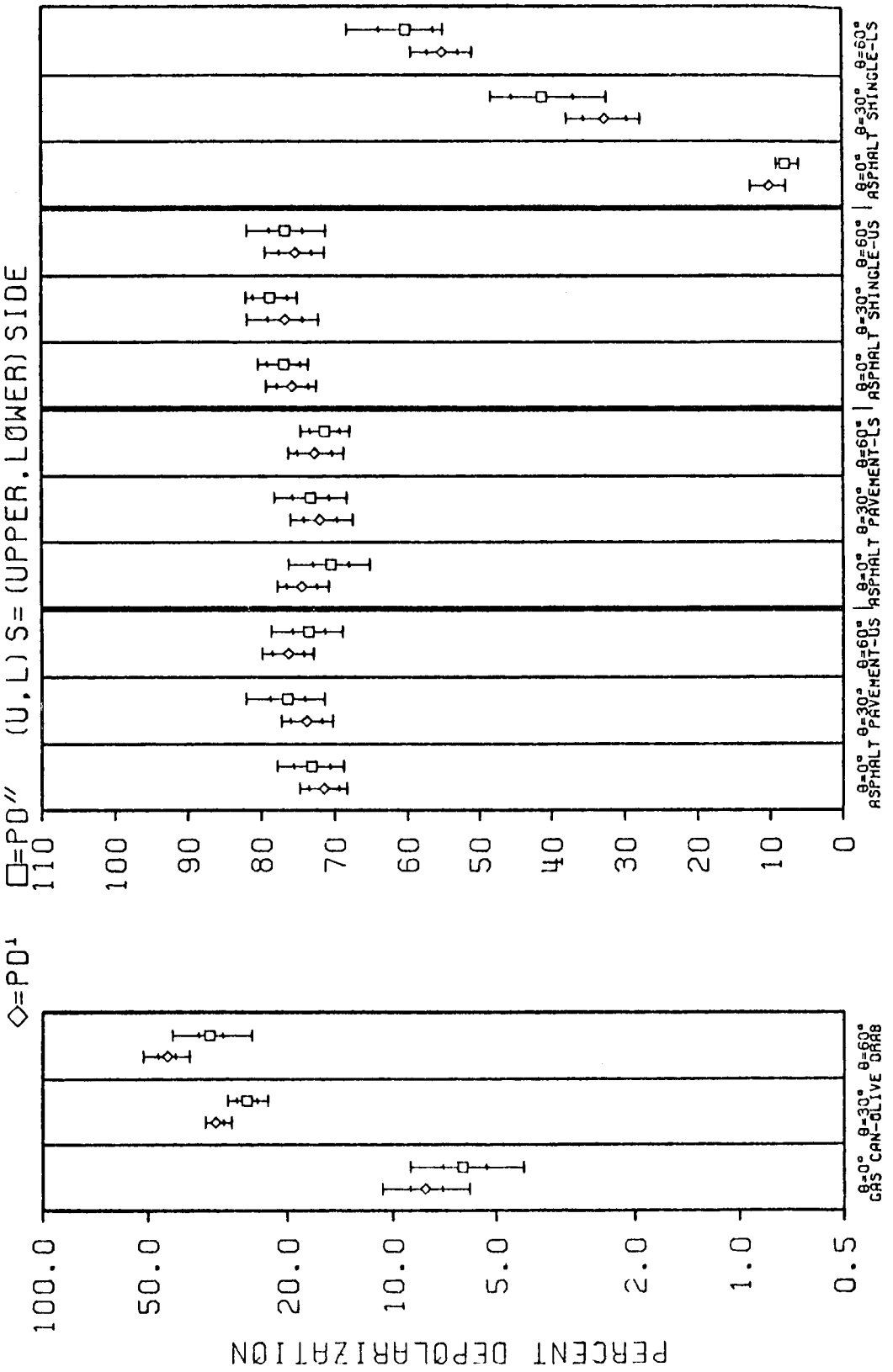


Figure 10. (continued)

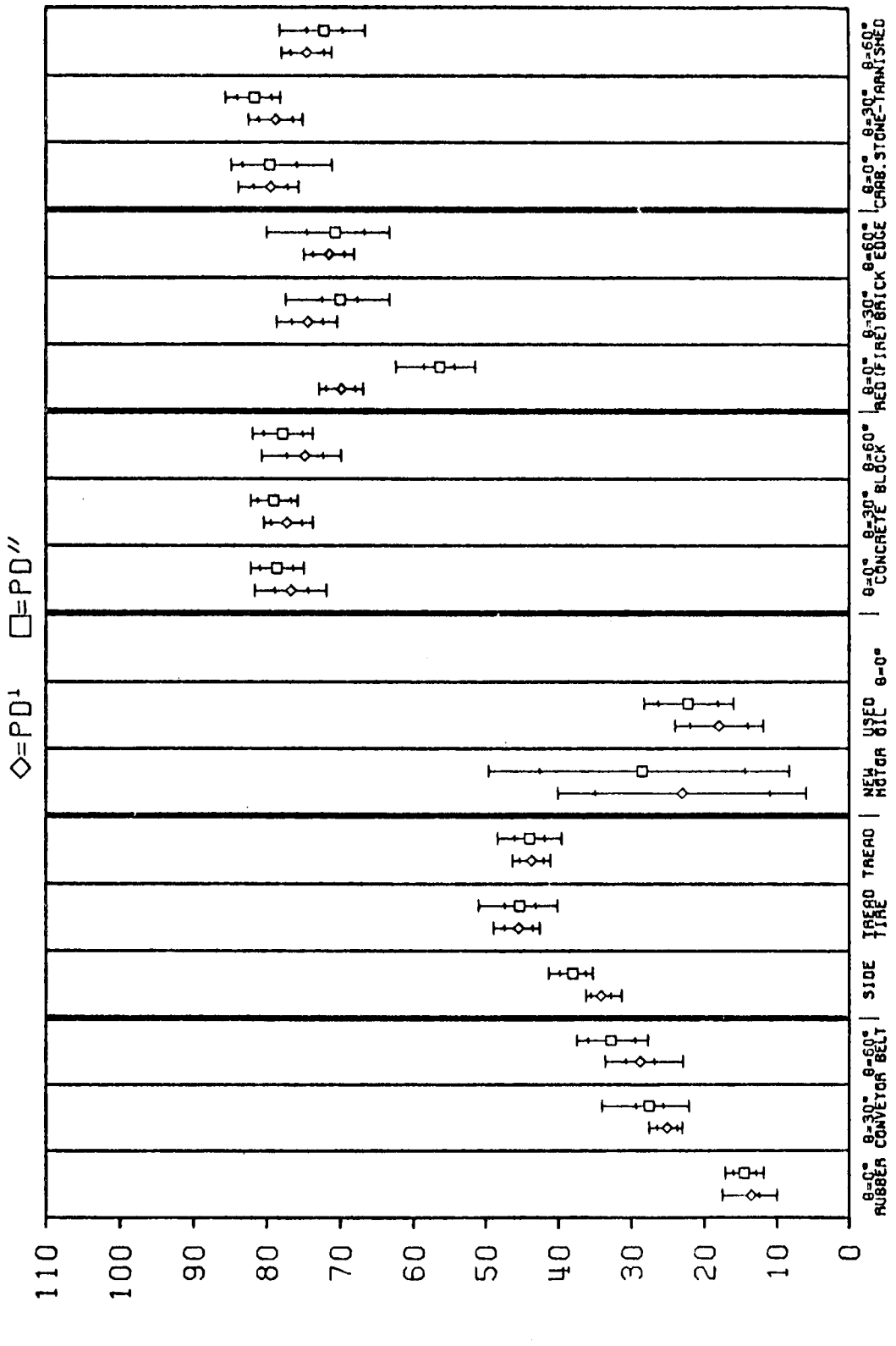


Figure 10. (continued)

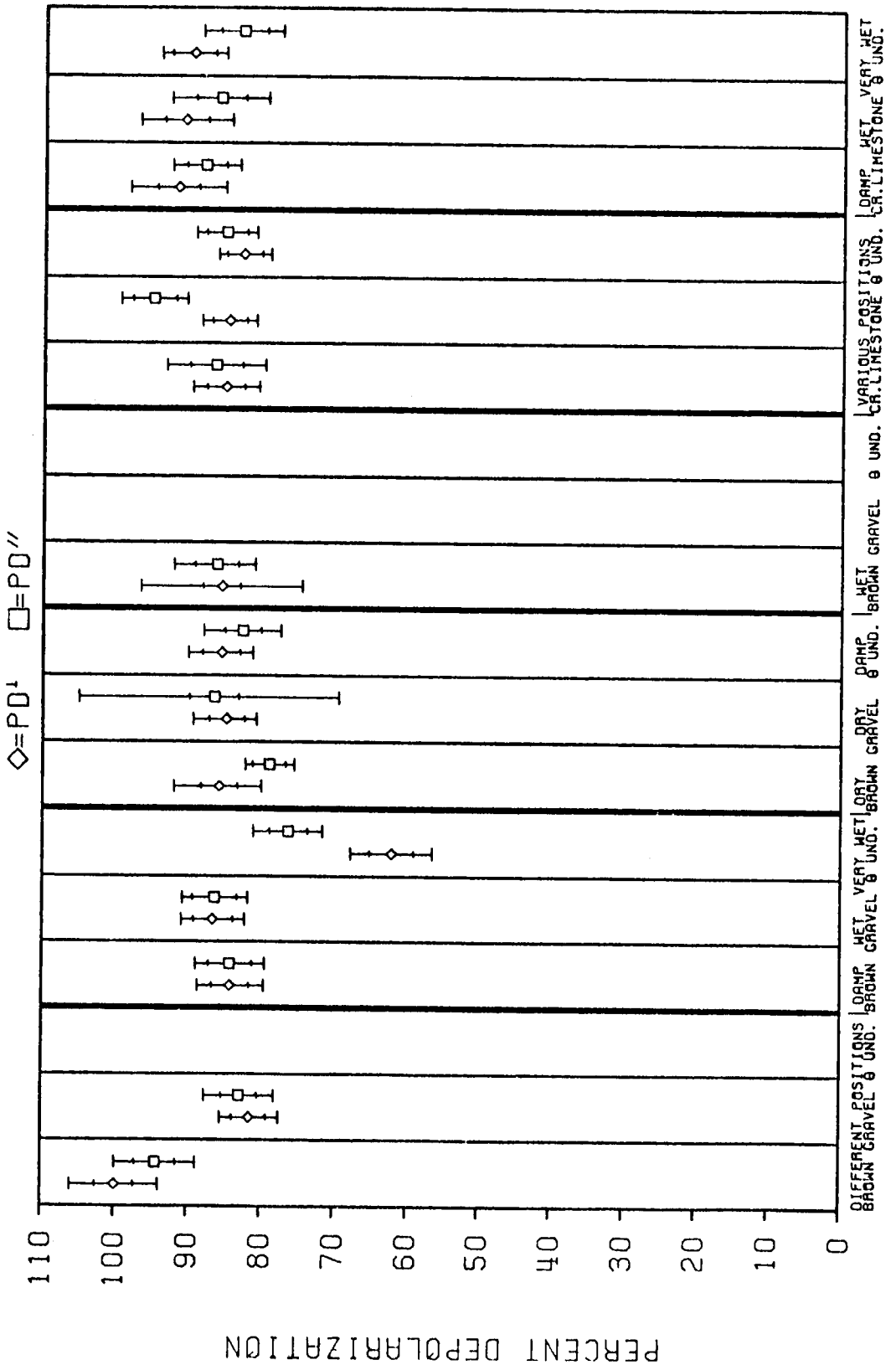


Figure 10. (continued)

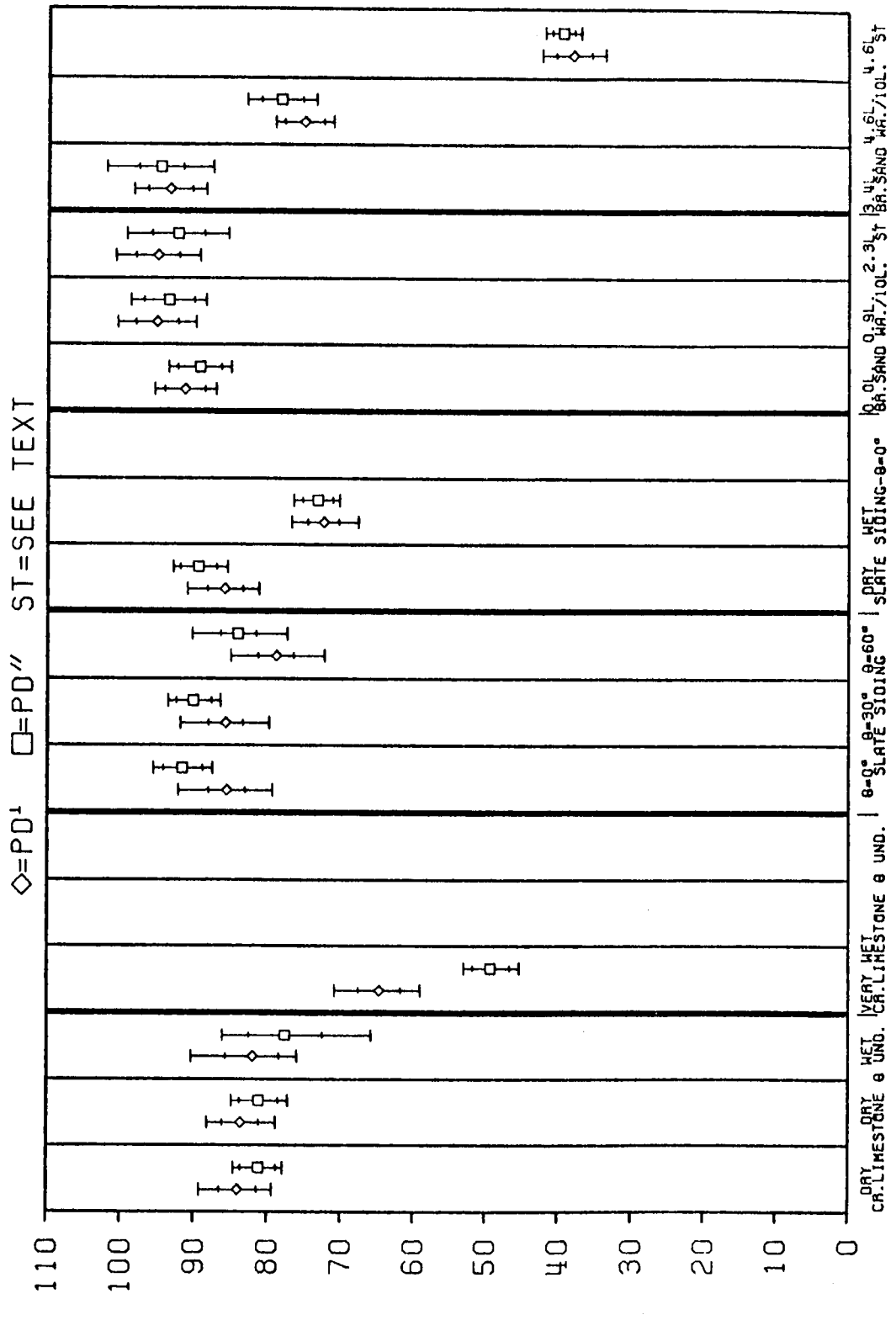


Figure 10. (continued)

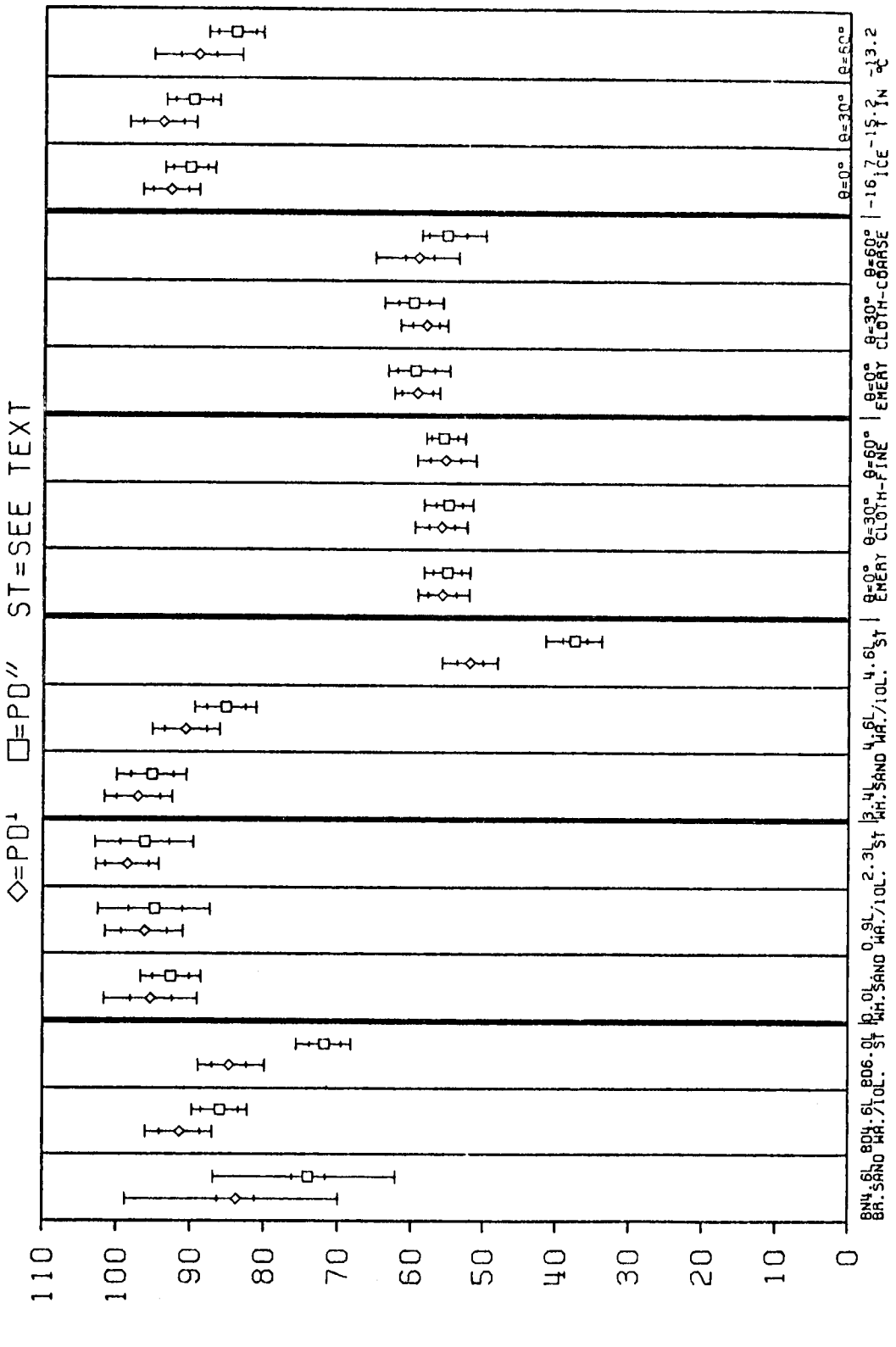


Figure 10. (continued)

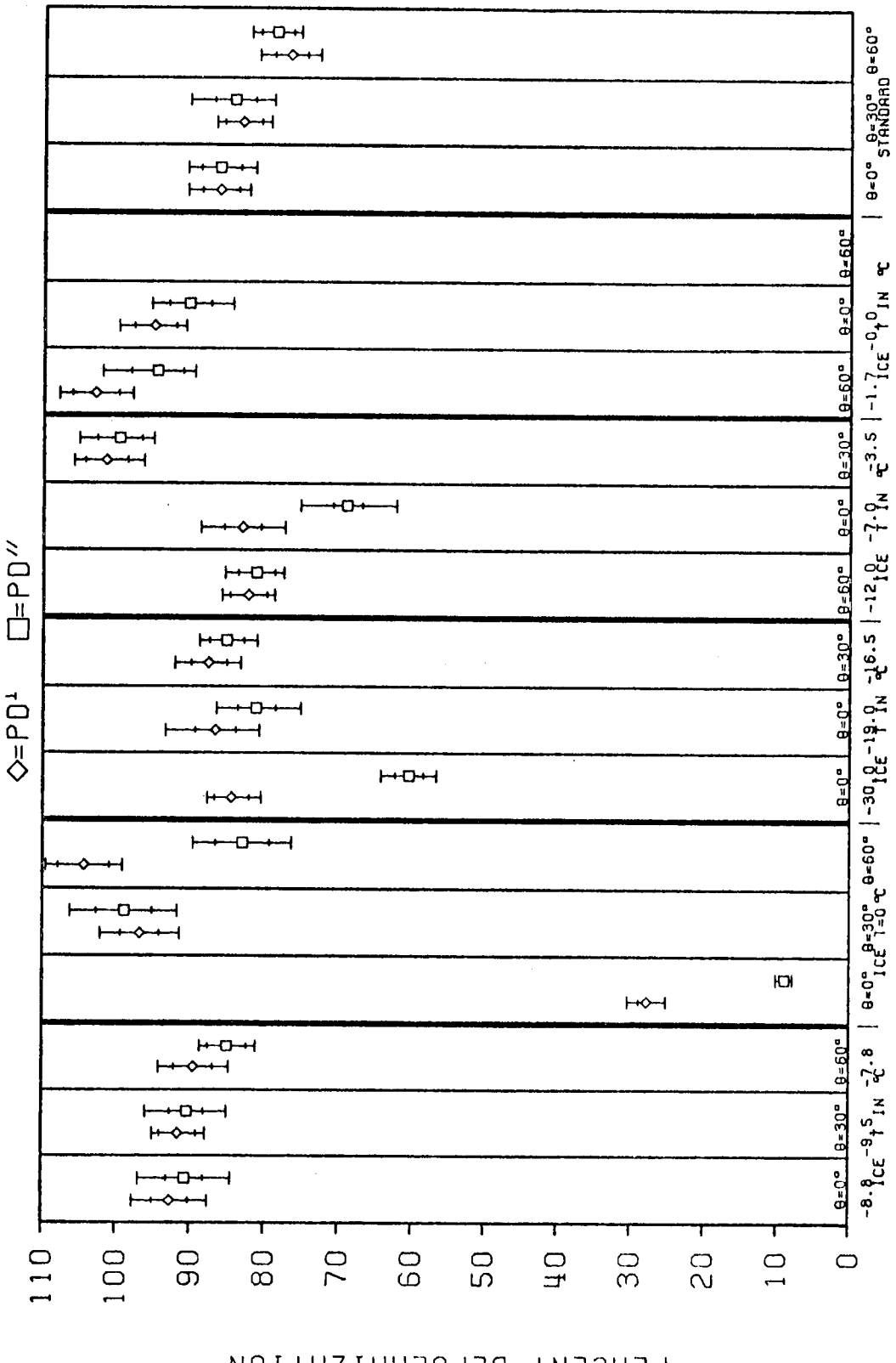


Figure 10. (continued)

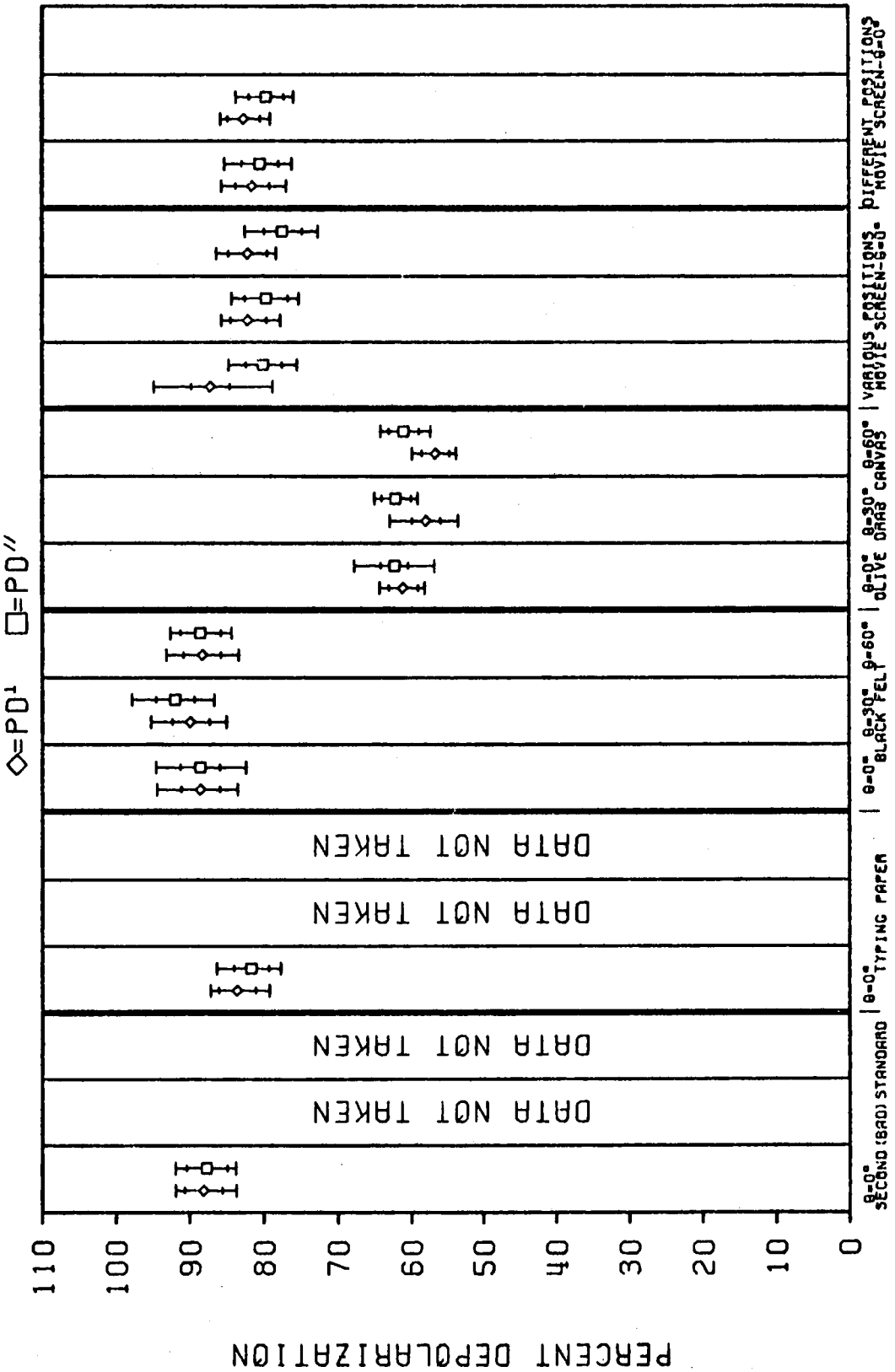


Figure 10. (continued)

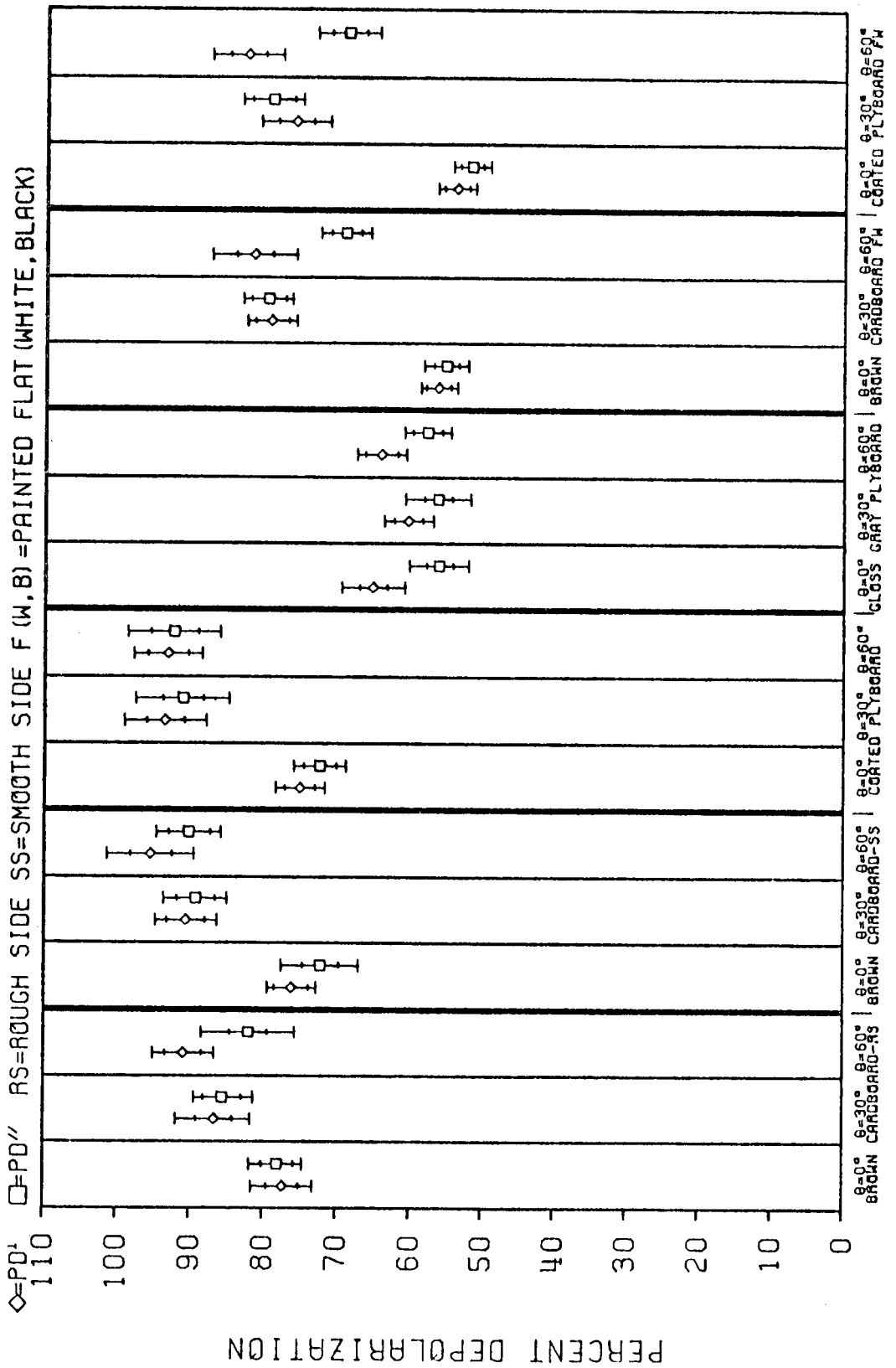


Figure 10. (continued)

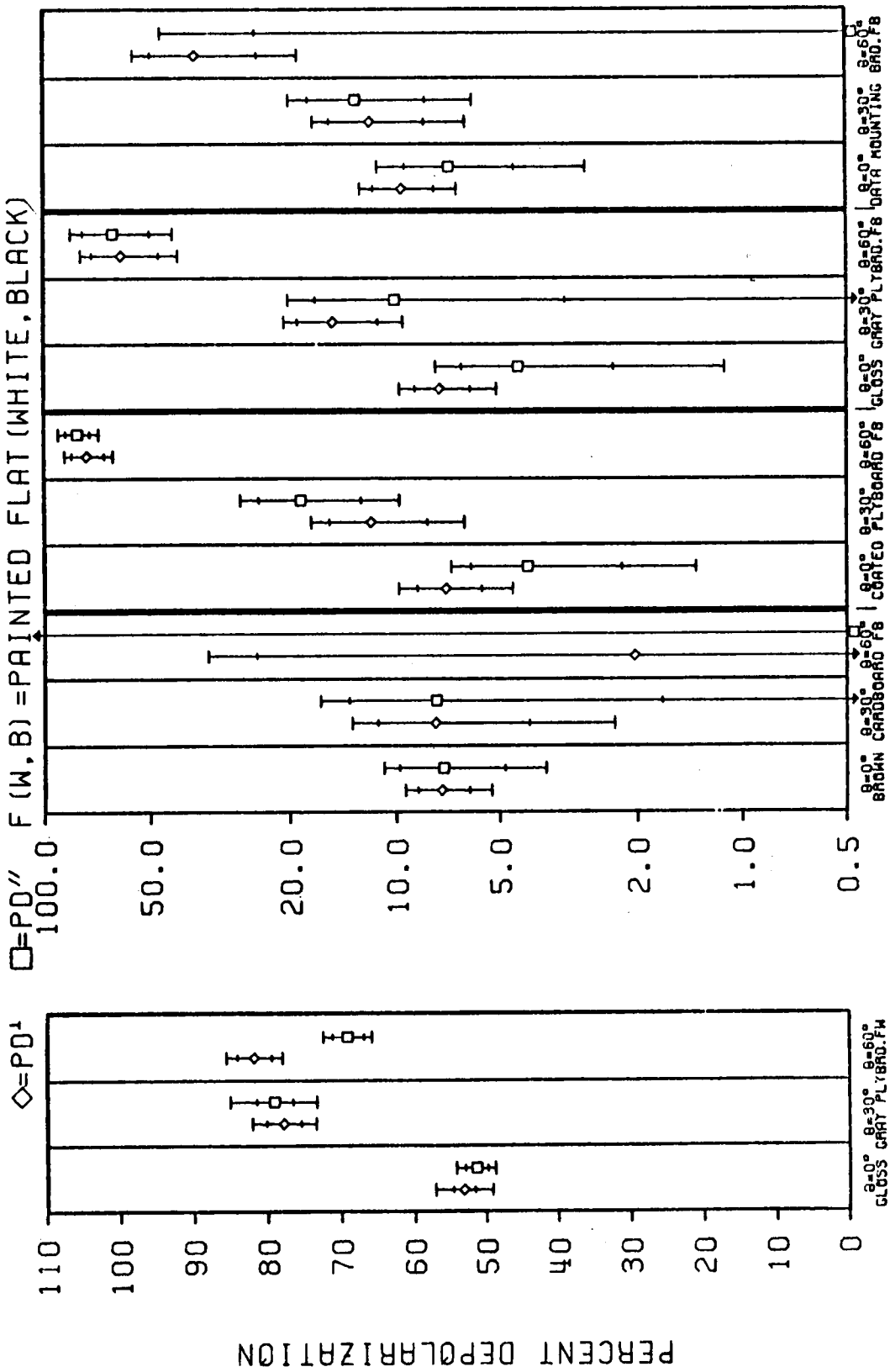


Figure 10. (continued)

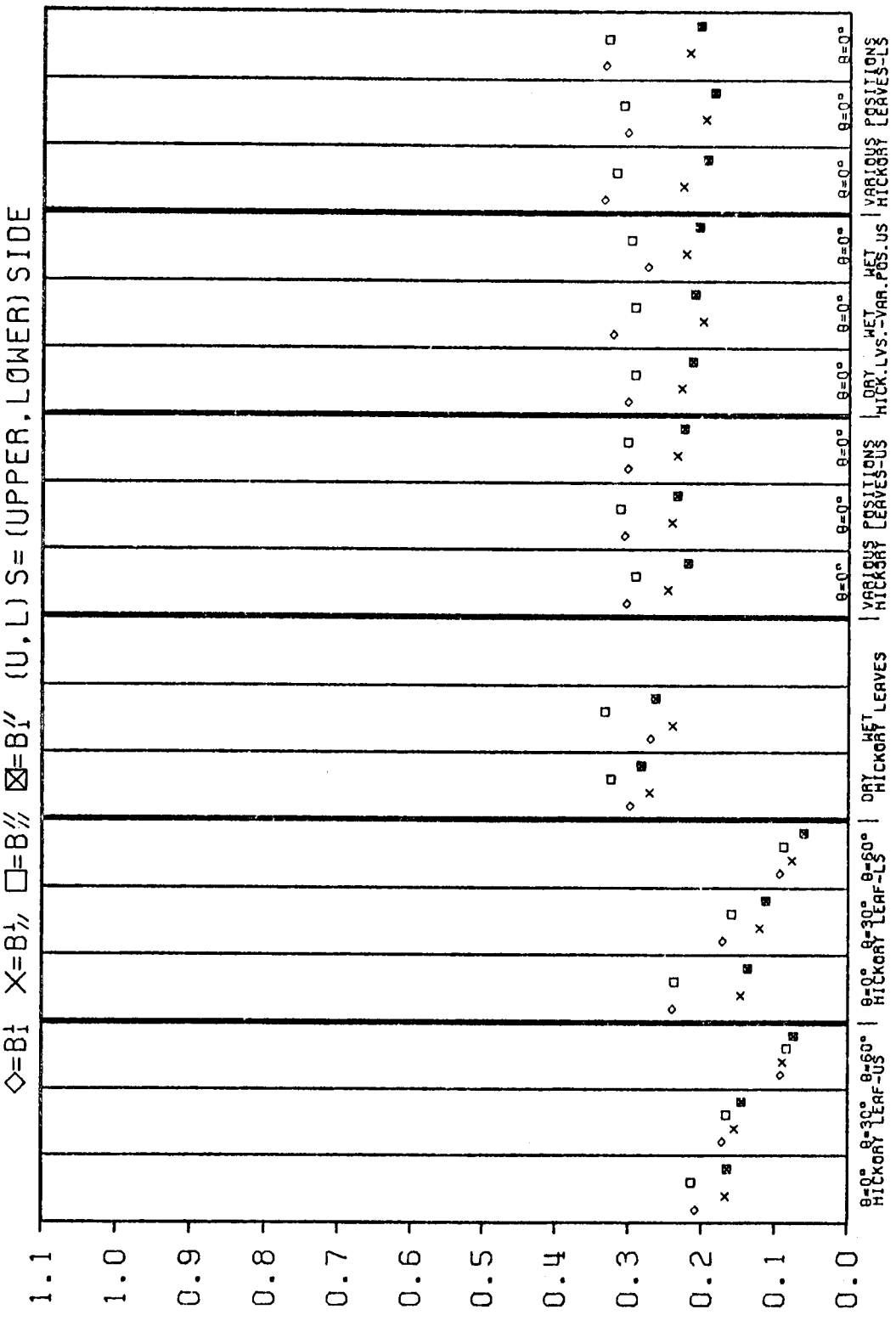


Figure 11. Basic backscattered fractions.

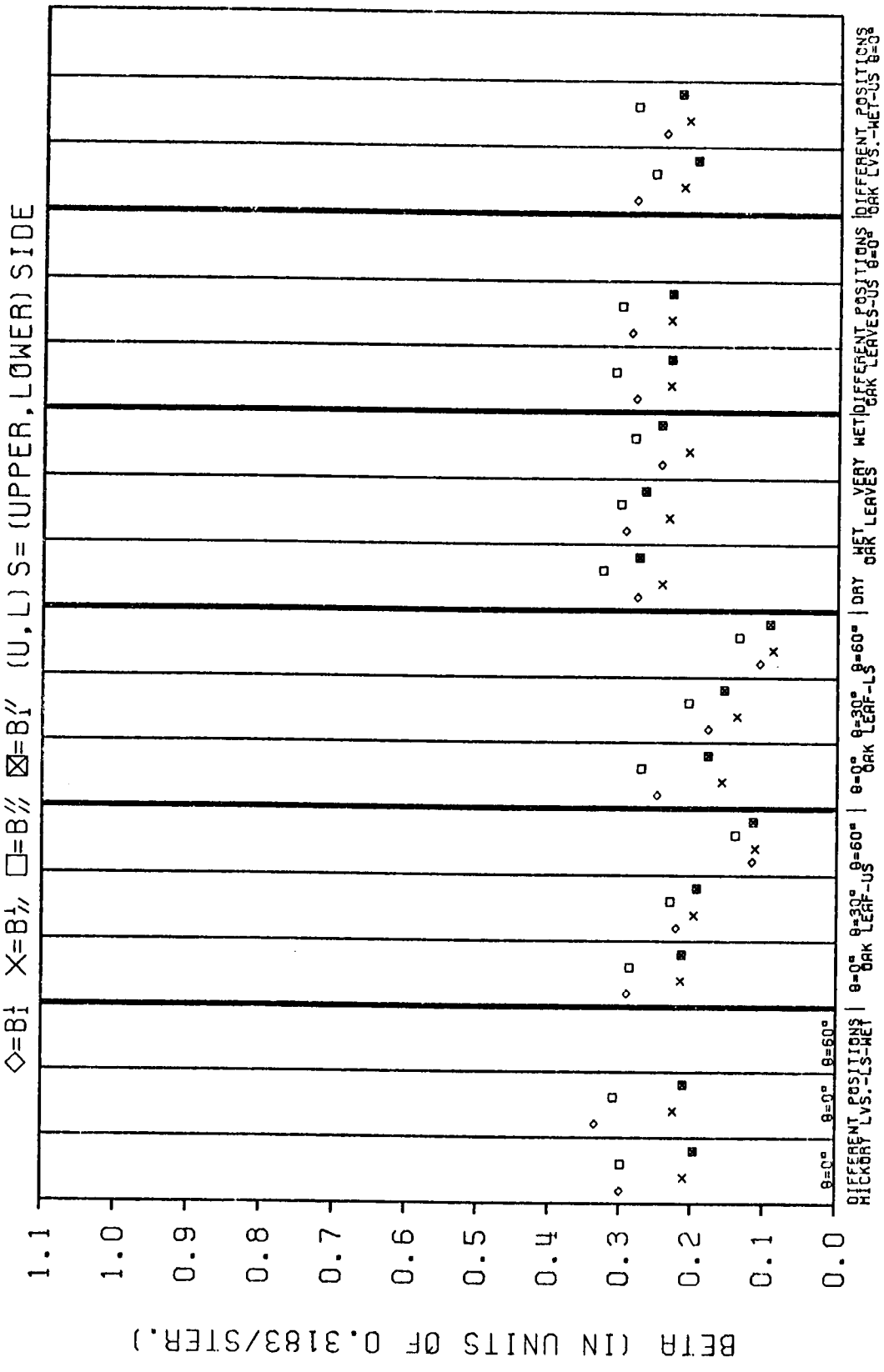


Figure 11. (continued)

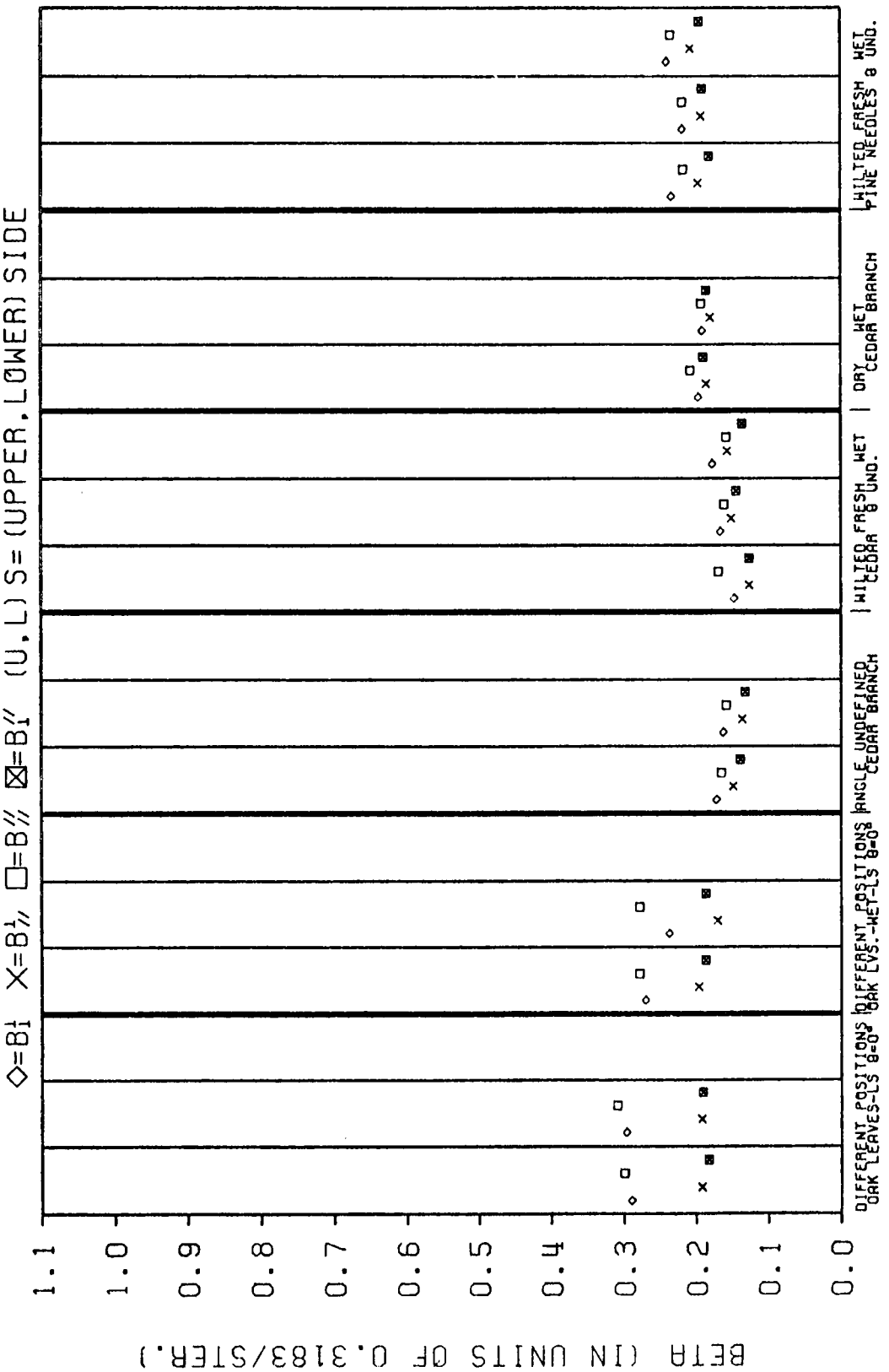


Figure 11. (continued)

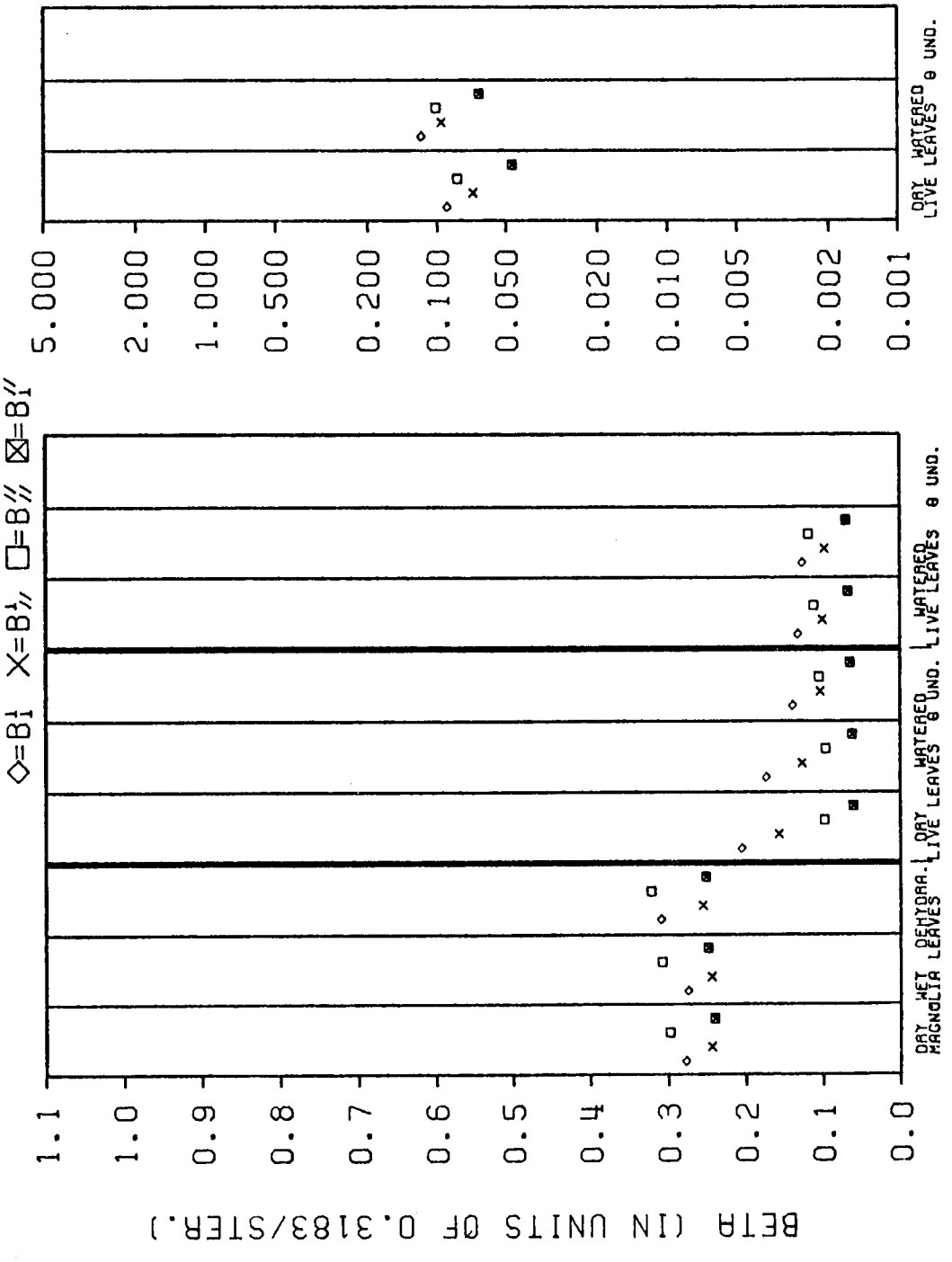


Figure 11. (continued)

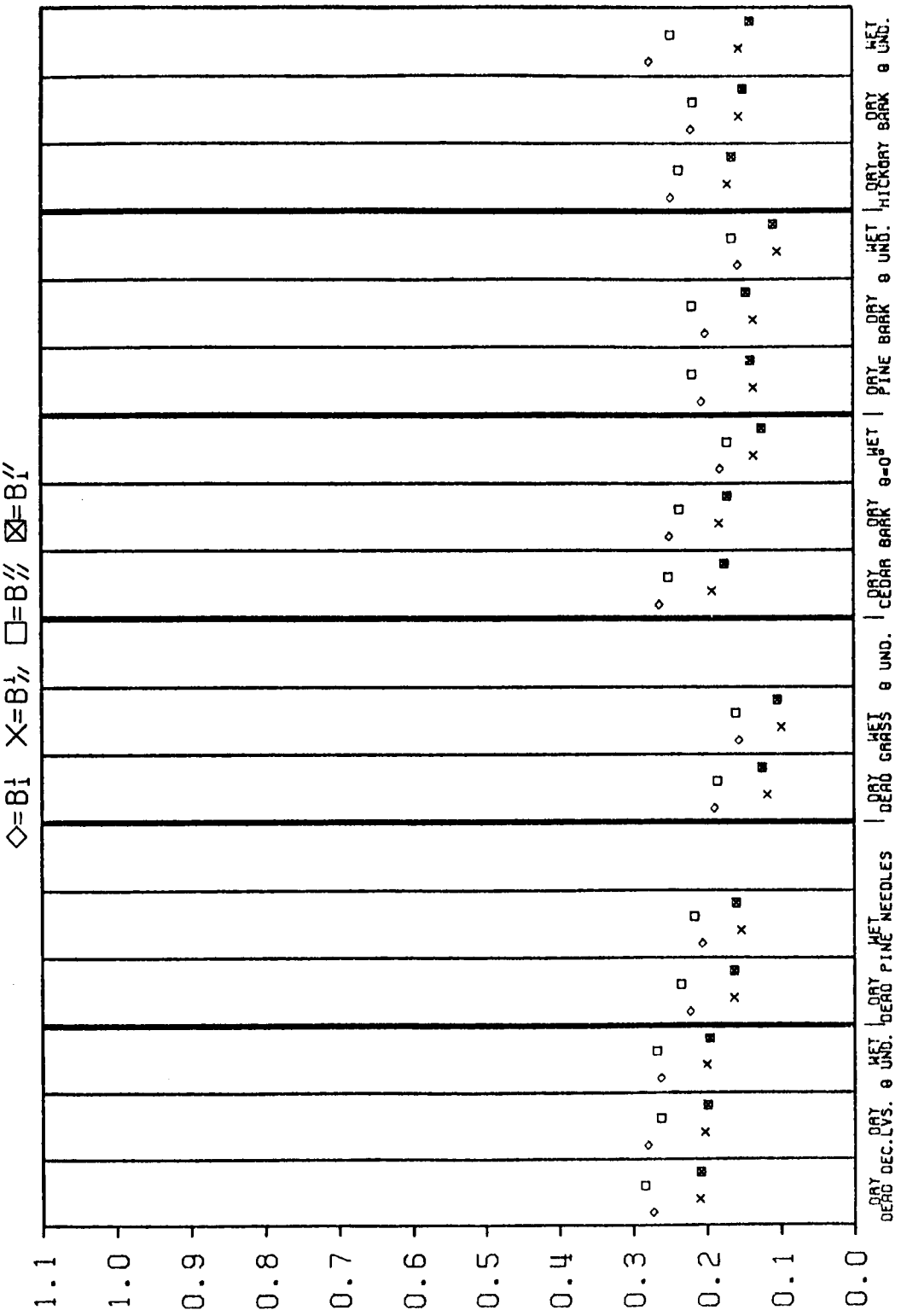


Figure 11. (continued)

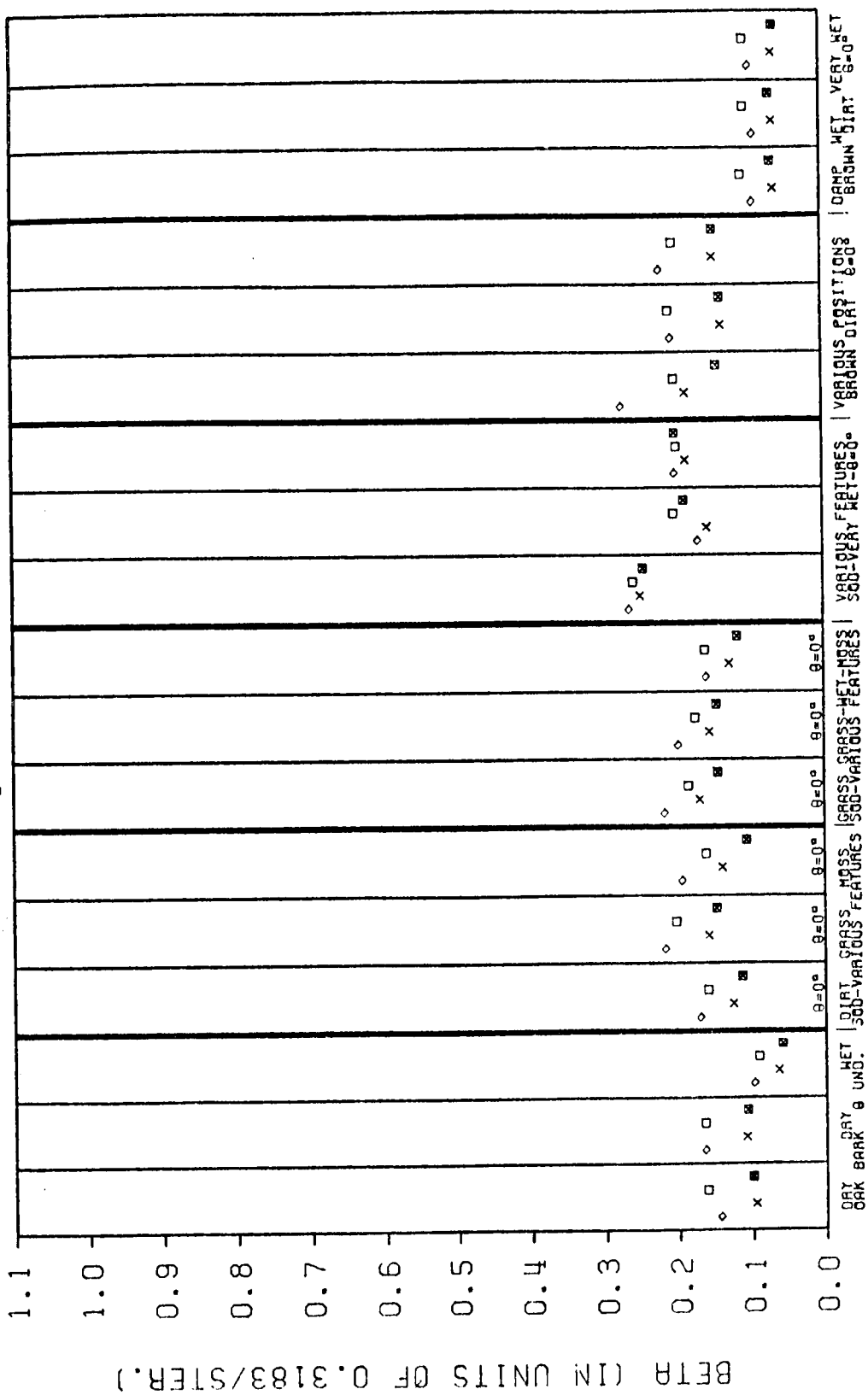


Figure 11. (continued)

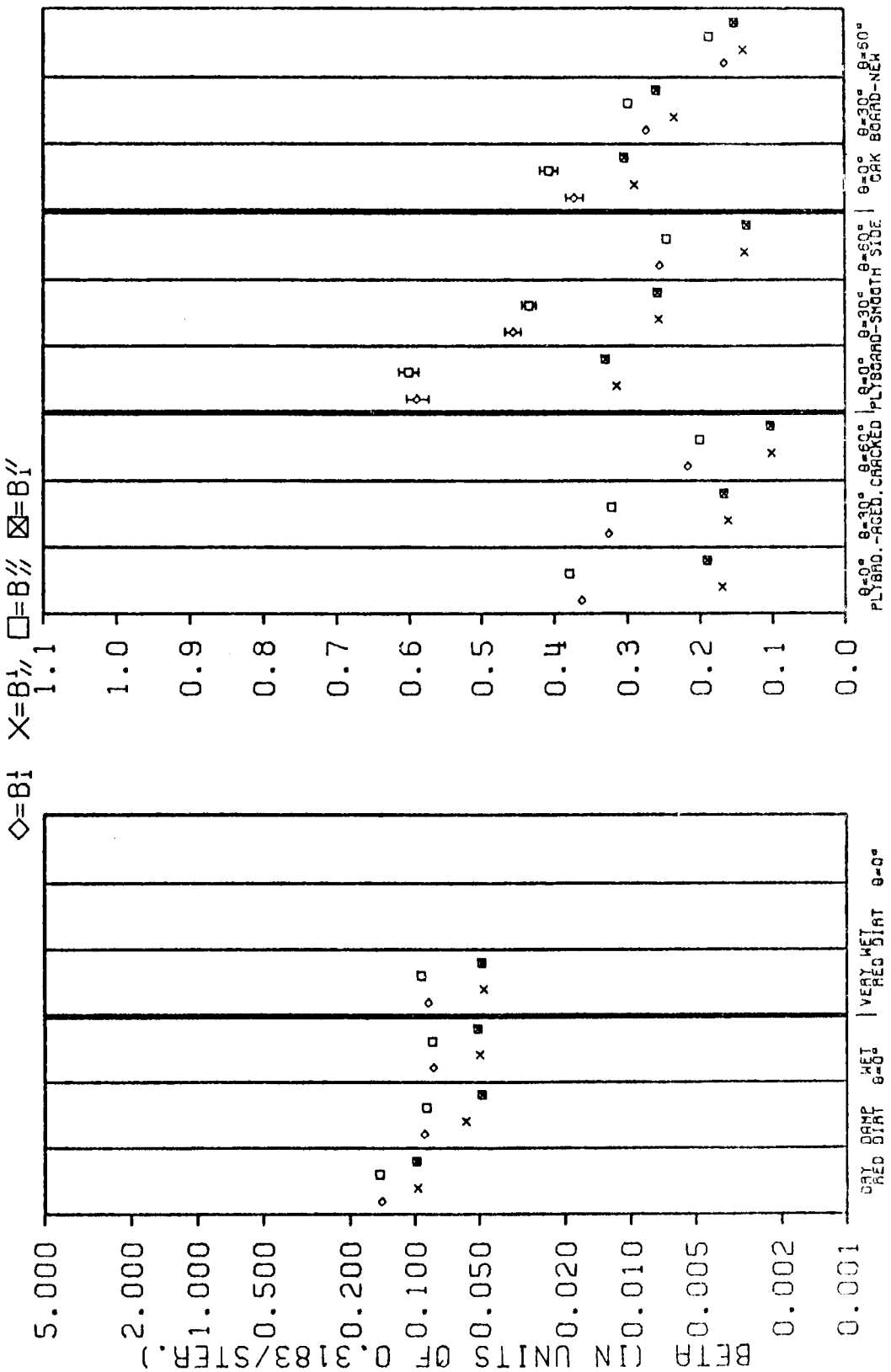


Figure 11. (continued)

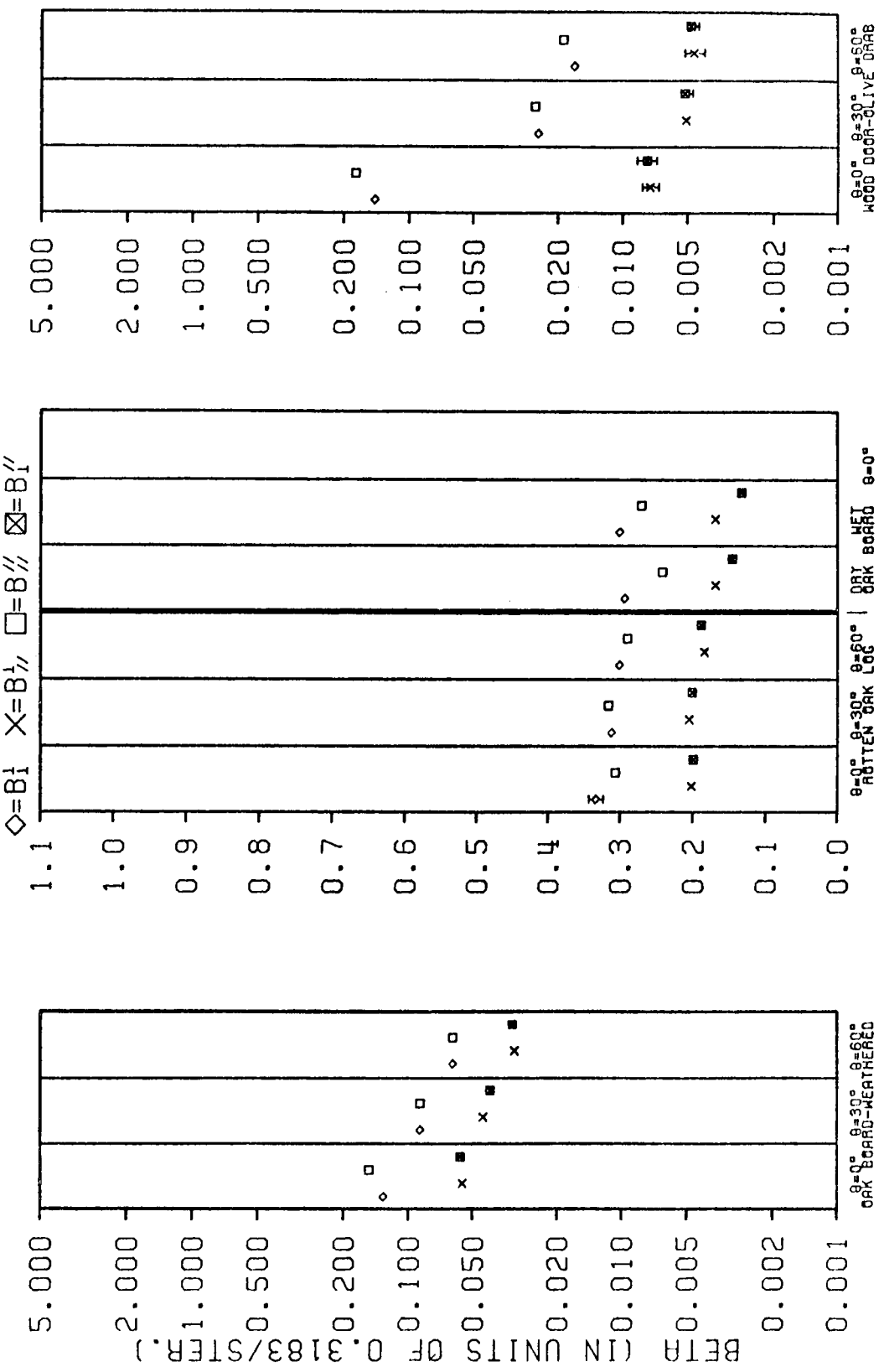


Figure 11. (continued)

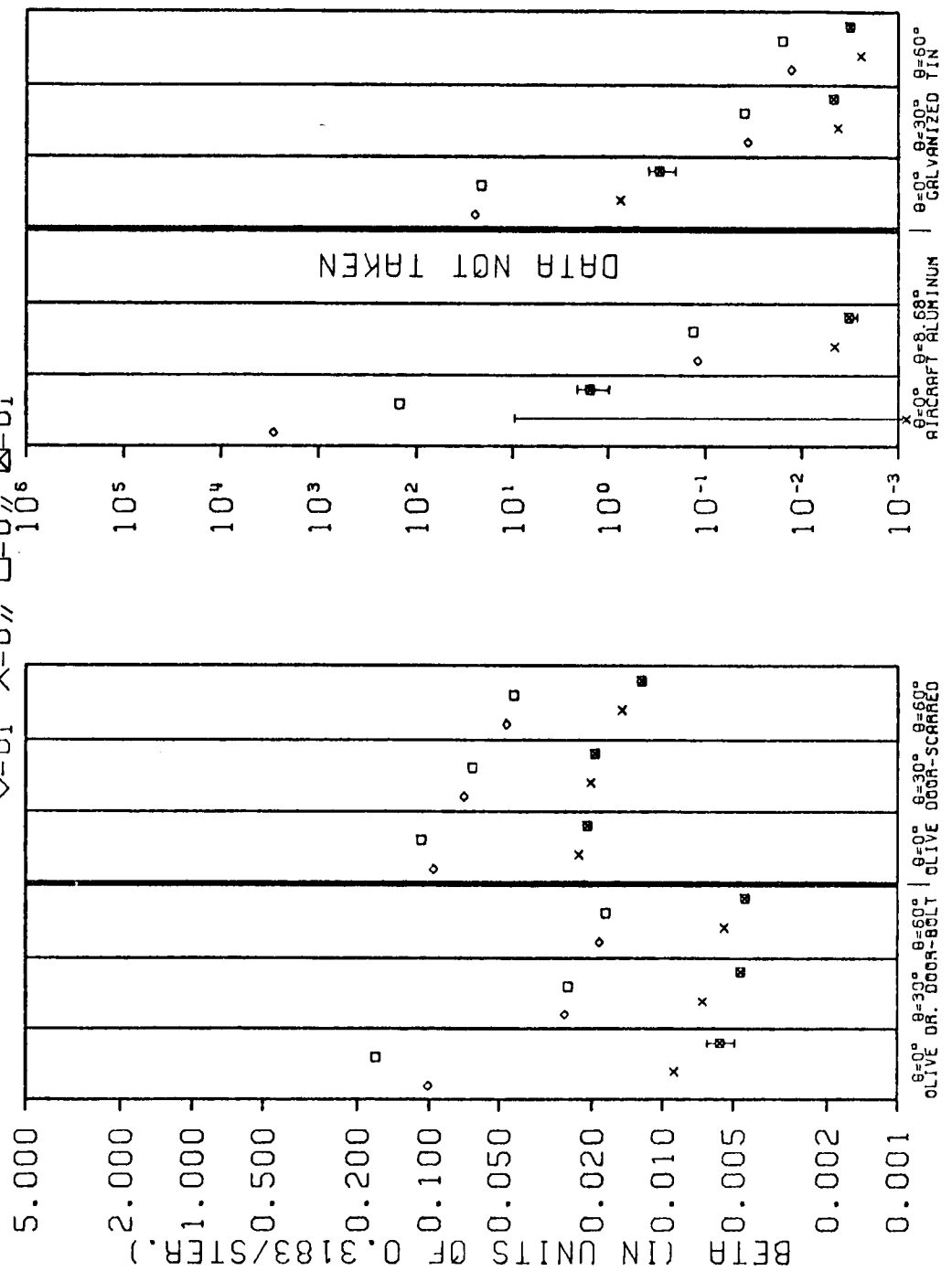


Figure 11. (continued)

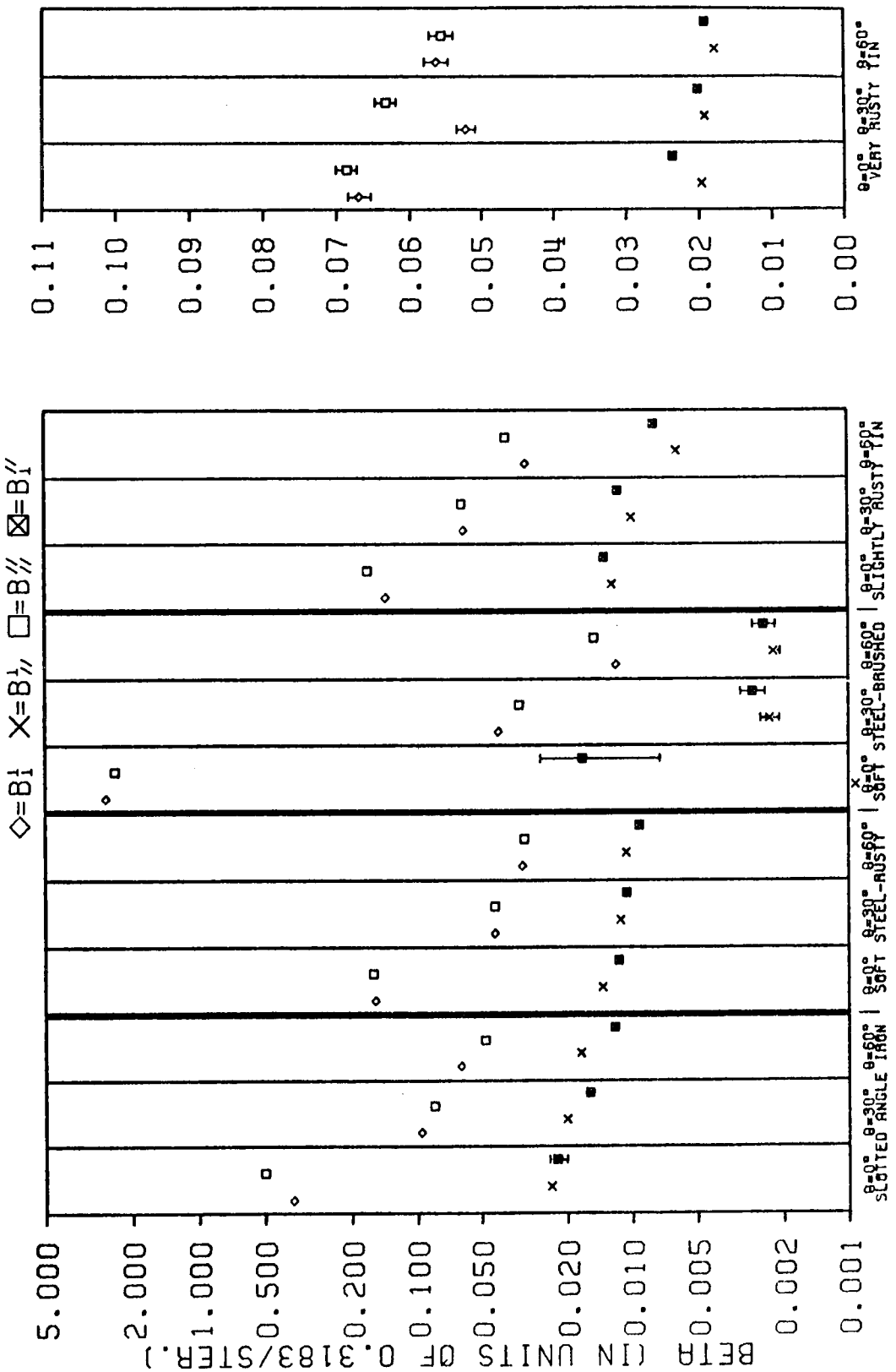


Figure 11. (continued)

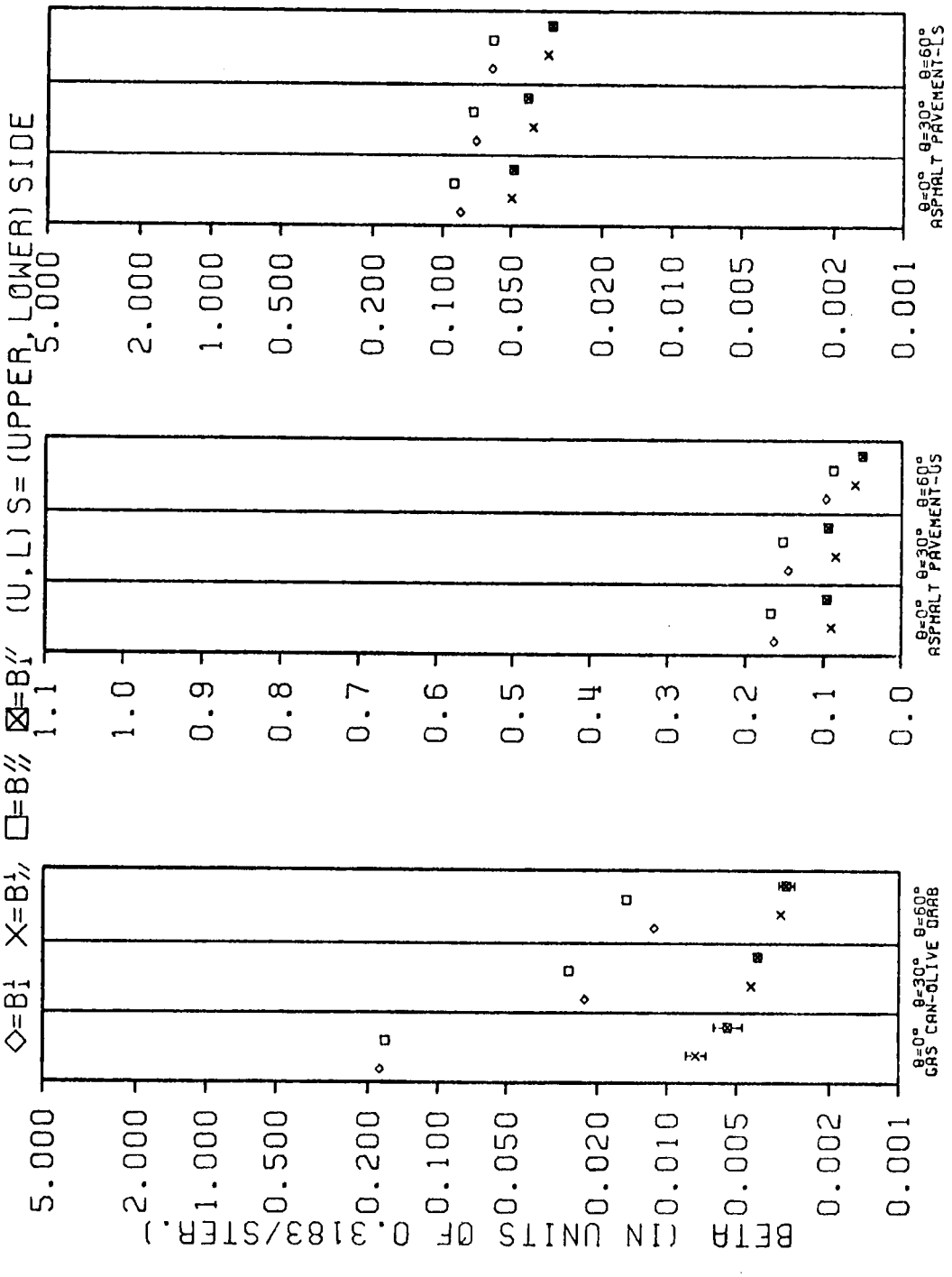


Figure 11. (continued)

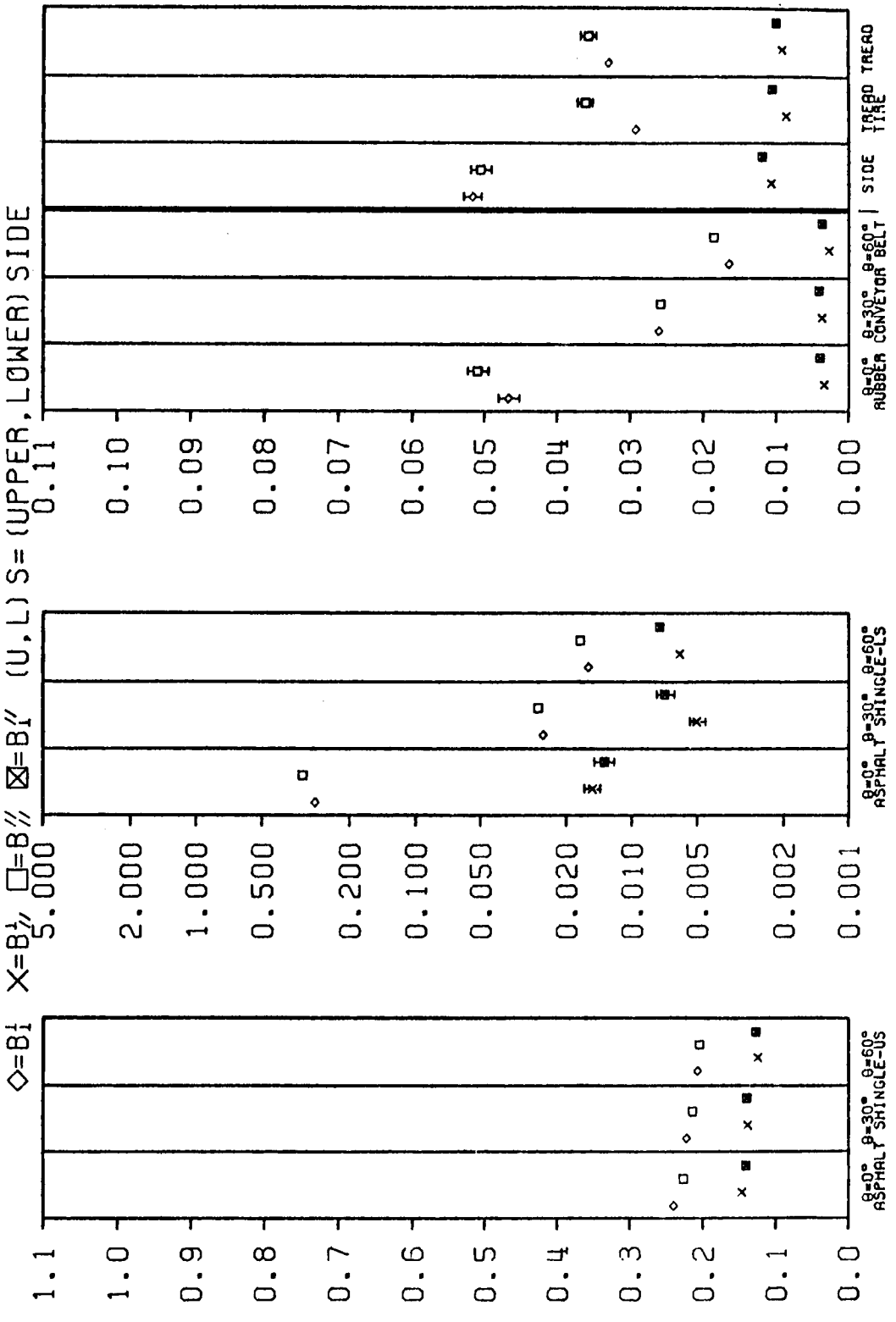


Figure 11. (continued)

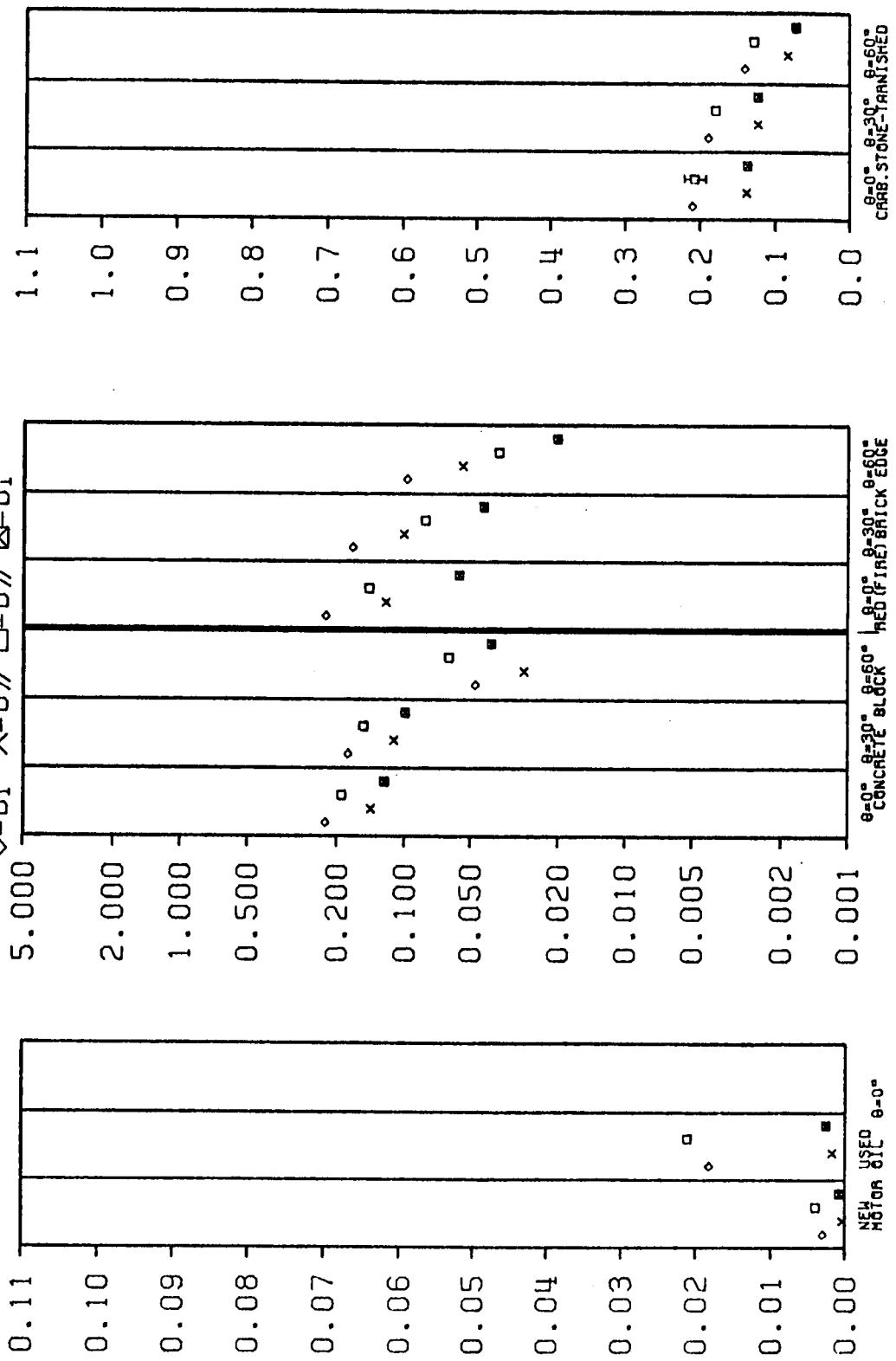


Figure 11. (continued)

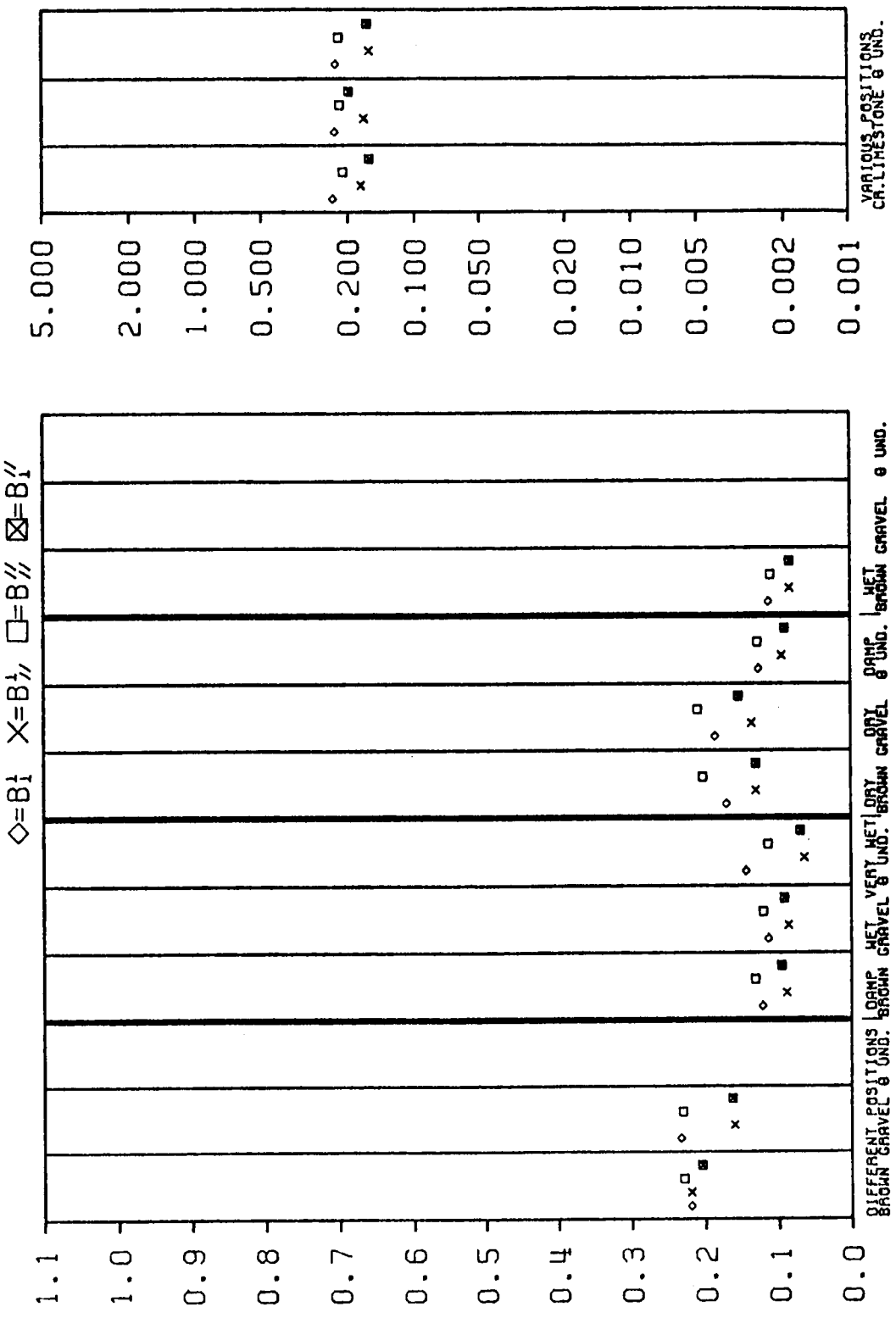


Figure 11. (continued)

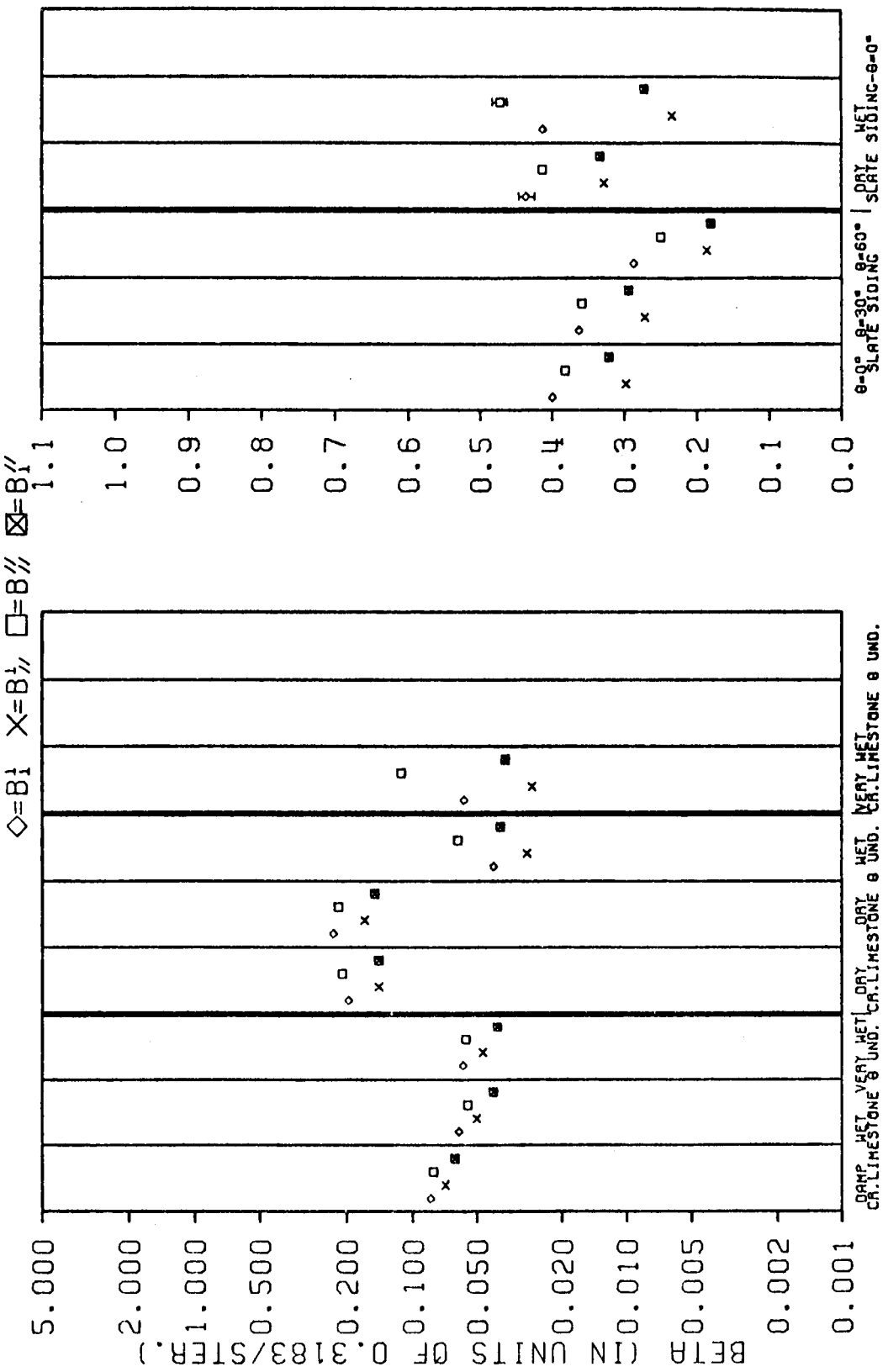


Figure 11. (continued)

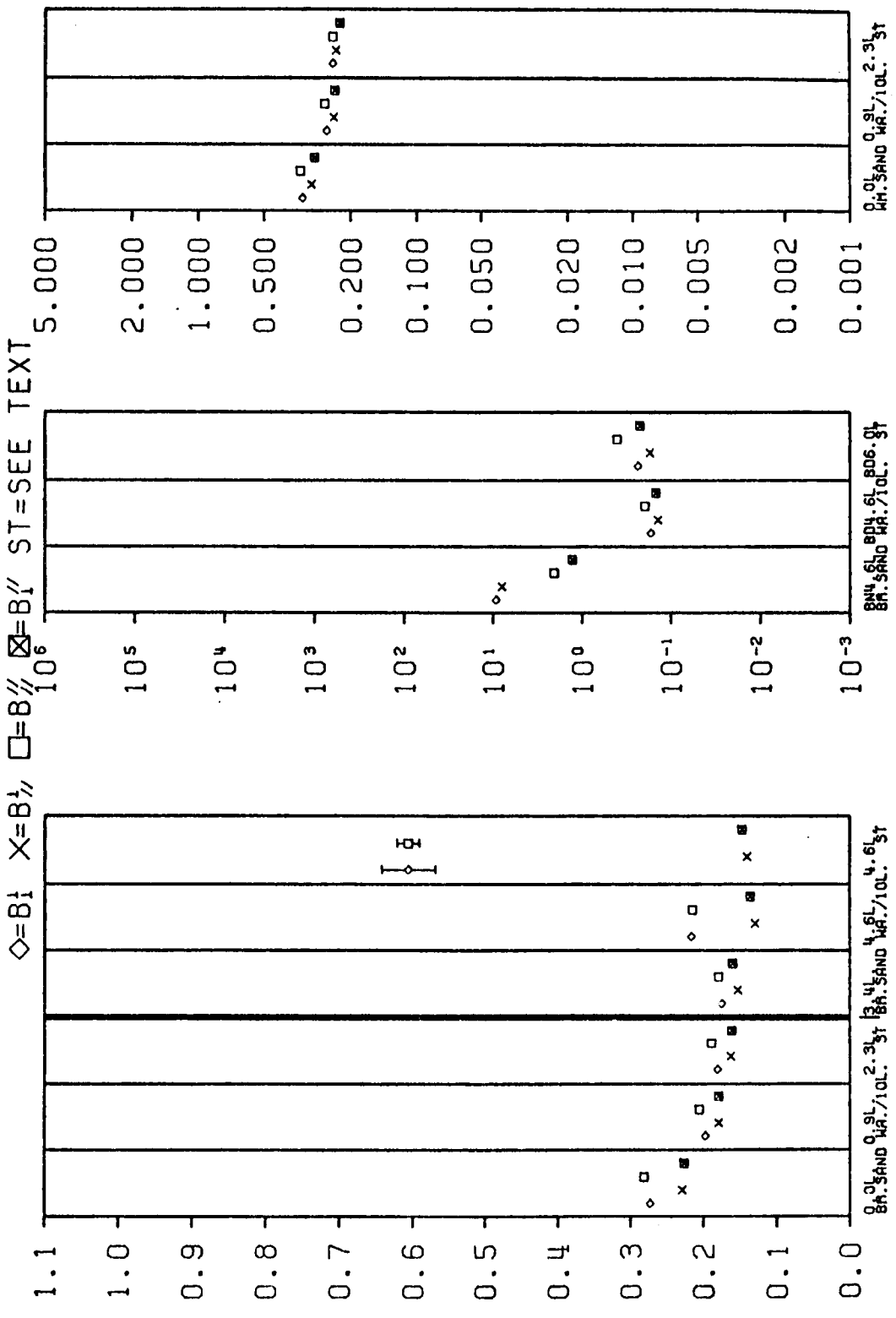


Figure 11. (continued)

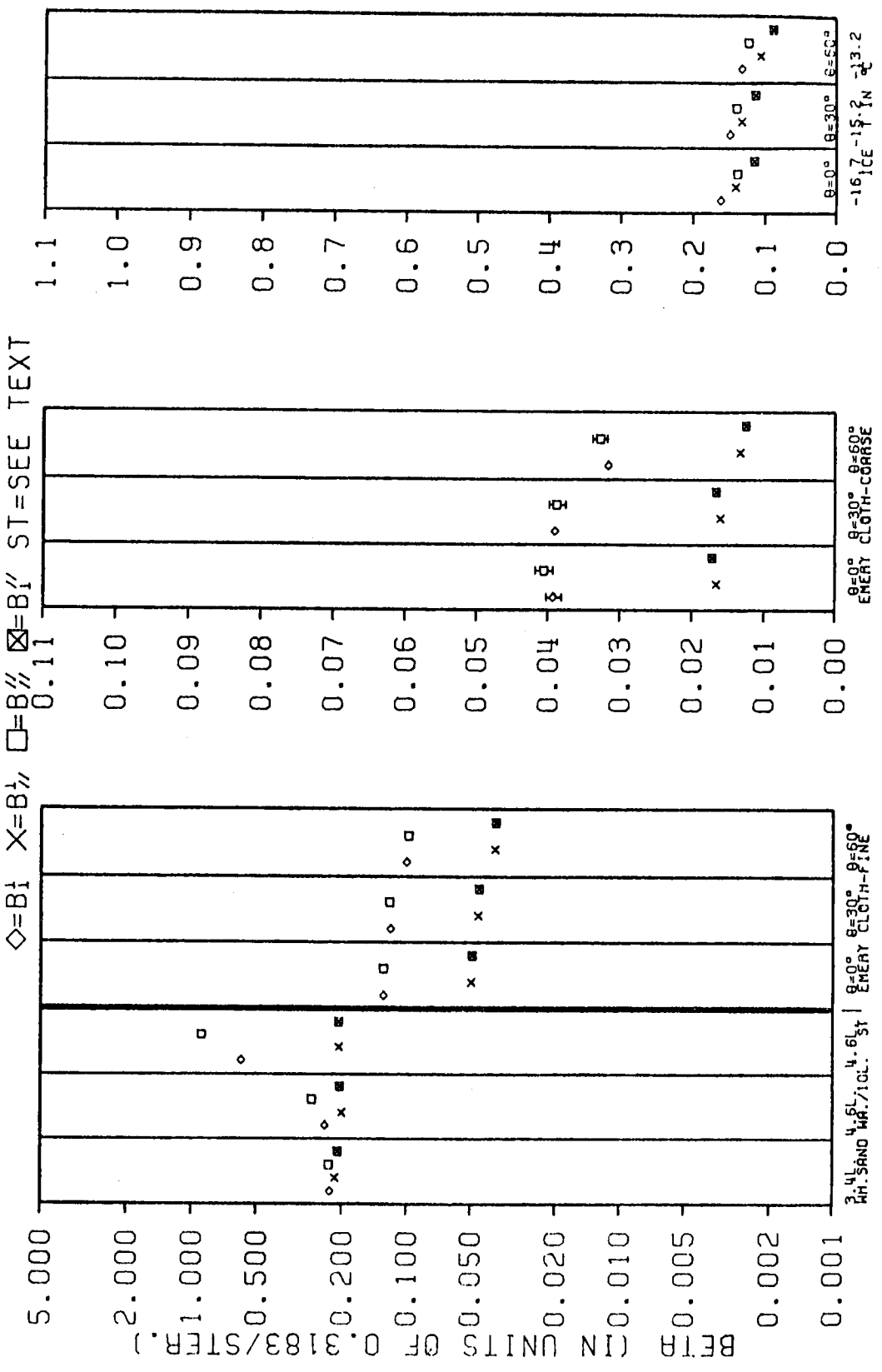


Figure 11. (continued)

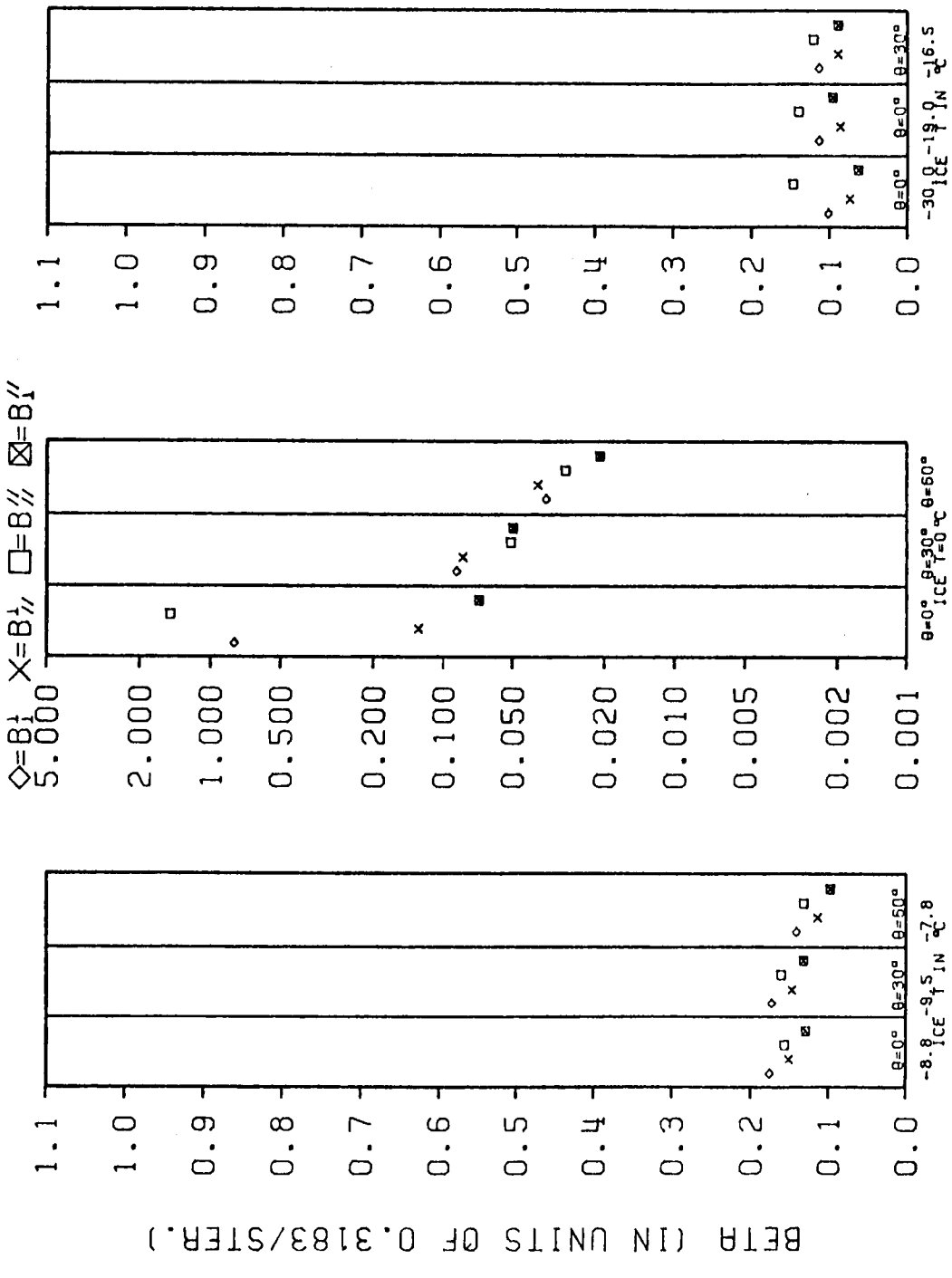


Figure 11. (continued)

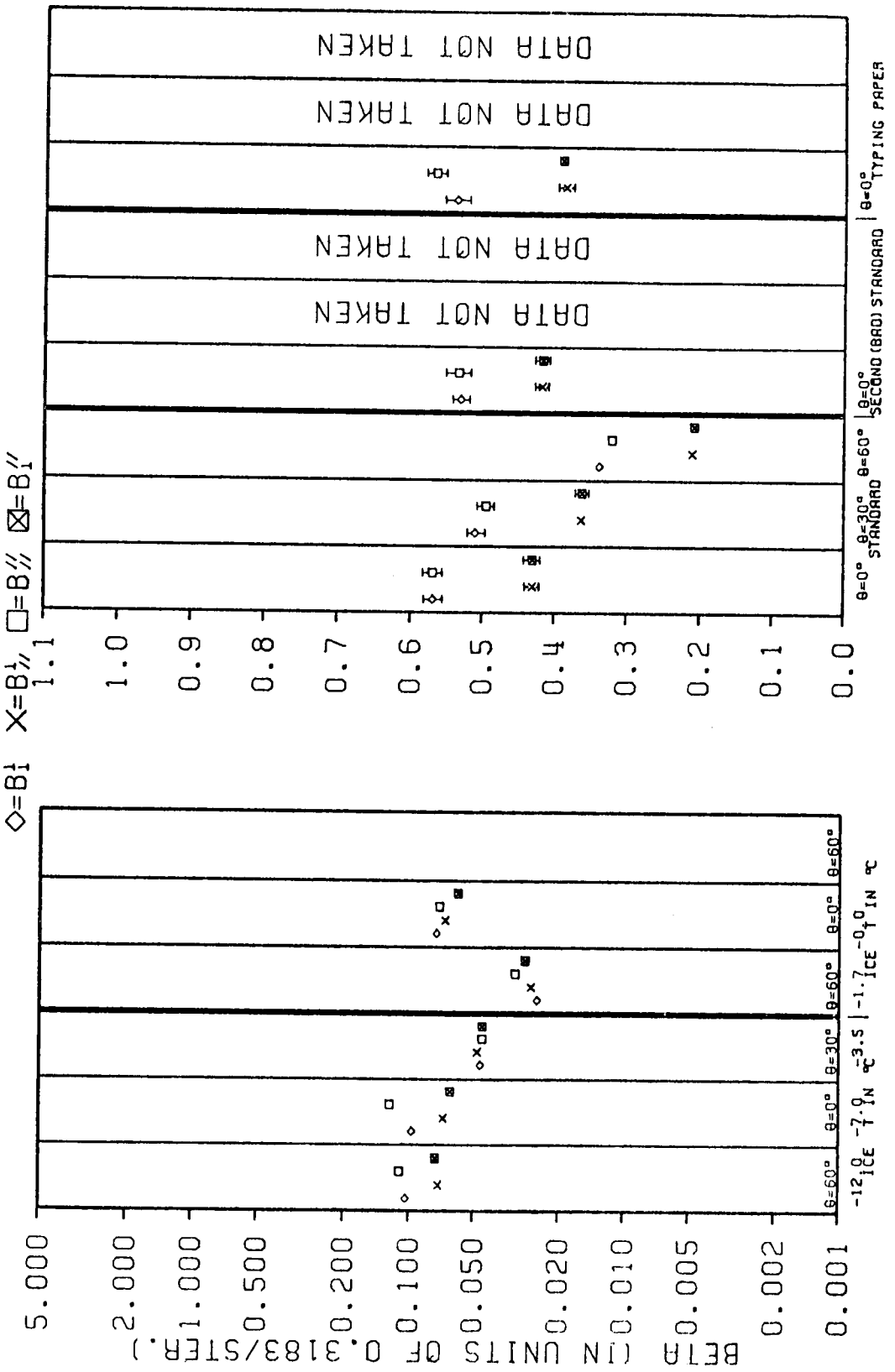


Figure 11. (continued)

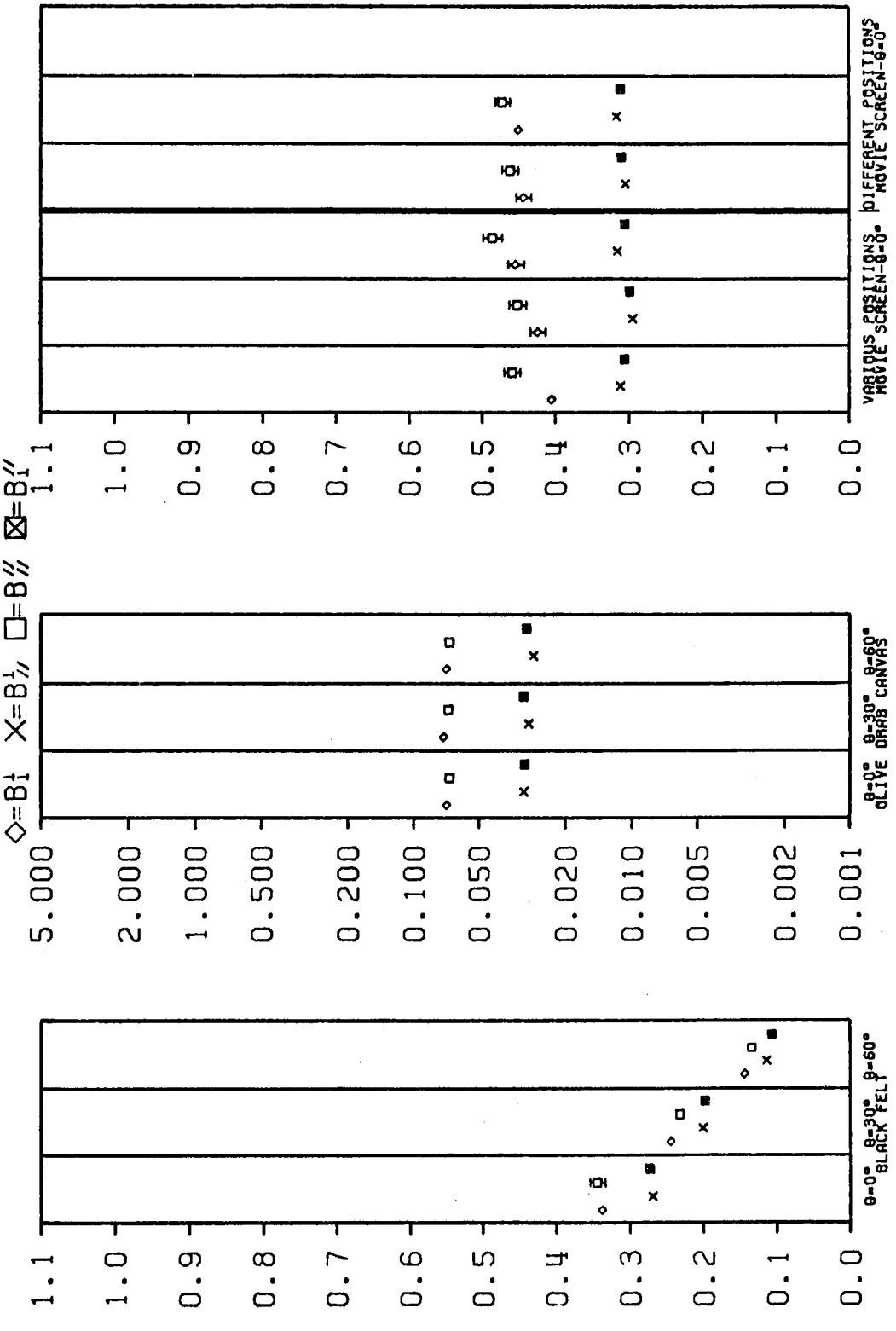


Figure 11. (continued)

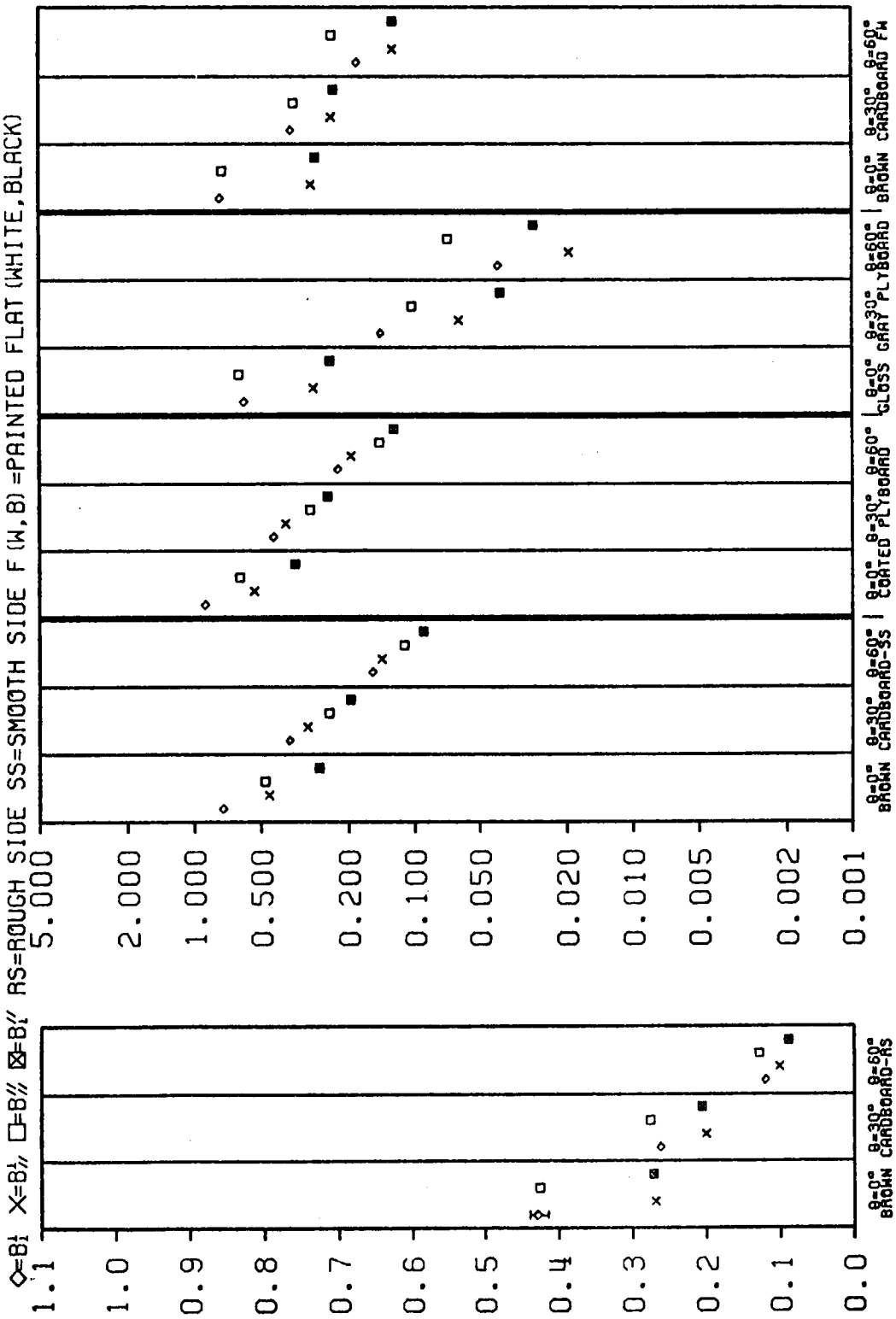


Figure 11. (continued)

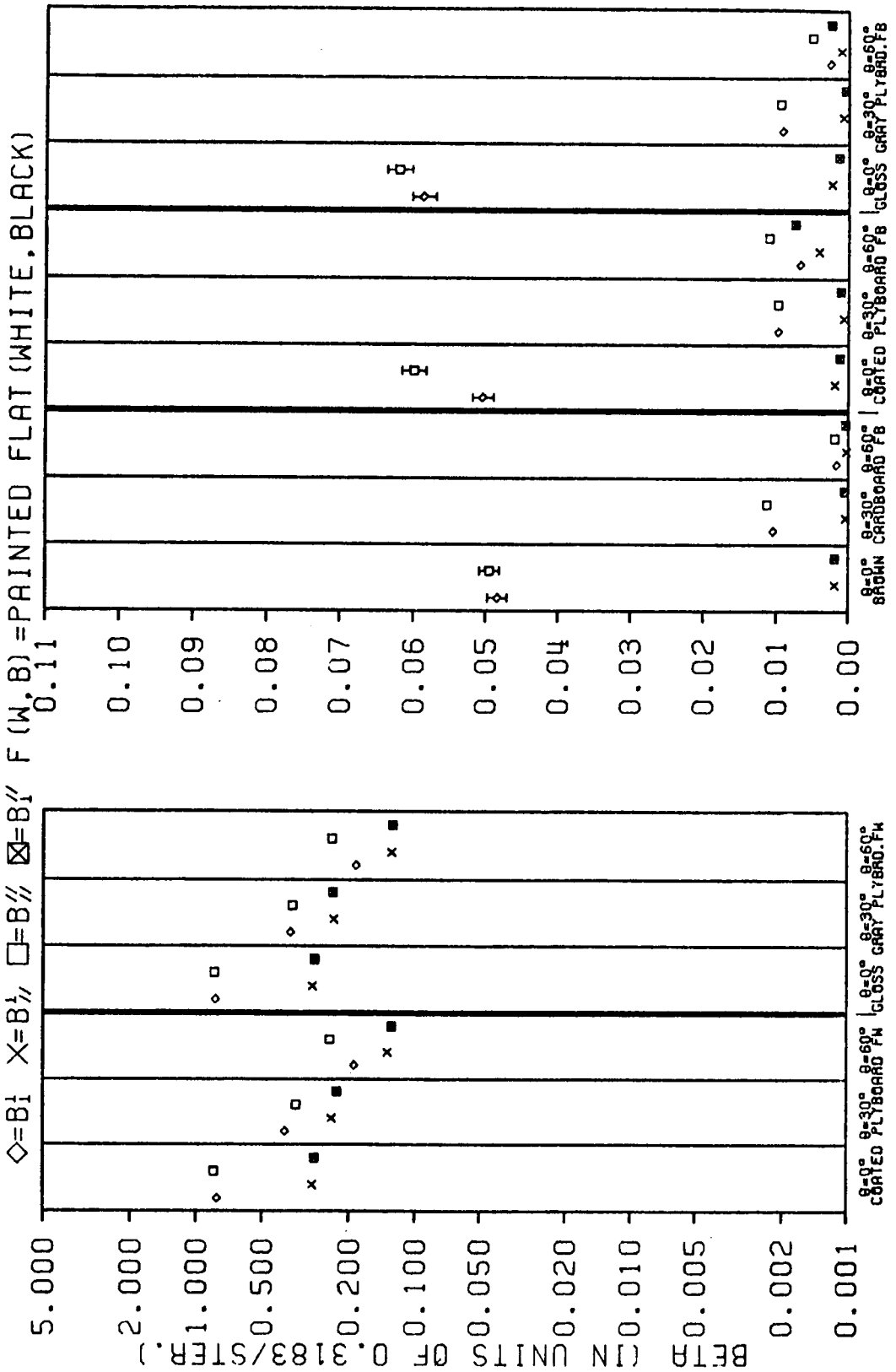


Figure 11. (continued)

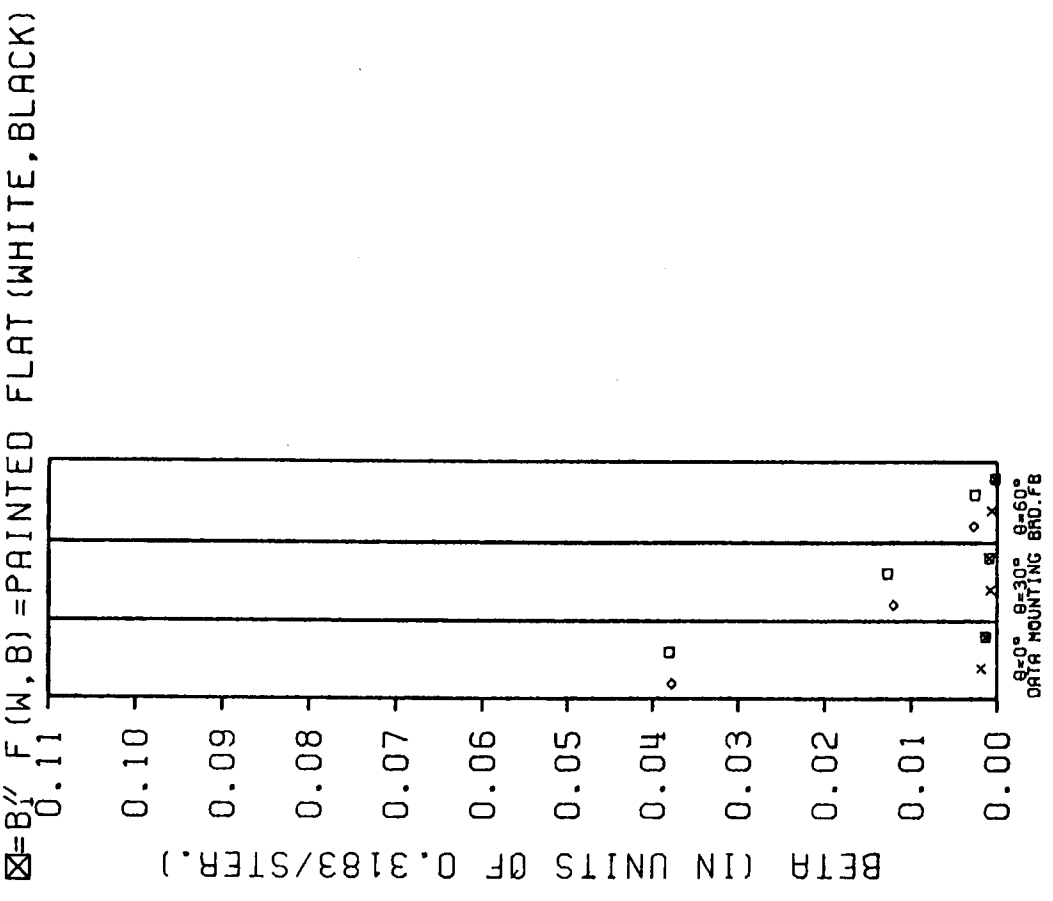


Figure 11. (continued)

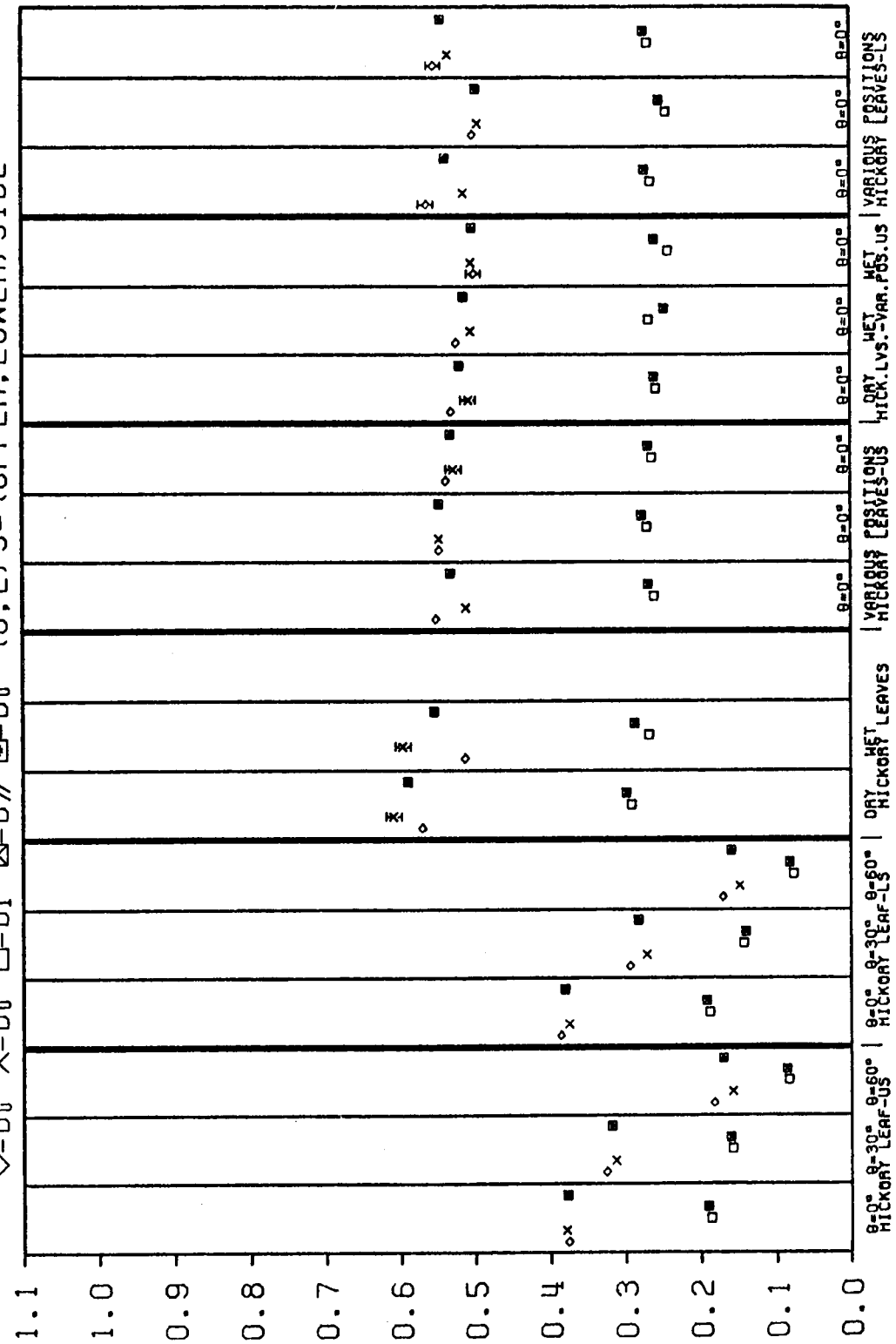


Figure 12. Backscattered fractions involving unpolarized radiation.

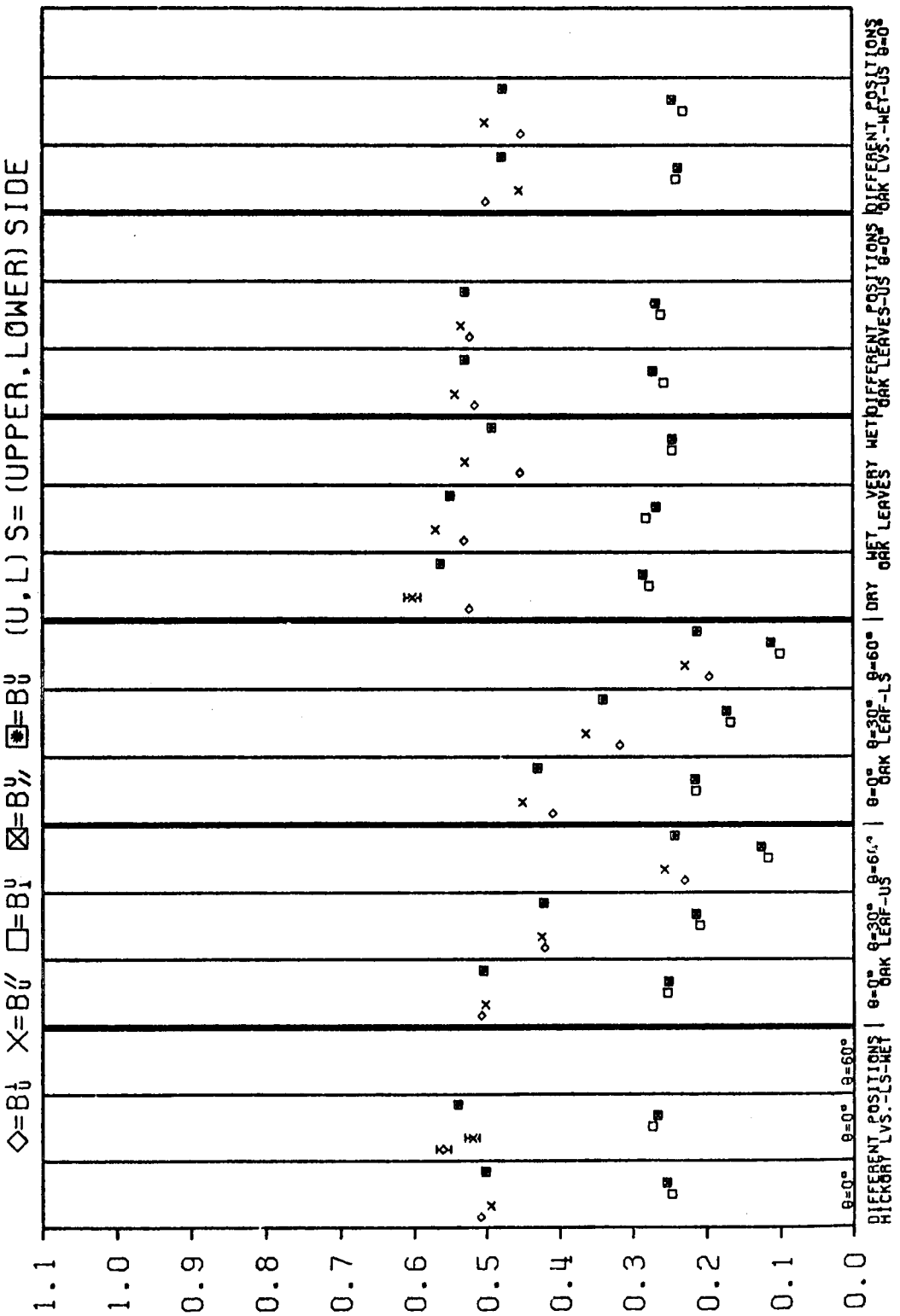


Figure 12. (continued)

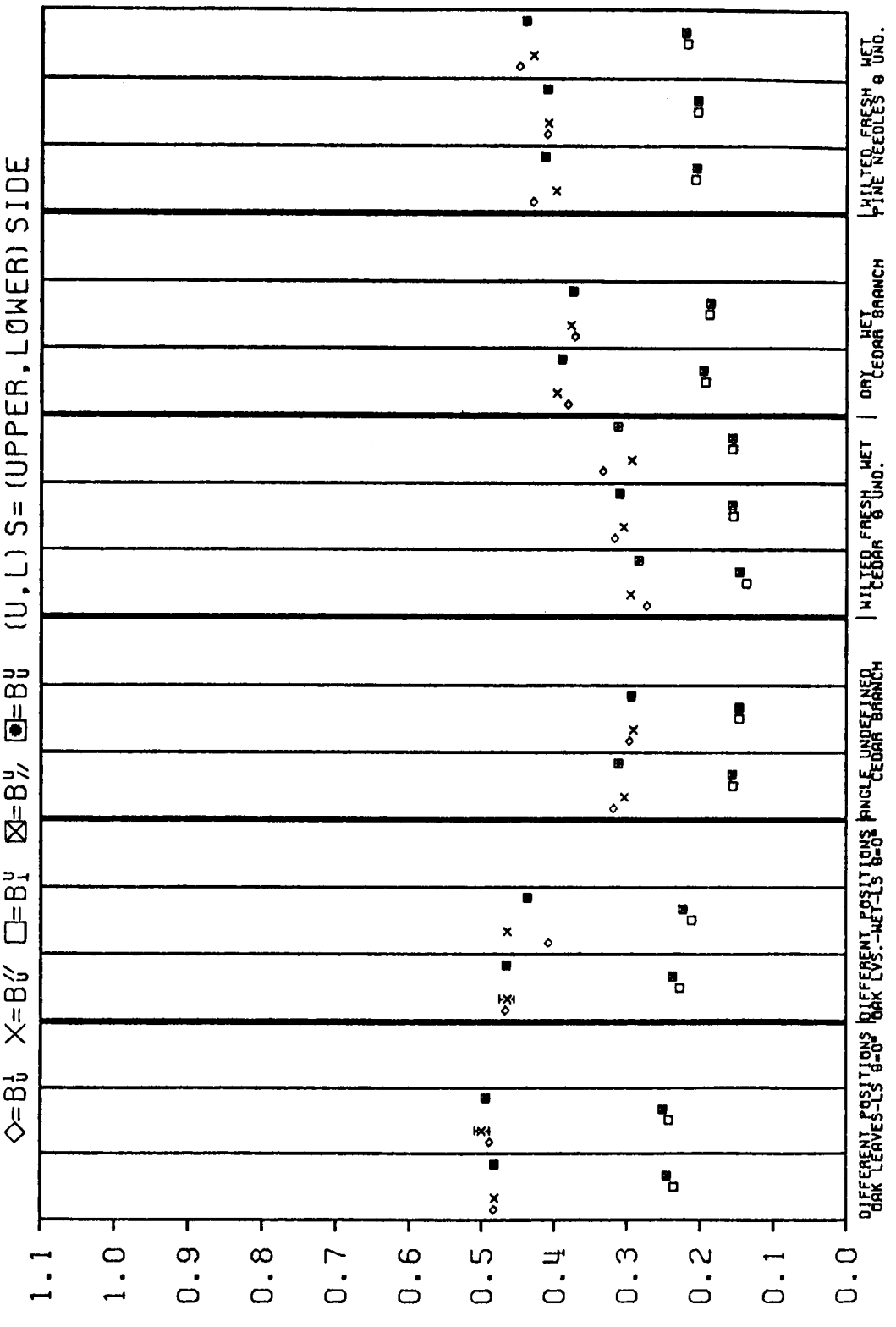


Figure 12. (continued)

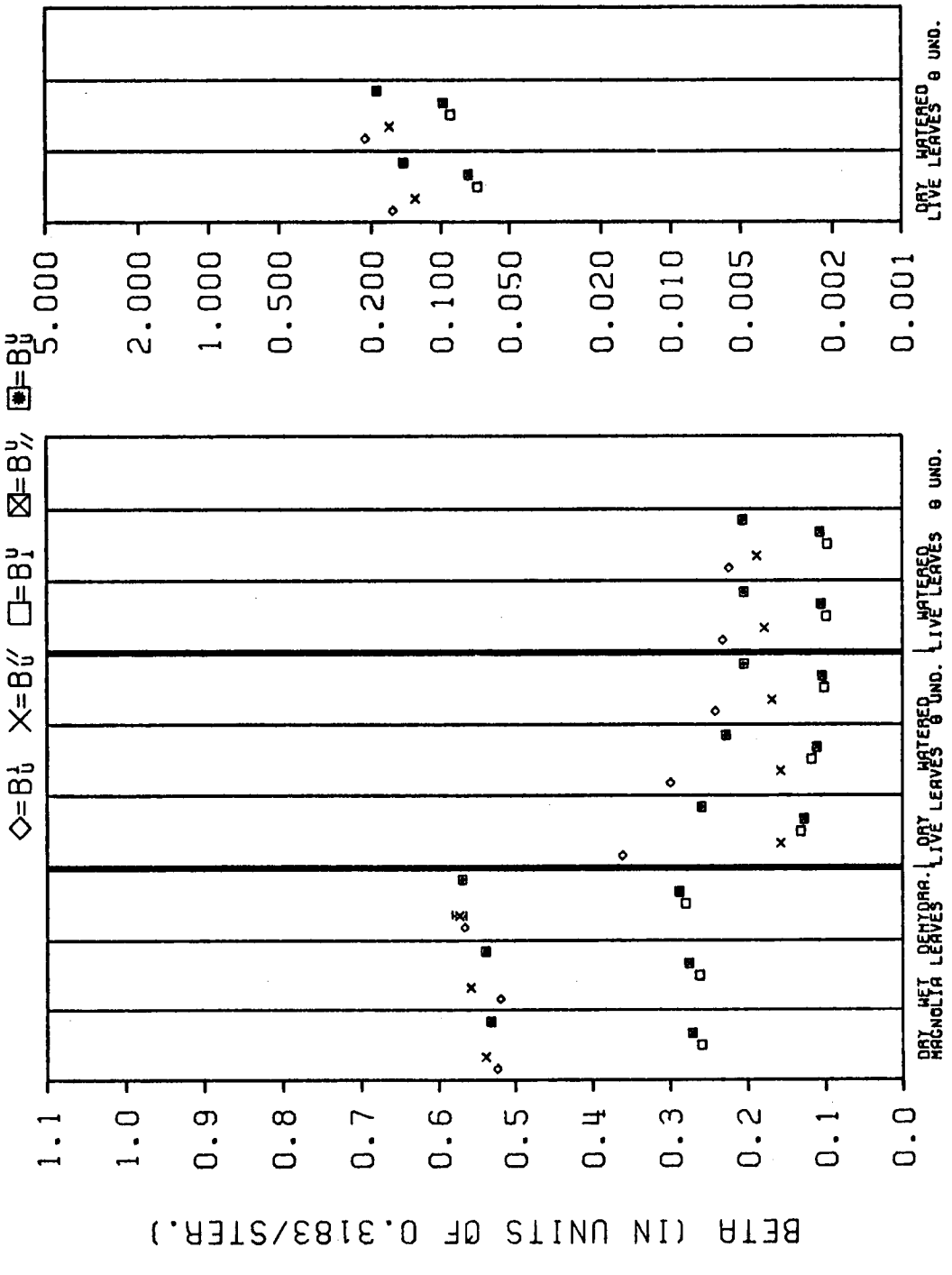


Figure 12. (continued)

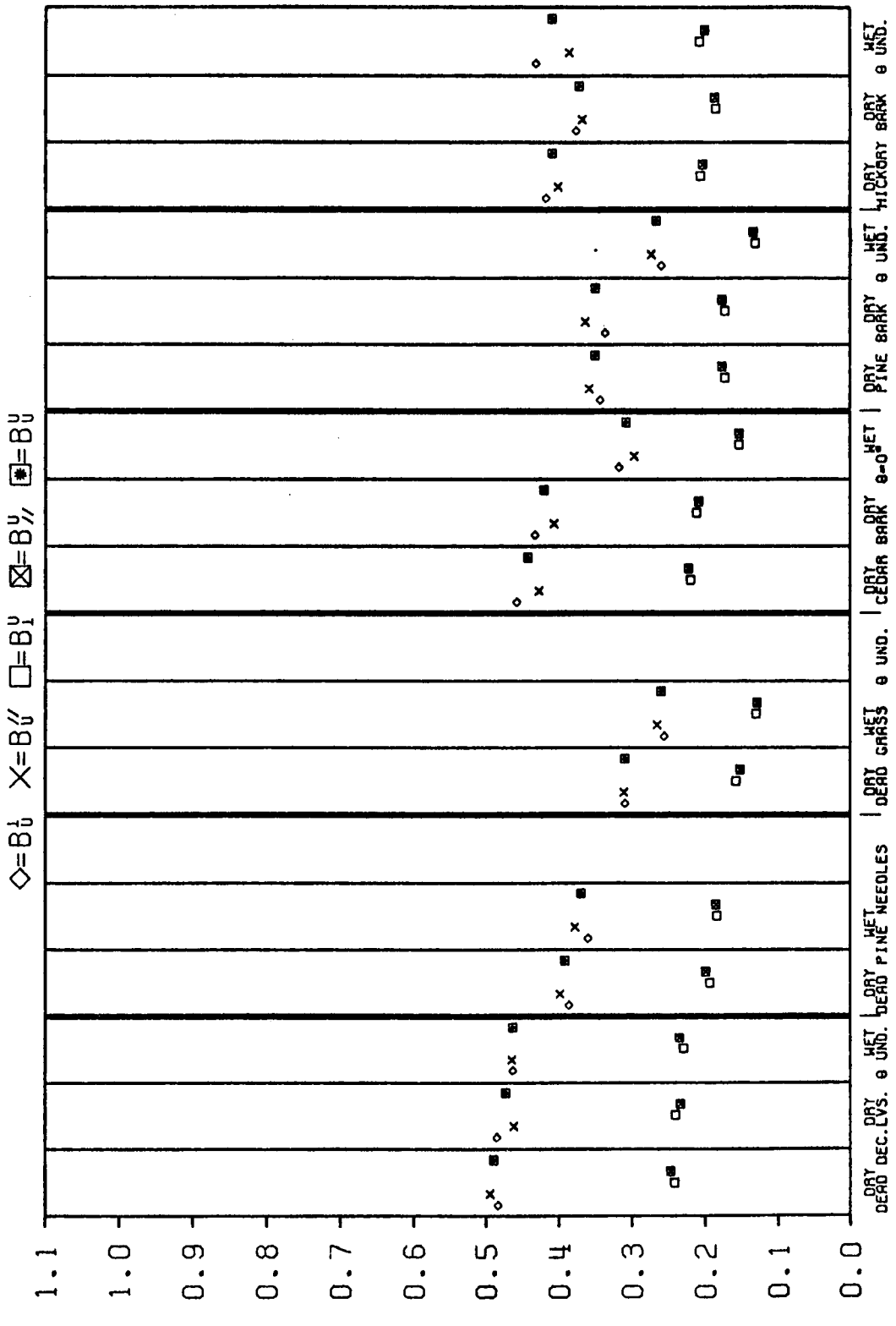


Figure 12. (continued)

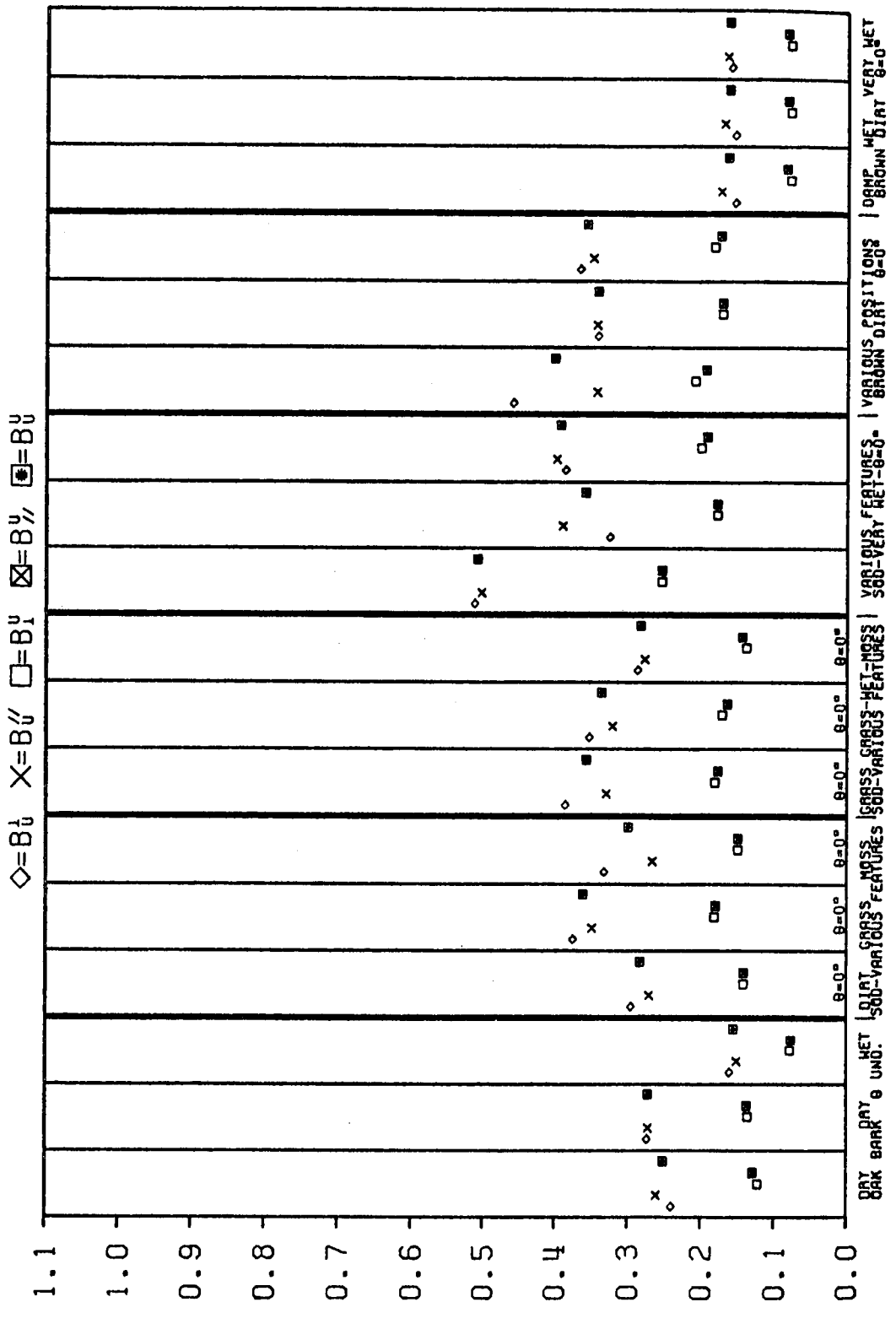


Figure 12. (continued)

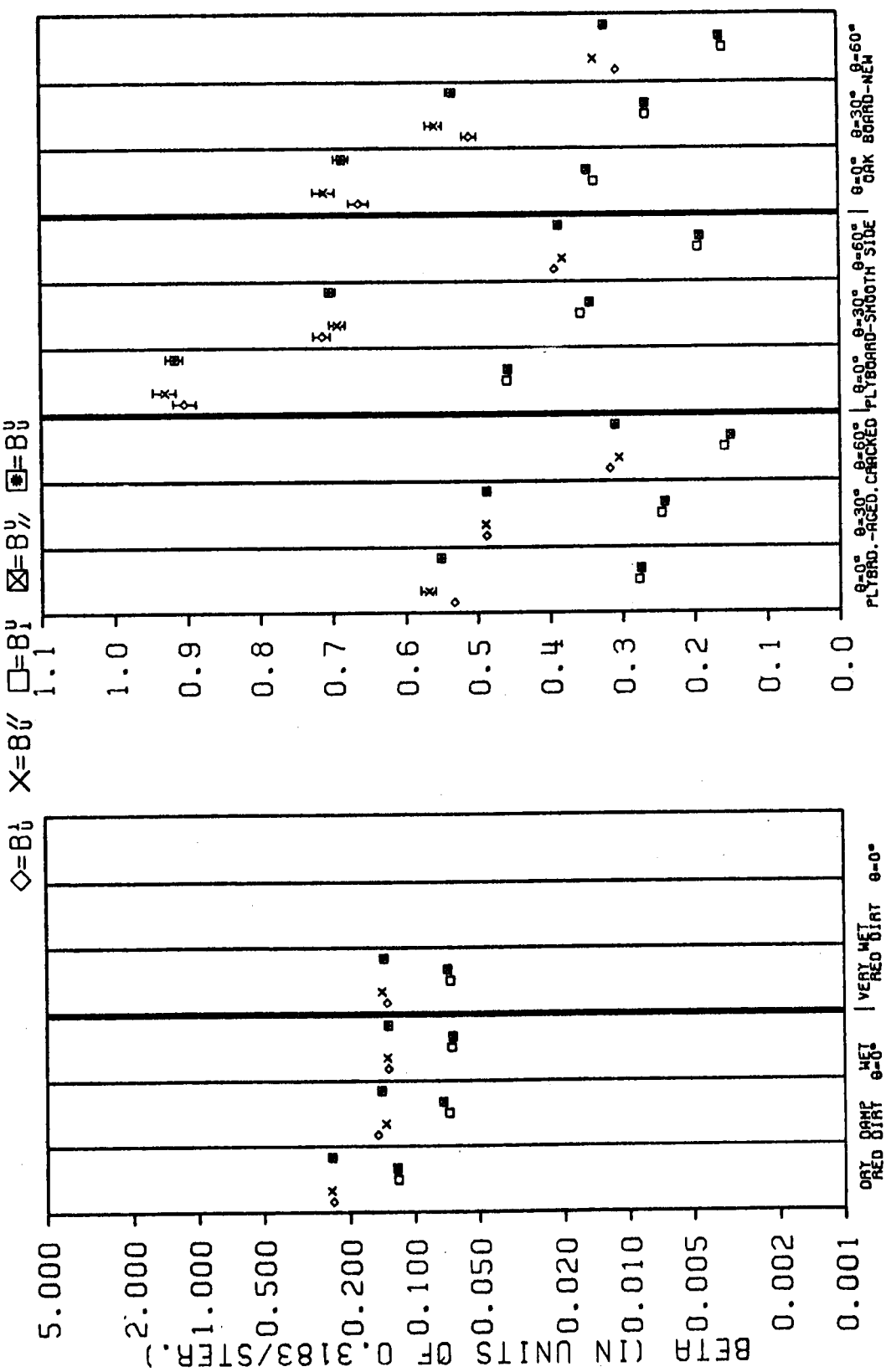


Figure 12. (continued)

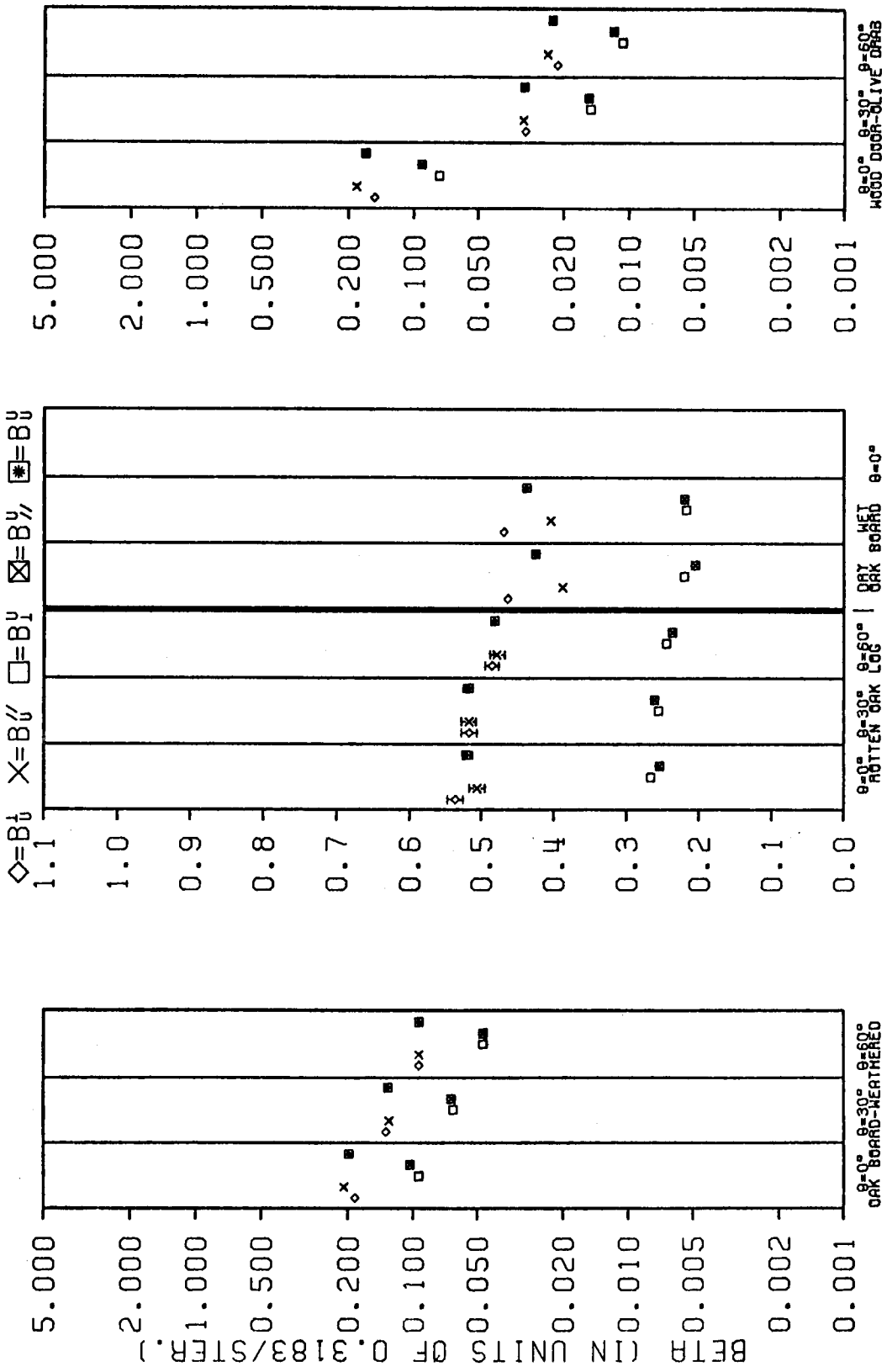


Figure 12. (continued)

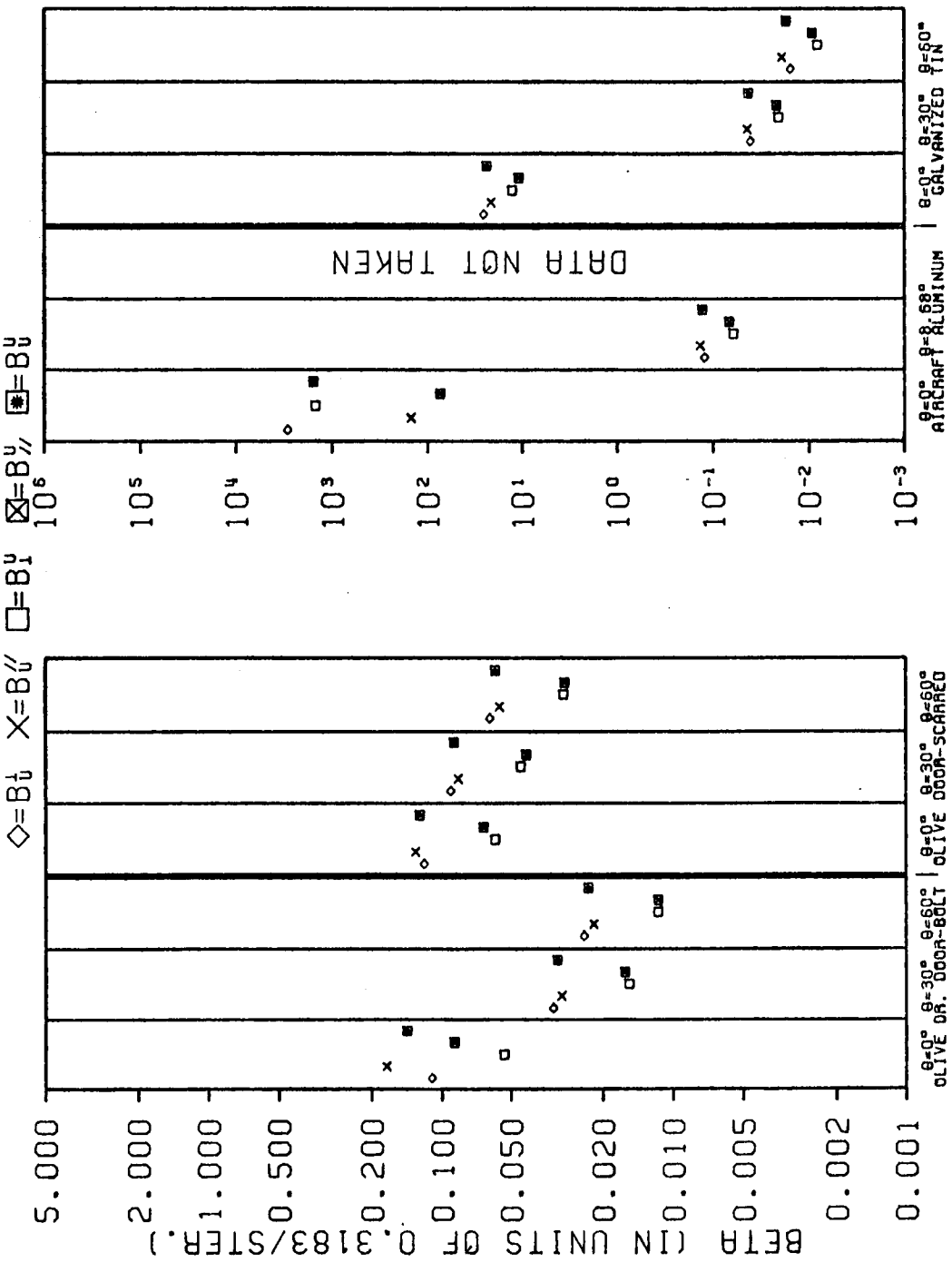


Figure 12. (continued)

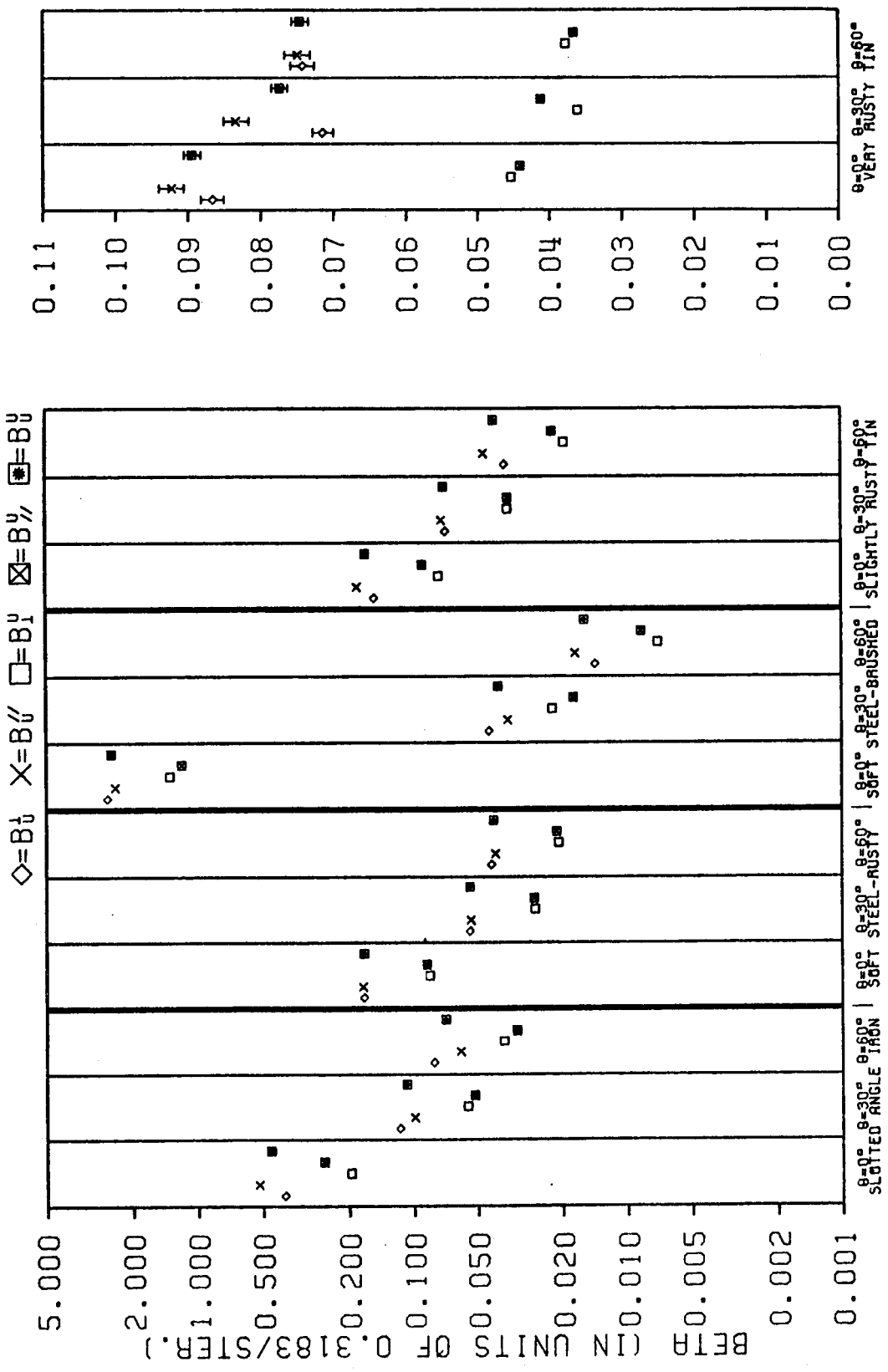


Figure 12. (continued)

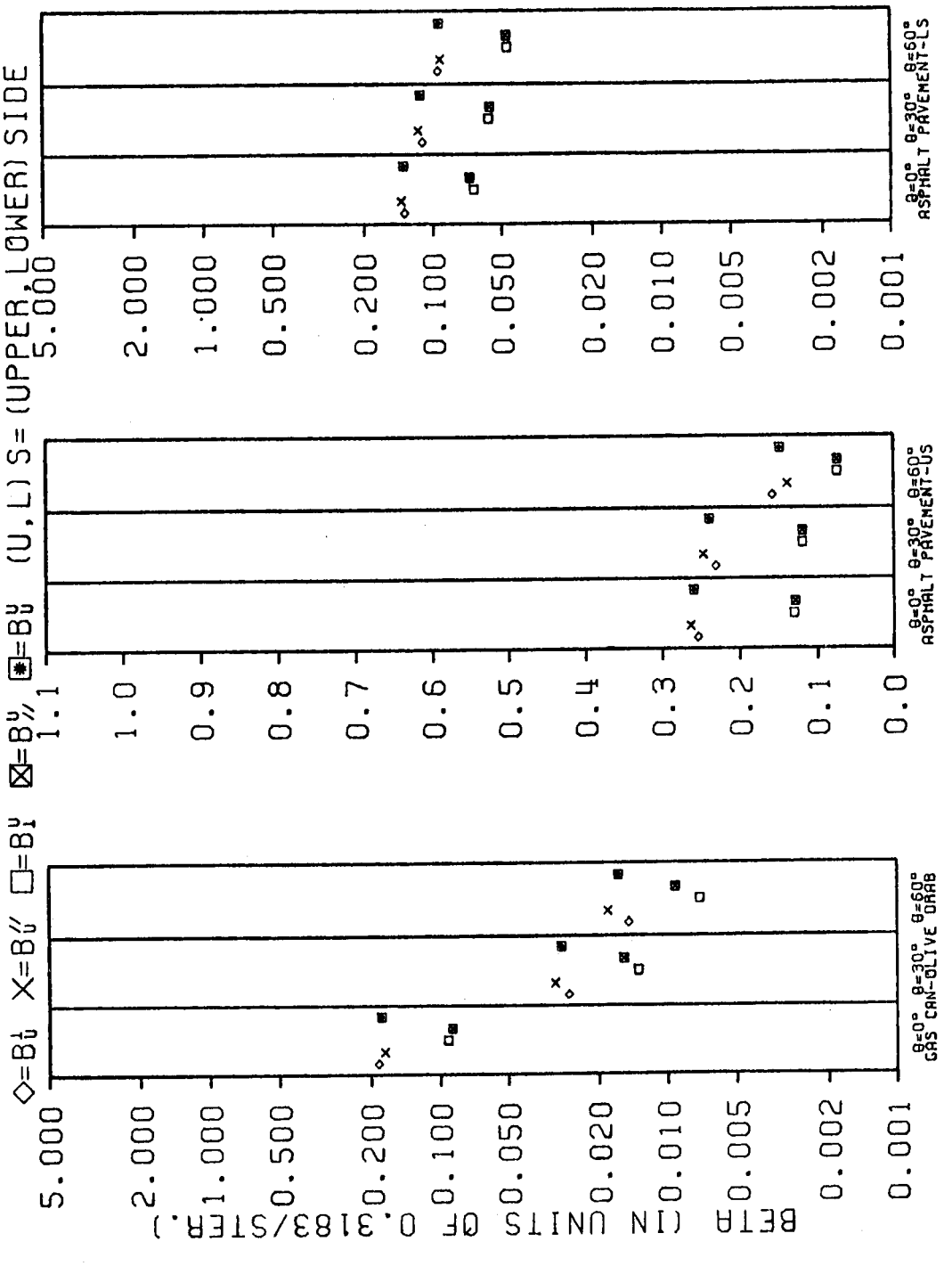


Figure 12. (continued)

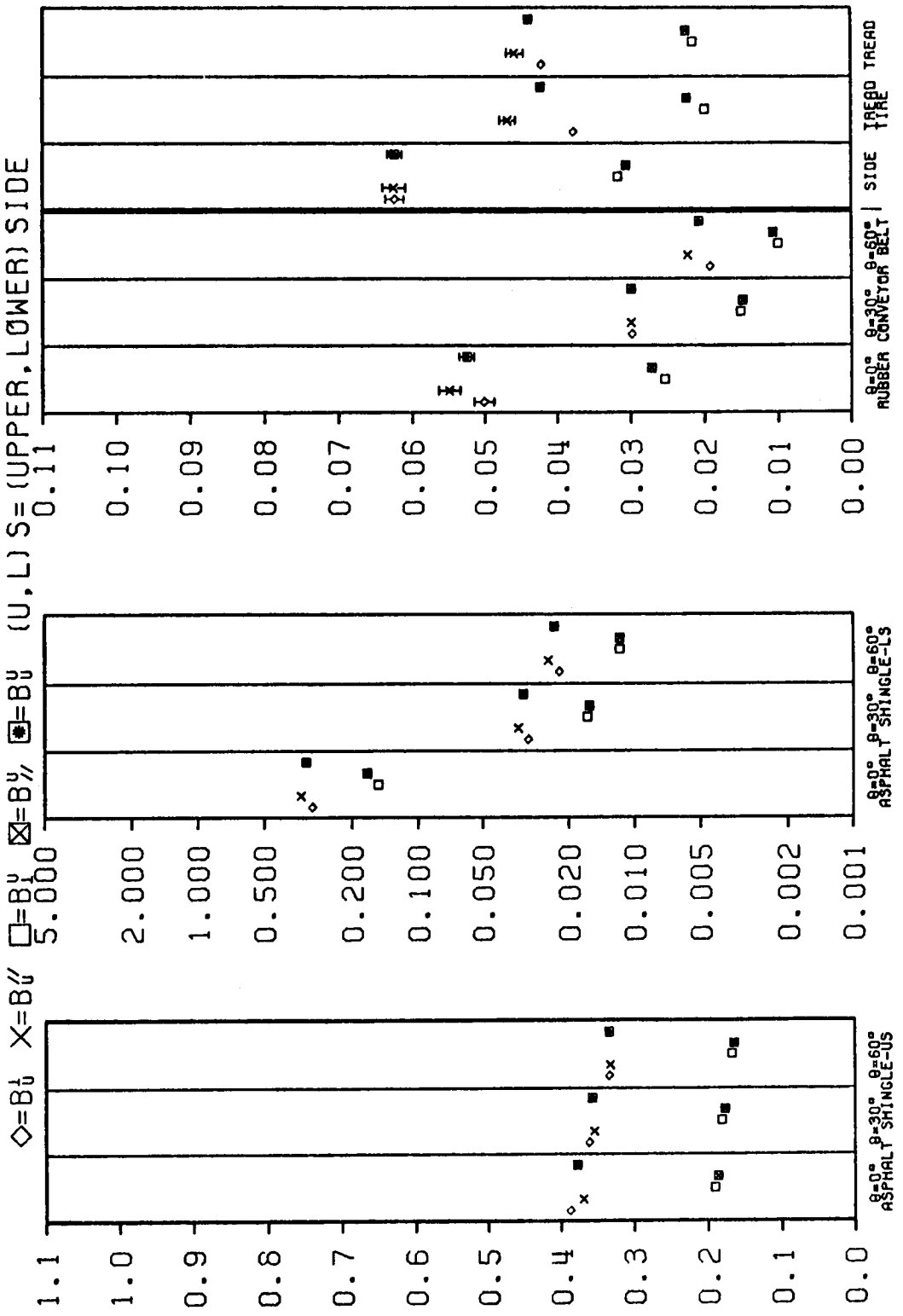


Figure 12. (continued)

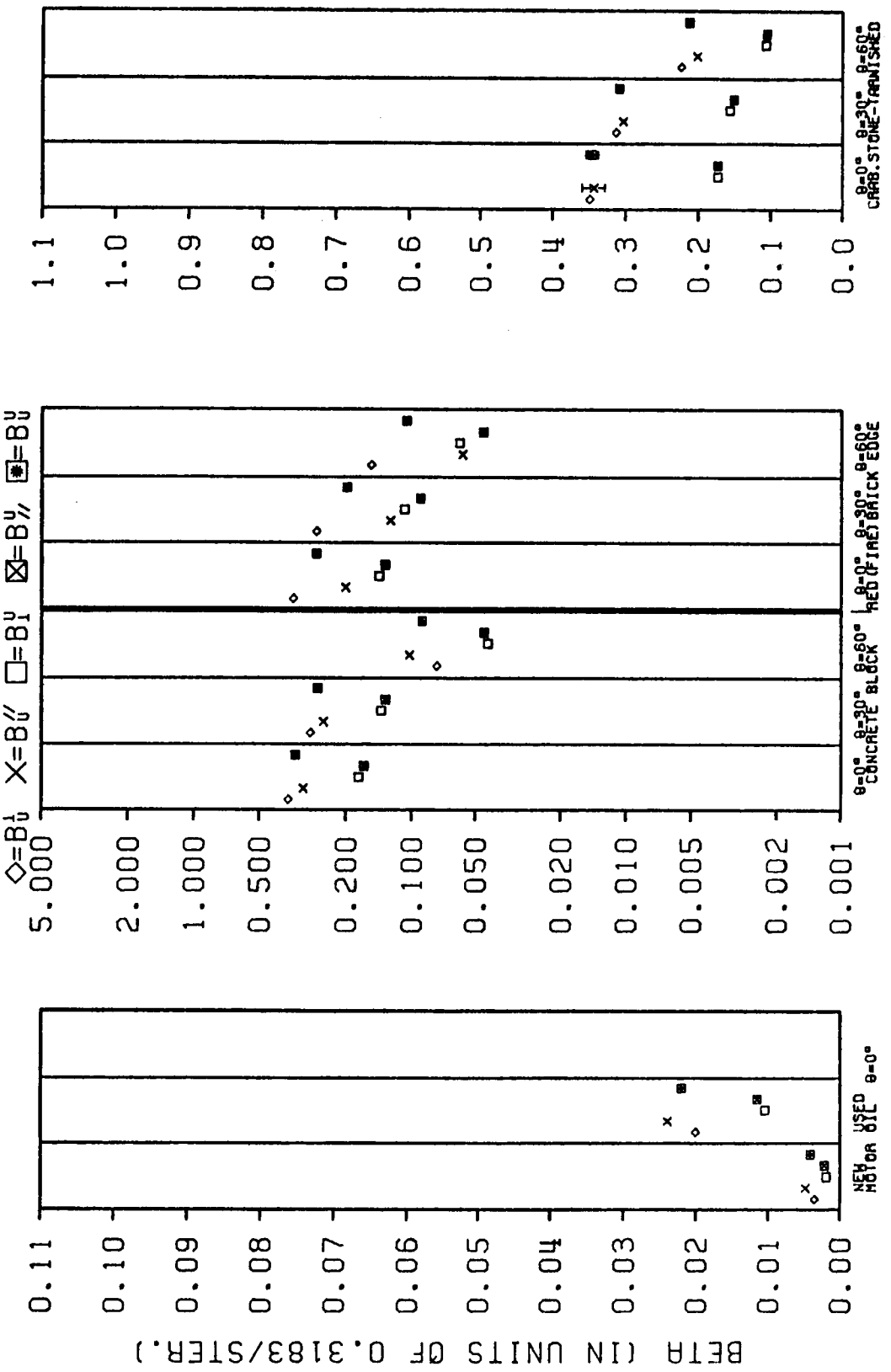


Figure 12. (continued)

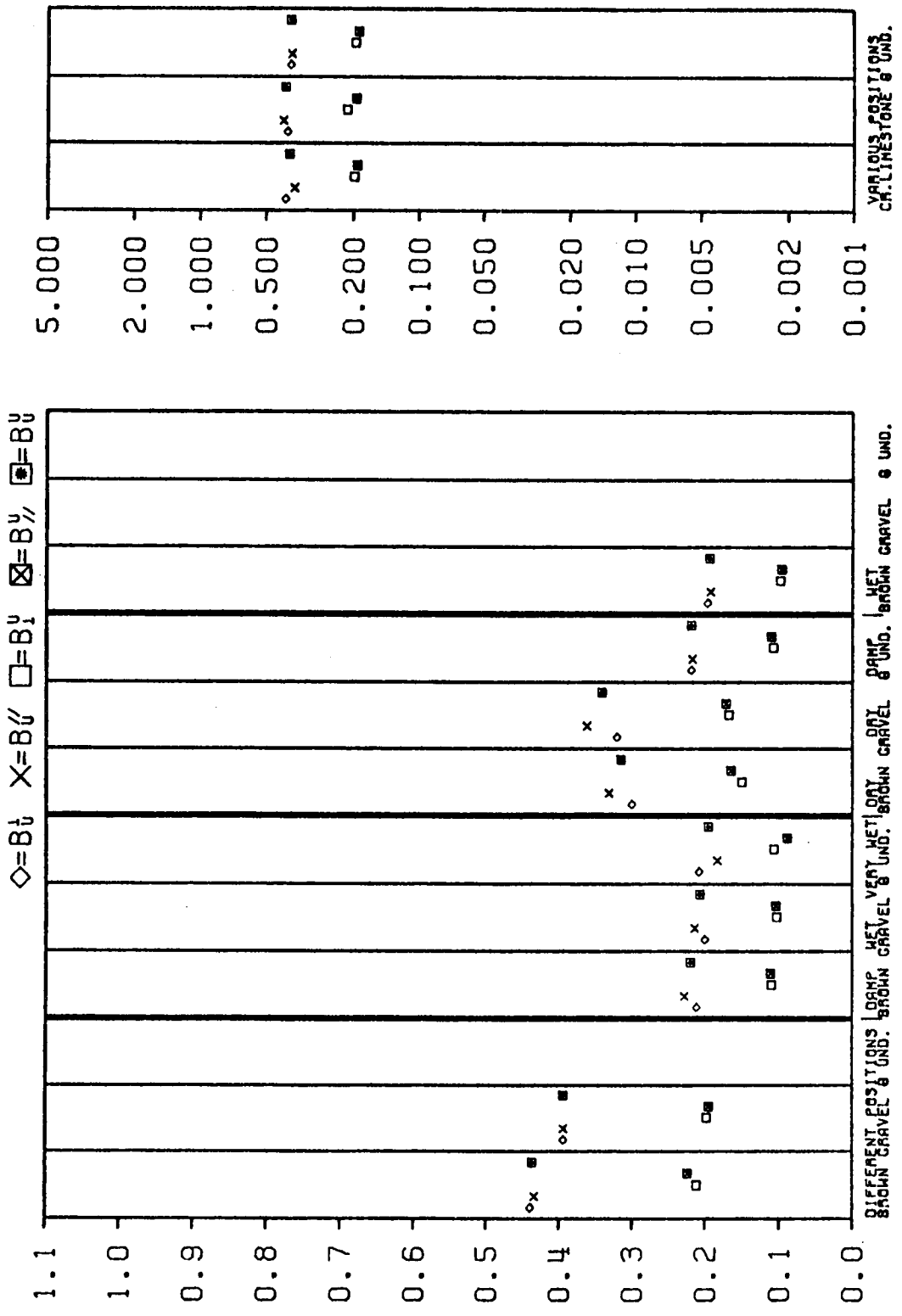


Figure 12. (continued)

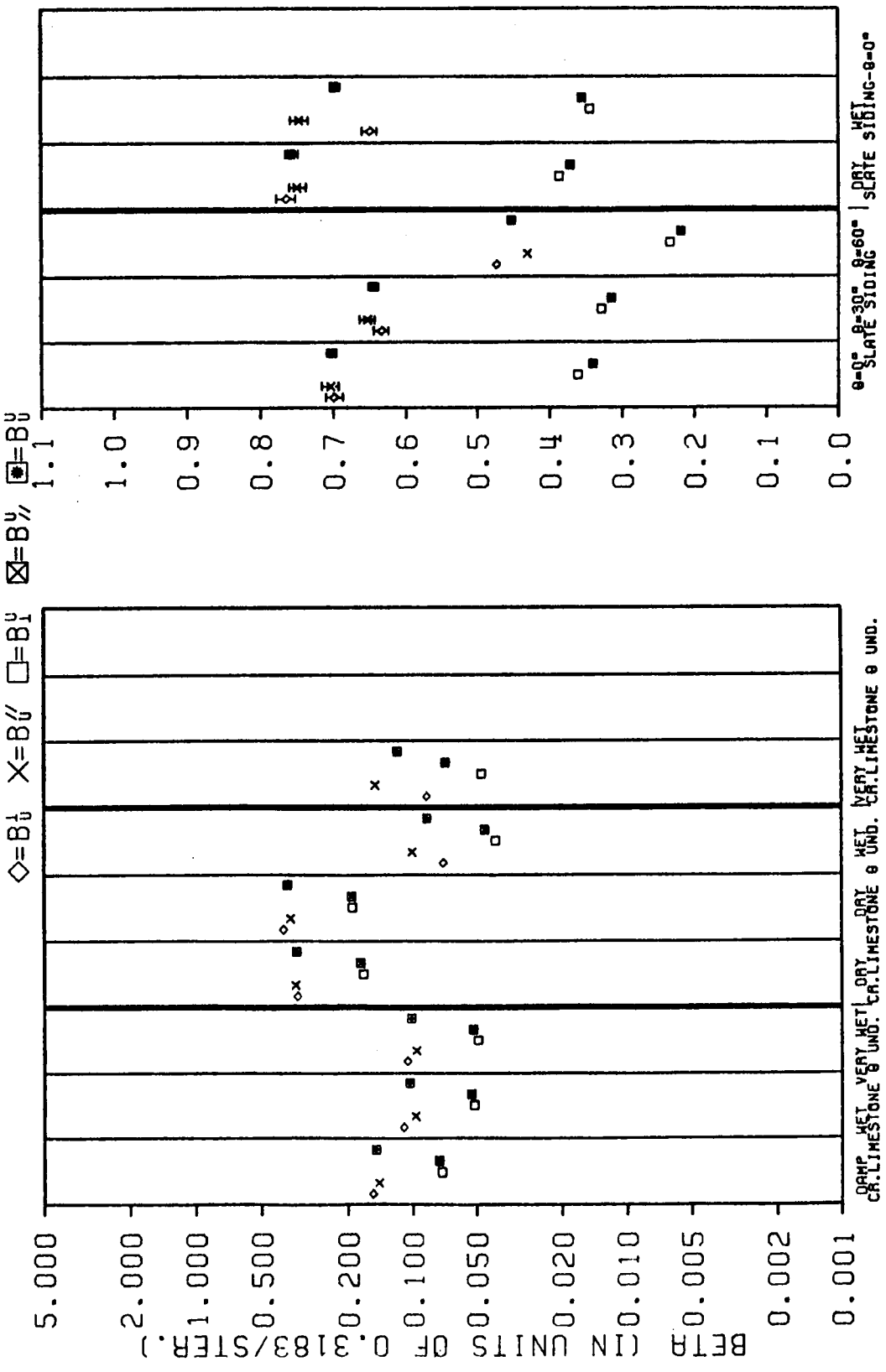


Figure 12. (continued)

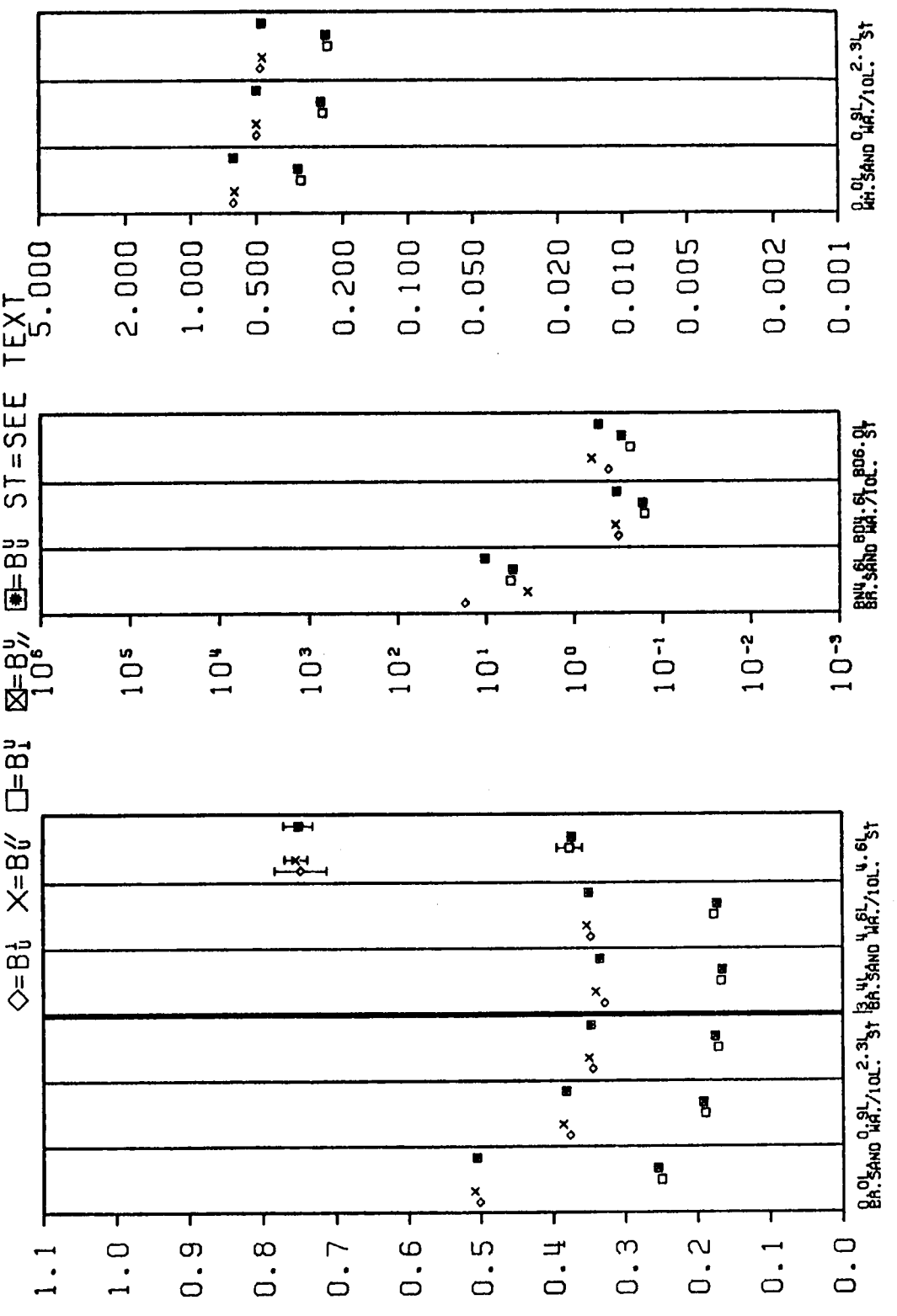


Figure 12. (continued)

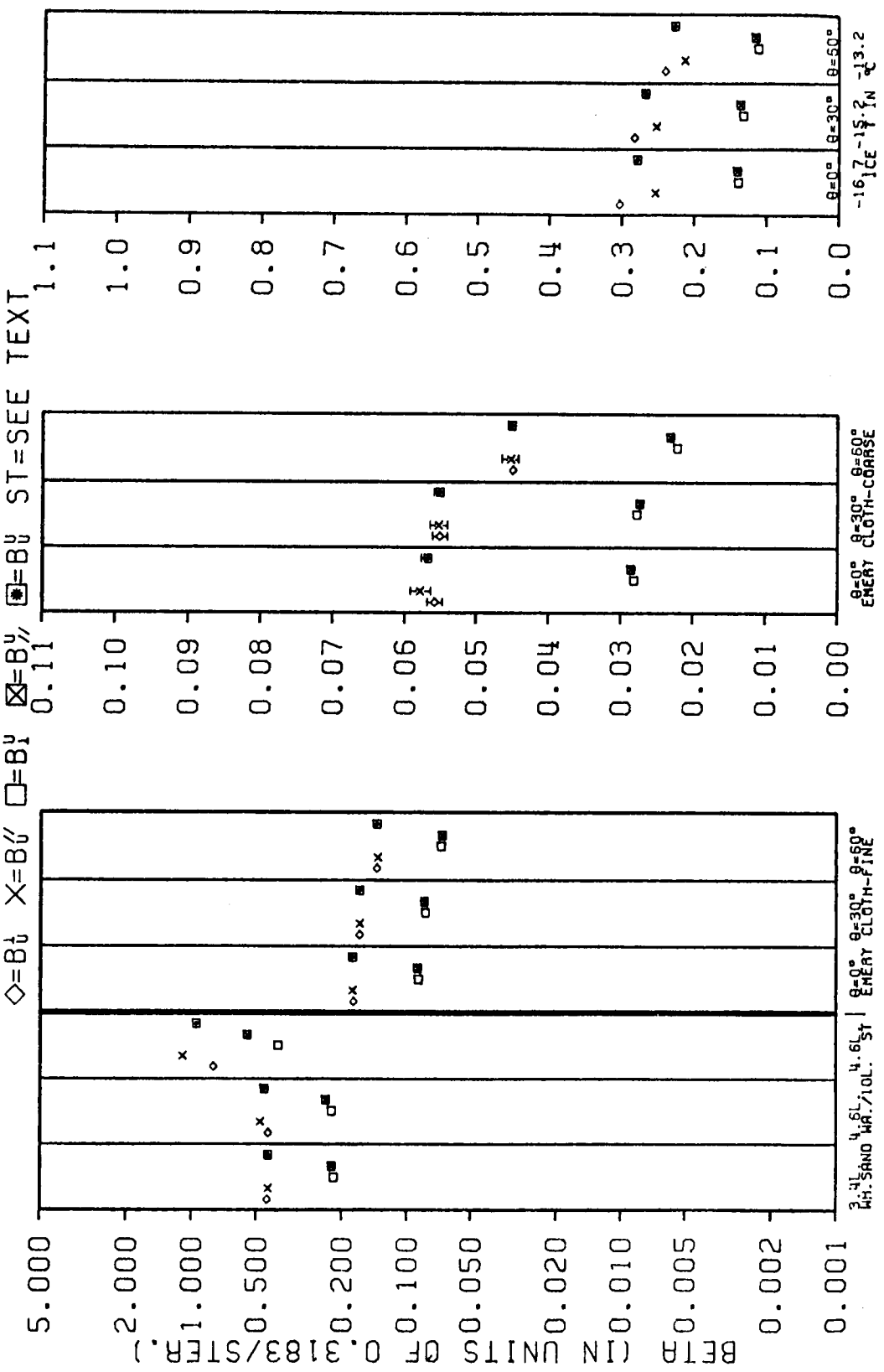


Figure 12. (continued)

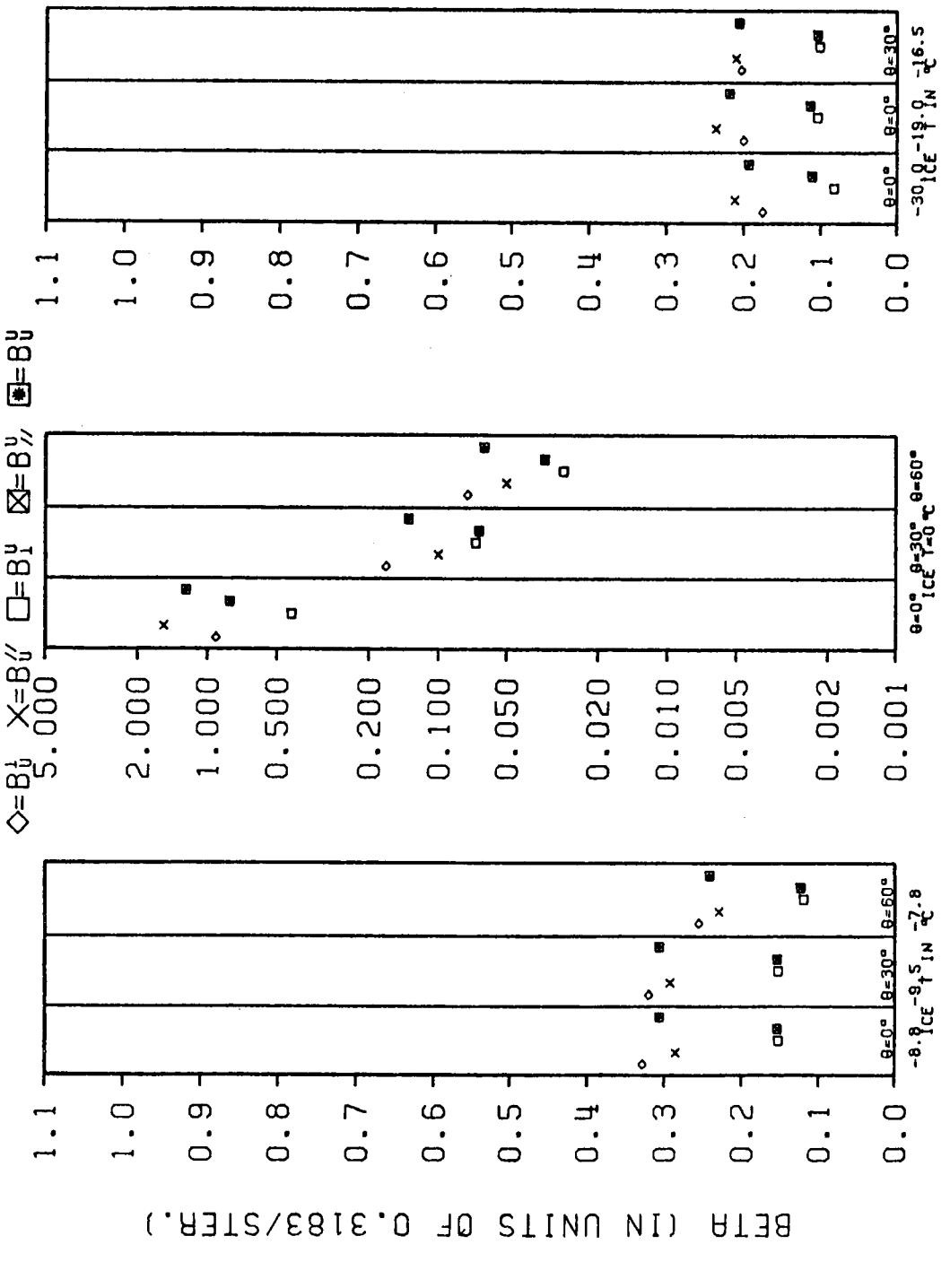


Figure 12. (continued)

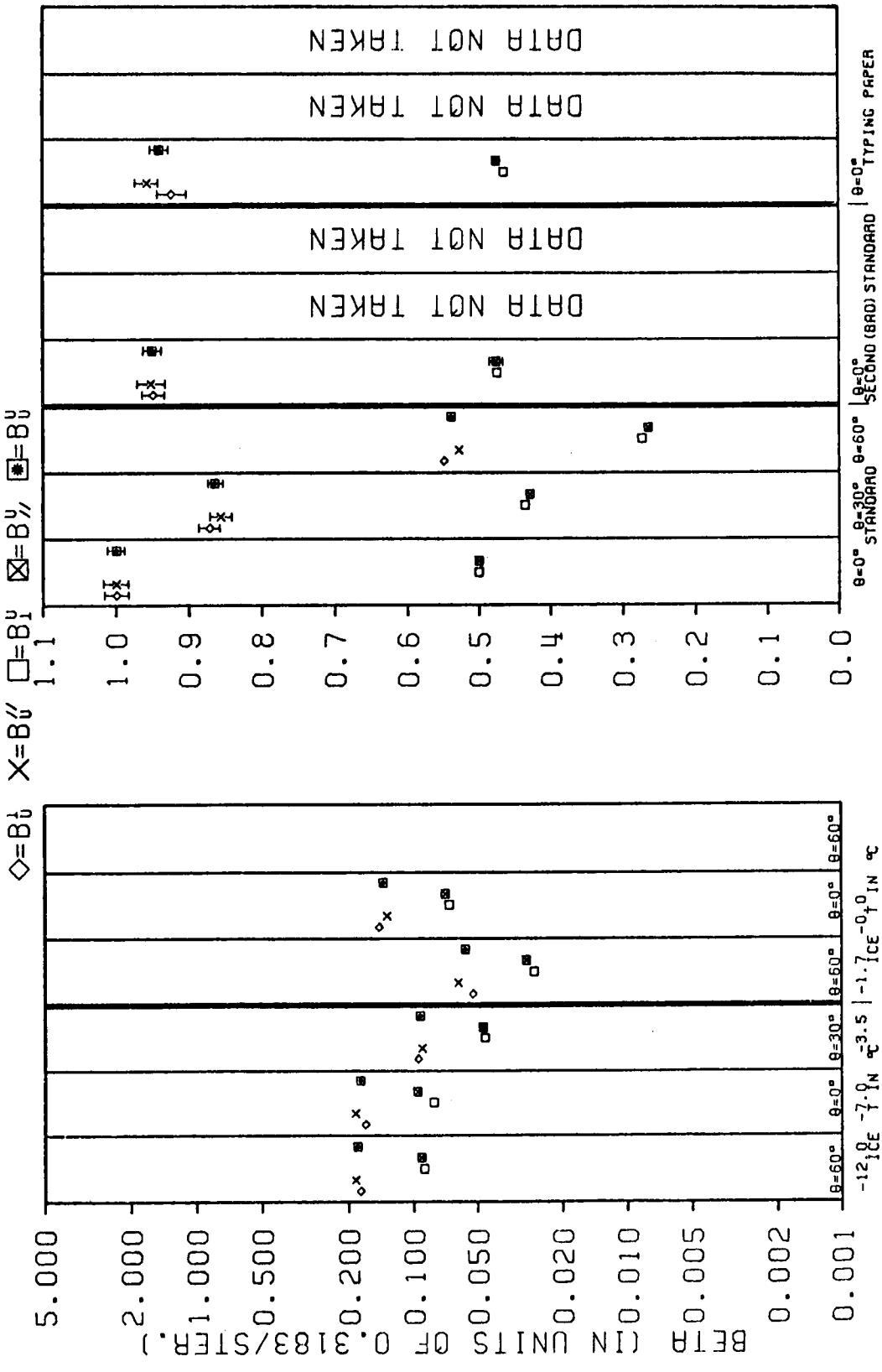


Figure 12. (continued)

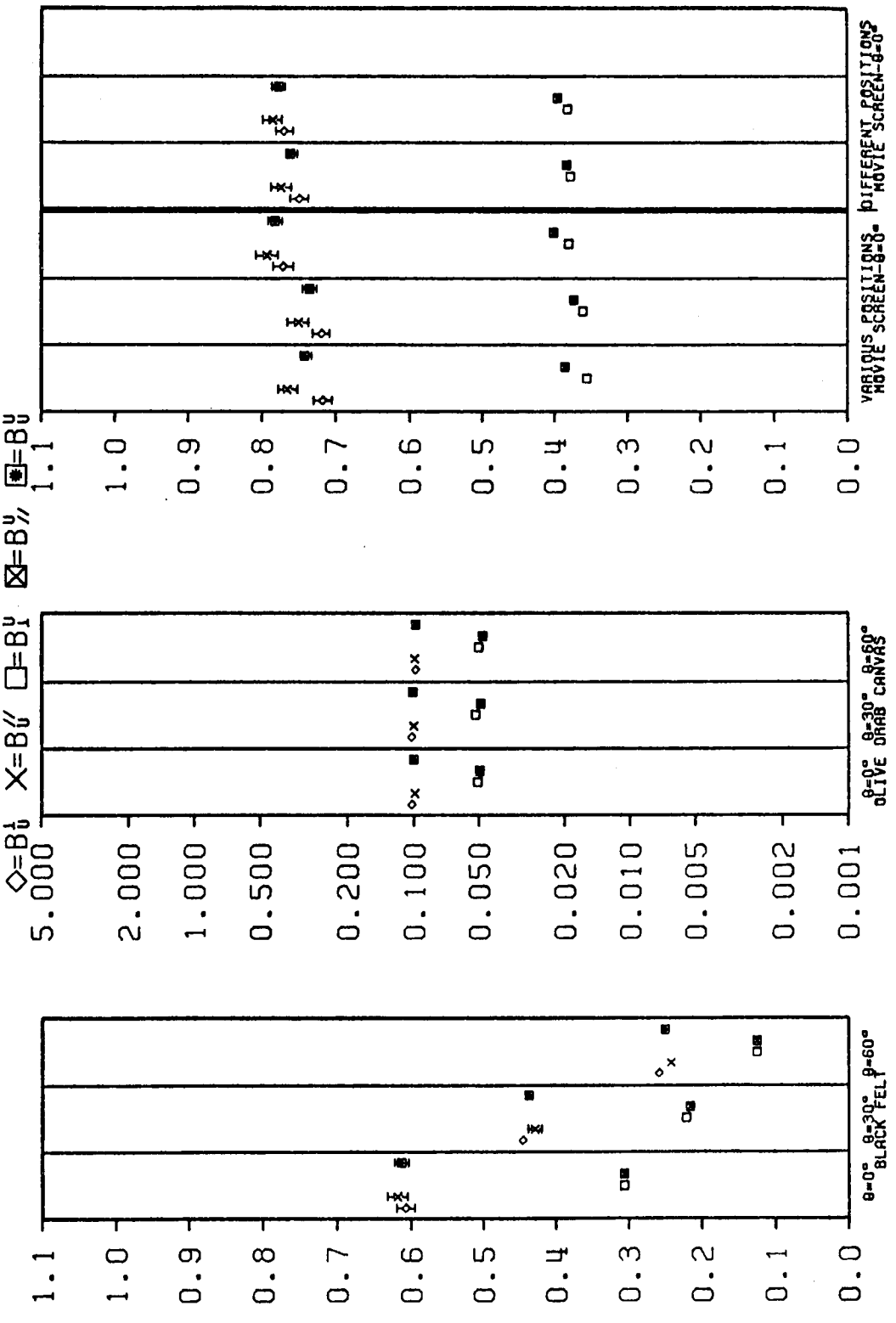


Figure 12. (continued)

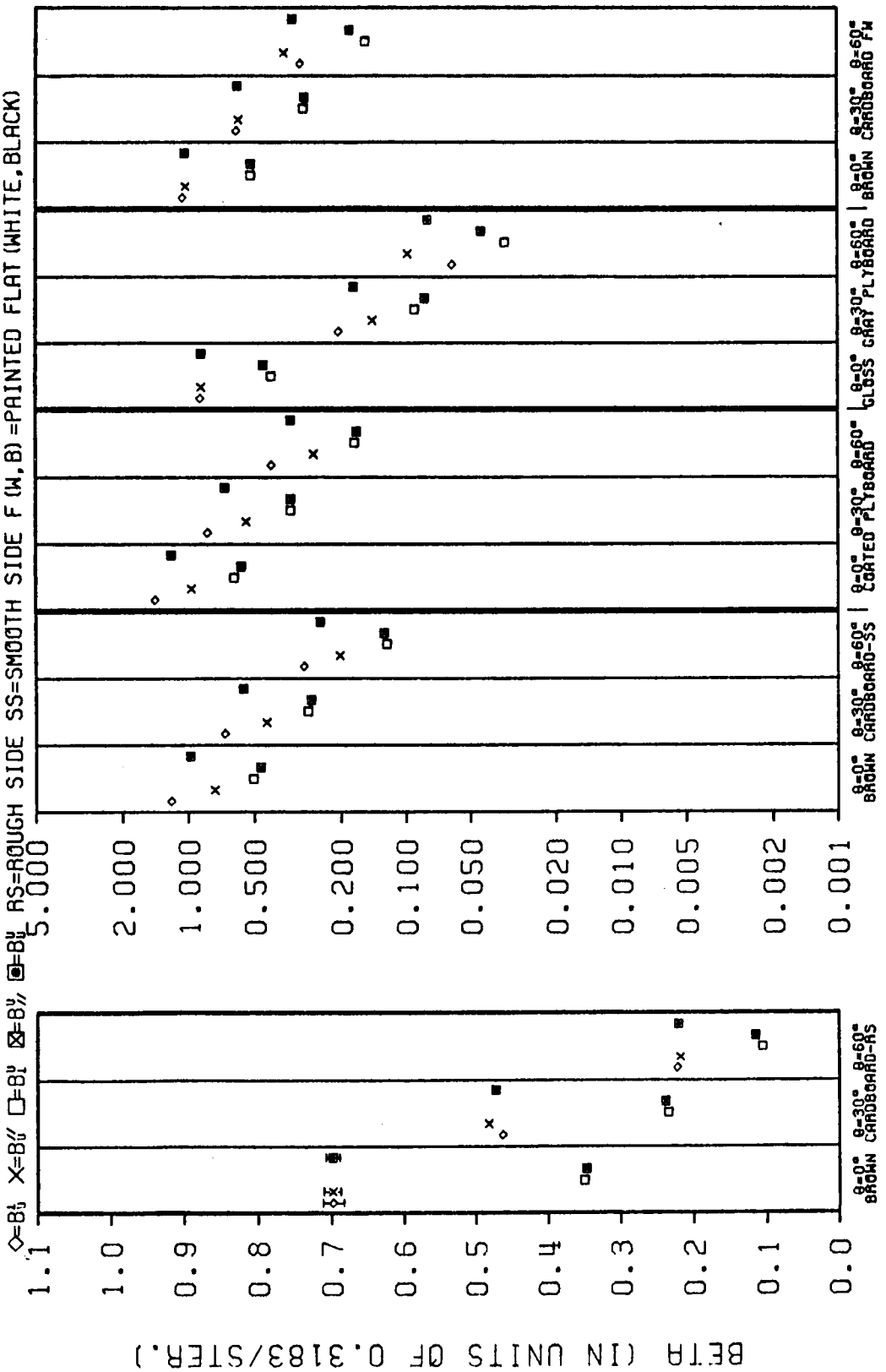


Figure 12. (continued)

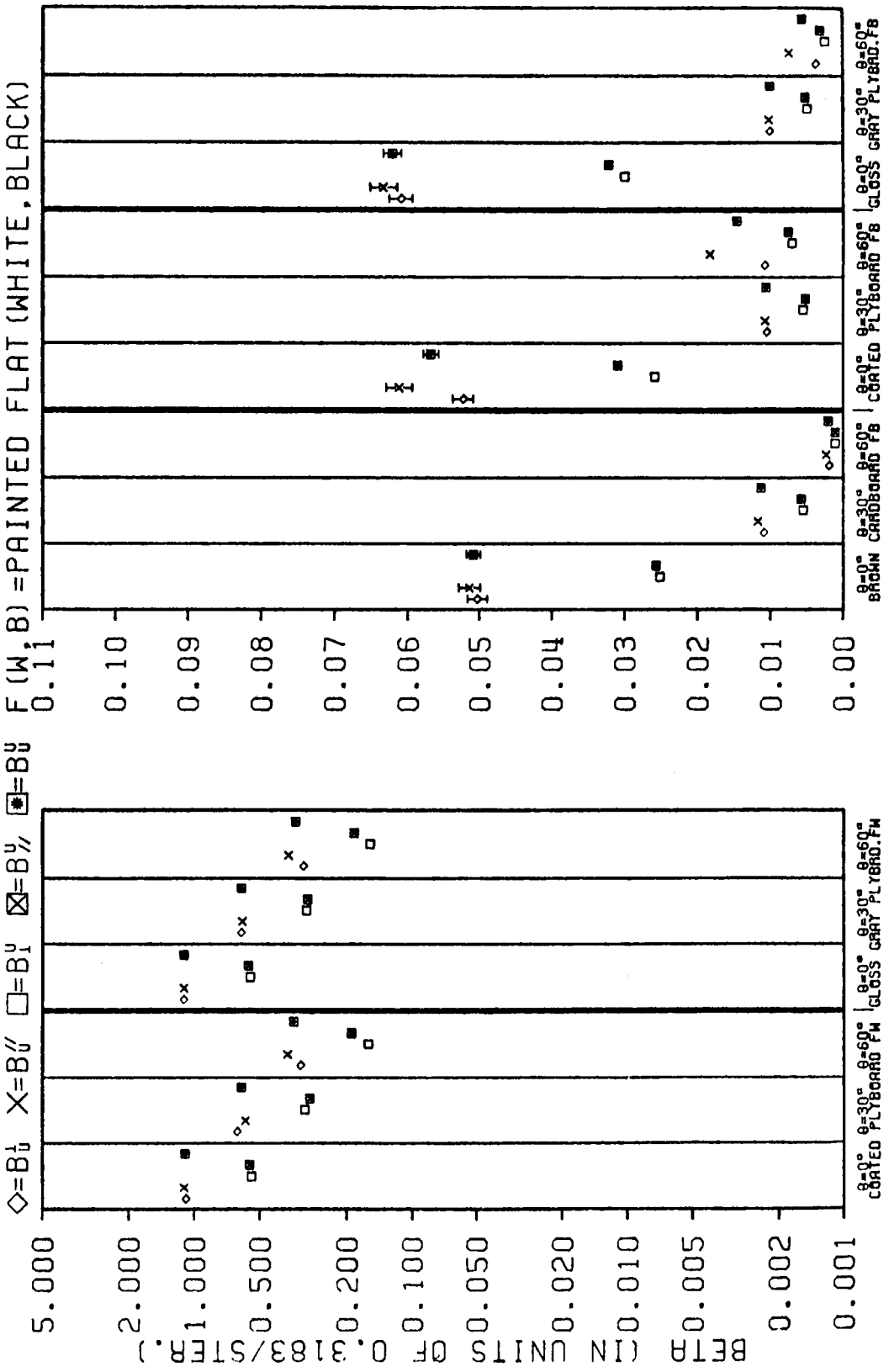


Figure 12. (continued)

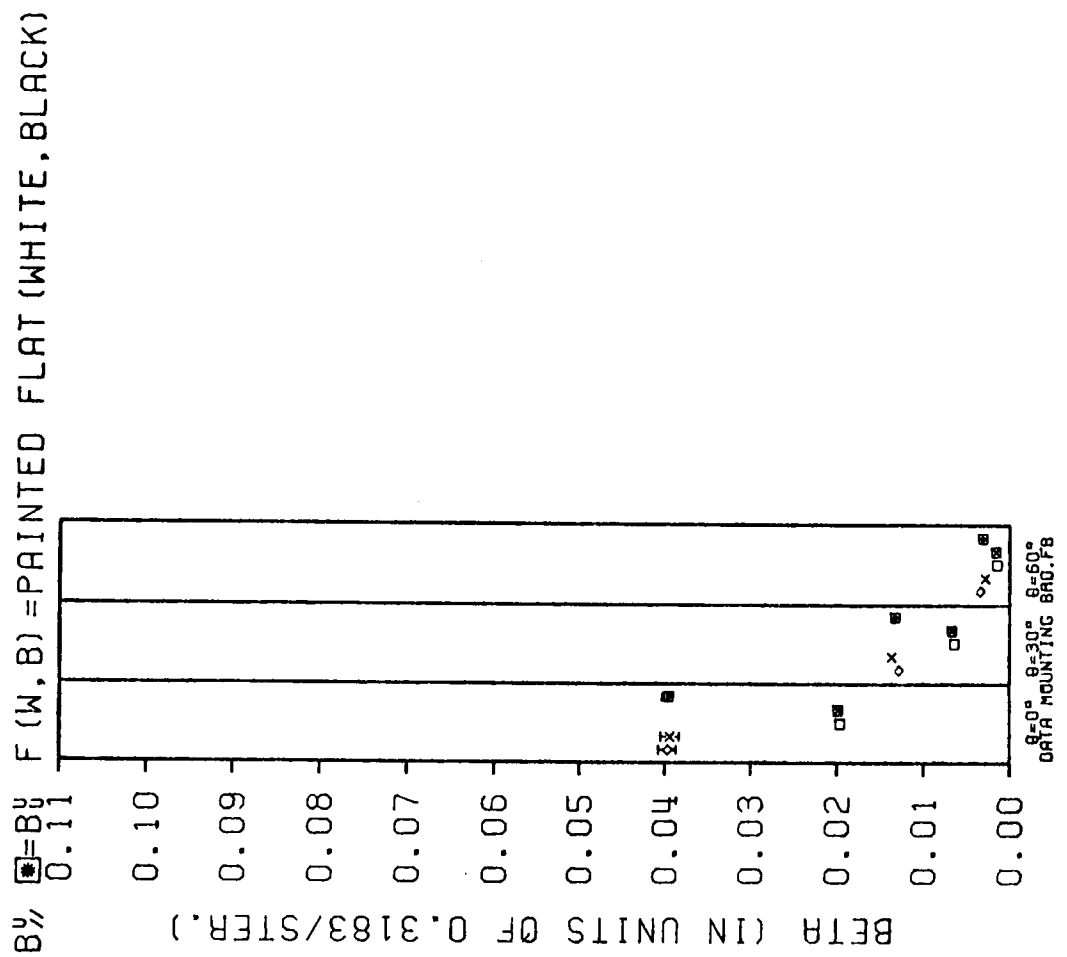


Figure 12. (continued)

The data are generally grouped in three sets of points representing the three angles of incidence at which the data were collected or in sets representing different surface conditions, such as dry or wet. If the angle of incidence is not given or is not obvious, it is discussed in the text.

The data are discussed in the general order in which they appear in each of the Figures 9, 10, 11, and 12. For the purpose of this discussion, the surfaces are collected into groups described in general as leaves, barks, dirts, woods, metals, petroleum products, rock-like surfaces, sands, ice, and miscellaneous. The miscellaneous group includes the good and bad standard surfaces, typing paper, black felt, canvas, a movie screen and cardboard. The effects produced by paints are also discussed.

The discussion is directed toward the polarization ratios and B_u^u the total fraction of unpolarized incident radiation which is backscattered. The latter are given in units of $\pi^{-1}\text{steradian}^{-1}$, that is, the values given are relative to a perfect diffuse reflector at zero degrees angle of incidence. When described in these units, the term relative backscattered fraction is used, and, therefore, B_u^u is referred to as the relative total backscattered fraction. The values discussed are generally the ones for zero angle of incidence (and zero angle of reflection), unless otherwise stated.

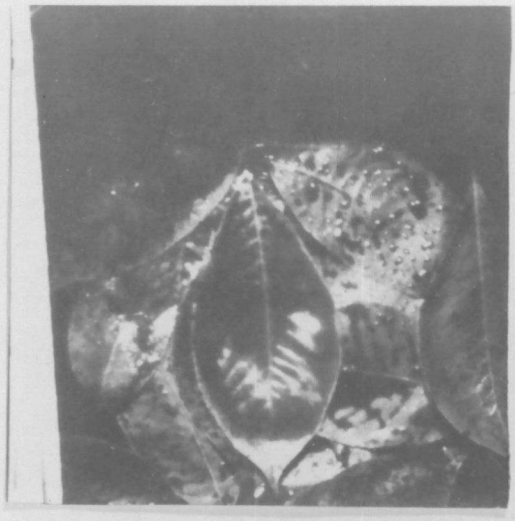
I. LEAVES

Data were collected from hickory, oak, cedar, pine, and magnolia leaves. Also data were collected from grass, moss, and clover in the form of a sod. Unless otherwise stated, all the leaves had been removed from the plant less than three hours prior to being used. The wet surfaces were obtained by spraying the surfaces with a garden hose nozzle.

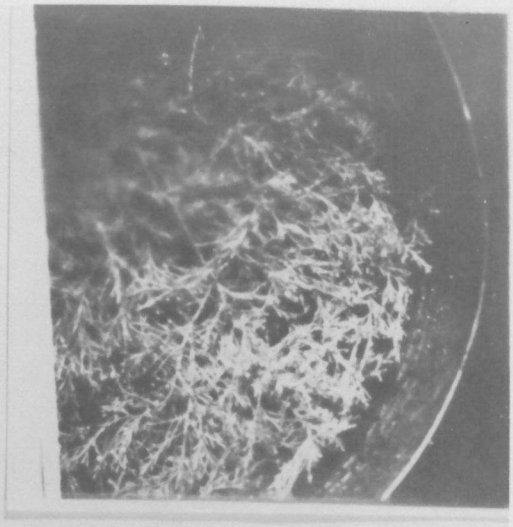
The first three sets of hickory leaf data; the first three sets of oak leaf data; the first and third sets of cedar data; and the magnolia leaf data were collected in the early summer during a very wet period. The first and third sets of cedar data were not taken from the same sample. The third set were taken from healthy cedar, whereas the first set were taken from cedar which contained dead undergrowth as the result of its being stunted by the overgrowth surrounding the cedar tree. The first data in the first set of the cedar data were taken from the greenest portion of the sample, and the other data were taken from a portion containing some exposed dead undergrowth. The backscattered fractions for the cedar branch used for the first set of data varied 10% over the surface. They decreased by 20% when the branch was oriented such that the laser beams were aimed approximately along the direction of growth of the cedar. The polarization ratios were

observed to be uniform for all positions and orientations of the cedar branch. The other leaf data and the grass, moss, and clover data were collected in mid-fall. All leaf samples contained only green vegetation except the cedar used for the first set of cedar data and those which are listed as dead. These contained no green vegetation. The dry-wet sets of data from hickory leaves and oak leaves without the angles given were collected from leaves piled into the holder under the mirror at an average of zero degrees angle of incidence, but without being placed in any particular orientation. The magnolia leaves had curved surfaces, and the angle of incidence may have differed from zero degrees because of this. When water was added, it wet the entire surface of each sample but one. The surface of the magnolia leaves, however, remained dry except for scattered water beads. Water also tended to sit in beads on all of the green vegetation and on the dead pine needles. The wet hickory leaves are shown in Figure 13a; the wet cedar is shown in Figure 13b; and the dry and wet magnolia leaves are shown in Figures 13c and 13d.

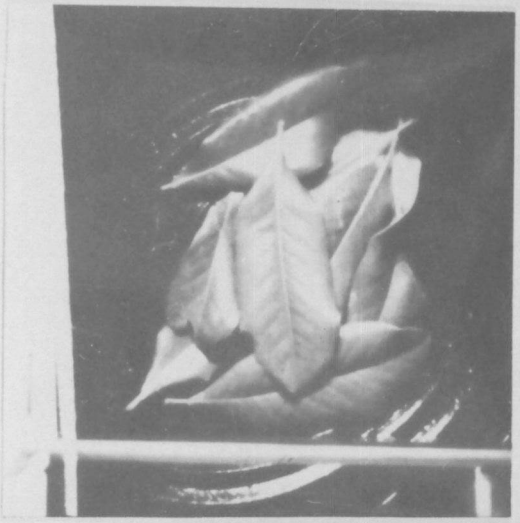
The polarization ratios for leaves were in the range of 0.6 to 0.9 for all data except the upper side of hickory and oak leaves where the angle of incidence was greater than thirty degrees. The ratios for the upper sides of the hickory and oak leaves were about 15% larger than the ratios



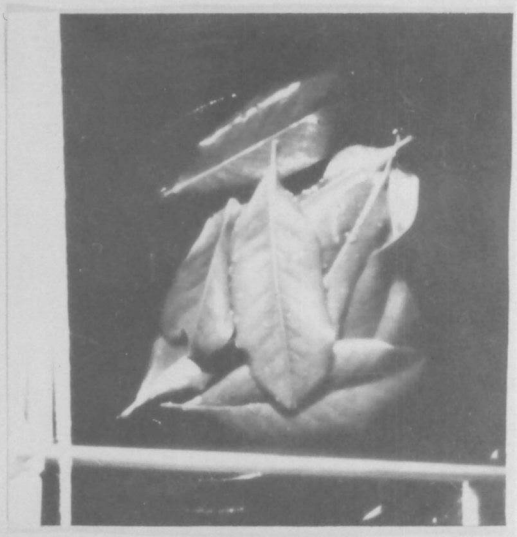
(a)



(b)



(c)



(d)

Figure 13. Leaves. (a) Hickory; (b) Cedar; (c) Dry magnolia; (d) Wet magnolia.

for the lower sides, although the lower sides looked rougher to the eye. The radiation is able to penetrate the leaf (4) to some extent, and volume effects or even scattering from the opposite side of the leaf could have been present. No distinctions could be seen between the ratios for the green summer leaves and the green fall leaves.

The polarization ratios for fresh pine and fresh cedar were noticeably larger than the ratios for wilted or dead samples. Two attempts were made to measure the dependence of the polarization ratios, percent depolarizations, and backscattered fractions on moisture content or freshness. Changes produced in these quantities by changes in the freshness of green vegetation have been observed using linearly polarized radiation at 0.6328 micrometers wavelength (5). The leaves of a live philodendren plant were used as samples. The plant was initially in a dehydrated state. Water was then added in a sufficient quantity to wet the entire volume of dirt surrounding the plant. As the result of the lack of a suitable mounting procedure, the leaves were not held in a particular orientation in the beam and shifted considerably as the plant stems began to straighten after the addition of the water. The first series of data with the live leaves were collected from the plant in a very dry state, and from the same plant thirty seconds after watering, fifteen minutes

after watering, thirty minutes after watering, and one hour after watering. The second series were collected from the plant in a dry state and from the same plant one minute after watering.

For grass, clover, and moss, the data were collected from a piece of sod on which a mixture of each was growing. Approximately 50% of the visual surface was white clay dirt. The polarization ratio went from approximately 0.7 to approximately 0.95 as water was added to the sod. This was possibly the result of the vegetation's becoming weighted by the water such that it shadowed more of the dirt. If this were true, the data labeled as dirt in the first set of the sod must have resulted from a higher percentage of scattering from vegetation than was visually apparent since they imply that the dirt and the vegetation have equivalent depolarization properties. The large value of the relative total backscattered fraction for the first data from the very wet sod was due to the specular reflection by a shallow water surface. The polarization ratio, however, was unchanged from the other data in the set, possibly because of particles on the surface of the water. None of the ratios from the other samples were noticeably affected by adding water except where some splitting is seen between the results from the two lasers, possibly due to a specular reflection from the water.

The relative total backscattered fractions varied from approximately 0.3 to 0.5 for most of the leaf surfaces. The low values of 0.22 for the live flower leaves were probably due to the angle of incidence being on the order of forty-five to seventy degrees. The total backscattered fractions changed little with the addition of water, although most samples became distinctly darker to the eye.

II. BARKS

Data were collected from the barks of cedar, pine, hickory, and oak trees. The cedar bark had the highest polarization ratio, although it appeared smoothest to the eye. Cedar was also the only bark which appeared smooth enough to have a defined angle of incidence. The polarization ratios were on the order of 0.7, and only the ratio for hickory changed when wet. The barks were wet by spraying them with a garden hose nozzle. Hickory was the only bark where water stood on the surface in the form of a film rather than soaking in, as was the case with the other barks. The relative total backscattered fractions from the barks were in the range of 0.25 to 0.4 and agreed with visual reflectivity by going down when wet, except in the case of hickory.

III. DIRTS

Data were collected from a dark brown top soil obtained in a wooded area and Tennessee red clay, a red

soil, as well as from a sparsely vegetated white clay sod discussed in Section II. The polarization ratios were approximately 0.65 for the dry soils and the dry sod. The relative total backscattered fractions were in the range 0.2 to 0.4. When water was added, the polarization ratios of the dirts decreased moderately while those of the sod increased. The relative total backscattered fractions of the bare soils decreased to about 0.15 while those of the sod increased. The behavior of the data from the sod was possibly due to the fact that its surface was covered with vegetation which was the predominate scatterer. The decrease of the total backscattered fraction of the dirts when water was added agreed with the visual change observed.

IV. WOODS

The wood surfaces from which data were collected consisted of new and aged plyboard, a freshly sawed oak board shown in Figure 14a, a weathered oak board shown in Figure 14b, a rotten oak log shown in Figure 14c, and a wooden door which had been painted olive drab shown in Figure 14d. The dry-wet data for the oak were taken from an oak board several months after it had been sawed, and had begun to turn brown. The polarization ratios were 0.5 for both the cracked plyboard and the new, smooth plyboard; 0.76 for the freshly sawed board; 0.4 for the weathered board; 0.6 for

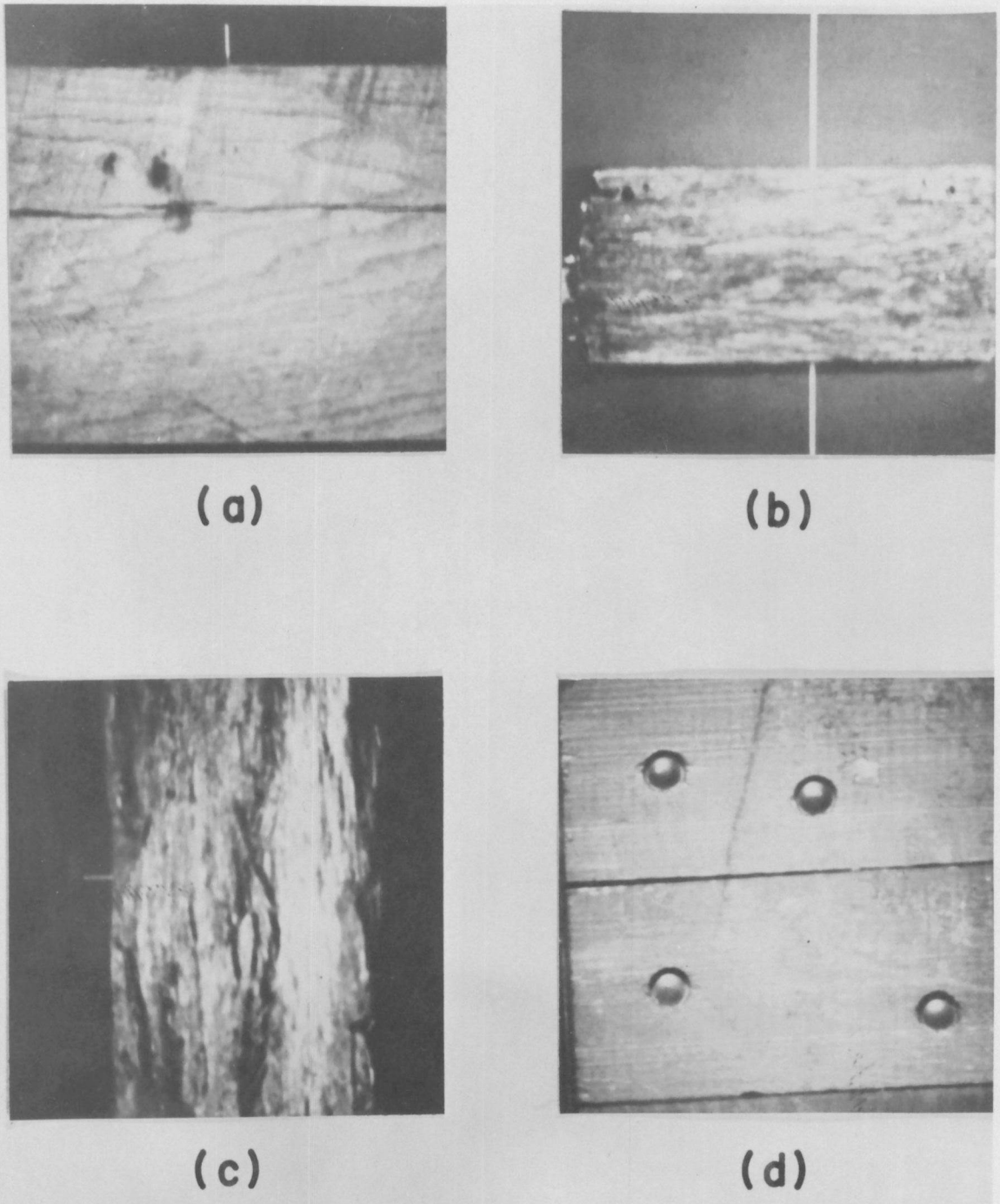


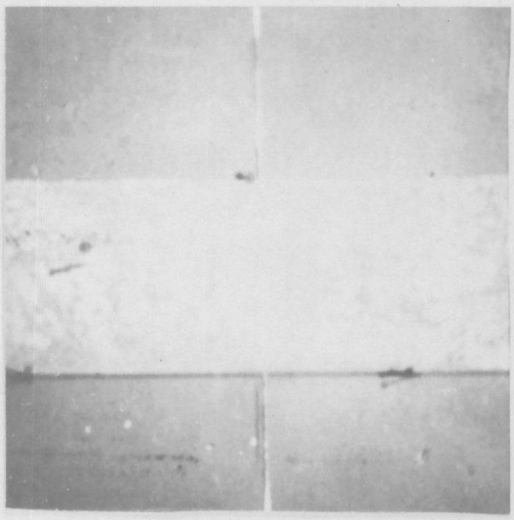
Figure 14. Woods. (a) Freshly sawed oak board; (b) Weathered oak board; (c) Rotten oak log; (d) Olive drab wooden door.

the rotten oak log; and 0.6 for the slightly aged oak board. The ratios agreed with visual roughness except for the closeness of the values for the two plyboards. The relative total backscattered fractions of 0.55 for the cracked plyboard; 0.9 for the new, smooth plyboard; 0.7 for the freshly sawed oak board; 0.2 for the weathered oak board; 0.5 for the rotten oak log; and 0.45 for the slightly aged oak board agreed with the apparent visual reflectivities, except that the value for the new plyboard appeared to be slightly greater than the apparent relative visual reflectivity. The polarization ratios for the olive drab door were 0.05 for a portion of the surface of the door which contained a painted bolt head and 0.2 for a portion of the surface of the door which had been scarred with about 80% of the paint removed therefrom. The scarred wood had just begun to age. The corresponding relative total backscattered fractions were 0.17 for the painted wood, 0.14 for the bolt head, and 0.12 for the scarred surface. The unscarred surface and the surface with the bolt head were specular reflectors. The scarred surface was not a specular reflector, although the value of the relative backscattered fraction was 30% of the typical value for the woods and 60% of the lowest value for the other woods indicating that the effects of the paint were still very large. The results for the surface with the bolt head are very similar to those of the painted surface without

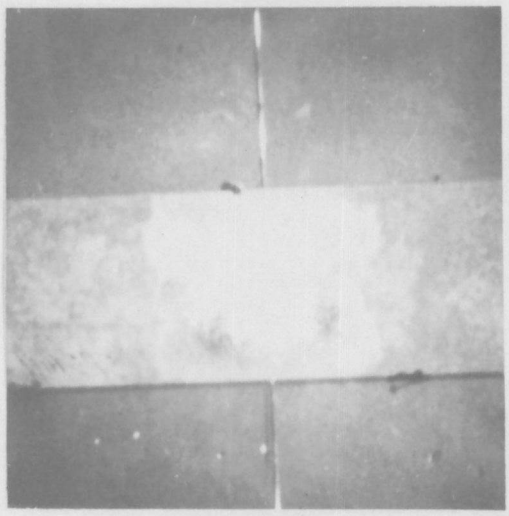
the bolt and do not positively identify the predominate scatterer. Although the laser beam was incident on the bolt head, the major portion of the scattered intensity from the bolt was possibly not scattered into the receivers, even at normal incidence, due to the shape of the bolt head.

V. METALS

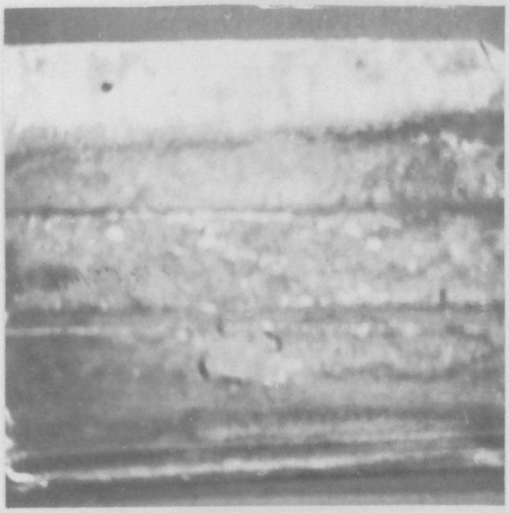
The metal surfaces from which data were collected were aircraft aluminum, galvanized tin, slotted angle iron painted a metallic gray, rusty soft steel shown in Figure 15a, soft steel with the rust removed by a steel brush shown in Figure 15b, rusty tin shown in Figure 15c, a gas can painted olive drab, and the bolt head described in the previous section. The polarization ratios were very low, ranging from zero to 0.1 (each of these could actually be on the order of 0.04 higher due to possible errors in the assigned values of the polarizer leakages discussed above), except for the very rusty tin which had a value of 0.3 for its polarization ratio. The relative total backscattered intensities were on the order of 10^3 for the aluminum; 10 for the galvanized tin; 2 for the brushed steel; 0.5 for the gray painted angle iron; 0.2 for the rusty steel, slightly rusty tin, and the gas can; and 0.09 for the very rusty tin. The metals



(a)



(b)



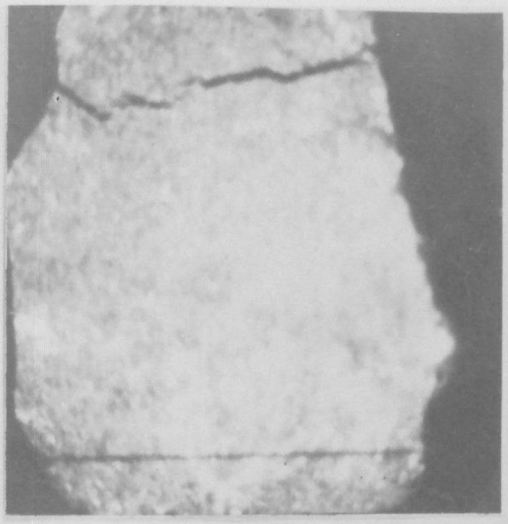
(c)

Figure 15. Metals. (a) Rusty soft steel; (b) Wire brushed soft steel; (c) Rusty tin.

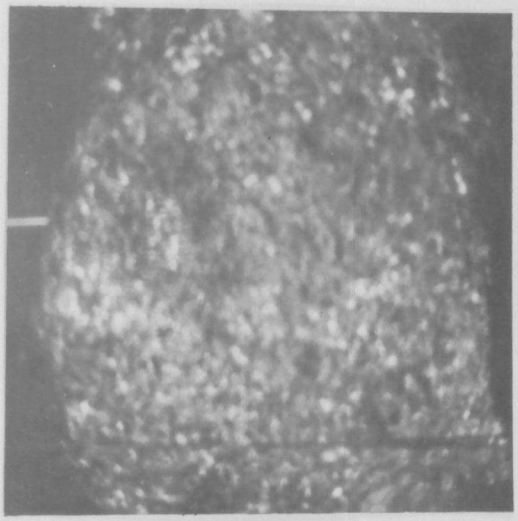
which were neither rusty nor painted were very specular reflectors, as the above figures indicate.

VI. PETROLEUM PRODUCTS

Data were collected from the worn and underside surfaces of a piece of asphalt street pavement shown in Figure 16a and Figure 16b; the upper and lower sides of an asphalt shingle; a rubber conveyor belt from a rock crusher shown in Figure 16c; a rubber tire with a universal tread taken from a riding mower; and new and used motor oil. Both the polarization ratios of 0.56 for the upper side and the lower side of the asphalt and 0.62 for the upper side of the asphalt shingle (gravel on tar paper and painted green) and the relative total backscattered fractions 0.25, 0.15, and 0.38, respectively, were relatively independent of angle of incidence suggesting that the angles of incidence to these grainy surfaces were not well-defined. The polarization ratios were 0.05 for the lower surface of the asphalt shingle and for the conveyor belt. The relative total backscattered fraction for the dark underside of the shingle, 0.3, was greater than might have been expected due to small white particles embedded in the tar paper. The conveyor belt and the motor oil had two of the lowest relative total backscattered fractions of the surfaces investigated with 0.05 for the belt, 0.004 for the new motor oil, and 0.021 for the used motor



(a)



(b)



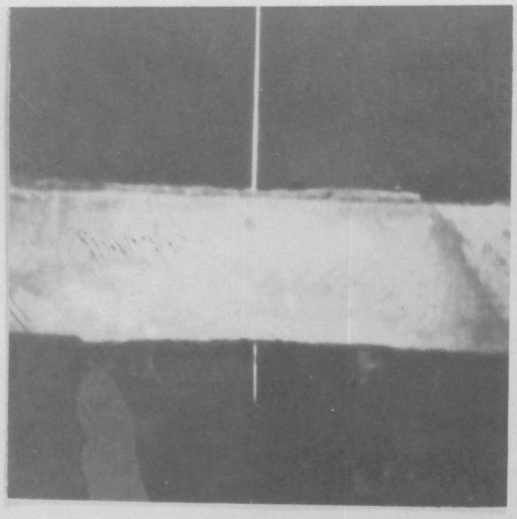
(c)

Figure 16. Petroleum products. (a) Asphalt upper surface; (b) Asphalt lower surface; (c) Rubber conveyor belt.

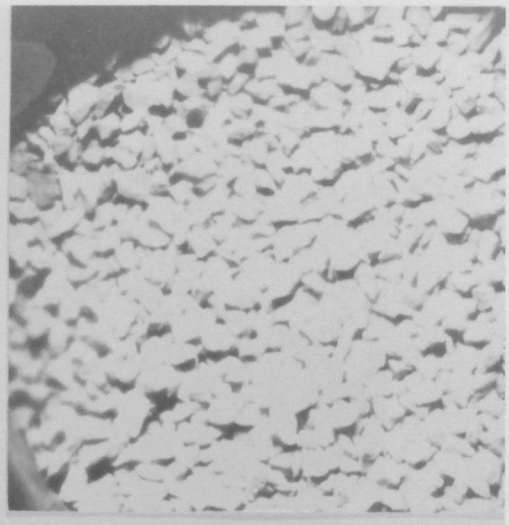
oil. There was also possibly a discernable difference between the polarization ratios of the new and used oils having values of 0.18 and 0.11, respectively. The underside of the shingle, the conveyor belt, and the oil were specular reflectors. The data were collected from the oil with the laser beams and fields of view of the receivers at a two degree angle of incidence to the surface so the specular nature of the motor oil was investigated by producing waves on the surface. The side and tread of the tire were arranged such that the angles of incidence to the surface were within 20^{o} of normal. The polarization ratios for the tire were on the order of 0.25; and the total backscattered intensities were 0.06 for the side wall and 0.04 for the tread.

VII. ROCK-LIKE MATERIALS

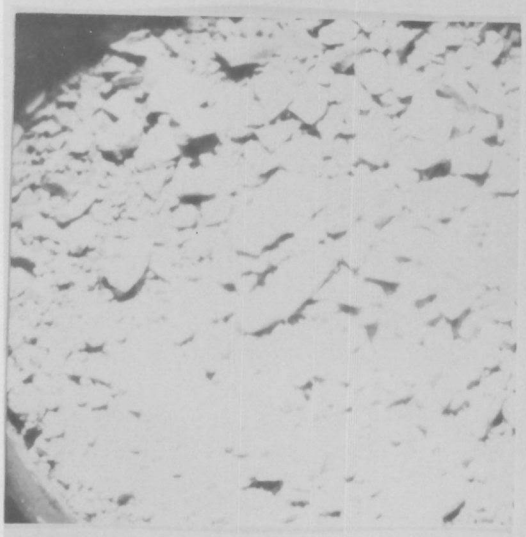
Data were collected from a concrete building block; a red fire brick (with smooth sides); a tarnished Crab Orchard stone (a limestone building stone from Crab Orchard, Tennessee) shown in Figure 17a; local brown river bottom gravel shown in Figure 17b; local crushed limestone shown in Figure 17c; and a piece of white painted slate siding which was weathered. The polarization ratios were 0.65 for the concrete block and the Crab Orchard stone and were 0.55 for the red fire brick. (The basic backscattered fractions for the red brick are dispersed in a



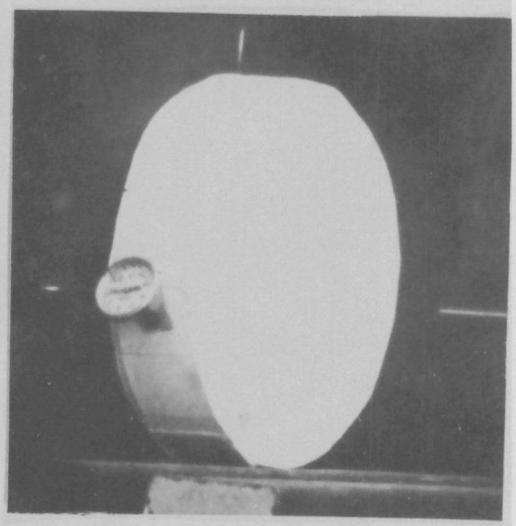
(a)



(b)



(c)



(d)

Figure 17. Stone and ice. (a) Crab Orchard stone; (b) Brown river gravel; (c) Crushed limestone; (d) Ice.

pattern which could have been caused by a temporary change in the parameters of a laser or detector-amplifier combination. The polarization ratio R'' at normal incidence appears to be the product of a system malfunction. The possibility of an anisotropic scatterer is also indicated.) The ratios change very little with changes in angle of incidence. The surfaces of the brick and the stone were not uniform with variations of up to 10% in the polarization ratios and backscattered fractions over the surfaces. The relative total backscattered fractions were approximately 0.3 for the block, the brick, and the stone. The nonuniformities in the stone were caused by three small white spots, each two millimeters in diameter, where the tarnished surface had recently been chipped. The polarization ratios for the brown gravel and the crushed limestone were on the order of 0.7 with deviations of about 15% observed over the surfaces and were decreased by the addition of water only when some of the radiation was being scattered by a water surface. The relative total backscattered fraction was 0.3 for the dry surfaces and changed to the range of 0.1 to 0.2 for the wet surfaces. The decrease agreed with the observed decrease in the visual reflectivity. The slate was one-half covered with weathered white paint, whereas the rest was unpainted and faded. The slate visually appeared nonuniform, but each section was a uniform reflector for radiation at the wavelength being considered.

The polarization ratio for the slate, 0.8, decreased slightly as the angle of incidence increased (possibly because a higher percentage of the radiation passed through the thin coat of paint and scattered from the slate at normal incidence than at larger angles of incidence) and decreased to 0.55 when wet, probably due to the specular reflection from a thin film of water and dissolved slate or paint forming a milky film covering the surface. The relative total backscattered fractions were 0.7 for the dry and the wet slate.

VIII. SANDS

Brown sand shown in Figure 18a, and white sand shown in Figure 18d, and emery cloth are included in this group. Water was mixed with the dry sand in known proportions given in liters of water per 10 liters of sand. The polarization ratios of both sands were about 0.9 until each sand was saturated with water although the texture of the sands appeared to change noticeably with each addition of water. The surface of the brown sand was periodically left in a very rough condition shown in Figure 18b, and the backscattered intensities were examined. No difference was observed in the data due to the condition of the surface. The surfaces of both sands were generally made level before data were collected to insure uniformity within the water and sand mixture. Both sands became saturated

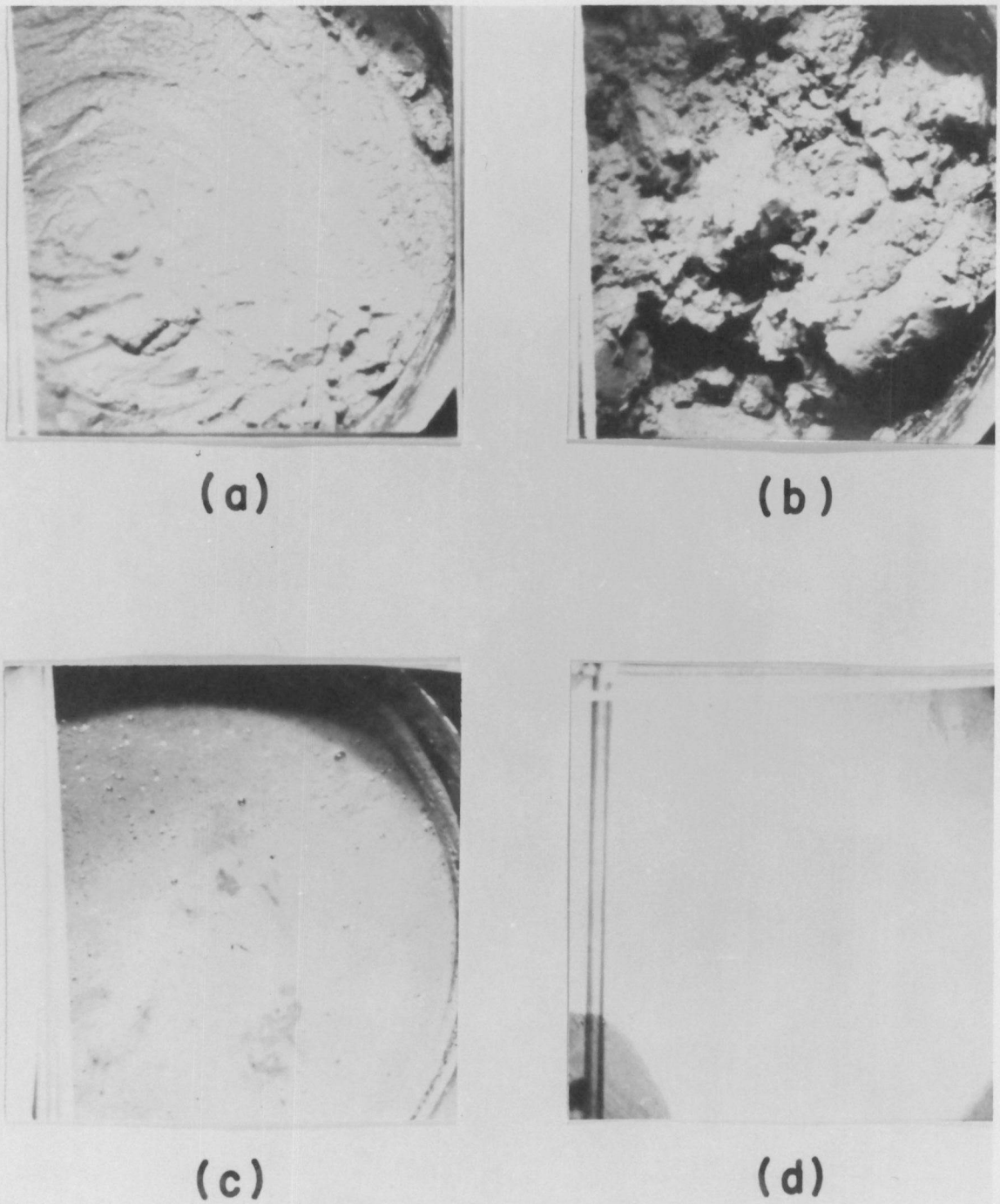


Figure 18. Sands. (a) Brown sand (smooth surface); (b) Brown sand (rough surface); (c) Brown sand (water and foam surface); (d) White sand.

when 4.6 liters of water per 10 liters of sand had been added. In each case there was a five to ten minute settling period during which the surfaces slowly became covered with water. In the case of the white sand, the water was relatively clear, and the polarization ratios continued to decrease as the depth of the water over the surface increased. The brown sand eventually became covered with a brown foam, shown in Figure 18c, and the polarization ratios increased to 0.75 as the water became murky after a low of 0.2 which occurred just after the water completely covered the surface and just before the foam began to form. The incident radiation was normal to the surface of the brown sand throughout the data in the last group labeled beam normal (BN) and then was deviated by 2^{o} (BD). The total backscattered intensity decreased almost two orders of magnitude after the incident beam was deviated due to the elimination of the specular reflection from the water surface. All of the white sand data were collected with the radiation hitting the surface at a 2^{o} angle of incidence. The polarization ratios of both the coarse and fine emery cloth were approximately 0.4 and were independent of angle of incidence. Visually, the fine grit cloth appeared very smooth while the coarse grit cloth appeared very rough. The fine grit cloth was rusty in color and had a relative total backscattered fraction of 0.2. The coarse grit cloth

was black and had a relative total backscattered fraction of 0.06. The backscattered fractions decreased moderately with increase in angle of incidence.

IX. ICE

Data were collected from a flat two inch thick piece of ice shown in Figure 17d, page 181. A thermometer was embedded two inches into the ice from the outer edge. The ice was covered with frost at ice temperatures less than -4 degrees Centigrade. The frost on the ice used for the first three data sets was formed during the freezing process, and the frost on the ice used for the fourth, fifth, and sixth data sets was formed when the ice was exposed to room air. The frost had a polarization ratio of 0.85 and a relative total backscattered fraction of 0.3 when it was formed in the freezer and had a temperature of -16 degrees Centigrade initially; and a polarization ratio of 0.75 and a total backscattered intensity of 0.2 when formed in the room air at an initial temperature of -30 degrees Centigrade. The ice gained a specular reflection component when the frost melted. At angles of incidence such that this component was not observed, the polarization ratios without the frost were generally on the order of 1.0 and were probably due to scattering from the center of the ice which was filled with air bubbles and imperfections and was visually opaque. At temperatures greater

than -4 degrees Centigrade in the interior of the ice, water flowed over the surface of the ice causing back-scattered fraction fluctuations of 40%, thus, causing similar fluctuations to show up in the polarization ratios.

X. MISCELLANEOUS

The miscellaneous group includes the standard surfaces, typing paper, black felt, canvas dyed olive drab, a movie screen and brown cardboard. The standard which was used as the standard surface had a polarization ratio of 0.75 and was Lambertian. The second (bad) standard made by pouring, which is described in Chapter II, Section IX, backscattered only 95% as much intensity at normal incidence as did the standard which was used, even though the area of the second standard surface which had the best appearance was used. The typing paper (100% cotton bond) had a polarization ratio of 0.7 and a relative total backscattered fraction equal to 95% of that of the good standard and would have made a good reference surface. The black felt had a polarization ratio of 0.8 which was relatively independent of angle of incidence. The only surprising result in the group was the relative total backscattered fraction of 0.6 for the black felt, which was also a slightly specular reflector. The olive drab canvas had a polarization ratio of 0.4 which possibly

showed some effects of the dye and a low relative backscattered fraction of 0.1 which was probably due to the olive drab dye. The movie screen had a polarization ratio of 0.7, and a relative total backscattered fraction of 0.75. The brown cardboard (from a shipping carton with a smooth exterior which had been printed on and a porous or rough interior) had a polarization ratio of 0.6 which differed slightly between the rough and smooth sides. The rough side had a relative total backscattered fraction of 0.7 and was slightly specular. The smooth side had a relative total backscattered fraction of 1.0 at normal incidence and was very specular. This agreed with the visual observation.

XI. EFFECTS PRODUCED BY PAINTS

The low polarization ratios and low backscattered fractions caused by olive drab paint on wood, metal, and cloth canvas surfaces have been described in Sections III, V, and X above. Data were taken from the smooth side of brown cardboard, varnished or shellacked plyboard, and plyboard painted gloss gray, both before and after they were painted with Krylon flat white and Krylon flat black. The surfaces were painted until no difference could be detected in the surface after the addition of a new coat. (About eight coats of paint were applied to each surface.) Data were also taken from the data mounting board described

in Chapter II, Section VII. The polarization ratios were 0.6 for the cardboard and the coated plyboard, and 0.45 for the gloss gray plyboard before painting. The respective relative total backscattered fractions were approximately 1.0 at normal incidence and the surfaces had large specular reflection components. After being painted flat white, the polarization ratios at normal incidence decreased by about one-third of their values. The total backscattered fraction increased slightly for the gray plyboard, and the surfaces became less specular. After being painted flat black, the polarization ratios decreased to 0.04 at normal incidence and increased with increasing angle of incidence to 0.8 for the cardboard, to 0.7 for the coated plyboard, and to 0.5 for the gray plyboard. The relative total backscattered fraction decreased to 0.05, and the surfaces became very specular reflectors. The data mounting board (plyboard painted flat black) had a polarization ratio of 0.05 which increased with increasing angle of incidence and a total backscattered intensity of 0.04 and had a noticeable specular reflection component. The polarization ratios for the data mounting board before it was painted should be the same as for the unpainted plyboard which was discussed in Section IV. These polarization ratios were 0.5 and varied little with the angle of incidence. The total backscattered intensity was 0.9, and it was a diffuse reflector.

The basic backscattered fractions for the smooth side of the cardboard and the unpainted coated plyboard indicate that the parallel laser decreased in output power during the collection of the data from these surfaces. The output power decreased to about 70% of its value just before and just after the data were collected. The values of $B_{\perp}''$ and $B_{/\!/}''$ for these surfaces should be about 40% larger while B_{U}'', $B_{/\!/}^{U}$, and B_{U}^{U} should be about 20% larger. Since the change did not occur during the time in which the data were being collected from a particular surface, the polarization ratios were not affected.

CHAPTER VI

CONCLUSIONS

The following conclusions are made for radiation at 0.9 micrometers wavelength incident on various commonly occurring surfaces.

1. No correlation was observed between the visual roughness of a surface and the fraction of the incident polarized radiation which was depolarized. This was probably due to surface penetration by the radiation.
2. The backscattered fractions of the surfaces behaved similarly in the visual range and at 0.9 micrometers except for a few very obvious cases such as the black felt.
3. The depolarization properties of surfaces were not changed by the addition of water as long as the surfaces were not masked by a relatively deep layer of water or as long as the surfaces were not modified by the water as was the case with the dirts.
4. The backscattered fractions of the surfaces were generally decreased by the addition of water.
5. Metallic surfaces are highly reflecting, very specular, and practically non-depolarizing

except when entirely covered by rust.

6. Petroleum products are very low reflectors, very specular, and depolarize very little.
7. Ice depolarizes essentially all of the diffusely backscattered radiation.
8. There is an indication that fresh vegetation depolarizes more than wilted vegetation.
9. Most common dielectric surfaces depolarize from 70% to 90% of the incident radiation which is found in the backscatter.
10. Most common dielectric surfaces reflect from 20% to 50% of the incident radiation in backscatter as compared to a perfectly diffuse 100% reflector.
11. Most common surfaces have a small specular reflection component. When the intensity of the specular component at 0^{o} angle of incidence is subtracted from the total backscattered intensity, the difference approximately obeys the cosine law.
12. When surfaces are painted, both the effects produced by the paint and the effects produced by the surface can usually be seen.

Two problems which could not be corrected occurred in the collection and the reduction of the data. One problem concerned the front surface aluminum mirror which was coated with an unknown substance. The mirror both depolarized and rotated the electric field of the radiation

which it reflected. All of the data collected using this mirror had to be discarded since all attempts to calibrate the effects of the mirror failed. The other problem involved the change of the polarizer leakages with time. The polarizers should have been checked several times during the experiment. Since they were checked only twice and the first check was several months prior to the experiment, the second set of leakage values obtained immediately after the end of the experiment were used in the calculations.

BIBLIOGRAPHY

BIBLIOGRAPHY

1. Shurcliff, W. A. Polarized Light, Production and Use. Cambridge: Harvard University Press, 1962.

2. Born, M., and E. Wolf. Principles of Optics. London: Pergamon Press, Ltd., 1970.

3. Corson, D., and P. Lorrain. Electromagnetic Fields and Waves. San Francisco: W. H. Freeman and Company, Inc., 1962.

4. Renau, J., P. Cheo, and H. Cooper. "Depolarization of Linearly Polarized EM Waves Backscattered from Rough Metals and Inhomogeneous Dielectrics," Journal of the Optical Society of America, 7:457-466, April, 1967.

5. Egan, W., J. Grusaukas, and H. Hallock. "Optical Depolarization Properties of Surfaces Illuminated by Coherent Light," Applied Optics, 7:1529-1534, August, 1968.

6. The Optoelectronics Data Book for Design Engineers. First Edition. Dallas, Texas: Texas Instruments, Inc., N.D.

7. Strong, C. L. "The Amateur Scientist," Scientific American, 228:114-119, March, 1973.

8. Jenkins, F., and H. White. Fundamentals of Optics. New York: McGraw Hill Book Company, Inc., 1957.

9. Grum, F., and G. Luckey. "Optical Sphere Paint and a Working Standard of Reflectance," Applied Optics, 7:2289-2294, November 1968.

10. Kneile, K. R. Private communication. Arnold Engineering Development Center, Arnold Air Force Station, Tennessee, February, 1976.

11. Guttman, I., and S. S. Wilks. Introductory Engineering Statistics. New York: John Wiley and Sons, Inc., 1965.

APPENDIX

APPENDIX I

RADIATION SCATTERED FROM A PERFECTLY REFLECTING LAMBERTIAN SURFACE

For a Lambertian surface, incident radiation is reflected in all directions such that the fraction reflected from a surface element per steradian in any direction is proportional to the cosine of the angle between the direction in which the radiation is reflected and the surface normal. A perfectly reflecting surface reflects 100% of the radiation incident on it.

Consider an element of area dA_t cut by a cone, shown in Figure 19a, whose vertex is one unit behind the surface element and whose axis is normal to the surface. Let I_1 be the intensity per unit area scattered from the surface element dA_t such that it appears to originate from the vertex of the cone and is uniform over dA_t. The area A_c intercepted by the cone at a distance R from the surface element dA_t is

$$A_c = (R + 1)^2 dA_t. \tag{77}$$

The intensity per unit area at a distance R from the surface is

$$I_2 = I_1/(R + 1)^2 . \tag{78}$$

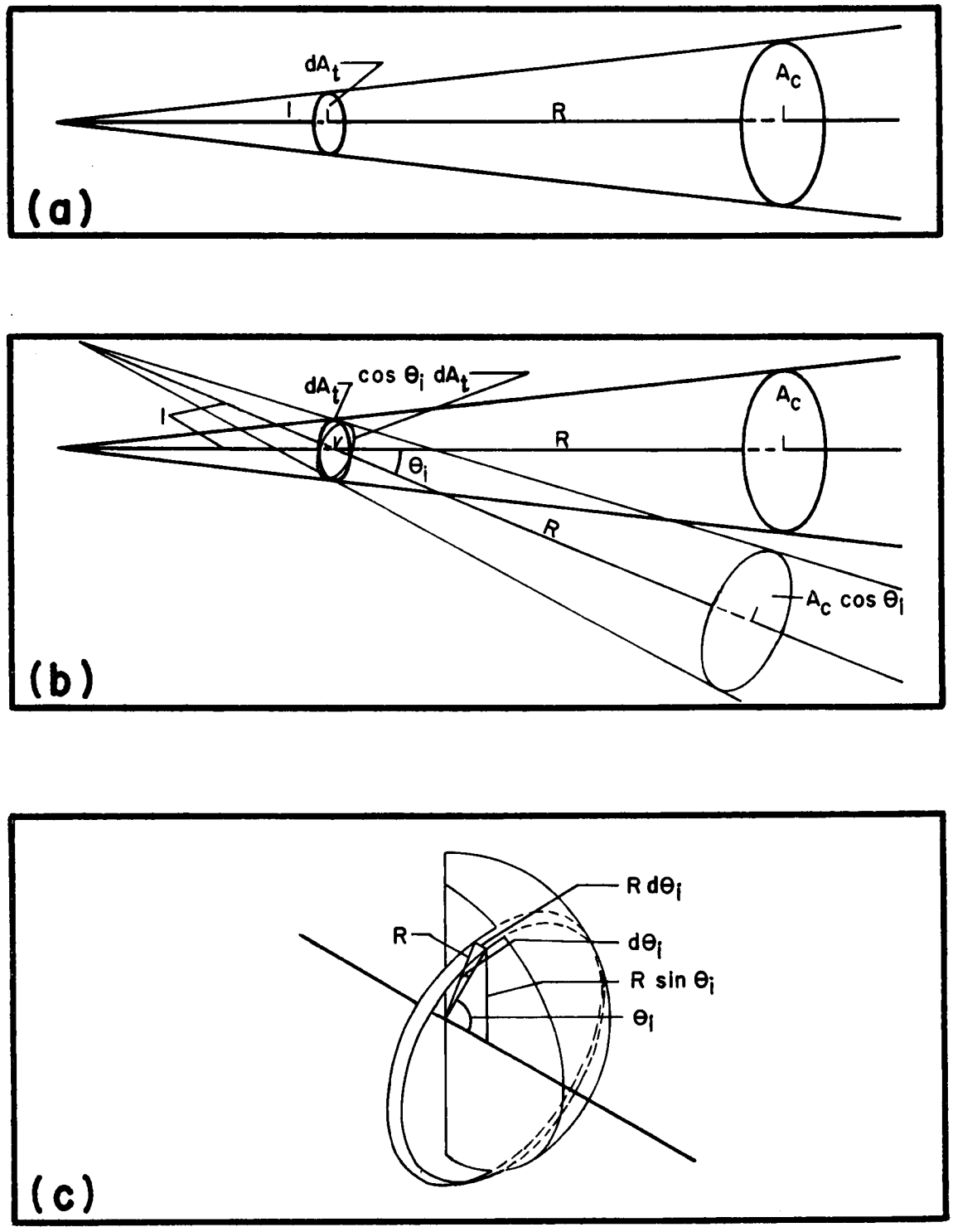


Figure 19. Sketches for deriving scattering equations. (a) Cone containing scattered radiation; (b) Scattering area viewed from an angle θ_i from the normal; (c) Annular band lying on the surface of a sphere of radius R.

For an observation point at an angle θ_i from the normal to the surface element, the surface which is normal to the line of sight (the surface viewed), shown in Figure 19b, is $\cos\theta_i dA_t$. The intensity I_3 per unit area at R, θ_i would be

$$I_3 = I_2\cos\theta_i = I_1\cos\theta_i/(R + 1)^2. \quad (79)$$

The points with equal R and θ_i lie on an annular band, shown in Figure 19c, centered on the surface normal having total area dA given by

$$dA = 2\pi(R\sin\theta_i)(Rd\theta_i). \quad (80)$$

The intensity of the radiation scattered through the annular band is

$$I_4 = I_3 dA = 2\pi I_3(R\sin\theta_i)(Rd\theta_i). \quad (81)$$

Then the intensity of the radiation scattered by dA_t into a direction which lies between $\theta_i=\theta_1$, and $\theta_i=\theta_2$ is

$$I_5 = \int_{\theta_1}^{\theta_2} \frac{2\pi I_1}{(R+1)^2} R^2\sin\theta_i\cos\theta_i d\theta_i$$

$$= \frac{\pi}{2}\frac{I_1R^2}{(R+1)^2}(\cos2\theta_2-\cos2\theta_1) . \quad (82)$$

The surface area between $\theta_i=\theta_1$ and $\theta_i=\theta_2$ at a distance R

from the surface is

$$A_1 = \int_{\theta_1}^{\theta_2} 2\pi(R\sin\theta_i)(Rd\theta_i). \tag{83}$$

The solid angle Ω_1 subtended by the surface area A_1 is

$$\Omega_1 = \frac{A_1}{(R+1)^2} = \frac{R^2}{(R+1)^2}(\cos\theta_2-\cos\theta_1). \tag{84}$$

Therefore, the intensity of radiation I_s per unit of solid angle scattered from dA_t into the annular cone which lies between $\theta_i=\theta_1$ and $\theta_i=\theta_2$ is

$$I_s = I_5/\Omega_1 = \frac{I_1}{4\pi}(\cos2\theta_2-\cos2\theta_1)/(\cos\theta_2-\cos\theta_1). \tag{85}$$

This result is completely general for any scattering surface dA_t centered around the normal from which θ_i is measured and where the boundary of A_t appears, from the point of observation, to be at least approximately centered at the point on the surface at which the normal intercepts the surface. In this case, the intensity scattered per unit area I_1 can be replaced by I_t, the total intensity scattered by the surface. Equation 85 then becomes

$$I_s = \frac{I_t}{4\pi}(\cos2\theta_2-\cos2\theta_1)/(\cos\theta_2-\cos\theta_1). \tag{86}$$

For a very small sample taken at normal incidence to the surface, that is, for $\theta_1=0$, and $\theta_2 \to 0$,

$$I_s = \lim_{\theta_2 \to 0} \frac{I_t}{4\pi} \frac{1-\cos 2\theta_2}{1-\cos \theta_2}$$

$$= I_t/\pi \simeq I_t/0.318310. \qquad (87)$$

For the receivers used, $\theta_1 \simeq 2.23 \times 10^{-3}$ milliradians and

$$I_s \simeq I_t(0.318316). \qquad (88)$$

For a perfect Lambertian reflector the intensity incident is I_t, the intensity scattered is I_s, and I_s/I_t is the total backscattered fraction of the incident intensity for normal incidence.

For unpolarized radiation normally incident, the power linearly polarized along direction ℓ is P^{ℓ} and the power linearly polarized along direction ℓ' orthogonal to ℓ is $P^{\ell'}$ where $P^{\ell}=P^{\ell'}=\frac{1}{2}P$ where P is the total intensity incident. Then as the power originally polarized along ℓ which is backscattered per steradian with polarization along d is ${}^{c}\sigma_d^{\ell}(0)P^{\ell}$, we have the power backscattered per steradian from an unpolarized normally incident beam as

$$\pi^{-1}P = {}^{c}\sigma_{\ell}^{\ell}(0)P^{\ell} + {}^{c}\sigma_{\ell}^{\ell}(0)P^{\ell} + {}^{c}\sigma_{\ell}^{\ell'}(0)P^{\ell'} + {}^{c}\sigma_{\ell}^{\ell'}(0)P^{\ell'} \qquad (89)$$

or

$$2\pi^{-1} = {}^{c}\sigma_{\ell}^{\ell}(0) + {}^{c}\sigma_{\ell}^{\ell}(0) + {}^{c}\sigma_{\ell}^{\ell'}(0) + {}^{c}\sigma_{\ell}^{\ell'}(0). \quad (90)$$

Since the standard was isotropic, ${}^{c}\sigma_{\ell}^{\ell} = {}^{c}\sigma_{\ell}^{\ell'}$, and ${}^{c}\sigma_{\ell}^{\ell} = {}^{c}\sigma_{\ell}^{\ell'}$, the backscattered fraction at normal incidence for incident radiation of either polarization is

$${}^{c}\sigma_{\ell}^{\ell}(0) + {}^{c}\sigma_{\ell}^{\ell}(0) = \pi^{-1}(\text{steradian})^{-1} . \quad (91)$$

When order of magnitude calculations were needed, the approximation of a 50% diffuse reflector,

$$I_s = \pi/2 , \quad (92)$$

was used.

For example, if 10^{-6} watts of scattered radiation need to be collected from a surface scattering a total of one watt, $I_5 = 10^{-6}$ watt,

$$I_s = \tfrac{1}{2}\pi^{-1}(1 \text{ watt}), \quad (93)$$

$$\Omega_1 = I_5/I_s = 2\pi \times 10^{-6}. \quad (94)$$

If the detector is to be twenty-five feet away, the area should be

$$A_1 = (\Omega_1)(300 \text{ inches})^2 \simeq 0.6 \text{ square inches}. \quad (95)$$

VITA

Robert L. Partin was born in Winchester, Tennessee, on January 8, 1948. He attended elementary and high school in Manchester, Tennessee. He graduated from Georgia Institute of Technology, Atlanta, Georgia, in March, 1970, with a Bachelor of Science degree in Physics.

He entered the University of Tennessee Space Institute, Tullahoma, Tennessee, in June, 1972. In 1973, he began research on optical discrimination techniques for surfaces utilizing backscatter from polarized laser radiation. He received the Master of Science degree in Physics in June, 1976.

He is married to the former Barbara Hobbs of Tampa, Florida. They have one child, Tracey.